



HAL
open science

Détection électrochimique, optique et par PCR de miARN dans des matrices biologiques pour le diagnostic du cancer

Yuanyuan Zhang

► **To cite this version:**

Yuanyuan Zhang. Détection électrochimique, optique et par PCR de miARN dans des matrices biologiques pour le diagnostic du cancer. Chimie théorique et/ou physique. Université Paris sciences et lettres, 2020. Français. NNT : 2020UPSLC023 . tel-03557666

HAL Id: tel-03557666

<https://pastel.hal.science/tel-03557666>

Submitted on 4 Feb 2022

HAL is a multi-disciplinary open access archive for the deposit and dissemination of scientific research documents, whether they are published or not. The documents may come from teaching and research institutions in France or abroad, or from public or private research centers.

L'archive ouverte pluridisciplinaire **HAL**, est destinée au dépôt et à la diffusion de documents scientifiques de niveau recherche, publiés ou non, émanant des établissements d'enseignement et de recherche français ou étrangers, des laboratoires publics ou privés.

THÈSE DE DOCTORAT
DE L'UNIVERSITÉ PSL

Préparée à l'École Nationale Supérieure de Chimie de Paris

**Détection électrochimique, optique et par PCR de
miARN dans des matrices biologiques pour le
diagnostic du cancer**

**Electrochemical, optical and PCR detection of miRNA in
biologically media for cancer diagnosis**

Soutenue par

Yuanyuan ZHANG

Le 13 Octobre 2020

Ecole doctorale n° 406

**Chimie Moléculaire de Paris
centre**

Spécialité

Chimie Moléculaire

Composition du jury :

Dr. Armelle RINGUEDE	Président
<i>Chimie ParisTech – Paris Sciences et Lettres</i>	
Pr. Benoît PIRO	Rapporteur
<i>Faculté des Sciences – Université de Paris</i>	
Dr. Jean GAMBY	Rapporteur
<i>Université Paris – Saclay</i>	
Pr. Claude JOLIVALT	Examinatrice
<i>Faculté des Sciences et Ingénierie – Sorbonne Université</i>	
Dr. Cyrine SLIM	Examinatrice
<i>Chimie ParisTech – Paris Sciences et Lettres</i>	
Dr. Mathieu LAZERGES	Directeur de thèse
<i>Faculté de Pharmacie de Paris – Université de Paris</i>	

Life is colorful, just follow your heart and believe in yourself.

Acknowledgments

The three-year Ph.D. life in *France* has given me a wealth of educational and life experience, which is inseparable from the support and guidance of all the people I received. Although no words can fully express my gratitude, I still want to express my gratitude to you here.

I will start by thanking my thesis supervisors, Dr. *Mathieu Lazerges*, Dr. *Fethi Bedioui*, Dr. *Cyrine Slim*, and Dr. *Sophie Griveau*. Each of you carried this project wholeheartedly, as well as tirelessly guide and revise the entire manuscript. *Mathieu*, I thank you for offering me be the executor of this project, which is an important and promising field for human health. Your extensive professional knowledge and broad vision benefited me a lot during my Ph.D. life, as well as for your humor and encouragement make my Ph.D. life more relaxed and enjoyable. As for *Fethi*, for your long-term vision and extensive experience in the research field enriched the project, thanks for your patience and friendly which supported me to complete the project.

I then come to thank the other supervisors who participated in guiding this project, *Cyrine Slim* and *Sophie Griveau*. *Cyrine*, your extensive analytical skills and knowledge helped me better understand various techniques, and for your patience, friendliness and quick feedback enables my project to proceed quickly and smoothly. *Sophie*, your extensive electrochemical theoretical knowledge and experimental skills provided powerful guidance for the subject, I thank for your patient guidance, your contributions of time and idea, it is very much appreciated.

I would like to thank *Philippe Nizard* and *Valérie Taly*, who collaborated in the PCR experiment part of this thesis. For them rich theoretical knowledge and experimental experience in PCR and have given great guidance and help to the PCR part of the experiment. I am also very grateful to other collaborators of project, *Gustavo Rivas* and *Fabiana Gutiérrez* for the many guidance and insightful discussion in the SPR and EIS biosensor experiment part.

I would also like to thank *Laurent Thouin* and *Eric aït-yahiatène* for their collaboration on part of the project, who took the time to answer my questions, providing gold microarrays and the guidance of fabrication of gold microelectrodes array using photolithography. I would also like to thank the technical and scientific contribution of the engineers and technicians of the microfabrication platform of the *Institute Pierre-Gilles de Gennes* (*Olivier Lesage* and *Nawel Cherkaoui*) for the masks and microfabrication tools made accessible by their work.

I would like to thank the members of the thesis jury: *Benoît PIRO*, *Jean GAMBY*, *Claude JOLIVALT* and *Armelle RINGUEDE*, thanks for your time and your interest in the overall work and I hope it will arouse your interest. I would then like to thank the members of my Ph.D. thesis committee, Dr. *Ludovic Tortech* and Dr. *Rodrigue Lescouëzec*, for their help, suggestion, supervision in my project and life time.

I would like to thank my lab members, they are also my friends, *Ménel Ben Ferej, Samantha Bourg, Jérémie Gouyon, Getnet Sewnet Kassahum, Sarah Boumati, Marion Gaudeau, Robin Nxele, Cindy lele, Fernando ESPINOLA, Amina HAMIDOU* and *Brenda DE CASTRO COSTA*, for their care of me, continued support and encouragement. I am very happy and fortunately to meet you in *Paris*, with your presence, my life has become more colorful. I also want to thank *François-Xavier GUILLON* for his help and guidance in the early stage of the experiment, and *Vincent Linden* for his help and contribution to this project. And the other members of the laboratory: *Anne, Bich-Thuy, Christian, Fanny, Camille, Laura* and the other trainees, doctoral students and post-docs too numerous to name them all.

I also would like to thank the members of Argentina lab, *Michael López Mujica* who is the collaborator in part of this project, thank him for helping me study and live in *Argentina*. Thanks for other lab members of: *Antoine, Pablo, Cecilia*, and other friend for inviting me to eat barbecue, go shopping, and eat ice cream, which left me with wonderful memories.

I gratefully acknowledge the funding received towards my PhD from *China Scholarship Council* and financial support from *CONICET, ANPCyT, SECyT-UNC (Argentina)* and *ECOS-SUD* program (A16E02).

I especially want to say a hearty thank you to the family of *Mathieu: Isabelle, Anna* and lovely little boy. The beef and bread made by *Isabelle* are very delicious, and watched movies with children is the happiest time. Your enthusiasm and friendliness are like my family, which gave me warm in *Paris*.

I gratefully thank my master supervisors *Yingshuai Liu* and *Changming Li*. It was you who led me to the path of scientific research and made me feel the charm of science. I not only learned a wealth of knowledge from you, but also learned a lot of philosophies on life. It is also your encouragement that gives me the confidence to keep moving forward on this path.

Finally, I would like to express my deep gratitude to my family: Mom, Dad, Grandma, Grandpa and brother, because their support gave me the courage to face three years of PhD life and allowed me to cross barriers that I could not see in my path.

Thank you!
Yuanyuan ZHANG
Paris, France
October 2020.

Trying to find their own a piece of the sky — struggle.

Reading Support

This doctorate presents the technological development of analytical tools allowing a direct detection of miRNAs: electrochemical (EIS and CA) and optical (RT-qPCR and SPR) biosensors which target miRNA-21, a biomarker implicated in hepatic cancers. The analytical performance of the biosensors developed as part of this doctorate is compared to that of PCR for the detection of miRNAs in human plasma samples.

The manuscript is divided into **3 Chapters**,

i) Chapter I – *State of art.*

This chapter mainly introduces the cancer and three nucleic acid cancer biomarkers (DNA, mRNA, miRNA) and different detection techniques. In addition, electrochemical nucleic acids biosensor was taken as an example to analyze the different electron transduction ways and the evolution of the detection limits.

ii) Chapter II – *Experiment Results: miRNA Quantification by Optical techniques*

In this chapter, firstly, we have carried out the detection of hybridization events to ensure that all nucleic acids can be correctly used to evaluate the performance of the four techniques proposed in this thesis.

Then we introduced two optic detection methods: *Reverse Transcription Real-time Polymerase chain reaction* (RT-qPCR) and *Surface Plasmon Resonance* (SPR)

iii) Chapter III – *Experimental Results: miRNA Quantification by Electrochemistry*

In this chapter, we introduced other two electrochemical detection methods: *Electrochemical Impedance Spectroscopy* (EIS) and *Chronoamperometry* (CA.)

iv) *General Conclusions*

This section summarizes and compares the performance of the four miRNA detection methods (Optical: RT-qPCR and SPR; Electrochemical: EIS and CA) previously designed.

v) *Appendices*

This section contains the production process of the gold UME array by photolithography, the cleaning of the array surface, the electrochemical theoretical knowledge and the measurement of DNA concentration by UV.

Contents

LIST OF ABBREVIATIONS	vi
RÉSUMÉ DE LA THÈSE	1
GENERAL INTRODUCTION.....	33
CHAPTER I: State of Art	36
LIST OF FIGURES	38
LIST OF TABLES	40
I.1. Cancer.....	41
I.2. Biomarkers.....	43
I.2.1. DeoxyriboNucleic Acid biomarkers (DNA).....	44
I.2.2. Messenger RiboNucleic Acids biomarkers (mRNA).....	46
I.2.3. MicroRNA biomarkers (miRNA or miR)	47
I.2.3.1. MicroRNA-21.....	50
I.3. Biomarker Quantification techniques	51
I.3.1. Nucleic acid amplification.....	51
I.3.1.1. Polymerase Chain Reaction (PCR).....	51
I.3.1.2. Quantitative Polymerase Chain Reaction (qPCR).....	54
I.3.1.3. Digital polymerase chain reaction (dPCR).....	63
I.3.1.4. qPCR detection of different targets	64
I.3.2. Biosensors transduction techniques.....	69
I.3.2.1. Probe immobilization method	70
I.3.2.2. The different type of Nucleic acid-based biosensor	75
I.4. Electrochemical Nucleic Acids Biosensors transduction pathway.....	91
I.4.1. Biosensors based on direct DNA oxidation.....	94
I.4.2. Biosensors based on electric properties of electrode-electrolyte interface.....	97
I.4.3. Biosensors based on redox probe labeling	100
I.4.4. Biosensors based on long range electron transfer	102
I.4.5. Biosensors based on catalyzed long-range electron transfer	105
I.4.6. Biosensors Based on Conducting polymers	106
I.4.7. Biosensors based on variation of faradic resistance	109
I.5. Object of the Thesis.....	113
References.....	115

CHAPTER II: Experimental Results	132
— miRNA Quantification by Optical techniques	132
LIST OF FIGURES	135
LIST OF TABLES	136
II.1. DNA hybridization studies	137
II.1.1. Ultraviolet method.....	137
II.1.2. The <i>Qubit</i> [®] dsDNA BR Assay	140
References.....	142
II.2. miRNA-21 quantification by RT- qPCR	143
miRNA-21 quantitative detection by Reverse Transcription Realtime Polymerase chain reaction (RT-qPCR): Stem-loop primer RT-qPCR vs Poly (A)-tail extension RT-qPCR	144
Abstract	144
Keywords	144
II.2.1. Introduction	145
II.2.2. Experimental	147
II.2.2.1. Material and methods	147
II.2.2.2. cDNA synthesis by stem-loop primer reverse transcription assay or Poly (A)-tail extension reverse transcription assay	147
II.2.2.3. miRNA purification from plasma.....	149
II.2.2.4. Real-time PCR (qPCR) using TaqMan probe	149
II.2.2.5. Absolute quantification of miRNA-21	151
II.2.3. Results and Discussion.....	152
II.2.3.1. Evaluation of the performances of two methods by analyzing miRNA-21 standard solutions in nuclease free water.....	152
II.2.3.2 Analysis of miRNA-21 standard solutions in plasma	158
Conclusions.....	160
References.....	160
Supplementary Information	162
II.3. miRNA-21 quantification by SPR	165
Label-free graphene oxide based-SPR genosensor for the quantification of microRNA21 ..	166
Abstract.....	166
Keywords	166
II.3.1. Introduction	167

II.3.2. Experimental	169
II.3.2.1. Material and methods	169
II.3.2.2. Construction of the biosensing platform	170
II.3.3. Results and Discussion.....	171
II.3.3.1. Construction and characterization of genosensor.....	171
II.3.3.2. Analytical performance of the genosensor	175
Conclusions.....	177
Acknowledgements.....	177
Compliance with ethical standards	177
References.....	178
Conclusion of the Chapter II	180
CHAPTER III: Experimental Results	181
—miRNA Quantification by Electrochemistry	181
LIST OF FIGURES	184
LIST OF TABLES	185
III.1. miRNA-21 quantification by EIS.....	186
Non-amplified impedimetric genosensor for quantification of miRNA-21 based on the use of reduced graphene oxide modified with chitosan	187
Abstract.....	187
Keywords	188
III.1.1. Introduction.....	188
III.1.2. Experimental	191
III.1.2.1. Reagents	191
III.1.2.2. Apparatus	191
III.1.2.3. Synthesis of RGO-CHIT	192
III.1.2.4. Construction of the biosensing platform.....	193
III.1.3. Results and discussion	194
Conclusions.....	201
Acknowledgements.....	201
Declaration of Conflict of Interest	201
References.....	201
Supplementary information	204
III.2. miRNA-21 quantification by Chronoamperometry.....	205

Electrochemical and reverse transcriptase real-time PCR analysis of miRNA-21	206
Abstract	206
Keywords	207
III.2.1. Introduction	207
III.2.2. Experimental section	209
III.2.2.1. Chemicals and biochemical compounds	209
III.2.2.2. Instruments	210
III.2.2.3. Plasma purification and RT-qPCR	210
III.2.2.4. Gold UME array fabrication and two-electrodes setup	211
III.2.2.5. Electrochemical measurements	212
III.2.2.6. Pretreatment of the gold ultramicroelectrodes (UME) array	213
III.2.2.7. Immobilization of DNA-probe self-assembled monolayer	213
III.2.2.8. Interfacial target oligonucleotide hybridization	214
III.2.3. Results and Discussion	215
III.2.3.1. Electrochemical response of gold UME array	215
III.2.3.2. Pretreatment of gold UME array	217
III.2.3.3. Calibration curve	221
III.2.3.4. Quantification of miRNA-21 in plasma based on RT-qPCR	222
III.2.3.5. The comparison between electrochemistry and RT-qPCR	223
Conclusions	223
References	224
Supplementary information	226
Conclusion of the Chapter III	230
General Conclusions	230
Appendices	235
LIST OF FIGURES	237
A.1. Introduction	239
A.2. Fabrication and Characterization of the Gold band UMEs array	239
A.2.1. Substrate Preparation	239
A.2.2. Photolithography Process	240
A.2.3. The metallization	243
A.2.4. Lift-off process	244
A.2.5. Fabrication of PolyDiMethylSiloxane wells (PDMS)	244

A.3. The gold band UMEs array surface cleaning.....	246
A.3.1. Gold UME array electrochemical response in sulfuric acid	246
A.3.2. Gold band UMEs array cleaning methods for bioanalytical purposes.....	249
A.3.2.1. Chemical and Electrochemical treatment method	249
A.3.2.2. Plasma treatment method	251
A.4. Gold electrode response in chloride solution.....	253
A.5. Electrochemical measurement methods.....	255
A.5.1. Mass Transport.....	256
A.5.1.1 Diffusion equations and current responses	257
A.5.2. The electrochemical measurement of planar electrode.....	258
A.5.2.1. Potential step methods (Amperometry)	258
A.5.2.2. Cyclical Voltammetry (CV).....	259
A.5.2.3. Electrochemical Impedance Spectroscopy (EIS).....	261
A.5.3. Ultramicroelectrodes (UME)	264
A.5.3.1. Potential step methods (Amperometry)	265
A.5.3.2. Cyclic voltammetry	266
A.5.4. Experiment set-up system	267
A.5.4.1. Three-electrode set-up.....	267
A.5.4.2. Two-electrode set-up.....	267
A.6. The concentration of nucleotides calculation	269

LIST OF ABBREVIATIONS

A

A	Adenine
AO	Acridine Orange
A	Absorbance

C

C_t	Cycle threshold
C	Cytosine
CA	ChronoAmperometry
CCD	Charge-Coupled Device
cDNA	complementary DNA
cfDNA	cell-free DNA
ctDNA	circulating tumor DNA
CRC	ColoRectal Cancer
CHIT	CHITosan

D

DPV	Differential Pulse Voltammetry
DTPA	DiThiol PhosphorAmidite
DNA	Deoxyribo Nucleic Acid
dsDNA	double-stranded DNA
dPCR	digital Polymerase Chain Reaction

E

EIS	Electrochemical Impedance Spectroscopy
EXPO5	EXPOrtin 5
E	PCR amplification Efficiency
EDC	1-Ethyl-3-(3-Dimethylaminopropyl) Carbodiimide
EB	Ethidium Bromide
Et	Ethanolamine

F

FRET	Förster Resonance Energy Transfer
-------------	-----------------------------------

G

G	Guanine
GO	Graphene Oxide
GCE	Glassy Carbon Electrode
Glu	Glutaraldehyde

H

HPLC	High Performance Liquid Chromatography
HCT	Human Colon Cancer

I

IUPAC	<i>International Union of Physical and Applied Chemistry</i>
--------------	--

L

LSV	Linear Sweep Voltammetry
LOD	Limit Of Detection
LOQ	Limit Of Quantification

M

mRNA	messenger RiboNucleic Acid
miRNA	micro RiboNucleic Acid
MCH	6-MerCapto-1-Hexanol
MWCNT	MultiWalled Carbon NanoTube
MGB	Minor Groove Binder
MPS	3-MercaptoPropane Sulfonate
MES	2-(N-Morpholino)-EthaneSulfonic Acid
MB	Methylene Blue

N

NCI	<i>National Cancer Institute</i>
NHS	N-HydroxysulfoSuccinimide
NTC	Non-Template Control
NFQ	Non-Fluorescent Quencher
NCD	Non-Communicable Disease

P

pri-miRNA	Primary miRNA
pre-miRNA	precursor miRNA
PCR	Polymerase Chain Reaction
PDDA	Poly(DiallylDimethylAmmonium Chloride)
PAA	Poly(Acrylic Acid)

Q

qPCR	quantitative Polymerase Chain Reaction
QD	Quantum Dot

R

RI	Reflective Index
RISC	RNA-Induced Silencing Complex
RT	Reverse Transcription
RT-qPCR	Reverse Transcription quantitative Polymerase Chain Reaction
R_{ct}	charge transfer Resistance

S

ssDNA	single-stranded DNA
SWV	Square Wave Voltammetry
SPR	Surface Plasmon Resonance
SAM	Self-Assembled Monolayer
SD	Standard Deviation

T

T	Thymine
TOMEHE	Thiazole Orange Methoxy HydroxyEthyl
TCEP-HCl	Tris(2-CarboxyEthyl)Phosphine hydrochloride
TO	Thiazole Orange

U

U	Uracil
3' UTR	3' UnTranslated Region
UME	UltraMicroElectrode

W

WHO	<i>World Health Organization</i>
ϵ	molar extinction coefficient
θ_{SPR}	SPR angle

RÉSUMÉ DE LA THÈSE

I. INTRODUCTION

Dans le domaine de la santé, trois champs d'études sont privilégiés pour améliorer la guérison des patients : le diagnostic, la mise au point de nouveaux traitements et le suivi du patient post-traitement. Selon l'*Organisation Mondiale de la Santé (OMS)*, avec un diagnostic précoce et un traitement adapté, les chances de guérison sont élevées pour de nombreux cancers [1]. L'amélioration du diagnostic et du traitement du cancer est une priorité puisqu'il représente la première cause de mortalité chez l'homme et la deuxième chez la femme avec environ 380000 nouveaux cas par an pour environ 150000 décès annuels en *France* [2].

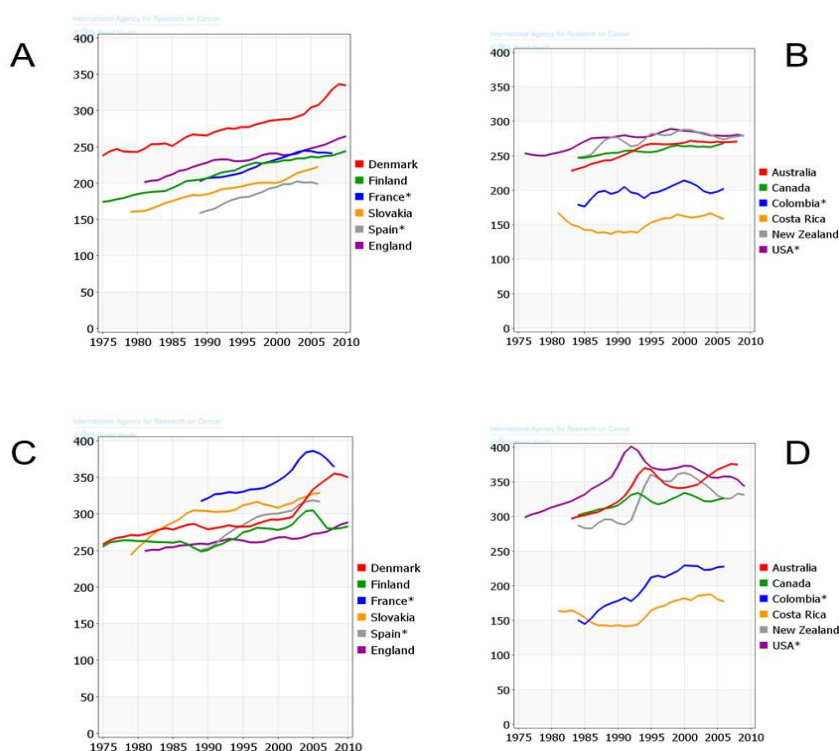


Figure 1. Incidence des cancers dans une sélection de pays en nombre de cas standardisés par l'âge pour 100000 individus: chez les femmes en Europe (A), chez les femmes en *Amérique* et *Océanie* (B), chez les hommes en *Europe* (C), chez les hommes en *Amérique* et *Océanie* (D).

De plus, l'incidence des cancers normalisée par la population est en hausse globale sur les quatre dernières décennies autant pour les hommes que pour les femmes (Figure 1) [3]. Ces chiffres montrent donc le besoin évident de dispositifs de diagnostic fiables, sensibles et précoces des cancers.

Cette thèse est dédiée au développement technologique d'outils analytiques permettant la détection et la quantification de miARNs: biocapteurs électrochimiques (spectroscopie d'impédance et chronoampérométrie) et optiques (Quantitative reverse transcription PCR (RT-qPCR)) et surface plasmon resonance (SPR)). La cible est le miRNA-21, un biomarqueur impliqué dans les cancers hépatiques. La performance analytique des biocapteurs développés dans le cadre de cette de la technique de référence, réaction de polymérisation en chaîne (PCR), pour la détection des miARNs dans des échantillons de plasma humain.

Les ADN et ARNs sont des biomolécules essentielles associées à de nombreux processus de l'organisme humain et par conséquent très souvent impliquées dans les mécanismes déréglés par les pathologies (proliférations cellulaires incontrôlées, maladies auto-immunes et neurodégénératives). La quantification de ces biomolécules est aujourd'hui réalisée par une technique de référence complexe mettant en jeu une étape préalable d'amplification de leur concentration par réaction en chaîne de la polymérase (PCR) suivie d'une mesure de fluorescence. Les limites de cette méthode sont un coût élevé, une durée d'analyse importante et l'erreur induite par l'étape préliminaire d'amplification : les miARN de séquences différentes ne sont pas systématiquement amplifiés de la même manière dans des conditions expérimentales identiques.

Ce manuscrit s'attache donc dans un premier temps à exposer la cible de ces biocapteurs, les acides nucléiques et plus précisément les miARNs, leur rôle biologique et la raison de ce choix, ainsi qu'un tour d'horizon des différentes méthodes optique et électrochimique de quantification d'acides nucléiques existants. La seconde partie est consacrée à l'exposé des résultats obtenus pour évaluer et comparer les performances des différentes techniques optiques : la RT-qPCR et la SPR. Enfin, la dernière partie expose les résultats des expériences réalisées pour évaluer et comparer les performances des méthodes électrochimiques sur des réseaux d'électrodes lithographiés. Deux modèles de biocapteurs électrochimiques ont été développés : un biocapteur impédimétrique basé sur l'utilisation d'oxyde de graphène modifié avec du chitosane ainsi qu'un biocapteur basé sur un réseau d'UltraMicroElectrodes (UMEs) pour une détection par chronoampérométrie.

II. ETAT DE L'ART

Nous présentons ici principalement l'état de l'art relatif aux trois biomarqueurs d'acides nucléiques (ADN, ARNm, miARNs,) et leurs différentes méthodes de détection (PCR, optique, massique et électrochimique). Ensuite, les différents types de voies de conduction électrochimiques sont introduits.

La définition du cancer du National Cancer Institute (NCI) est un terme qui désigne les maladies dans lesquelles des cellules anormales se divisent sans contrôle et peuvent envahir les tissus voisins [4]. Selon les estimations de l'Organisation mondiale de la santé (OMS) en 2018, le cancer est la deuxième cause de décès (22 % du total des décès) dans le monde. La détection précoce et précise du cancer est très importante pour le diagnostic clinique, le contrôle de la toxicité efficace et, finalement, pour le succès du traitement des cancers. Aujourd'hui, une variété de biomarqueurs pouvant prédire le cancer à un stade précoce ont été découverts et l'ARNm est l'un des biomarqueurs prometteurs du cancer.

II.1. Les biomarqueurs miARNs

Les biocapteurs d'acides nucléiques peuvent cibler deux types d'espèces biologiques qui sont d'une part les acides désoxyribonucléiques (ADN) et d'autre part les acides ribonucléiques (ARN). L'ARN est une molécule transcrite à partir de l'ADN. Sa structure, découverte en 1960 par Jacob et Monod [5], est proche de celle de l'ADN. L'ARN est constitué d'un groupement phosphate, d'un groupement ribose (sucre), et d'une base aromatique purine ou pyrimidine qui peut être l'adénine (A), l'uracile (U), la cytosine (C) ou la guanine (G). L'ARN est une molécule moins stable que l'ADN car son groupement ribose peut être hydrolysé en milieu aqueux [6]. L'hydrolyse du groupement sucre est un équilibre chimique, et l'ARN est hydrolysé lentement au cours du temps selon le mécanisme donné sur la Figure 2.

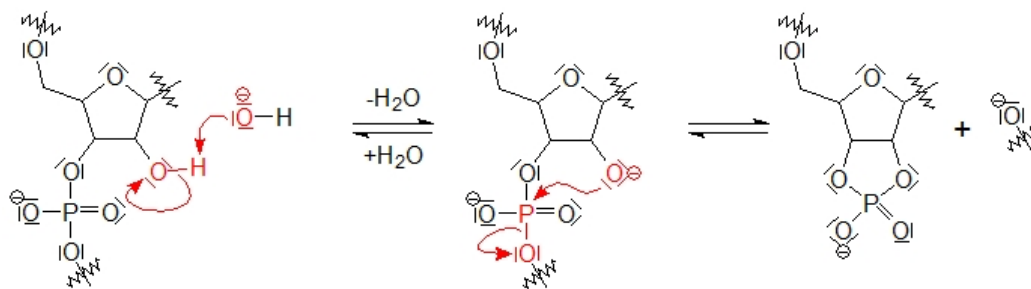


Figure 2. Mécanisme d'hydrolyse de l'ARN en milieu aqueux

La thymine et l'uracile diffèrent l'un de l'autre par un groupement méthyle. Les nucléotides A et U sont complémentaires et forment un complexe par deux liaisons hydrogènes (Figure 3).

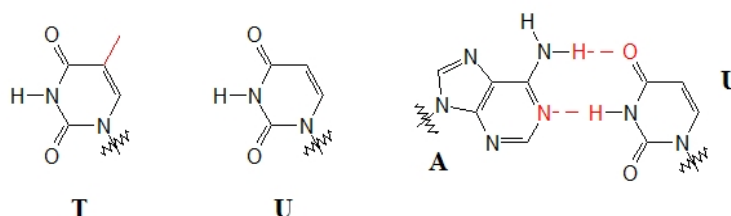


Figure 3. Structures de la Thymine (T), de l'Uracile (U) et du complexe Adénine-Uracile (A-U)

Les microARNs sont de petits ARN de longueur de base ~ 20 , ils régulent l'expression des gènes au niveau post-transcriptionnel en réduisant au silence les transcriptions de la cible par une complémentation de paires de bases avec la miARN. Les miARNs sont des régulateurs de divers processus biologiques notamment le développement, la différenciation cellulaire, la régulation du cycle cellulaire et l'apoptose. On les trouve dans presque tous les organes et dans divers fluides corporels, y compris le sang, l'urine et la salive. De plus en plus de travaux montrent que les miARNs deviennent des candidats idéaux comme biomarqueurs non invasifs de diagnostic et de pronostic dans les applications cliniques (tableau 1).

Tableau 1. Exemples de miARNs oncogènes [7].

MicroRNA	Cancer type	Function
miR-9	AML	Specifically overexpressed in MLL-rearranged AML and promotes leukemia progression.
miR-17-92	AML	Up-regulated in MLL-rearranged AML and targets p21 and RASSF2.
miR-21	Breast cancer	Overexpression of miR-21 contributes to proliferation and metastasis.
miR-27a	NSCLC	Promotes proliferation in NSCLC cells.
miR-30a/c	RCC	Downregulation leads to increased expression of HIF2a.
miR-126	AML	Up-regulated in core-binding factor (CBF) leukemia.
miR-181a/b	Breast, liver and colon cancers	Promote tumorigenesis and tumor progression.
miR-196a	Gastric cancer	Promoted EMT, migration and invasion.
miR-196b	AML	Upregulated in MLL-rearranged AML and targets Fas.
miR-421	Gastric cancer	Marker of circulating tumor cells.

AML, Acute Myeloid Leukemia; *NSCLC*, Non-Small Cell Lung Cancer; *RCC*, Renal Cell Carcinomas.

II.2. Techniques de quantification de miARNs

Les méthodes de RT-qPCR ainsi que divers biocapteurs (optiques, massiques et électrochimiques) sont couramment utilisés pour quantifier les miARNs.

a). Amplification des acides nucléiques

i). *La PCR (La réaction en chaîne par polymérase)*

Actuellement, la méthode utilisée pour quantifier les micro-ARNs, et plus largement les acides nucléiques, est la PCR (polymerase chain reaction) qui consiste à amplifier in vitro un fragment d'ADN donné, à l'aide d'une réaction enzymatique, pour obtenir 10^6 à 10^9 copies du fragment en quelques heures. Cette technique de biologie moléculaire est combinée à une méthode de détection classique comme la fluorescence pour doser des échantillons d'acides nucléiques ne contenant que quelques copies d'une séquence connue. La PCR a été développée dans les années 1980 par Kary Mullis qui reçut le prix Nobel de chimie en 1993 [8]. Il s'agit de synthétiser des copies du fragment initial à l'aide d'une enzyme, la DNA polymérase, de deux amorces (courts oligonucléotides de 20 à 25 bases) chacune complémentaire d'une extrémité

d'un des deux brins (par exemple, une amorce complémentaire de l'extrémité 3' du premier brin, et l'autre amorce complémentaire de l'extrémité 3' du second brin), et des quatre nucléotides qui sont les réactifs. Chaque cycle est composé de trois étapes : une étape de dénaturation pour séparer les deux brins d'ADN en chauffant, une étape d'hybridation des amorces sur les brins séparés en diminuant la température, et une étape d'élongation en augmentant de nouveau la température pour permettre l'action de l'enzyme. Il faut 30 à 40 cycles pour pouvoir quantifier les fragments d'ADN. De plus, les variations de température importantes nécessitent d'utiliser une enzyme thermo-résistante comme la polymérase issue d'une bactérie thermophile vivant dans les sources d'eau chaude, *Thermus Aquaticus*, appelée Taq polymérase et découverte en 1966 par Brock [9]. La PCR peut être intégralement automatisée mais il subsiste malgré tout des limitations à la quantification d'ADN par cette méthode. Tout d'abord, c'est une méthode onéreuse tant par l'appareillage nécessaire pour réaliser les cycles thermiques rapides que par les réactifs nécessaires (Taq polymérase, amorces spécifiques, nucléotides).

ii). La RT-qPCR (La réaction en chaîne par polymérase quantitative) en temps réel

La RT-qPCR est basée sur la PCR pour amplifier rapidement et spécifiquement toute petite quantité d'ARN cible *in vitro*, puis contrôler la fluorescence dans chaque cycle de PCR. En raison de la courte séquence des miARN matures (la longueur moyenne est d'environ 22 nucléotides), une méthode de PCR (tests de microARN TaqMan) adaptée aux miARNs a donc été mise au point par l'extension des miARNs matures courts (ou ADNc). Elle comporte principalement deux procédures : La transcription inverse du miARN en un ADNc étendu, puis la réaction en chaîne de la polymérase quantitative en temps réel (qPCR) avec la sonde TaqMan. Il existe deux grandes approches pour obtenir un ADNc étendu. La première consiste à utiliser une amorce RT de type tiges-boucles pour obtenir un ADNc étendu lors de l'étape de transcription inverse (figure 4a). La deuxième consiste à étendre d'abord le miARN par la méthode d'addition d'une queue poly(A) (figure 4b), puis à obtenir une version étendue de l'ADNc dans l'étape de transcription inverse suivante et à l'utiliser dans l'étape de qPCR.

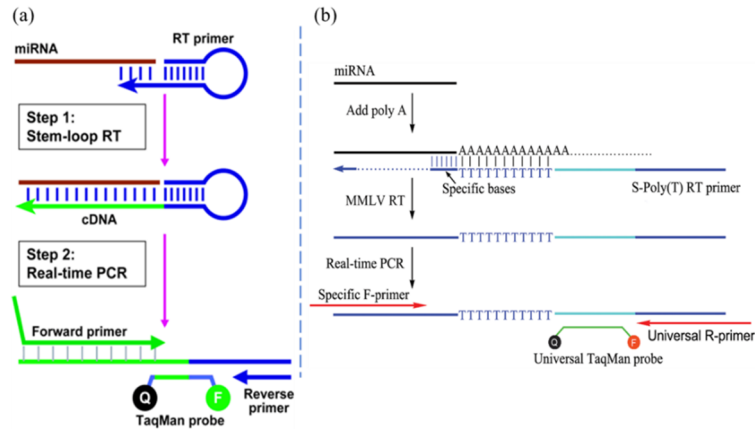


Figure 4. Description schématique des dosages des miARNs TaqMan par la méthode de l'amorce de type tige-boucle (a) ou de l'addition d'une queue poly(A) (b) pour la quantification des miRNA [10, 11].

iii). TaqMan qPCR - quantification absolue

La quantification absolue est une méthode qui consiste à utiliser une courbe standard connue pour calculer la concentration des échantillons inconnus. Pour la courbe standard, un échantillon standard de concentration connue est dilué dans une série de différentes concentrations et on effectue ensuite une qPCR (figure 5a). Le logarithme des concentrations standards est ensuite tracé sur l'axe X, et la valeur C_t correspondante est mesurée sur l'axe Y (figure 5b). Le calcul de concentration de l'échantillon est basé sur la valeur C_t mesurée et l'équation de la courbe d'étalonnage selon la formule suivante [12]:

$$C_t = slope \times \log (Concentration) + intercept$$

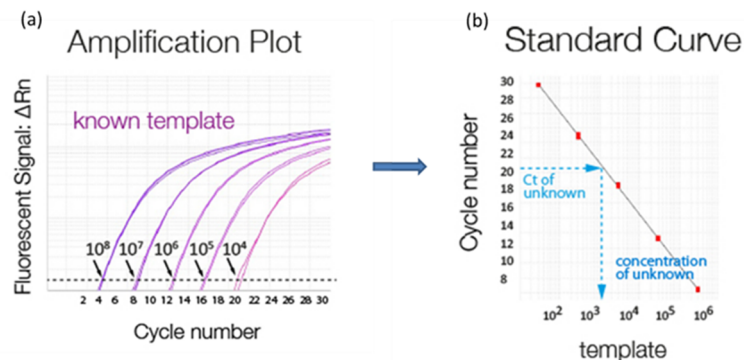


Figure 5. Schéma de quantification absolue par qPCR, (a) courbe d'amplification d'un échantillon dilué en série de concentration connue utilisé pour générer une courbe standard. (b) La courbe standard est tracée à partir de l'échantillon de concentration connue.

b). Les différents types de biocapteurs pour la détection des miARN

Le terme "biocapteur" (abréviation de "capteur biologique") est un dispositif de détection analytique sensible à la biomolécule d'intérêt et contenant deux composants principaux : le biorécepteur et le transducteur (figure 6). Il convertit les réactions biologiques en signaux spécifiques (électrochimiques, optiques, acoustiques, massiques, thermiques) et fournit des informations d'analyse quantitatives ou semi-quantitatives [13].

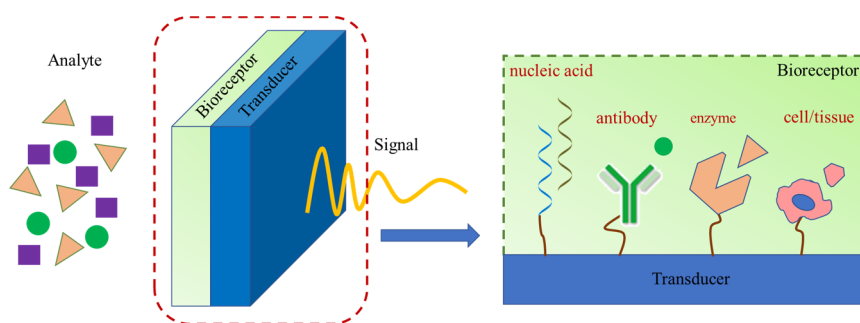


Figure 6. Schéma général d'un biocapteur.

Les biocapteurs d'acide nucléique (biocapteur d'ADN) sont basés sur les propriétés d'une molécule d'ADN simple brin (sonde), qui est capable de reconnaître les brins d'ADN spécifiques par un événement d'hybridation [14]. Les séquences spécifiques d'ADNs sont immobilisées sur la surface du support solide et agissent comme des éléments de reconnaissance moléculaire, puis l'événement d'hybridation est converti en un signal facilement mesurable, tel qu'un changement de température optique, un changement de masse, de courant ou de potentiel. Par conséquent, de nombreux types de biocapteurs existent en fonction de la méthode de transduction et de détection choisie [15].

i). Les biocapteur optiques

Les capteurs optiques sont certainement ceux offrant le plus large éventail de modes de transduction. Il s'agit alors de traduire un évènement biologique, dans ce cas précis, l'hybridation de deux simples brins d'acides nucléiques, en un signal optique, comprenant la

spectrophotométrie ultraviolette, visible et infrarouge en modes de transmission ou de réflectance. Il peut s'agir de l'émission ou de l'absorption d'une fluorescence, d'un changement de couleur, d'une luminescence ou d'un signal de résonance plasmonique de surface (SPR). Ce signal optique peut ensuite être traduit et collecté sous forme de signal électrique pour un traitement numérique et exploité pour contrôler la reconnaissance de l'ADN [16].

Résonance plasmonique de surface (SPR)

En 1982, Liedberg *et al.* ont démontré l'utilité de la SPR comme biocapteur optique et l'ont utilisé pour la première fois pour l'analyse des interactions antigènes-anticorps. La SPR est un phénomène optique physique, il reflète l'indice de réflexion (IR) dans le champ évanescent sur un métal. Le capteur SPR est également un réfractomètre optique basé sur la surveillance d'un changement de l'angle de résonance dû à une modification de l'indice de réfraction du matériau diélectrique à la surface du capteur SPR résultant de la réaction de liaison de surface. La variation de l'angle de résonance du SPR est très sensible et proportionnelle à la densité des molécules biologiques qui se trouvent dans le champ évanescent (<500 nm) sur l'autre surface du métal (figure 7). Ainsi, le biocapteur SPR peut détecter l'association et la dissociation de molécules biologiques sur la surface d'un film d'or en temps réel et sans marquage. Les changements des paramètres optiques de la surface sont causés par des réactions biochimiques, comme l'affinité de l'anticorps et de l'antigène, du récepteur et du ligand, et des fragments d'ADN complémentaires dans des conditions physiologiques [17-20].

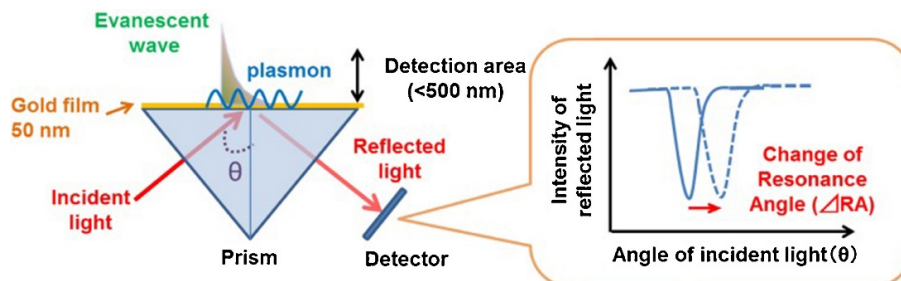


Figure 7. Schéma descriptif d'un capteur SPR.

ii). Les biocapteur électrochimiques

Les biocapteurs électrochimiques d'ADN exploitent l'affinité de l'ADN simple brin pour un brin complémentaire d'ADN simple brin afin de détecter des séquences spécifiques d'ADN en détectant les changements de signal électrochimique en présence ou en absence d'ADN complémentaire. Il convertit directement l'événement d'hybridation de l'ADN en un signal électrique, ce qui améliore considérablement la sensibilité par rapport aux autres moyens de détection (optique, masse). La figure 8 illustre la conception de base d'un biocapteur électrochimique d'ADN : des brins d'ADN sont immobilisés sur une surface électroactive (électrode) comme sonde pour construire un biocapteur d'hybridation de l'ADN, puis les modifications des paramètres électriques (par exemple, le courant, le potentiel, la conductance, l'impédance et la capacité) causées par l'hybridation sont mesurées. De nombreux types de transductions existent d'ores et déjà dans la littérature et seront détaillés dans la suite de ce manuscrit. Les biocapteurs électrochimiques d'ADN ont été rapidement développés dans le domaine de l'analyse de l'ADN ces dernières années en raison des différents avantages : (i). La transduction est directe car le processus biochimique est traduit en réponse électrique (ii). Une détection sans marquage devient possible, ce qui évite de modifier la séquence de l'ADN (iii). Le protocole de mesure électrochimique est également adapté à la fabrication à grande échelle de dispositifs miniaturisés. De plus, ils offrent une réponse rapide, une simplicité, une bonne sensibilité et sélectivité, une commodité expérimentale et un faible coût par rapport aux autres méthodes de détection des acides nucléiques [21].

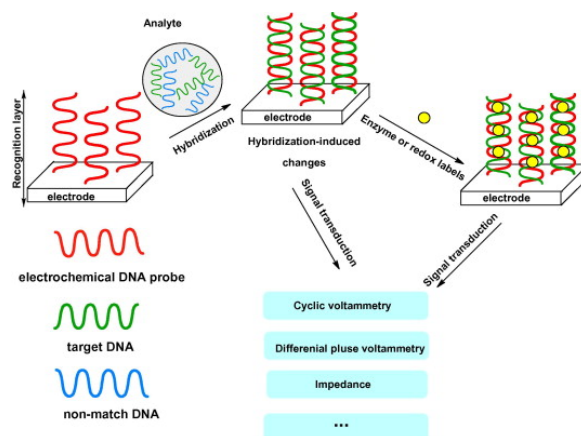


Figure 8. Schéma de conception d'un biocapteur électrochimique d'ADN [22].

Conclusion

Il existe différents types de biocapteurs pour la détection des miARNs, ayant chacun des avantages et des inconvénients. Par exemple, les biocapteurs électrochimiques font l'objet d'intérêt en raison de leur bonne sélectivité, de leur grande sensibilité et précision, et de leur miniaturisation facile. En effet, l'électrochimie est le seul mode de transduction qui permet de convertir un évènement biologique directement en un signal électrique sans conversion intermédiaire, qui nécessiterait des composants supplémentaires et entraînerait une modification du signal au cours de la transduction. Ce point clé fait de l'électrochimie une méthode de transduction appréciée des chercheurs. Par conséquent, les biocapteurs électrochimiques font l'objet de nombreuses recherches dans la communauté scientifique ces deux dernières décennies, néanmoins ces capteurs sont souvent perturbés par des substances interférentes électroactives.

Les capteurs optiques ont une vitesse de réponse rapide, les changements de signal ne sont pas affectés par les interférences électroniques ou magnétiques, mais ils nécessitent un équipement coûteux. Les biocapteurs piézoélectriques peuvent évaluer dynamiquement la réaction d'affinité, l'inconvénient est que le cristal doit être calibré et l'équipement reste souvent assez coûteux. Néanmoins, aucun biocapteur n'a réussi à supplanter la PCR jusqu'à présent. C'est la raison pour laquelle il est nécessaire de poursuivre les recherches dans ce domaine au vu des résultats apportés par les différents groupes développant ces thématiques.

II.3. Les différents types de transduction électrochimique

L'hybridation de la cible sur la sonde immobilisée à la surface de l'électrode est suivie en réalisant des mesures électriques avant et après l'hybridation permettant à la fois la détection et la quantification du fragment d'ADN. La méthode choisie pour construire le biocapteur va également jouer un rôle primordial dans les performances de robustesse et de sélectivité du capteur. Dans un premier temps, il est intéressant d'exposer les différentes techniques de transduction électrochimiques sans marquage de la cible afin d'en étudier les caractéristiques

et de choisir celle qui semble correspondre le mieux aux contraintes imposées par ce travail. Les capteurs peuvent être classés dans 7 grandes familles selon la méthode de transduction adoptée.

a). Transduction basée sur l'oxydation de la guanine

L'événement d'hybridation peut être traduit par l'oxydation de la guanine (figure 9). Le signal d'oxydation électrochimique augmente après l'hybridation en raison de l'oxydation supplémentaire des groupes guanine cibles. Le nombre de bases G après hybridation étant plus grand qu'avant l'hybridation, l'intensité du pic d'oxydation mesurée est plus grande et permet de quantifier la cible dans l'échantillon.

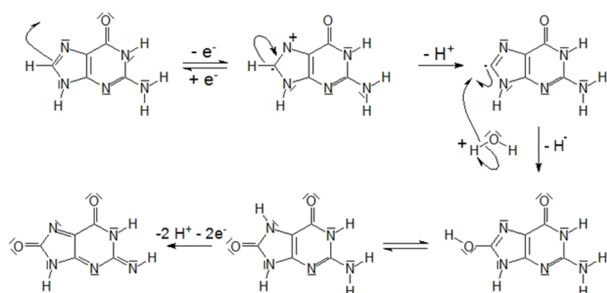


Figure 9. Mécanisme d'oxydation de la guanine

b). Transduction non-faradique

La transduction non faradique est basée sur la modification des propriétés électriques de l'interface électrode-solution en raison de l'hybridation : la conductivité et la capacité électriques sont toutes deux modifiées. La variation de la capacité interfaciale peut être mesurée par des techniques électrochimiques non transitoires comme la spectroscopie d'impédance ou la voltampérométrie cyclique.

c). Transduction basée sur des sondes marquées par une molécule rédox

Le principe de cette transduction est basé sur la mesure de la réponse redox d'une sonde ADN marquée avec une molécule électroactive, dans une configuration « classique » ou « en épingle à cheveux ». Dans le cas d'une configuration « en épingle à cheveux », le courant peut augmenter ou diminuer en fonction de la nature de la transduction et de la séquence de la sonde ADN.

d). Transduction basée sur le transfert d'électrons longue distance non catalysé

Cette transduction utilise des sondes ADN greffées à la surface de l'électrode. Il s'agit d'utiliser une propriété fondamentale de l'ADN, c'est-à-dire l'augmentation de la conductivité électronique du duplex d'ADN par rapport au simple brin du fait de l'empilement π des bases du duplex permettant le transfert des électrons à travers la couche d'ADN un peu comme le long du squelette d'une molécule aromatique. En effet, dans la configuration de l'hélice double brin, les bases aromatiques sont orientées vers l'intérieur de l'hélice, dans le plan perpendiculaire à l'axe de cette hélice. De cette manière, les bases de l'ADN se retrouvent empilées d'une façon « semblable à une pile de pièces de monnaie » avec un espace entre chaque base de l'ordre de 3 à 4 Å. Cet espace interbase est alors semblable à celui mesuré entre deux plans graphène du graphite, ce qui permet de confirmer que le passage d'électrons d'une base à une autre est possible, tout comme il est observé entre deux plans du graphite. Dans la première génération de capteurs basés sur le transfert d'électrons longue distance, un médiateur rédox cationique en solution est utilisé. Au cours de l'hybridation, avec l'augmentation des charges négatives à la surface de l'électrode, l'attraction électrostatique du médiateur rédox dans la couche d'ADN augmente. Par conséquent, l'intensité mesurée du signal de ce médiateur augmente également, permettant la détection de l'hybridation (Figure 10). Cependant, le rapport signal/bruit n'est pas optimal puisque l'attraction électrostatique n'est pas spécifique au duplex ADN et se produit également avec la couche de sonde simple brin.

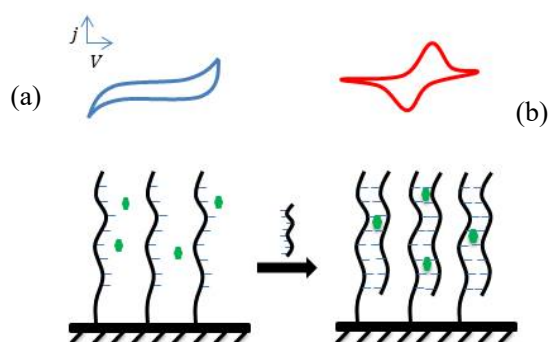


Figure 10. Schéma de la transduction basée sur le transfert d'électrons longue distance non catalysé d'espèces rédox cationiques (cercles verts) avant (a) et après (b) hybridation.

e). Transduction basée sur le transfert d'électrons longue distance catalysé

Une percée majeure des biocapteurs basés sur le transfert d'électrons à longue distance a été réalisée en utilisant deux systèmes redox. Cette méthode utilise des sondes redox anioniques en solution à une concentration de l'ordre du millimolaire (mM), et un intercalant redox de l'ADN dans une quantité catalytique de l'ordre du micromolaire (μM). La diffusion de la sonde redox au sein de la couche d'ADN chargée négativement est empêchée par des répulsions électrostatiques avec des squelettes d'ADN phosphate chargés négativement. De plus, la concentration de l'intercalant est très faible, ce qui donne un courant très faible. La réponse électrochimique unique de ce système est le signal redox de la sonde électrocatalysé par le transfert d'électrons à longue distance renforcé par l'intercalant redox (figure 11). Cette technique permet donc de discriminer une cible parfaitement complémentaire d'une autre contenant un seul mismatch. Cette technique est donc parfaitement sélective et donc très adaptée à l'application souhaitée.

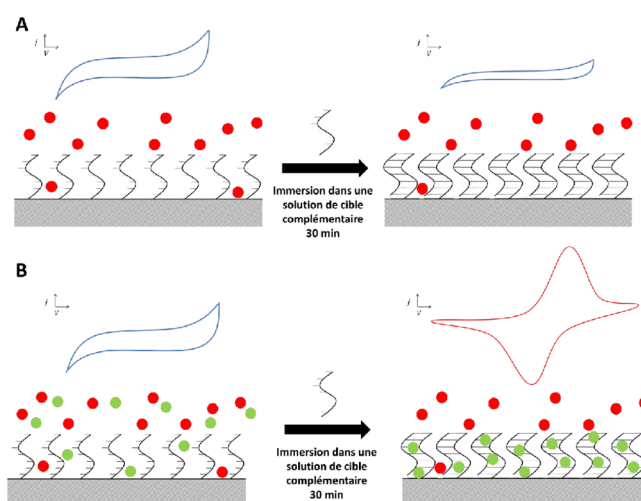


Figure 11. Transduction basée sur le transfert d'électrons longue distance depuis une sonde redox anionique en solution (cercles rouges) non catalysés (A) ou catalysés (B) par un intercalant redox (cercles verts).

f). Transduction basée sur la réponse électrochimique des polymères conducteurs

L'oxydation réversible de polymères conjugués organiques, comme le polypyrrole, peut être utilisée pour effectuer la transduction de l'hybridation. La transduction est basée sur la

variation de la charge d'oxydoréduction du polymère après l'hybridation. En effet, l'oxydation du polypyrrole le fait passer d'un état où les monomères sont libres à un état beaucoup plus contraint appelé structure quinoïde. Après hybridation de la sonde greffée sur le polymère à la cible complémentaire, les duplex ADN sont plus encombrants et plus raides que les sondes seules. Aussi, le passage à la structure quinoïde plus contraintes demande plus d'énergie, d'où une charge électrique plus importante pour oxyder le polypyrrole.

g). Transduction basée sur la résistance faradique

Des capteurs basés sur l'augmentation de la résistance faradique peuvent également être envisagés pour la détection d'acides nucléiques. Cette méthode de transduction utilise des sondes ADN greffées à la surface de l'électrode et un médiateur rédox en solution. Lors de l'hybridation, l'encombrement stérique de la couche d'ADN augmente empêchant d'autant plus la diffusion du médiateur rédox en solution vers l'électrode (Figure 12). L'hybridation entraîne donc une diminution de l'intensité du signal du médiateur rédox mesurée. Le développement des nanomatériaux tels que les nanoparticules ou les nanotubes de carbone au cours des dernières années a permis d'améliorer considérablement les limites de détection de ce type de capteurs. L'utilisation des nanomatériaux permet d'augmenter considérablement la surface active et par conséquent de multiplier le nombre de sondes ADN immobilisées. La sensibilité du capteur est donc améliorée. De plus, les nanomatériaux permettent d'intégrer des étapes de concentration au protocole pour améliorer encore la sensibilité de la méthode.

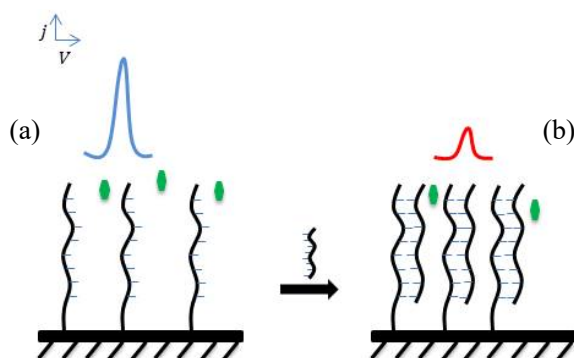


Figure 12. Schéma de la variation de résistance faradique d'un biocapteur ADN avant (a) et après (b) hybridation

II.4. Objectif de la thèse

Les micro-acides ribonucléiques (miARNs) sont des biomarqueurs émergents pour de nombreuses maladies, en particulier les cancers. Ils présentent un intérêt majeur pour la santé humaine car leur quantification permet d'établir un diagnostic avec un nombre d'analyses nettement inférieur à celui basé sur la quantification des micro-acides ribonucléiques messagers (ARNm). La quantification de ces biomolécules est aujourd'hui réalisée par une technique complexe mettant en jeu une réaction de polymérisation en chaîne (PCR), et il serait intéressant de développer d'autres dispositifs permettant une quantification fiable, rapide, sans amplification et facile à mettre en place au niveau clinique. Les limites de la méthode PCR sont son coût élevé, sa longue durée d'analyse et l'erreur induite par les étapes préliminaires d'amplification. La détection directe des miARNs, c'est-à-dire sans amplification préalable par PCR, constitue un défi dans le diagnostic médical. Ce doctorat présente le développement technologique d'outils analytiques permettant une détection directe des miARNs : des biocapteurs électrochimiques et optiques qui ciblent le miARN21, un biomarqueur impliqué dans les cancers hépatiques. Les performances analytiques des biocapteurs développés dans le cadre de ce travail sont comparées à celles de la PCR pour la détection des miARNs dans les échantillons de sang d'origine humaine.

III. Résultats - Quantification du miARN 21 par des méthodes optiques

III.1. Études de l'hybridation de l'ADN

L'ADN double brin absorbe moins de lumière UV que l'ADN simple brin dénaturé en raison des interactions d'empilement entre les bases, qui est appelée l'effet hypochrome [23]. Il permet de vérifier l'hybridation des deux brins d'ADN et d'évaluer la complémentarité des deux acides nucléiques, et de fournir les preuves d'hybridation pour une détection électrochimique ultérieure.

Tableau 2. Séquences d'échantillons d'ADN et de miARN.

Nom	Séquence
DNA probe (P)	1-DTPA-5' TCA ACA TCA GTC TGA TAA GCT A 3'
DNA target (T)	5' TAG CTT ATC AGA CTG ATG TTG A 3'
miRNA-21	5' UAG CUU AUC AGA CUG AUG UUG A 3'
mismatch DNA target (mT)	5' TAG CTT ATC A CA CTG ATG TTG A 3'
Random DNA target (rT)	5' CAG TCG TAA GCT CTG AGT CTA T 3'

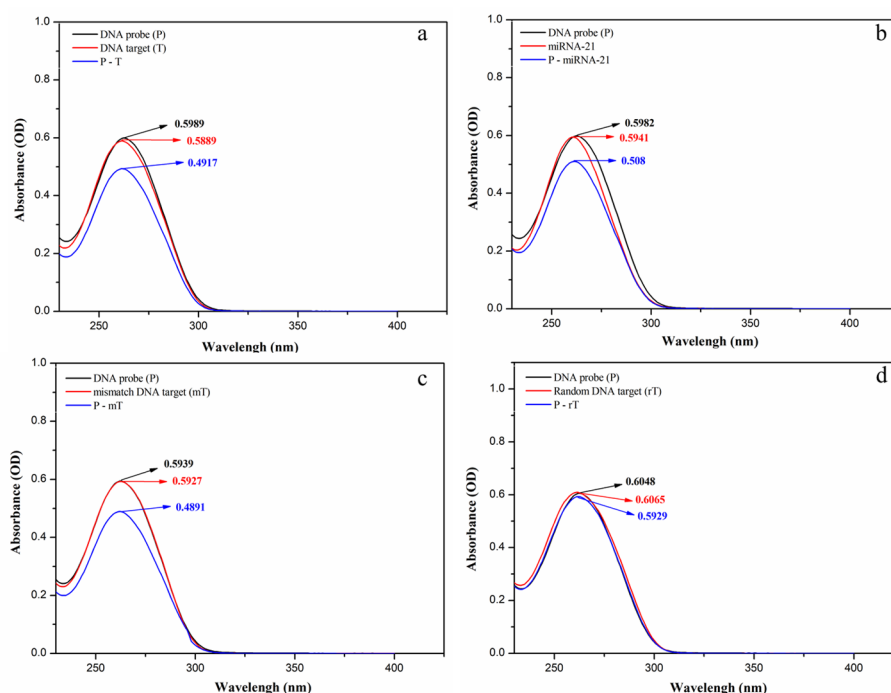


Figure 13. Spectres d'absorbance UV de différents ADN simple brin avant et après leur mélange. a: sonde ADN-DTPA et sa cible ADN complémentaire; b: sonde ADN-DTPA et miARN 21; c: sonde ADN-DTPA et cible ADN complémentaire (une base); d: sonde ADN-DTPA et cible ADN aléatoire. La plage de détection est comprise entre 200 et 450 nm et la résolution est fixée à 1 nm.

La figure 13 montre les spectres d'absorbance UV de l'ADN simple brin (tableau 2) et de l'ADN double brin (les sondes ADN s'hybrident respectivement à toutes les cibles). Lorsque la cible est une cible complémentaire (figure 13a), un miARN 21 (figure 13b) ou bien une cible non complémentaire (figure 13c), nous observons une diminution de l'absorbance après le mélange de la sonde et de la cible (hybridation). En outre, lorsque la cible est un ADN aléatoire (randomisé) (figure 13d), l'absorbance ne change pratiquement pas après le mélange. Nous démontrons donc que l'hybridation a lieu dans les trois premières solutions mélangées aux cibles et elles peuvent donc être utilisées pour élaborer et évaluer la plateforme électrochimique de biocapteurs.

III.2. Quantification du miRNA-21 par RT- qPCR

a). Introduction

Parmi les miARNs découverts, le miARN 21, indique, en fonction de son niveau d'expression dans les tissus, une variété de maladies et leurs progressions. Malgré le développement de différentes méthodes pour quantifier les miARNs, la PCR quantitative reste la méthode de référence pour valider d'autres méthodes. Dans ce travail, la sensibilité et la sélectivité de la détection des miARN-21 ont été évaluées à l'aide de deux méthodes : la méthode d'addition d'une queue poly(A) et la transcription inverse de l'amorce type tige-boucle (kits TaqMan®). La figure 14 montre le schéma des deux méthodes de RT-PCR utilisées.

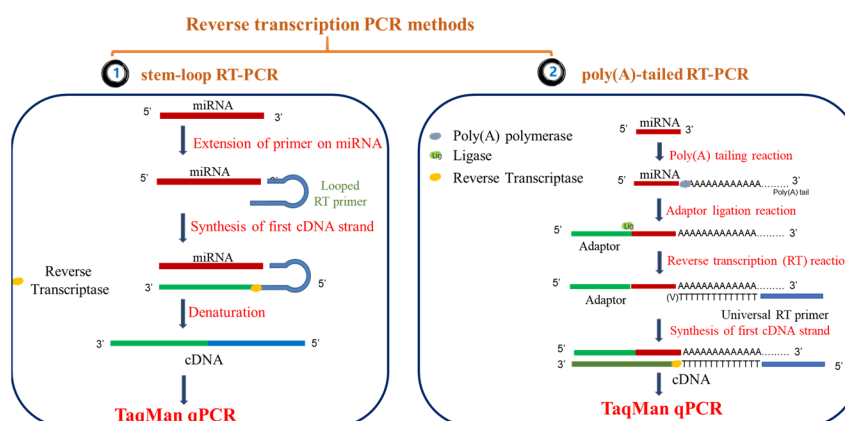


Figure 14. Schéma des deux méthodes de transcription inverse (RT) des miARN.

La méthode RT-PCR qui utilise des amorces de transcription inverse en tige-boucle spécifiques

à la cible consiste à obtenir un ADNc étendu dans l'étape de transcription inverse en utilisant une amorce RT à tige-boucle (appelée test microARN TaqMan®). La RT-PCR à queue poly(A) consiste à étendre le miARN d'abord par l'addition d'une queue poly(A), puis à obtenir une version étendue de l'ADNc dans l'étape de transcription inverse suivante (appelée tests microARN avancés TaqMan®). Les ADNc obtenus par transcription inverse sont ensuite utilisés dans l'étape suivante de qPCR, et le miARN est quantifié en contrôlant la fluorescence de la sonde TaqMan pour chaque cycle de qPCR.

b). Courbes de calibration qPCR en suivant les deux méthodes

Les courbes d'étalonnage ont été tracées pour évaluer et comparer la performance des tests miARN TaqMan® et miARN avancés TaqMan®. Les deux courbes ont été tracées pour les valeurs logarithmiques de la concentration diluée en série du miARN-21 standard et les valeurs de Ct correspondantes en utilisant le qPCR sur l'axe X et l'axe Y respectivement.

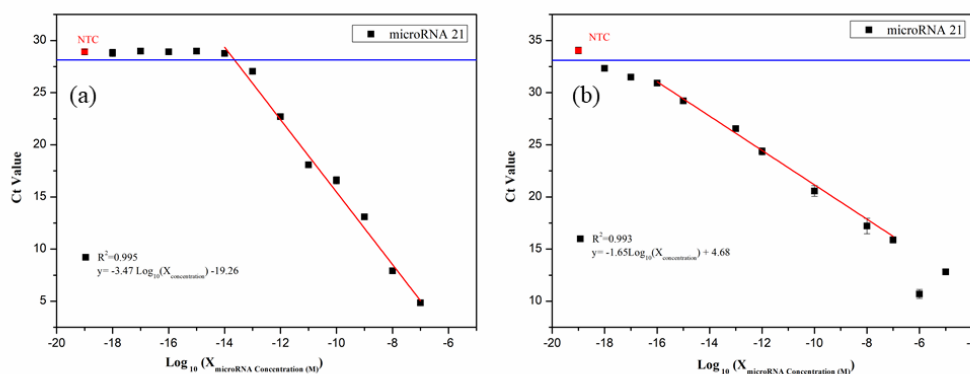


Figure 15. Courbes d'étalonnage qPCR pour différentes concentrations de miARN 21 suivant les tests de miARN TaqMan® (a) et les tests de miARN avancés TaqMan® (b). Les valeurs des concentrations en série du miARN-21 s'étendent entre 10^{-5} mol L⁻¹ à 10^{-18} mol L⁻¹, chaque point a été répété 6 fois minimum.

La figure 15 montre les courbes d'étalonnage pour le miARN-21 dans de l'eau désionisée en utilisant les tests de microARN TaqMan® (a) et les tests de microARN avancés TaqMan® (b). Les performances de détection sont résumées dans le tableau 3. Même si la méthode de transcription inverse de l'amorce type tige-boucle est plus rapide et moins contraignante que la méthode d'extension à queue poly(A), cette dernière étant plus sensible. Ainsi, dans ce qui suit,

la méthode d'extension à queue poly(A) sera utilisée pour quantifier le miARN-21 dans le plasma.

Tableau 3. Comparaison des performances de deux méthodes de détection de miARN-21 par RT-qPCR.

Method	Dynamic range	LOD	LOQ
stem-loop primer reverse transcription (<i>TaqMan</i> [®] microRNA Assay)	10 ⁻⁷ M to 10 ⁻¹⁴ M	22 fM	31 fM
poly(A)-tail extension method (<i>TaqMan</i> [®] advanced microRNA Assay)	10 ⁻⁷ M to 10 ⁻¹⁶ M	6 aM	15 M

c). Analyse des solutions standards de miARN-21 dans le plasma

Le miARN-21 standard a été dilué dans des solutions de plasma purifié ne contenant pas de miARN-21. Ensuite les tests avancés de microARN *TaqMan*[®] ont été utilisés pour quantifier le miARN-21 dans le plasma contenant d'autres miARN, et évaluer la spécificité et la sensibilité de la méthode. La figure 16 montre la courbe d'étalonnage qPCR en utilisant différentes concentrations de miARN-21 dans le plasma purifié.

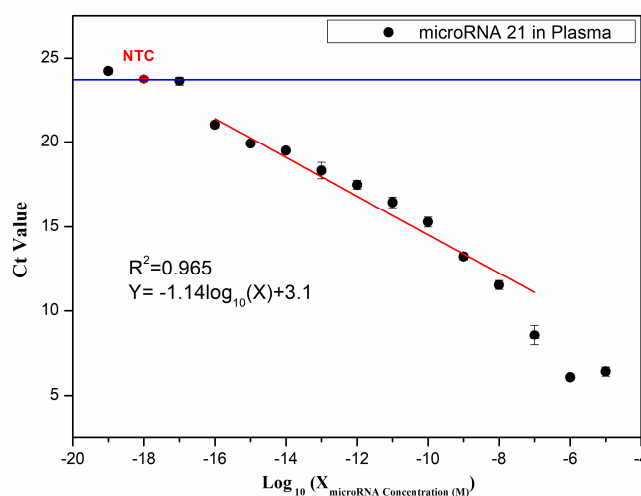


Figure 16. Courbe de rendement d'amplification qPCR (points noirs) et la courbe d'étalonnage qPCR d'un échantillon de miARN-21 de concentration différente dans le plasma (droite rouge) en utilisant les tests avancés miARN *TaqMan*[®].

La courbe montre une plage dynamique comprise entre 10⁻⁸ mol L⁻¹ et 10⁻¹⁶ mol L⁻¹, et les LOD et LOQ sont respectivement de 0,87 et 1,85 amol L⁻¹.

La fiabilité des tests avancés de miARN TaqMan® a été évaluée en analysant le plasma de donneur sain et l'ARN total de la lignée cellulaire HCT116 pour détecter le niveau d'expression du miARN-21. Le C_t du plasma d'un donneur sain est de 25,5 ce qui est proche de la valeur du contrôle négatif (NTC). Le C_t de la lignée cellulaire HCT116 est de 17,82, ce qui est inférieur au C_t (24,2) du contrôle négatif NTC qui montre la présence de miARN-21 dans cette lignée cellulaire HCT116. Selon l'équation linéaire de la courbe d'étalonnage du miARN-21 dans le plasma, la concentration de miARN-21 est de $1,22 \times 10^{-13} \text{ mol L}^{-1}$.

III.3. Quantification du miARN-21 par SPR : Biocapteur SPR à base d'oxyde de graphène sans marquage pour la quantification du miARN 21

Ce travail est axé sur le développement d'un biocapteur pour la quantification du miARN-21 en utilisant la résonance plasmonique de surface (SPR) pour la transduction de l'hybridation. La plateforme de biodétection a été construite en auto-assemblant deux bicouches de poly(chlorure de diallyldiméthylammonium) (PDDA) et d'oxyde de graphène (GO) sur une surface en or modifiée avec du 3-mercaptopropane sulfonate (MPS), puis en immobilisant de manière covalente la sonde ADN (figure 17). Le GO a été utilisé pour permettre l'immobilisation de la sonde ADN ainsi que pour augmenter la sensibilité de la détection. Dans la suite, nous examinons l'influence du nombre de bicouches PDDA/GO sur la réponse plasmonique de la plateforme, l'optimisation de la quantité de sonde d'ADN immobilisée, l'optimisation du temps d'hybridation ainsi que la performance analytique du biocapteur.

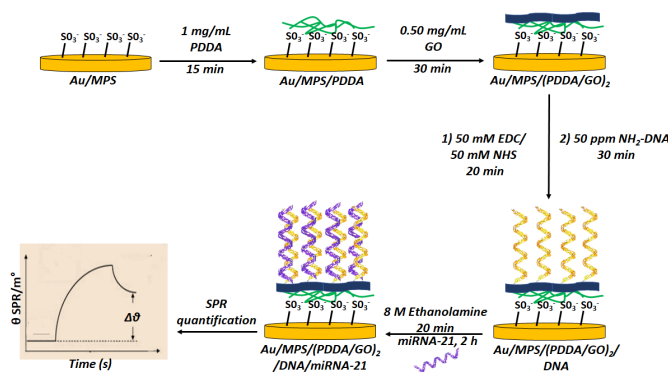


Figure 17. Schéma des différentes étapes de la construction du biocapteur SPR du microARN-21.

a). Construction et caractérisation du biocapteur SPR

La transmittance élevée de la feuille de graphène, le confinement et la propagation élevés des polaritons de plasmon de surface font du graphène un matériau aux propriétés intéressantes pour la construction de biocapteurs SPR [24-26]. Le biocapteur SPR a été conçu de telle manière à pouvoir suivre en temps réel les différentes étapes de sa construction et la détection de l'évènement de biodétection.

La figure 18a montre les profils du signal SPR obtenus lors des différentes étapes de construction de l'ensemble du biocapteur Au/MPS/(PDDA/GO)₂/DNA et la reconnaissance des cibles miARN 21.

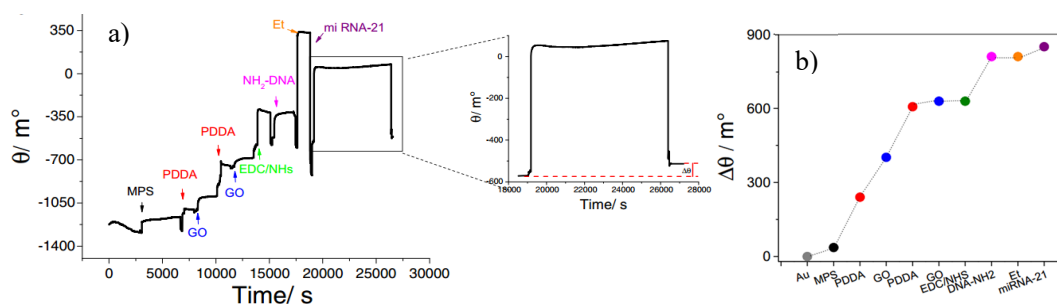


Figure 18. a) Evolution du signal SPR en fonction du temps (Sensorgramme SPR) obtenu lors de la construction du biocapteur microARN-21. La partie encadrée montre le signal obtenu après l'addition du microARN-21. b) $\Delta\theta_{SPR}$ calculée à partir du sensorgramme obtenu en a).

Le signal analytique en présence de microARN-21 a été obtenu à partir de la modification du signal SPR θ_{SPR} avant et après l'ajout de la cible et le rinçage avec la solution tampon +Tween. (voir encadré de la figure 18a). Afin de pouvoir évaluer les variations du signal SPR, la figure 18b montre l'incrément de $\Delta\theta_{SPR}$ après l'incorporation de chaque couche de la plate-forme de biodétection et après l'hybridation avec le miARN-21.

b). Performances analytiques du biocapteur

Les conditions expérimentales optimisées (sonde ADN de 50 ppm et temps d'hybridation de 120 min) ont été choisies et utilisées pour la construction de la courbe d'étalonnage du miARN-

21. Nous obtenons une relation linéaire entre 1,0 fM et 10 nM, une limite de détection de 0,3 fM. Des séquences présentant une unique base non-complémentaire (mismatch) ont été utilisées pour éprouver la sélectivité du capteur. Il s'agit de montrer que, pour un fragment cible différent d'un seul nucléotide, la réponse obtenue varie de manière à détecter cette différence pour la quantification du microARN-21 dans des échantillons d'urine enrichis. Cet aspect est primordial dans l'optique d'obtenir un biocapteur très sélectif et d'éviter les faux positifs.

En comparant les deux techniques optiques, on constate que la RT-qPCR est plus sensible que la SPR, tandis que la SPR est plus pratique et ne nécessite pas d'étape d'amplification.

IV. Résultats - Quantification du miARN 21 par des méthodes électrochimiques

IV.1. Biocapteur impédimétrique non amplifié pour la quantification du miRNA 21 basé sur l'utilisation d'oxyde de graphène réduit modifié avec du chitosan

Nous présentons ici un biocapteur pour la quantification du microARN-21 utilisant la spectroscopie d'impédance électrochimique (SIE) pour la transcription de l'hybridation. La plate-forme de détection a été obtenue par immobilisation covalente d'oxyde de graphène réduit (RGO) modifié avec du chitosane (CHIT) sur une surface d'or thiolé et par fixation covalente supplémentaire de la sonde d'ADN aminé. Le GO a été utilisé pour fournir les groupes carboxyliques pour la fixation covalente du CHIT et, ensuite réduit pour améliorer l'électroactivité de la plate-forme résultante, tandis que le CHIT a servi de pont entre le thiol et la sonde ADN aminée. La figure 19 montre le schéma des différentes étapes de la construction du biocapteur miARN-21. Les trois électrodes et la sonde redox $[\text{Fe}(\text{CN})_6]^{3-/4-}$ ont été utilisés pour détecter l'hybridation à partir du changement de la résistance de transfert de charge (R_{ct}). Les trois électrodes sont configurées comme suit : Un fil de platine et Ag/AgCl ont été utilisés comme contre-électrode et référence, respectivement, et les électrodes à disque d'or ont été

utilisées pour réaliser le biocapteur.

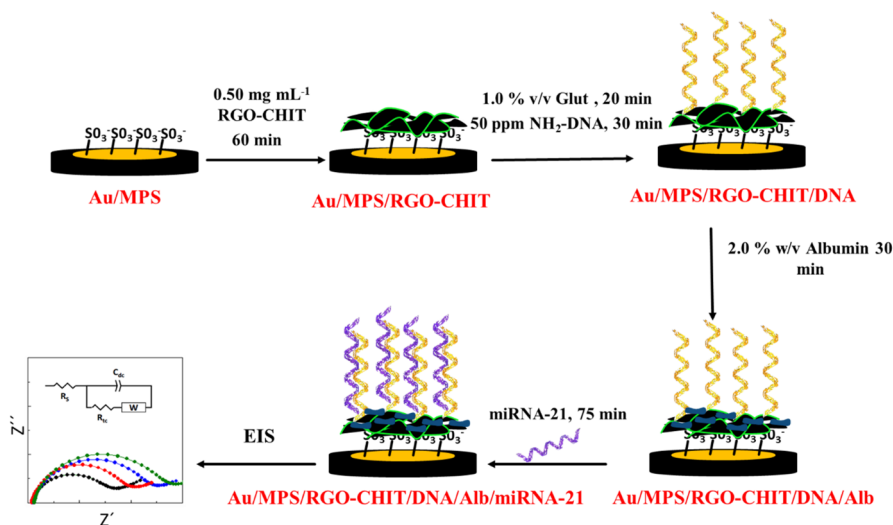


Figure 19. Schéma des différentes étapes de la construction du biocapteur miARN-21.

Dans ce qui suit, nous abordons la caractérisation de la plate-forme de biodétection et les performances analytiques du biocapteur construit.

La figure 20 montre les diagrammes de Nyquist obtenus après chaque étape de construction de du biocapteur et après l'hybridation. Les points expérimentaux sont représentés par des ronds pleins, tandis que les lignes continues représentent la concordance avec le modèle.

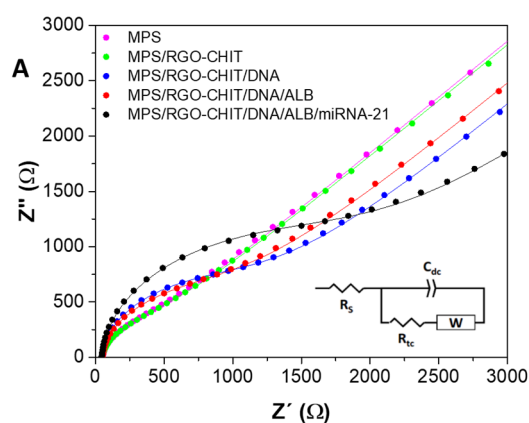


Figure 20. Diagrammes de Nyquist obtenus après chaque étape de construction du biocapteur et après l'hybridation avec le miARN-21 à une concentration de 10^{-8} M. Sonde rédox $[\text{Fe}(\text{CN})_6]^{4-/3-}$ à 10^{-3} M; Gamme de fréquences: 10 KHz à 10 mHz; Amplitude: 10 mV; Potentiel de travail: 0,2 V. Électrolyte support: Solution tampon de phosphate 0,05 M pH 7,40 avec NaCl 0,5 M.

L'immobilisation de la sonde d'ADN sur la plateforme Au/MPS/RGO-CHIT entraîne l'augmentation prévue du R_{ct} en raison de l'effet de blocage de la couche d'acide nucléique non conductrice et de la répulsion électrostatique avec la sonde redox. En outre, une fois l'hybridation avec le miARN-21 à une concentration de 10^{-8} M effectuée, il y a une augmentation importante de la R_{ct} principalement dû à l'augmentation de la charge négative due à la formation de la double hélice et à la répulsion consécutive de la sonde redox chargée négativement.

Grâce à l'optimisation des conditions expérimentales, nous avons sélectionné un temps d'hybridation de 75 min qui donne le meilleur compromis entre la sensibilité, la reproductibilité et le temps d'analyse.

La figure 21 montre la courbe de R_{ct} en fonction de logarithme de la concentration de miARN-21. Il existe une relation linéaire pour toute la gamme comprise entre $1,0 \times 10^{-12}$ M et $1,0 \times 10^{-8}$ M de miARN-21, avec une limite de détection de 300 fM.

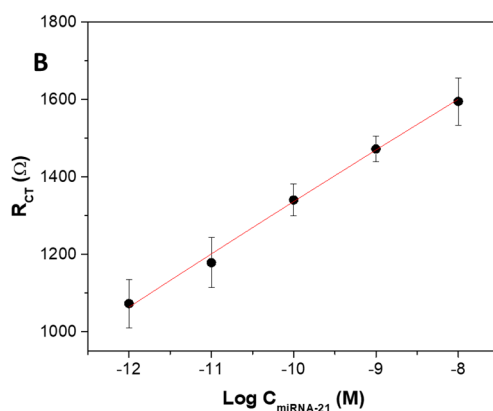


Figure 21. Courbe de calibration obtenue à partir de la réponse impédimétrique avec la sonde $[\text{Fe}(\text{CN})_6]^{3-/4-}$ à une concentration de 10^{-3} M sur Au/MPS/RGO-CHIT/ADN pour différentes concentrations de miARN-21; Gamme de fréquences: 10 KHz à 10 mHz; Amplitude: 10 mV; Potentiel redox: 0,2 V. Electrolyte support: Solution tampon de phosphate 0,050 M pH = 7,40 avec 0,5 M NaCl.

D'autre part, une séquence présentant une unique base non-complémentaire (mismatch) ainsi qu'une séquence totalement non complémentaire ont été utilisées pour vérifier la sélectivité du

capteur. Aucune réponse n'a été observée dans le cas de la séquence totalement non complémentaire par rapport au blanc, alors que pour la séquence présentant une unique base non-complémentaire, le Rct n'est que de 24,2 % par rapport à la séquence complémentaire, ce qui indique clairement que le biocapteur est capable de discriminer des séquences non complémentaires et des séquences à unique base non complémentaire (mismatch) avec d'excellents résultats. Le biocapteur obtenu a été utilisé avec succès pour la quantification du microARN-21 dans des échantillons enrichis de sérum sanguin, d'urine et de salive humains.

IV.2. Quantification par Chronoampérométrie: Analyse électrochimique du miRNA-21 sans marquage basée sur l'utilisation d'un réseau d'ultramicroélectrodes

Dans cette section, un biocapteur électrochimique d'ADN ciblant le miRNA-21 a été conçu en utilisant un réseau d'ultra-microélectrodes (UME) en utilisant la Chronoampérométrie (CA) pour détecter l'hybridation. Le réseau UME est un système d'analyse complet, automatisé et transportable. La figure 22 illustre le micro dispositif à réseau d'UME en or à 10 bandes.

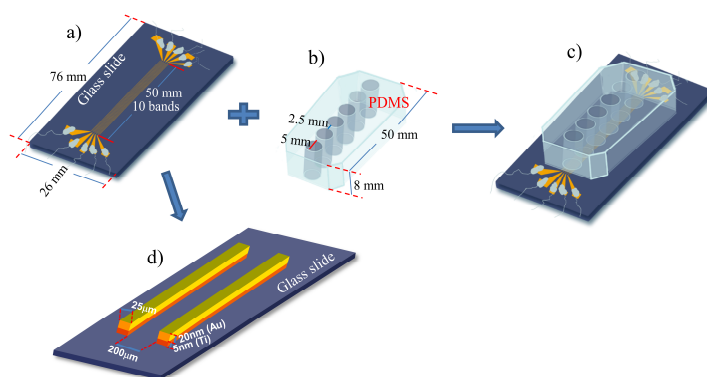


Figure 22. Schéma de la plate-forme et du microdispositif de réseau d'UMEs en or à 10 bandes, a) Réseau d'UMEs en or à 10 bandes. b) Puits en PDMS. c) Plate-forme de réseau d'UMEs à bande d'or. d) Vue en coupe des UMEs à bande montrant les couches d'or et de sous-couche de titane ainsi que les dimensions.

Un design comprenant dix microbandes d'or interdigitées sur une lame de verre (Figure 22) a été réalisé par des techniques de lithographie optique et de lift-off. Le design est défini par un

masque optique en négatif, obtenu par lithographie avec un faisceau d'électrons haute résolution. Ce masque a ensuite été répliqué par lithographie optique sur un substrat en verre en une fine couche de matériau AZ-5214 photo-résistant déposé par centrifugation. Ensuite, une couche de titane de 5 nm d'épaisseur est déposée sur le substrat en verre développé pour augmenter l'adhésion de l'or sur le dispositif. Puis une couche d'or d'une épaisseur de 20 nm est déposée par évaporation à la surface du dispositif. Après cette étape, la couche photo-résistante est dissoute, ne laissant alors que les dépôts métalliques en contact direct avec le verre. Toutes les bandes présentent des dimensions identiques (0.5 cm de longueur, 25 µm de largeur) et sont espacées de 200 µm.

Un montage à deux électrodes a été utilisé dans ce travail. Le réseau des dix microbandes d'or est placé au milieu du puits PDMS (figure 22c) et fonctionne comme électrode de travail, et la contre-électrode est un fil d'or d'un diamètre de 1 mm qui est également considéré comme une pseudo-électrode de référence.

a). Performances électrochimiques des dispositifs de détection à réseau d'UMEs

La réponse par chronoampérométrie en utilisant la sonde redox $[\text{Fe}(\text{CN})_6]^{3-/4-}$ sur le réseau d'UME a été mesurée et a permis d'évaluer la performance électrochimique du réseau d'UMEs. Le courant limite mesuré est proche du courant théorique obtenu à partir de 5 électrodes indépendantes. Ce résultat démontre que l'écart de 200 µm entre les électrodes du réseau est suffisant pour éviter le recouvrement des champs de diffusion des électrodes. En d'autres termes, la réponse électrochimique de chaque électrode ne dépend pas des réponses des autres électrodes. L'intérêt du réseau étant d'augmenter le rapport signal/bruit.

b). Prétraitement des réseaux d'électrodes d'or

Afin d'optimiser les performances du réseau d'UME en or avant l'immobilisation des sondes d'ADN, différents traitements de surface ont été réalisés :

i. prétraitement chimique acide (H_2SO_4) ;

ii. prétraitement chimique de base (KOH + H₂O₂) ;

iii. Prétraitement électrochimique (+ 1,2 V) ;

iv. Prétraitement au plasma (Ar) ;

v. Prétraitement thermique (flamme).

L'efficacité de blocage du transfert d'électrons à longue distance par la monocouche de la sonde d'ADN simple brin après le prétraitement (méthodes i à iv) a été calculée en mesurant le courant en régime stationnaire avant (I_{Au}) et après la formation de la monocouche d'ADN (I_{ss}) (Figure 23a), tous les traitements permettent d'immobiliser la sonde d'ADN à la surface de l'électrode. De plus, l'efficacité d'hybridation de la cible d'acide nucléique a été calculée avec un courant en régime stationnaire (I_{ssDNA}) avant et (I_{dsDNA}) après l'hybridation (Figure 23b). L'efficacité d'hybridation obtenu après le traitement à la flamme est la plus élevée parmi les différents traitements, ce traitement a donc été choisi pour préparer la matrice en or pour les expériences ultérieures.

Les conditions expérimentales ont également été optimisées : NaH₂PO₄ a été choisi comme solution tampon et utilisé dans toutes les procédures expérimentales, un intercalant le bleu de méthylène à une concentration de 5mM, une durée d'incubation de 30 min a été choisie pour réaliser l'hybridation et la mesure électrochimique.

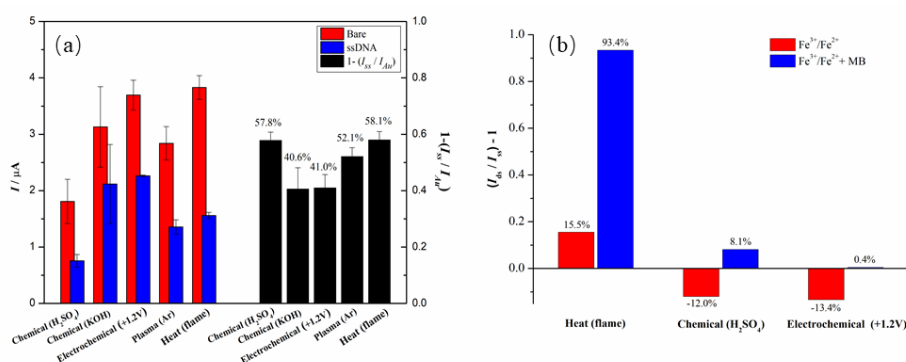


Figure 23. Efficacité de blocage du transfert d'électrons à longue distance (a) et efficacité d'hybridation (b) après les différents prétraitements de la surface d'or. Le courant est mesuré par chronoampérométrie dans une solution de NaCl 0,5 M, 5 mM [Fe(CN)₆]^{3-/4-}, 5M bleu de méthylène.

La figure 24 montre la courbe d'étalonnage obtenue avec différentes concentrations de miARN-21 dans le tampon NaH_2PO_4 avec le réseau d'UMEs à bande d'or par chronoampérométrie. Le signal représenté correspond à la différence du courant après (I_{ds}) et avant (I_{ss}) hybridation.

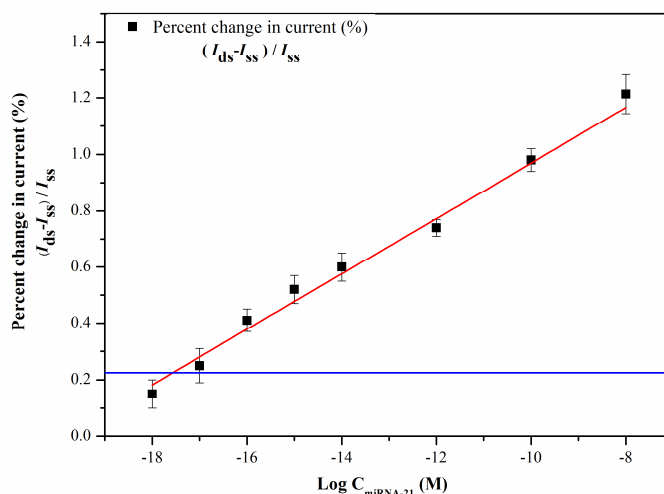


Figure 24. La courbe d'étalonnage obtenue par chronoampérométrie avec différentes concentrations de miARN-21 dans le tampon NaH_2PO_4 sur le réseau d'UMEs à bande d'or.

La relation est linéaire sur une gamme de concentration comprise entre $1,0 \times 10^{-18}$ M et $1,0 \times 10^{-8}$ M de miARN-21. La limite inférieure de détection est de $5,7 \times 10^{-18}$ mol L^{-1} (valeur obtenue à partir de 3 fois l'écart-type, où l'écart-type est l'écart type du signal à blanc). Le biocapteur électrochimique du miARN 21 constitue une méthode de test d'hybridation à la fois rapide, simple, fiable et peu coûteuse et qui permet de détecter les molécules de miARN allant du femtomolaires aux attomolaires.

V. Conclusion

Ce travail de thèse a été consacré au développement technologique d'outils analytiques permettant une détection directe des miARNs. Il s'agit de biocapteurs électrochimiques (EIS et CA) et optiques (RT-qPCR et SPR) qui ciblent le miARN21, un biomarqueur impliqué dans les cancers hépatiques. La performance analytique des biocapteurs développés a été comparée à celle de la PCR qui est la technique de référence pour la détection des miARNs dans les

échantillons biologiques. Le tableau 4 résume les performances des quatre méthodes de quantification des miARN-21 développées dans ce travail. Elles ont toutes permis d'obtenir une large gamme dynamique de quantification allant du femtomolaire à l'attomolaire. En comparant les différents résultats nous pouvons conclure que le biocapteur à transduction SPR permet de détecter dynamiquement tout le processus d'interaction des biomolécules sur la surface du substrat en temps réel et sans marquage. Le processus de détection de l'hybridation est pratique, rapide et d'une grande sensibilité. La technique électrochimique permet des tests d'hybridation de l'ADN rapides, simples, fiables et peu coûteux. Elle permet une détection sans marquage et sans amplification. De plus, l'impédance est un outil efficace pour l'étude des processus à la surface d'électrodes. Elle permet d'obtenir de plus amples informations cinétiques et structurales aux interfaces comparée à d'autres techniques électrochimiques. La modification de la surface de l'électrode avec les couches RGO-CHIT a permis d'améliorer la sensibilité de la plate-forme, et obtenir une quantification sensible, sélective, simple et rapide du miARN-21.

L'utilisation de la voie de transfert d'électrons catalysée à longue distance qui, grâce au signal faradique, ne se limite pas aux espèces redox adsorbées à la surface du biocapteur, ce qui améliore considérablement la sensibilité du biocapteur. Cette voie a permis la quantification du miARN-21 à l'échelle attomolaire. De plus le réseau de bande UMEs offre une plus grande fiabilité et sensibilité au système électrochimique du biocapteur ADN qui grâce à la miniaturisation et l'intégration ouvre les perspectives de la commercialisation.

Tableau 4. Résumé des performances de quatre méthodes de quantification pour le miARN-21.

Méthodes de détection		Gamme linéaire	LOD (M)	Echantillon réel
Optiques	RT-qPCR	10^{-16} M to 10^{-8} M,	8.7×10^{-19}	Plasma
	SPR	10^{-15} M to 10^{-6} M	3×10^{-16}	Urine
Electrochimiques	EIS	10^{-12} M to 10^{-8} M	3×10^{-13}	salive, urine et serum
	CA	10^{-18} M to 10^{-12} M	3×10^{-18}	-

Références

1. « OMS | Cancer » W. [En ligne]. Disponible sur. In. <http://www.who.int/mediacentre/factsheets/fs297/fr/>. [Consulté le: 09-févr-2017].
2. « Les chiffres clés du cancer en France » Lclc. [En ligne]. Disponible sur. In. http://www.ligue-cancer.net/article/6397_les-chiffres-cles-des-cancers [Consulté le: 19-juin-2017].
3. OMS FSbC, 2012. [En ligne]. Disponible. In. http://globocan.iarc.fr/Pages/fact_sheets_cancer.aspx; [Consulté le: 10-juill-2017].
4. Institute NC. NCI Dictionary of Cancer Terms. In. <https://www.cancer.gov/publications/dictionaries/cancer-terms/def/cancer>; 2019.
5. Jacob F, Monod J. Genetic regulatory mechanisms in the synthesis of proteins. *Journal of molecular biology* 1961,**3**:318-356.
6. Williams N. DNA hydrolysis: mechanism and reactivity. In: *Artificial Nucleases*; Springer; 2004. pp. 3-17.
7. Price C, Chen J. MicroRNAs in cancer biology and therapy: Current status and perspectives. *Genes & Diseases* 2014,**1**:53-63.
8. Saiki RK, Scharf S, Faloona F, Mullis KB, Horn GT, Erlich HA, *et al.* Enzymatic amplification of beta-globin genomic sequences and restriction site analysis for diagnosis of sickle cell anemia. *Science* 1985,**230**:1350-1354.
9. Brock TD, Freeze H. *Thermus aquaticus* gen. n. and sp. n., a nonsporulating extreme thermophile. *Journal of bacteriology* 1969,**98**:289-297.
10. Chen C, Ridzon DA, Broomer AJ, Zhou Z, Lee DH, Nguyen JT, *et al.* Real-time quantification of microRNAs by stem-loop RT-PCR. *Nucleic acids research* 2005,**33**:e179-e179.
11. Kang K, Zhang X, Liu H, Wang Z, Zhong J, Huang Z, *et al.* A novel real-time PCR assay of microRNAs using S-Poly (T), a specific oligo (dT) reverse transcription primer with excellent sensitivity and specificity. *PloS one* 2012,**7**:e48536.
12. Formisano-Tréziny C, de San Feliciano M, Gabert J. Development of plasmid calibrators for absolute quantification of miRNAs by using real-time qPCR. *The Journal of Molecular Diagnostics* 2012,**14**:314-321.
13. Turner A, Karube I, Wilson GS. *Biosensors: fundamentals and applications*; Oxford university press; 1987.
14. Wang J. DNA biosensors based on peptide nucleic acid (PNA) recognition layers. A review. *Biosensors and Bioelectronics* 1998,**13**:757-762.
15. Mulchandani A, Bassi AS. Principles and applications of biosensors for bioprocess monitoring and control. *Critical reviews in biotechnology* 1995,**15**:105-124.
16. Leatherbarrow RJ, Edwards PR. Analysis of molecular recognition using optical biosensors. *Current opinion in chemical biology* 1999,**3**:544-547.
17. Homola J. Present and future of surface plasmon resonance biosensors. *Analytical and bioanalytical chemistry* 2003,**377**:528-539.
18. Homola J, Koudela I, Yee SS. Surface plasmon resonance sensors based on diffraction gratings and prism couplers: sensitivity comparison. *Sensors and Actuators B: Chemical* 1999,**54**:16-24.
19. Ritzefeld M, Sewald N. Real-time analysis of specific protein-DNA interactions with surface plasmon resonance. *Journal of amino acids* 2012,**2012**.
20. Yanase Y, Hiragun T, Ishii K, Kawaguchi T, Yanase T, Kawai M, *et al.* Surface plasmon resonance for cell-based clinical diagnosis. *Sensors* 2014,**14**:4948-4959.
21. Zhang S, Wright G, Yang Y. Materials and techniques for electrochemical biosensor design and construction. *Biosensors and Bioelectronics* 2000,**15**:273-282.
22. Liu A, Wang K, Weng S, Lei Y, Lin L, Chen W, *et al.* Development of electrochemical DNA biosensors. *TrAC Trends in Analytical Chemistry* 2012,**37**:101-111.
23. HISATOME M, MARUYAMAN, IKEDA K, FURUTERA T, ISHIKAWA T, YAMAKAWA K. Synthesis and some spectroscopic properties of porphyrin derivatives connected with nucleobases (adenine, thymine, guanine and cytosine) by alkanamide chains. *Chemical and pharmaceutical bulletin* 1996,**44**:1801-1811.
24. Grigorenko A, Polini M, Novoselov K. Graphene plasmonics. *Nature photonics* 2012,**6**:749-758.
25. Jung I, Rhyee J-S, Son JY, Ruoff RS, Rhee K-Y. Colors of graphene and graphene-oxide multilayers on various substrates. *Nanotechnology* 2011,**23**:025708.
26. Primo EN, Kogan MJ, Verdejo HE, Bollo S, Rubianes MD, Rivas GA. Label-free graphene oxide-based surface plasmon resonance immunosensor for the quantification of galectin-3, a novel cardiac biomarker. *ACS applied materials & interfaces* 2018,**10**:23501-23508.

GENERAL INTRODUCTION

Currently, non-communicable diseases (NCDs) are the leading cause of death worldwide [1]. According to estimates from the World Health Organization (WHO) in 2018 [2], cardiovascular disease has a mortality rate of 44%, and cancer has a mortality rate of 22%. In addition, cancer is expected to be the leading cause of death in countries around the world in the 21st century and the single most important obstacle to increasing life expectancy [2]. The high mortality rate of cancer is generally due to a late-stage diagnosis and limited access to timely standard treatment. Because cancer cells can invade surrounding tissue or leave the original tumor and migrate to other areas of the body (called metastasis). Thus, it is important to detect cancer early to avoid this migration. The early and accurate detection of cancer is highly important for clinical diagnosis, effective toxicity monitoring, and ultimately for the successful treatment of cancers. At present, most diagnostic methods used by clinicians rarely provide early diagnosis, are either invasive (such as blood samples and biopsies), or very expensive (such as MRI, PET, and CT). Therefore, it is very important to develop economical, non-invasive, fast, and easy to operate techniques to improve early diagnosis.

The National Cancer Institute (NCI) definition of a biomarker is [3] “a biological molecule found in blood, other body fluids, or tissues that is a sign of a normal or abnormal process, or of a condition or disease. It also called molecular marker and signature molecule and may be used to see how well the body responds to a treatment for a disease or condition, such as cancer.” Currently, large numbers of studies have found that more and more biomarkers (e.g., proteins, nucleic acids, antibodies, peptides, and metabolites) can be used for early diagnosis of diseases. Among them, Nucleic acid biomarkers (DNA, mRNA, and miRNA) have many clinical applications due to the rapid development of nucleic acid sequencing and other technologies in the past decade [4-6].

Compared with DNA biomarkers, RNA biomarkers regulate gene expression at the

transcription and post-transcription levels [7], which can more dynamically reflect the state of the cell and the regulatory process. Moreover, compared with mRNAs, miRNAs are more sensitive, more stable, and more specific. They were found in almost all organs and various body fluids including blood, urine, and saliva. More and more evidence show that miRNAs are becoming ideal candidates as non-invasive diagnostic and prognostic biomarkers in the early stage clinical applications. However, their concentration in biological fluids is low, between 10^{-12} and 10^{-17} M, the quantification of these biomolecules is carried out by complex techniques involving polymerase chain reaction (PCR). Therefore, it would be interesting and challenging to develop a simple device that can perform reliable and rapid quantification without previous amplification. And now, in order to improve the sensitivity and detection ability of the miRNA quantification method, which has developed into a research field.

In order to overcome the above challenges, this work presents the technological development of analytical tools allowing direct detection of miRNAs: electrochemical and optical biosensors that target miRNA-21. The analytical performance of the biosensors developed as part of this work is compared to that of PCR for the detection of miRNAs in blood samples of human origin.

The first chapter presents the important role of biomarkers in clinical diagnosis and justifying the choice of miRNA biomarker during this thesis. In addition, it focuses on the presentation of miRNA quantitative technology, followed by an introduction to the evolution of the electronic transduction method and detection limit of the nucleic acid electrochemical biosensor.

The second chapter presents the results of two optical miRNA quantification methods used in this thesis, Reverse Transcription Real-time Polymerase chain reaction (RT-qPCR) and Surface Plasmon Resonance (SPR) technologies for miRNA quantification. Here, two RT-qPCR methods, stem-loop primer reverse transcription and poly(A)-tail extension are used, and then the miRNA-21 samples are amplified by polymerase chain reaction (PCR) while monitoring the fluorescence of the TaqMan probe. Showing the sensitivity of these two techniques, and then used in the quantification of miRNA-21 in the real sample.

The third chapter presents the results of two electrochemical miRNA biosensors. Which the Electrochemical Impedance Spectroscopy (EIS) and Chronoamperometry (CA) detection techniques were used to monitor the changes in the electrochemical characteristics of the electrode surface during the electrode construction process and DNA probe and miRNA target reactions on the electrode surface, showing the feasibility and sensitivity of such biosensor.

Finally, the last chapter summarizes and compares the miRNA quantification performance of the three sensors we constructed during the thesis (SPR, Electrochemical biosensor), and then compares them with the classic nucleic acid quantitative method PCR, which is the reference method. The analysis of the real sample and the comparison with RT-PCR showed that the self-made electrochemical biosensor is possible for the analysis of miRNA for clinical diagnosis.

References

1. Bray F, Ferlay J, Soerjomataram I, Siegel RL, Torre LA, Jemal A. Global cancer statistics 2018: GLOBOCAN estimates of incidence and mortality worldwide for 36 cancers in 185 countries. *CA: a cancer journal for clinicians* 2018,**68**:394-424.
2. Organization WH. Geneva: *World Health Organization*. who.int/gho/database/en/. Accessed June 21, 2018.; 2018.
3. Institute NC. NCI Dictionary of Cancer Terms. In. <https://www.cancer.gov/publications/dictionaries/cancer-terms/def/biomarker>; 2019.
4. Carlomagno N, Incollingo P, Tammaro V, Peluso G, Rupealta N, Chiacchio G, *et al*. Diagnostic, predictive, prognostic, and therapeutic molecular biomarkers in third millennium: a breakthrough in gastric cancer. *BioMed research international* 2017,**2017**.
5. Kosaka N, Iguchi H, Ochiya T. Circulating microRNA in body fluid: a new potential biomarker for cancer diagnosis and prognosis. *Cancer science* 2010,**101**:2087-2092.
6. Ortiz-Quintero B. Cell-free microRNAs in blood and other body fluids, as cancer biomarkers. *Cell proliferation* 2016,**49**:281-303.
7. Mazumder S, Datta S, Ray JG, Chaudhuri K, Chatterjee R. Liquid biopsy: miRNA as a potential biomarker in oral cancer. *Cancer Epidemiology* 2019,**58**:137-145.

CHAPTER I: State of Art

Contents

CHAPTER I: State of Art	36
LIST OF FIGURES	38
LIST OF TABLES	40
I.1. Cancer	41
I.2. Biomarkers	43
I.2.1. DeoxyriboNucleic Acid biomarkers (DNA).....	44
I.2.2. Messenger RiboNucleic Acids biomarkers (mRNA).....	46
I.2.3. MicroRNA biomarkers (miRNA or miR)	47
I.2.3.1. MicroRNA-21.....	50
I.3. Biomarker Quantification techniques	51
I.3.1. Nucleic acid amplification.....	51
I.3.1.1. Polymerase Chain Reaction (PCR).....	51
I.3.1.2. Quantitative Polymerase Chain Reaction (qPCR).....	54
I.3.1.3. Digital polymerase chain reaction (dPCR).....	63
I.3.1.4. qPCR detection of different targets	64
I.3.2. Biosensors transduction techniques.....	69
I.3.2.1. Probe immobilization method	70
I.3.2.2. The different type of Nucleic acid-based biosensor	75
I.4. Electrochemical Nucleic Acids Biosensors transduction pathway	91
I.4.1. Biosensors based on direct DNA oxidation.....	94
I.4.2. Biosensors based on electric properties of electrode-electrolyte interface.....	97
I.4.3. Biosensors based on redox probe labeling	100
I.4.4. Biosensors based on long range electron transfer	102
I.4.5. Biosensors based on catalyzed long-range electron transfer	105
I.4.6. Biosensors Based on Conducting polymers	106
I.4.7. Biosensors based on variation of faradic resistance	109
I.5. Object of the Thesis	113
References.....	115

LIST OF FIGURES

Figure I.1. The top four cause of death among all non-communicable diseases (NCD) by world area in 2018 [2].....	41
Figure I.2. Distribution of cases and deaths by world area (a) and 10 most common cancers (b) in 2018 [1].	42
Figure I.3. The three major nucleic acid biomarkers: DeoxyriboNucleic Acid (DNA), messenger RiboNucleic Acid (mRNA), and micro RiboNucleic Acid (miRNA) [18].	44
Figure I.4. Origins and range of alterations in cell-free DNA. DNA from cells are released through a combination of apoptosis, necrosis and secretion. In the bloodstream, cfDNA may exist as either free or associated with extracellular vesicles such as exosomes [27].	45
Figure I.5. The biogenesis of microRNAs processing [58].....	48
Figure I.6. The miR-21 location of (a) gene location, (b) Chromosome 17 and (c) the sequence. The human microRNA-21 gene is located on plus strand of chromosome 17q23.2 [66].	51
Figure I.7. The exponential amplification of the gene in PCR [71].	52
Figure I.8. The schematic diagram of polymerase chain reaction (PCR).	54
Figure I.9. Separation result of agarose gel electrophoresis, DNA fragments are detected with ethidium bromide [73].	55
Figure I.10. Amplification curve or reaction dynamic of PCR. In endpoint PCR, detection of amplicons occurs in the plateau phase. In real-time qPCR, quantitation of amplicons occurs during the exponential phase.	56
Figure I.11. Depictions of the more commonly used types of fluorescent detection probes used in quantitative real-time PCR [75].	58
Figure I.12. Quantification strategies in real-time quantitative PCR: absolute quantification and relative quantification [76].	60
Figure I.13. Schematic of absolute quantitative by qPCR, (a) Amplification plot of a serially diluted sample of known concentration used to generate a standard curve. (b) The standard curve is plotted by the known concentration sample.	62
Figure I.14. Schemes of typical digital PCR (dPCR) workflow. Generally, dPCR is conducted following the steps of preparation, partitioning, amplification, and analysis [89].	64
Figure I.15. Steps of mRNA real-time reverse transcription PCR [93].	65
Figure I.16. One-Step RNA real-time reverse transcription PCR.	66
Figure I.17. Two-Step real-time reverse transcription PCR.	66
Figure I.18. Specificity of TaqMan miRNA assays between stem-loop and linear RT primers [94].	67
Figure I.19. Schematic description of TaqMan miRNA assays [94].	68
Figure I.20. Schematic representation of the S-Poly(T) Plus method for miRNA quantification[99].	69
Figure I.21. General diagram of a biosensor.	70
Figure I.22. The basic of electrostatic adsorption for immobilization of DNA probes [111].	71
Figure I.23. Some common methods of DNA covalent binding on different electrochemical transducer surfaces [106].	73

Figure I.24. The covalent immobilization methods of amine-labeled DNA probe on electrodes modified with different functional groups [111].	74
Figure I.25. DNA probes immobilization on the gold electrode surface via chemisorption technique due to the strong affinity interaction between the thiol group and gold [111].	74
Figure I.26. The biotinylated HBV DNA probe immobilization process on the streptavidin modified MWCNT surface and the hybridization event [125].	75
Figure I.27. The scheme of an optical biosensor, it is a compact analytical device containing a biorecognition sensing element integrated with an optical transducer system [128].	76
Figure I.28. a: Standard MB in its closed (left) and open (right) conformations. b: Representative fluorescence emission spectra of the closed MB (black) and the open MB (red) in the absence and presence of the target, respectively [133].	78
Figure I.29. Some common planar polyaromatic compounds fluorescent intercalating dyes, which can be widely used as fluorescent probes. They can be specifically inserted into double-stranded DNA and then activated for emission, thereby the fluorescence signal is enhanced [144].	79
Figure I.30. Schematic of single-QD-based DNA nanosensors. a, Conceptual scheme showing the formation of a nanosensor assembly in the presence of targets. b, Fluorescence emission from Cy5 on illumination on QD caused by FRET between Cy5 acceptors and a QD donor in a nanosensor assembly. c, Experimental setup [147].	81
Figure I.31. Multitarget Label-Free chemiluminescence detection protocol based on different carrier vehicles [151].	82
Figure I.32. Schematic diagram of the hairpin-DNA probe detection for DNA hybridization [152].	83
Figure I.33. Schematic representation of colorimetric detection of ToLCNDV DNA using AuNP conjugated bifunctional oligonucleotide probes and the self-assembly of gold clusters [154].	84
Figure I.34. Schematic description of SPR sensor [159].	85
Figure I.35. Immobilization of probe oligonucleotides on SPR-based biosensor and the effect of hybridization on the absorbance values [160].	86
Figure I.36. General design of electrochemical DNA biosensor [167].	88
Figure I.37. Guanine oxidation mechanism.	94
Figure I.38. Transduction based on electrochemical oxidation of guanine: before (left) and after (right) hybridization (guanine groups are red).	95
Figure I.39. Double hydrogen bonded complexes of inosine with A, T and C bases.	95
Figure I.40. Transduction based on electrochemical oxidation of guanine, Differential Pulsed Voltammetry (DPV) response before (blue) and after (red) hybridization. The signal before hybridization is silenced by substitution of guanine with inosine.	96
Figure I.41. <i>LOD</i> evolution of electrochemical DNA-biosensors based on guanine oxidation.	97
Figure I.42. Electrochemical transduction of DNA hybridization based on electric properties of electrode-electrolyte interface: linear sweep voltammetry response.	98
Figure I.43. <i>LOD</i> evolution of electrochemical DNA-biosensors based on electric properties of electrode-electrolyte interface.	99
Figure I.44. Illustration of redox probe electrochemical transduction pathway with classic (left, bottom) and hairpin (left, top) DNA-probes tagged with redox groups (green circle symbols).	100

Figure I.45. LOD evolution of electrochemical DNA-biosensors based on redox probe labelling.	102
Figure I.46. Hybridization detection based on long-range electron transfer of cationic redox species and evolution of limit of detection.....	102
Figure I.47. LOD evolution of electrochemical DNA-biosensors based on long-range electron transfer. .	104
Figure I.48. Hybridization detection based on catalyzed long-range electron transfer (green triangles are redox indicators and green circles are redox intercalators.	105
Figure I.49. LOD evolution of electrochemical DNA-biosensors based on catalyzed long-range electron transfer.	106
Figure I.50. Reversible pyrrole oxidation of polypyrrole response of probe (P) and probe-target (P-T) and evolution of limit of detection (red circle: single mismatched detection).....	107
Figure I.51. LOD evolution of electrochemical DNA-biosensors based on conducting polymers.....	109
Figure I.52. Illustration of DNA biosensor variation of faradic resistance.	109
Figure I.53. LOD evolution of electrochemical DNA-biosensors based on faradic resistance increase. ...	112

LIST OF TABLES

Table I.1. Detection of cfDNA with different tumour types.	46
Table I.2. Examples of mRNA-associated with cancer specimens.	47
Table I.3. Examples of tumor-suppressor miRNAs [65].....	49
Table I.4. Examples of oncogenic miRNAs [65].	49
Table I.5. Comparison of different types of biomarkers.	50
Table I.6. Performances of miRNA detection platforms and assays [168].	90
Table I.7. DNA detection limits of biosensors based on guanine oxidation.	96
Table I.8. DNA detection limits of biosensors based on electric properties of electrode-electrolyte interface.	98
Table I.9. Detection limit of electrochemical DNA-biosensors based on redox probe labelling.	101
Table I.10. Detection limit of electrochemical DNA-biosensors based on long-range electron transfer. ...	103
Table I.11. Detection limit of electrochemical DNA-biosensors based on catalyzed long-range electron transfer.	106
Table I.12. Detection limit of electrochemical DNA-biosensors based on conducting polymers.....	108
Table I.13. Detection limit of electrochemical DNA-biosensors based on faradic resistance increase.	110

I.1. Cancer

Currently, noncommunicable diseases (NCDs) are the leading cause of death worldwide. According to the estimates from the World Health Organization (WHO) in 2018, Among them, the number of deaths caused by cancer is the second in the world (22% of the total deaths) (Figure I.1), and cancer will become the main cause of death around the world in the 21st century and the most important obstacle to extending life [1, 2].

The *National Cancer Institute (NCI)* definition of cancer is a term for diseases in which abnormal cells divide without control and can invade nearby tissues [3]. It is caused by a mutation or genetic instability in the original normal cell. Most cancers take several years to form and can appear at any age.

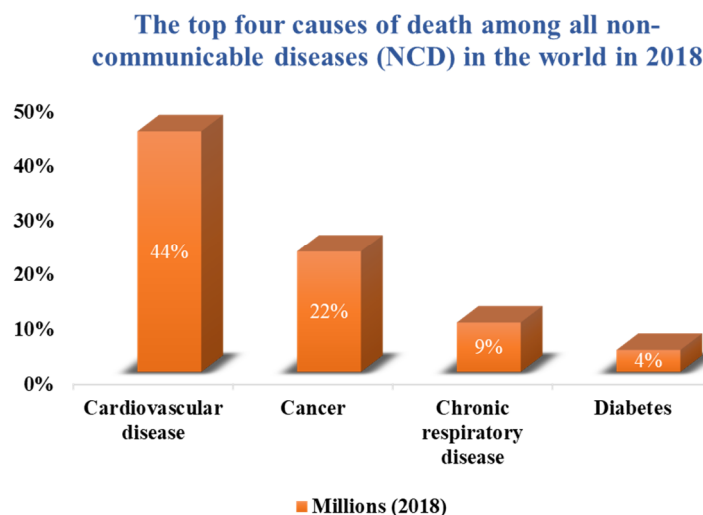


Figure I.1. The top four cause of death among all non-communicable diseases (NCD) by world area in 2018 [2].

GLOBCAN estimates 18.1 million new cancer cases and 9.6 million cancer deaths in 2018 by analyzing 185 countries and 36 types of cancer by age and sex (Figure I.2), lung cancer is the most commonly diagnosed cancer (11.6% of the total cases) and the main cause of cancer death (18.4% of the total cancer deaths) (Figure I.2a). Liver cancer is also one of the cancers with higher cancer mortality (8.2% of the total cancer deaths) (Figure I.2b).

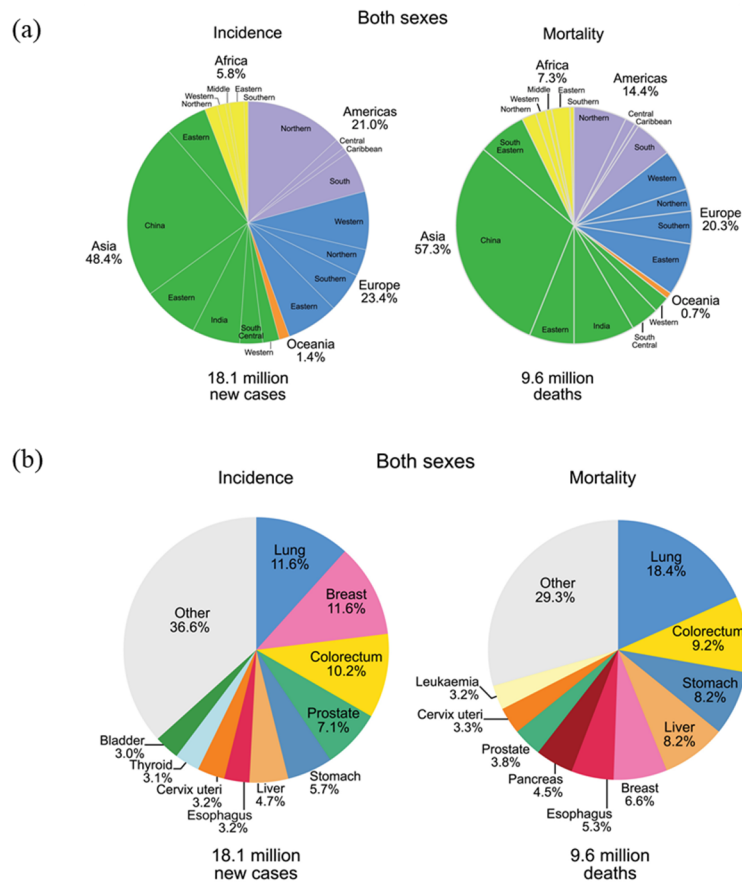


Figure I.2. Distribution of cases and deaths by world area (a) and 10 most common cancers (b) in 2018 [1].

Cancer is a frightening disease and survival rates tend to be poor. Over the years, more and more research in cancer field due to the high and rising mortality rate worldwide. Although it differs depending on the type of cancer and where it occurs, cancer can be cured if it intervenes correctly at the right time. The high mortality rate of cancer is probably due to a late stage diagnosis and limited access to timely standard treatment. Cancer cells can invade surrounding tissue or leave the original tumor and migrate to other areas of the body (metastasis). Thus, it is important to detect cancer early to avoid this migration. The early and accurate detection of cancer is highly important for clinical diagnosis, effective toxicity monitoring, and ultimately for the successful treatment of cancers.

Biomarkers that can predict cancer at an early stage have been discovered. The detection of biomarkers has formed an independent research field.

I.2. Biomarkers

Currently, there are many definitions of biomarkers. The *International Union of Physical and Applied Chemistry (IUPAC) Gold book* definition of a biomarker is [4-6]:

« *A parameter that can be used to identify a toxic effect in an individual organism and can be used in extrapolation between species, or as an indicator signaling an event or condition in a biological system or sample and giving a measure of exposure, effect, or susceptibility.* »

World Health Organization (WHO) has definition the term “biomarker” is [7, 8]:

« *Any measurement reflecting an interaction between a biological system and an environmental agent, which may be chemical, physical or biological.* »

The *National Cancer Institute (NCI)* definition of biomarker is [3]:

« *A biological molecule found in blood, other body fluids, or tissues that is a sign of a normal or abnormal process, or of a condition or disease. It also called molecular marker and signature molecule and may be used to see how well the body responds to a treatment for a disease or condition, such as cancer.* »

Biomarkers can be used in research and diagnosis, to screen the type of disease, estimate the risk of disease, monitor the disease stage and the progression of therapy to evaluate the safety and effectiveness of new drugs or new therapies. Some biomarkers only represent one specific disease. Biomarkers can be cells, molecules, they may be classified into three types, according to the application [9-11]: predictive, prognostic and diagnostic:

Predictive Biomarkers are usually measured before treatment and can indicate the possible effects of specific therapies on patients and guide treatment decisions [12, 13];

Prognostic Biomarkers inform doctors about the risks of clinical outcomes, such as disease recurrence or progression [14, 15];

Diagnostic Biomarkers are used to identify particular diseases or condition of interest or to

identify individuals with a subtype of the disease [14, 16, 17].

Another classification of biomarkers is based on the structure which can be cellular or molecular (Figure I.3), such as proteins (e.g., an enzyme or receptor), nucleic acids (e.g., a DNA, mRNA, microRNA or other non-coding RNA), antibodies, peptides and metabolites.

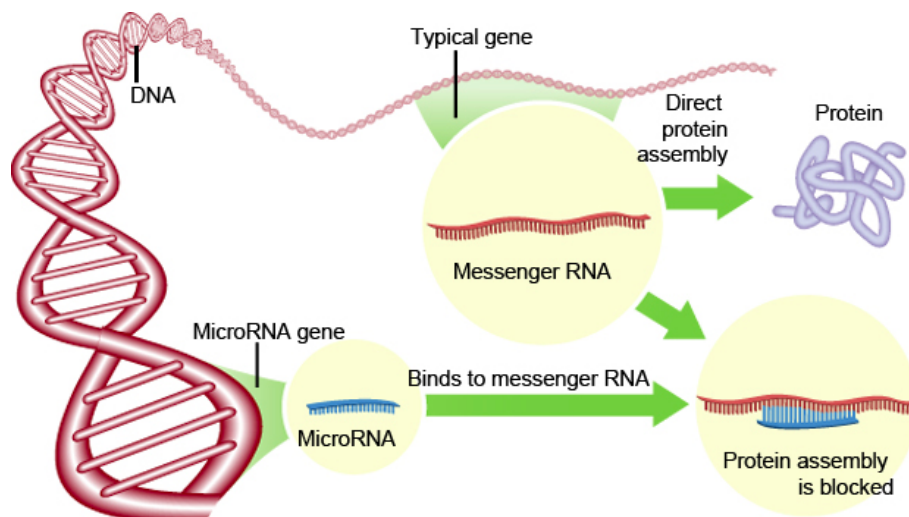


Figure I.3. The three major nucleic acid biomarkers: DeoxyriboNucleic Acid (DNA), messenger RiboNucleic Acid (mRNA), and micro RiboNucleic Acid (miRNA) [18].

I.2.1. DeoxyriboNucleic Acid biomarkers (DNA)

In 1953, *James Watson, Francis Crick, Maurice Wilkins and Rosalind Franklin* discovered the mystery of the DNA double helix structure [19, 20]. Nucleic acid biomarkers have many clinical applications due to the rapid development of nucleic acid sequencing in the past decade. The main nucleic acid biomarkers are circulating DNA, mRNA, and miRNA. During tumor development, their levels increase due to release by both cancer cell death and secretion [21-23]. In addition, the levels of circulating viral nucleic acids have also increased in certain cancer patients. Some circulating nucleic acid concentrations of healthy people and patients differ greatly, which the concentration of the tumor-related circulating nucleic acid biomarkers are generally associated with the tumor burden and the progression of the disease [24, 25]. Moreover, the circulating DNA biomarkers are stable in body fluids (blood, urine, saliva) and can be used directly to monitor disease progression without processing tumor tissue biopsy

[24]. Cell-free nucleic acids (cfDNA) were first discovered by *Mandel and Métais* in the form of DNA fragments in the non-cellular part of blood in 1948 [26]. In addition to blood, cfDNA is also found in urine, saliva and other body fluids in subsequent studies. The cfDNA can be released through a combination of apoptosis, necrosis and secretion of both normal and tumor cells (Figure I.4).

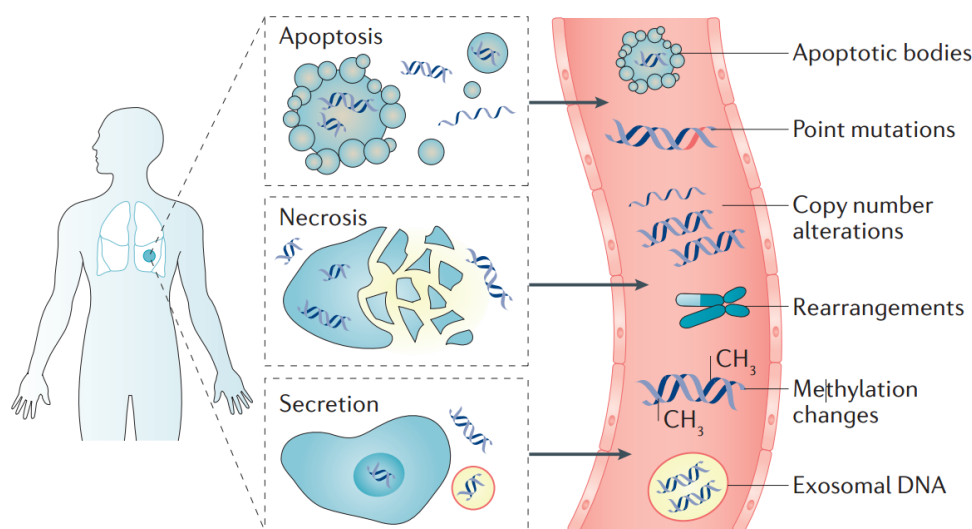


Figure I.4. Origins and range of alterations in cell-free DNA. DNA from cells are released through a combination of apoptosis, necrosis and secretion. In the bloodstream, cfDNA may exist as either free or associated with extracellular vesicles such as exosomes [27].

cfDNA from tumor cells are often called circulating tumor DNA (ctDNA). Cancer patients have increased levels of cfDNA compared to unaffected patients. In cancer patients, the proportion of ctDNA as a component of the overall cfDNA varies greatly, from less than 0.1% to more than 90% [28, 29], Table I.1 shows the cfDNA and associated with different tumour types. Genetic modifications of cfDNA molecules reflect the genome of the cell of origin [30-32]. The nature of ctDNA is related to tumor, the quantification of information related to tumor burden on ctDNA allow to evaluated disease nature and stage. For example, the detection of mutant K-ras gene sequences in plasma is a potential prognostic factor in colorectal or pancreatic cancer [33].

Table I.1. Detection of cfDNA with different tumour types.

Cancer	cfDNA	Gene	Ref.
Pancreatic	Mutation	K-ras/ KRAS2	[34]
	Microsatellite	486/273/2952	[35]
	Methylation		[36]
Colorectal	Mutation	K-ras/p53/APC	[37]
	Microsatellite	311/852/1085	[38]
	Methylation	hMLH1/p16INK4a/DAPK	[33, 39]
Hepatocellular Carcinoma	Mutation	p53/exon7/ser-249	[40]
	Microsatellite	74 markers from 17 chromosomal arms	[41]
	Methylation	P15/P16INK4a	[42]
	Viral DNA		[43]
Breast	Mutation	P53 exons 5-8	[44]
	Microsatellite	DM-1/D17S1325	[45]
	Methylation	APC/RASSF1A/DAP-kinase	[46]
	Mitochondrial		[47]
Lung	Mutation	p53 exons/K-ras	[48]
	Microsatellite	GPX1/D3S1259/D13S227/p53	[49]
	Methylation	p16INK4a/RASSF1A/DAPKinase	[50]

I.2.2. Messenger RiboNucleic Acids biomarkers (mRNA)

In 1961, *François Jacob* and *Jacques Monod* discovered the mRNA role in protein synthesis [51, 52]. This role was confirmed by the experiment of Brenner, Jacob and Meselson [53]. Messenger RNA (mRNA) is a type of single-stranded RNA, it transmits a sequence of genomic DNA to the ribosome for protein synthesis. Dysregulation of this process is associated with the development and progression of cancers [54]. Many tumor-associated mRNA species were found in plasma and serum: Table I.2 list mRNA-associated with cancer specimens. With the discovery of more and more mRNAs associated with different tumor, the presence of tumor mRNA in plasma and serum affords the opportunity to diagnose or stratify patients with cancer when tissue is not readily available [55].

Table I.2. Examples of mRNA-associated with cancer specimens.

mRNA Genes	Selected Cancers
REF/Aly	Dysregulated in colon, stomach, pancreas, testis cancers, and others.
THO	Dysregulated in ovarian, testis, skin, breast, nonsmall cell lung cancers, and others.
CRM1	Overexpressed in cervical, glioma, ovarian, pancreatic cancers, and others.
Nup88	Overexpressed in breast, colorectal, ovarian, hepatocellular cancers, and others.
Nup214	Chromosomal translocation resulting in acute myeloid leukemia and acute nonlymphocytic leukemia.
GANP	Overexpressed in lymphoma.
eIF4E	Overexpressed in acute myeloid leukemia, lymphoma, breast cancer, and others.
CNE-2	Nasopharyngeal carcinoma.
A375	Malignant melanoma.

Cancers listed for each factor above are examples and do not represent a complete list [56].

I.2.3. MicroRNA biomarkers (miRNA or miR)

MiRNA are small RNA ~20-base length. Lee *et al.* first discovered in 1993 the miRNA gene lin-4 in a transparent circle worm specie (*Caenorhabditis Elegans*). About 1900 miRNAs have been reported in humans since this discover [57]. miRNAs regulate gene expression at the post-transcriptional level by silencing target transcripts through base-pair complementation with mRNA (Figure I.5). miRNAs are regulator of various biological processes including development, cell differentiation, regulation of cell cycle and apoptosis. They were found in almost all organ and various body fluids including blood, urine, and saliva. More and more evidences show that miRNAs are becoming ideal candidates as non-invasive diagnostic and prognostic biomarkers in clinical applications.

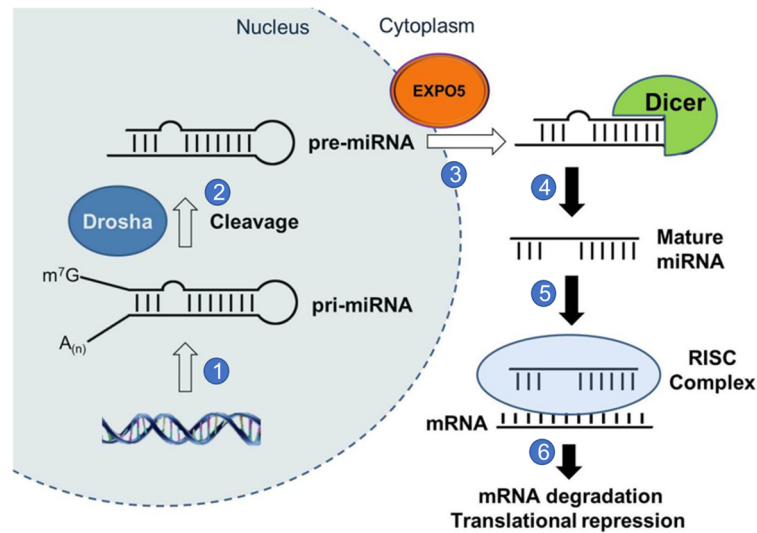


Figure I.5. The biogenesis of microRNAs processing [58].

The bioforming of miRNAs processing goes through several steps, as shown in Figure I.5, which contains:

- i).** miRNAs are initially transcribed as primary-miRNA (pri-miRNA) with stem-loop structure by RNA polymerase II [59].
- ii).** Following, pri-miRNA is cleaved in nucleus by RNase III enzyme, yielding to precursor miRNA (pre-miRNA) [60, 61].
- iii).** After nuclear processing, the pre-miRNA is then exported into the cytoplasm from nucleus by exportin 5 (EXPO5) [62-64].
- iv).** In cytoplasm, the RNase III enzyme Dicer complex cleaves the pre-miRNA to its mature length double strand RNA duplex by removing the stem-loop structure.
- v).** The single-strand mature miRNA forms a complex with a protein call RNA-Induced Silencing Complex (RISC).
- vi).** The complex of miRNA with the RISC binds to target mRNA to repress their translation or induce their degradation. The complex of miRNA with the RISC can pair with mRNA to regulate gene expression and a variety of other biological processes.

Table I.3. Examples of tumor-suppressor miRNAs [65].

MicroRNA	Cancer type	Function
miR-29b	AML	Represses Sp1 which resulted in c-KIT inhibition.
miR-34b/c	Lung cancer	A positive feedback between p53 and miR-34 mediates tumor suppression in human lung cancer.
miR-126	Breast, lung, and colon cancers	Plays a critical tumor-suppressor role in tumor initiation and metastasis.
miR-150	AML	A critical tumor-suppressor gatekeeper in AML by targeting FLT3 and Myb.
miR-15	Breast cancer	Downregulates RAD51 and sensitize cancer cells to irradiation.
miR-181a/b	AML	Their increased expression is associated with good prognosis and hinders tumor cell growth.
miR-375	Breast cancer	Forced expression re-sensitizes cells to tamoxifen treatment.
miR-494	Lung cancer	Regulated by ERK1/2 it modulates proliferation and apoptosis response.
miR-495	AML; gastric cancer	Specifically down-regulated in MLL-rearranged AML; Shown to block migration and invasion
miR-551a	Gastric cancer	Forced expression leads to a block in migration and invasion

AML, Acute Myeloid Leukemia

Table I.4. Examples of oncogenic miRNAs [65].

MicroRNA	Cancer type	Function
miR-9	AML	Specifically overexpressed in MLL-rearranged AML and promotes leukemia progression.
miR-17-92	AML	Up-regulated in MLL-rearranged AML and targets p21 and RASSF2.
miR-21	Breast cancer	Overexpression of miR-21 contributes to proliferation and metastasis.
miR-27a	NSCLC	Promotes proliferation in NSCLC cells.
miR-30a/c	RCC	Downregulation leads to increased expression of HIF2a.
miR-126	AML	Up-regulated in core-binding factor (CBF) leukemia.
miR-181a/b	Breast, liver and colon cancers	Promote tumorigenesis and tumor progression.
miR-196a	Gastric cancer	Promoted EMT, migration and invasion.
miR-196b	AML	Upregulated in MLL-rearranged AML and targets Fas.
miR-421	Gastric cancer	Marker of circulating tumor cells.

AML, Acute Myeloid Leukemia; NSCLC, Non-Small Cell Lung Cancer; RCC, Renal Cell Carcinomas.

Conclusion

Nucleic acid are biomarkers of various diseases that and can reflect the real-time status of cells. Compared with DNA biomarkers, RNA biomarkers regulate gene expression at the transcription and post-transcription levels, which can more dynamically reflect the state of the cell and the regulatory process. Moreover, compared with mRNAs, miRNAs are more sensitive, more stable, and more specific. The Table I.5 shows the comparison of DNA, mRNA and miRNA.

Table I.5. Comparison of different types of biomarkers.

	DNA	mRNA	miRNA
Biological function	Genetic information carrier	Transmit genetic information	Regulatory factor: regulate gene expression
Content / Human cell	~ 6 pg	0.5~1.5 pg/10 ⁵ molecules	-
Content / Plasma (1mL)	1 ~ 1000 ng	1 ~ 1000 ng	-
Biological stability	Stable in the alkaline solution	Easy degradation	More stable than mRNA
A feature used as a biomarker	Mutation, epigenetic modification	Expression profiles	Expression profiles
Examples	Mutation: P53 exons 5-8 (Breast)	eIF4E (Breast)	miR-375 (Breast)

I.2.3.1. MicroRNA-21

MicroRNA-21, also known as hsa-mir-21, miRNA-21 or ,miR-21 is one of the first miRNAs discovered, located on the chromosomal positive strand 17q23.2 (Figure I.6 a and b). The miRNA-21 sequence is UAG CUU AUC AGA CUG AUG UUG A (Figure I.6c), it plays an important role in a variety of biological functions and diseases, including development, cancer, cardiovascular disease and inflammation. In the study of cancer, it found that miR-21 is of oncogenic nature, it is overexpressed in most cancer types, such as liver, lung, breast, stomach, prostate, colon and pancreas ones. Additionally, it was found that miR-21 is also overexpressed in biological fluids (blood, tear, urine), which makes it a very promising biomarker and allows noninvasive and early cancer diagnosis, and therefore can improve the cure rate of cancer.

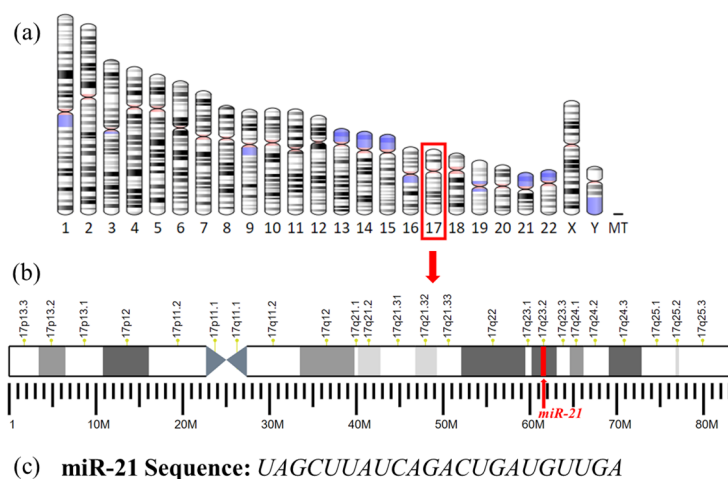


Figure I.6. The miR-21 location of (a) gene location, (b) Chromosome 17 and (c) the sequence. The human microRNA-21 gene is located on plus strand of chromosome 17q23.2 [66].

miRNA are excellent biomarkers that can predict different cancers through its quantitative detection in the early stages of cancer, but their concentration in biological fluids is between 10^{-12} and 10^{-17} M and it is a real challenge to quantify them without previous amplification. At present, in order to improve the sensitivity and detection ability of miRNA quantification method, which has developed into a research field. There are contain RT-qPCR and different types of biosensor (optic, mass and electrochemical).

I.3. Biomarker Quantification techniques

I.3.1. Nucleic acid amplification

I.3.1.1. Polymerase Chain Reaction (PCR)

Polymerase Chain Reaction (PCR) is a molecular biology technique widely used to amplify specific DNA segment, it can quickly and specifically exponentially amplify any target DNA of small amount in vitro (Figure I.7), thus, widely used in biomedical science, criminal forensics, archeological fields and many other aspects. In 1971, Khorana first proposed the concept of nucleic acid amplification in vitro, however, it didn't receive much attention and it couldn't be verified by experiments at that time due to the immature methods of gene sequence analysis

and the thermostable DNA polymerase have not yet been discovered [67]. In 1983, Kary Mullis came up with the PCR principle again, developed the PCR technique to practice [68-70] and patented in 1985, he was awarded the Nobel Prize in Chemistry in 1993 for this invention.

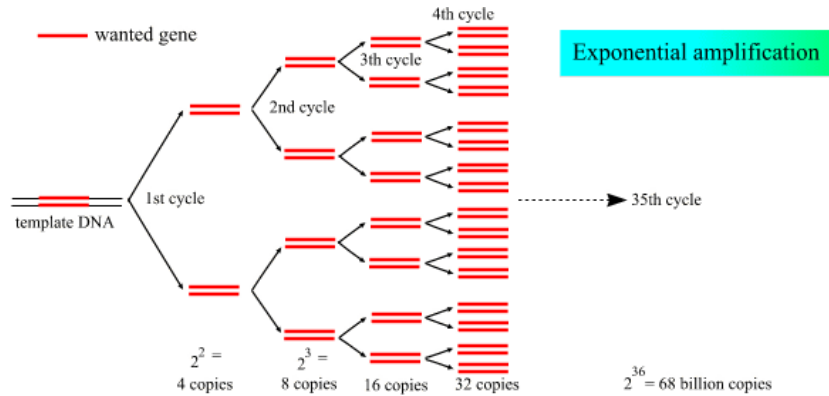


Figure I.7. The exponential amplification of the gene in PCR [71].

1). PCR principle

PCR is based on using the ability of DNA polymerase in a specific buffer condition that contains specific primers, nucleotides to synthesize new strand of complementary DNA based on the offered template strand, then through more cycles to cloned and amplify DNA template to billions of copies in just a few hours.

2). PCR components

Five components are required to set up PCR: DNA template, DNA polymerase, Primer, nucleotides and buffer.

a). DNA template: The sample DNA is usually a double-stranded DNA that contains the target sequence.

b). DNA Polymerase: A type of enzyme that synthesizes new strands of DNA complementary to the target sequence. The most commonly used enzyme is Taq DNA polymerase, it purified or cloned from *Thermis aquaticus* which lives in hot springs and resists temperatures above 100 °C [72].

c). Primer: To achieve amplification of nucleotide sequences, it is necessary to add primers which complement with the 3' ends of the target sequence. Primers are short stretches of single stranded DNAs which often contain only 10-30 bases in size. Due to DNA polymerase only can add nucleotide onto a preexisting 3'-OH group, thus it needs a primer to provide the first nucleotide before amplification.

d). Nucleotides: The four deoxyribonucleoside triphosphates A, T, G, and C (dATP, dTTP, dGTP, dCTP) are the necessary components to construct the new strand of DNA and which provide the energy for polymerization and the building blocks for DNA synthesis.

e). Buffer system: Includes magnesium and potassium to provide the optimal conditions for DNA denaturation and renaturation, also important for polymerase activity, stability and fidelity.

3). PCR procedures

PCR technique procedure is a thermal cycling that involves series of heating and cooling process. It refers to use DNA as a template with specific primers as the extension starting point, and then replicating the template in vitro through denaturation, annealing and extension steps, that carried out automatically by the DNA thermocycler machine and repeated for 30 or 40 cycles to get a huge number of gene sample copies.

The three major PCR stages (Figure I.8):

a). Denaturation (94-96 °C):

The denaturation step is to separate double-stranded DNA into two single strands which works as template of PCR. When the double-stranded DNA is heated to 94-96 °C, the hydrogen bonds of double-stranded DNA helix will be broken to form single stranded DNA, which used as PCR template.

b). Annealing (50-70 °C):

During the annealing, the mixture reagents are cooled to 50-70 °C, so that the DNA primers enable to complementary bind to the part of template DNA. If the reaction reagents only contain one kind of primer, there is only one kind of template strand is copied.

c). Extension (Elongation, 72 °C):

After the temperature raise to 72 °C that is the ideal temperature for the polymerase, then polymerase extends the primers to complementary sequence through adding nucleotides according to the target DNA template.

During one cycle of PCR, both single strands are copied, then one double-stranded DNA template is amplified into two separate double-stranded DNA. These two double-stranded DNA are available for further amplification in the next cycle. As the PCR cycles are repeated, more and more DNA copies are generated which is exponential increase.

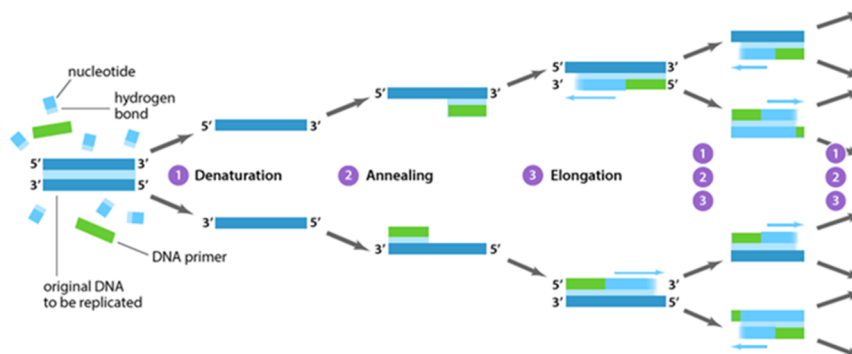


Figure I.8. The schematic diagram of polymerase chain reaction (PCR).

I.3.1.2. Quantitative Polymerase Chain Reaction (qPCR)**1). Endpoint Polymerase chain reaction (Endpoint PCR)**

After PCR experiment process, the PCR product must be detected and analyzed to determine whether the PCR was successful and then used for other applications. Endpoint PCR is one of DNA qualitative and semi-quantitative method through gel electrophoresis.

Gel electrophoresis is widely used to identify and analyze DNA fragment through separating DNA by size (e.g., length in base pairs) to achieve qualitative and semi-quantitative detection. The oligo sample will be loaded into wells of the gel, and apply a current to the gel, the DNA (and RNA) molecule have the negative charge because of the phosphate groups of phosphate backbone, therefore when placed in an electric field, DNA fragments will migrate to the positive electrode. Which the shorter DNA fragments migrate faster than longer ones. Then, the approximate length of unknown samples can be identified through comparing with DNA ladder (a collection of DNA fragments of known lengths).

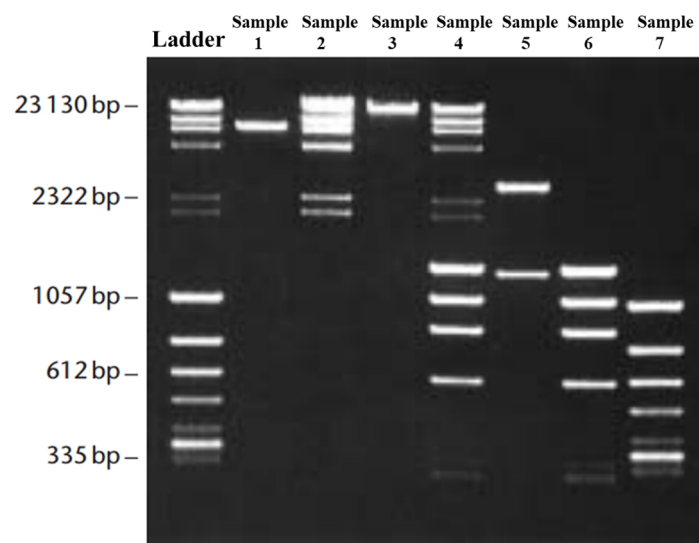


Figure I.9. Separation result of agarose gel electrophoresis, DNA fragments are detected with ethidium bromide [73].

The Figure I.9 shows lanes of agarose gel that detected with ethidium bromide, the first right lane is the DNA ladder, it is a DNA size standard reference that contains DNA fragments of known lengths and the other lanes added different DNA samples [73]. The DNA standard and DNA samples start migrating through the gel to the positive electrode, when the current is loaded on the gel. The shorter base DNA will pass through the gel holes faster than the longer ones, such the DNA samples will be separated and the shorter the DNA fragments are closer to the positive electrode of the gel and the longer DNA fragments are closer to the well. After the DNA sample fragments have been separated, the DNA fragments will glow when the gel is

stained with the DNA-binding dye and placed under UV light. In the Figure I.9, each individual band contains a large number of same size DNA fragments and the brighter the band, the more DNA fragments there are. In addition, the approximate size of DNA sample fragments can be determined based on comparing the DNA sample bands with the DNA ladder.

The gel electrophoresis can only determine the approximate amount and size of the DNA sample simply based on the distance and brightness of the DNA band on the gel, so the sensitivity is limited. More importantly, gel electrophoresis is performed at the end of PCR, when DNA fragment amplification has reached the plateau phase (Figure I.10). In the plateau phase, the amplification product no longer increases exponentially, so there is no linear relationship between the end product and input template, and the initial DNA copy number cannot be calculated through the amplification end product. So, in order to semi-quantifying gene expression by endpoint PCR before reaching a plateau, the expressed gene can be estimated by using diluted DNA samples as inputs, or collecting the amplicons at specific PCR cycles for estimating the expressed genes via gel band intensity.

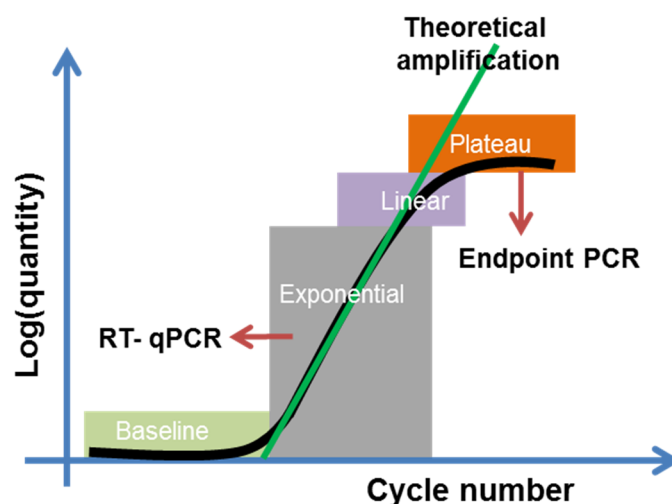


Figure I.10. Amplification curve or reaction dynamic of PCR. In endpoint PCR, detection of amplicons occurs in the plateau phase. In real-time qPCR, quantitation of amplicons occurs during the exponential phase.

2). Real-time quantitative Polymerase chain reaction

Real-time quantitative Polymerase chain reaction is known as the qPCR or RT-PCR, which is reported by Higuchi et al in 1993 [74]. qPCR is able to real-time monitor the progression of the PCR amplification by fluorescent signal, when the amplification is occurring, the kinetics of fluorescence accumulation during the thermal cycle is directly related to the starting number of DNA copies. Since the 1997, the first qPCR instrument came to the market, the accurate and fast quantification of gene expression and copy number is realized.

In the process of qPCR, fluorescence signals are collected once per cycle, then the curve with the fluorescence intensity as the Y-axis and the number of cycles as the X-axis is called the PCR amplification curve (Figure I.10). In the beginning few cycles, although the target product increased exponentially, the total fluorescence intensity can't reach the detection limit of the instrument, so the fluorescence intensity detected by the instrument did not change. The average value of the fluorescence intensity in this period is called the baseline. When the fluorescence signal reaches a certain intensity, the increase in fluorescence intensity can be truthfully measured by the instrument and the minimum fluorescence intensity that can be measured by the instrument is called the fluorescence threshold. However, in practice the fluorescence threshold can be artificially set, which usually take the mean fluorescence intensity from 3rd to 15th cycle and plus 10 times of standard deviation or the highest fluorescence value of negative control. It always is set in the exponential phase of the PCR amplification curve.

During the PCR amplification, the number of amplification cycles that occur when the fluorescence signal of the amplification product reaches the set threshold is called the cycle threshold (C_t). The C_t value is related to the number of templates in the reaction tube (copy number) and has a linear relationship with the logarithm of the starting copy number of the template. Which the more start copies, the smaller the C_t value.

Currently, there are mainly five different kinds of fluorescent probes for qPCR detection:

SYBR Green, TaqMan, Molecular Beacons, hybridization probe and Scorpions (Figure I.11). SYBR Green dye is a non-sequence-specific detection method though binding to the minor groove of the DNA double helix. The other three fluorescent probes are sequence-specific probe which generates fluorescence depend on Förster Resonance Energy Transfer (FRET) coupling of the dye molecule and a quencher moiety. Among of them, the most common real-time fluorescence quantification PCR is SYBR Green method and TagMan probe method [75].

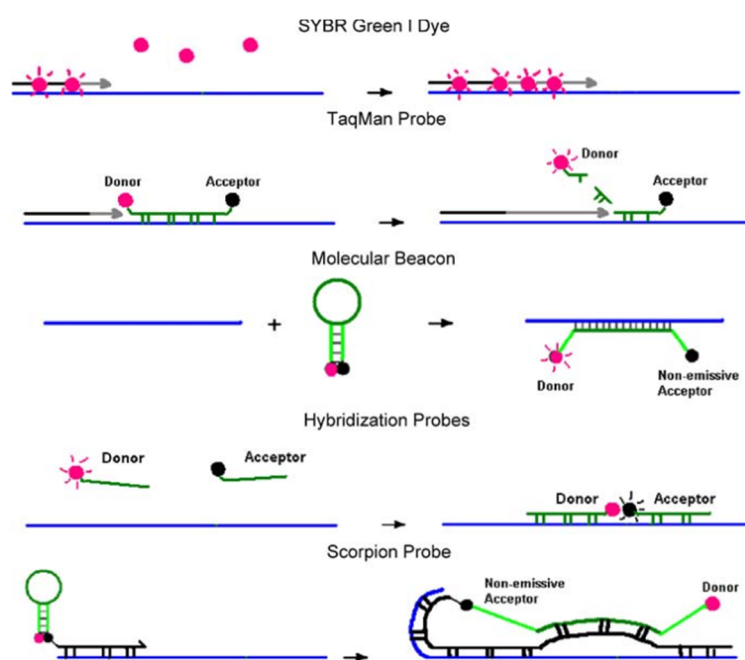


Figure I.11. Depictions of the more commonly used types of fluorescent detection probes used in quantitative real-time PCR [75].

a). SYBR Green method

SYBR Green method is a non-specific double stranded DNA binding dye with a green excitation wavelength, with a maximum absorption wavelength of about 497 nm and a maximum emission wavelength of about 520 nm. It can be combined with all dsDNA double helix grooves. SYBR Green emits weak fluorescence when it is free, until it binds to double-stranded DNA, the fluorescence will be greatly enhanced, and the increase in the fluorescence signal will be completely synchronized with the increase of the PCR product. The advantage

of this method is that the detection method is simple and low cost, it can monitor the amplification of any dsDNA sequence, due to the fluorescent dye can combine to any dsDNA, even the non-specific amplification products and primer dimers will cause false positive results, so the specificity is not as good as the probe method. Because the denaturation temperature of non-specific products and primer dimers is lower than the target product, the signals can be collected and identified by software analysis instruments during the dissociation curve reaction. If there is only a single peak in dissociation curve, it indicates that the specificity of the amplification product is good, while the presence of the heterozygous peak, the specificity of amplification is poor, and there is non-specific amplification, such as primer dimer, etc.

b). TaqMan probe method

TaqMan probe method is a highly specific quantitative PCR technique, it uses the TaqMan probe to hybridize with the target gene sequence in the amplification product to improve the specificity of the product detection. Even if there are non-specific amplified fragments in the amplification product, as long as it is not complementary to the probe, no fluorescence is generated. The TaqMan probe sequence is complementary to a part sequence of the target fragment, which the 5' end of the probe is labeled with fluorescence reporter group and the 3' end of the probe is labeled with the fluorescence quenching group. At this moment, the fluorescence energy of reporter group is quenched by quenching group, so the instrument can't pick up the fluorescence signal. During the PCR annealing step, both primers and probes can be bound to the target gene template. Next, in the elongation step, the primers extend and the Taq polymerase moves along the DNA template. When it moves to the TaqMan probe, which was hydrolyzed and the fluorescence reporter group was released by the 3', 5' circumscribed nuclease activity of Taq polymerase. Then quenching mechanism eliminated, the fluorescence reporter group produces the fluorescence signal.

According to the classification of quantitative method, qPCR can be divided into two categories: absolute quantification and relative quantification. Absolute quantification usually determines the

copy number of interest genes by using a calibration curve with known concentrations (Figure I.12) [76]. Relative quantification refers to the variation of target sequence relative to another reference sequence in a given sample.

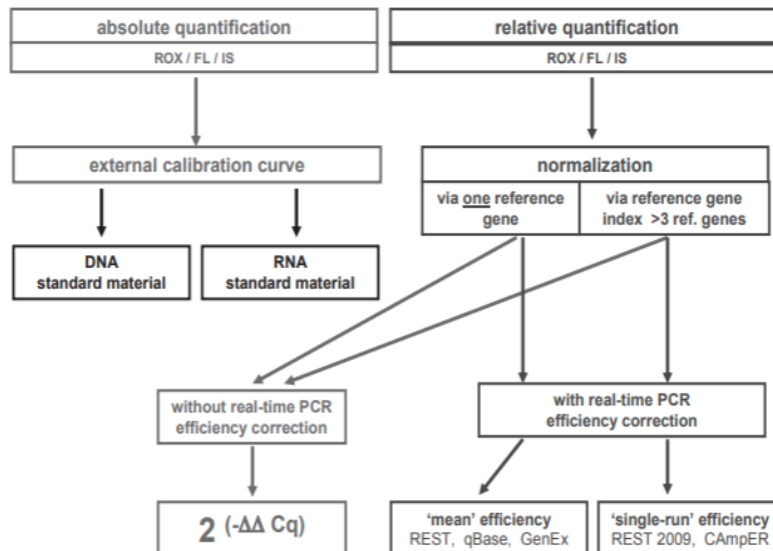


Figure I.12. Quantification strategies in real-time quantitative PCR: absolute quantification and relative quantification [76].

PCR amplification efficiency

PCR amplification efficiency (E) plays an important role both in absolute and relative quantification, it should be the first things to be done when running the qPCR assay. One way of determining the amplification efficiency is by calibration curve that plot by the C_T values of serial 10-fold dilutions of the target along with corresponding concentrations. It can easily and quickly provide repeatable PCR amplification efficiency [77]. The PCR amplification efficiency (E) calculated with the slope of the standard curve:

$$E = 10^{-1/slope} - 1$$

Theoretically, the PCR amplification efficiency should be 100% (the slope of calibration curve

is -3.3) during the exponential phase, it means that polymerase enzyme is working at maximum capacity and all the target sequence double during each replication cycle. However, in practice, the amplification efficiency is not equal to 100%, and when the efficiency is low than 100%, it is due to the presence of contaminants, for the degradation of nucleic acid [78]. In addition, the bad primer design and non-optimal reagent concentrations or reaction conditions also can lead to poor amplification efficiency. On the other side, the amplification efficiency may be over 100% because of polymerase activators, unspecific products and primer dimers, the inhibition of reverse transcriptase and the errors of pipetting or diluting [79-81].

Typically, the desired amplification efficiencies of PCR should be range from 90% to 110% ($-3.6 \geq \text{slope} \geq -3.3$). There is a quantitative relationship between the starting target sequence and the PCR product at any given cycle:

$$x_n = x_o (1 + E)^n$$

Where x_n is the amount of target sequence at amplification cycle n , x_o is the initial amount of target, and E is the amplification efficiency. The E values are included between 0 (no amplification) and 1 (every amplicon is replicated during each cycle) [82].

c). Absolute quantification

Absolute quantification is a method of using a known standard curve to calculate the quantity of unknown samples. For the standard curve, a standard sample of known concentrations is diluted into a series of different gradient concentrations and carries out qPCR (Figure I.13a). Then, the logarithm of the standard concentrations is plotted on the X-axis, and the corresponding C_t value is measured as the Y-axis (Figure I.13b). The calculation of sample magnitude based on the C_t value and the equation of the calibration range, the formula is as follows [83]:

$$C_t = \text{slope} \times \log (\text{Concentration}) + \text{intercept}$$

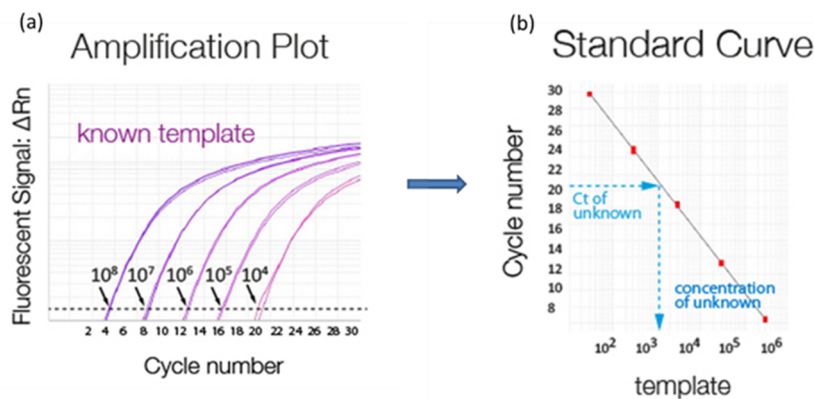


Figure I.13. Schematic of absolute quantification by qPCR, (a) Amplification plot of a serially diluted sample of known concentration used to generate a standard curve. (b) The standard curve is plotted by the known concentration sample.

d). Relative quantification

There are two kinds of relative quantification methods. One is by comparing standard curves, and the other is by comparing C_t value.

i). The standard curve comparison method:

It is a way based on the standard curve of the standard sample to analyze the variation of a target with the magnitude of another reference.

ii). The C_t value comparison method (the $2^{-\Delta\Delta C_t}$ method)

This method is presented the data of target sample gene relative to reference sample gene. It amplifies the target sample gene fragment and the reference sample gene fragment in two reaction tubes or one reaction tube at the same time, then calculate the relative amount of target and the reference sample based on the C_t . The premise of this method is that the amplification efficiency of target sample gene and reference sample gene are basically the same, the deviation of amplification efficiency will impact the actual quantity estimation, which is one of the difficulties in the application of this method.

The method was reported previously in Applied Biosystems User Bulletin No. 2 (P/N 4303859)

and ref. 15 [84-87]

$$\text{Fold change} = 2^{-\Delta\Delta C_t}$$

The first ΔC_t is the difference in C_t between the target gene and internal control:

$$\Delta C_t = C_t (\text{target gene}) - C_t (\text{internal control})$$

The $\Delta\Delta C_t$ is the difference in ΔC_t as described in the above formula between the target and reference samples. The target sample can be the treated sample or the diseased state sample and the reference sample corresponds to the untreated control or the normal state sample. The full form is:

$$\begin{aligned} \Delta\Delta C_t &= \Delta C_t (\text{target sample}) - \Delta C_t (\text{reference sample}) \\ &= [(C_t \text{ target gene} - C_t \text{ internal gene})_{\text{target sample}} - (C_t \text{ target gene} - C_t \text{ internal gene})_{\text{reference sample}}] \end{aligned}$$

I.3.1.3. Digital polymerase chain reaction (dPCR)

Digital PCR is an improvement biotechnological of conventional polymerase chain reaction methods, and it developed in parallel with real-time PCR in the 1990s [88]. It is the absolute quantitation method of DNA samples, a highly diluted target molecules are distributed into multiple isolated reaction chambers (liquid drop, multi-compartment chip). So that each reaction chamber contains one or more copies of the target molecules (positive) while others do not contain copies (negative), then record the fluorescence signal of each amplification cycle, the process is shown in the Figure I.14 [89]. The copy number of the target sample is determined from the fraction of negative reactions using a statistical model (Poisson distribution) without based on standard curve of the known samples and the reference sample

to carry out quantitation, which with the advantages of higher sensitivity and accuracy.

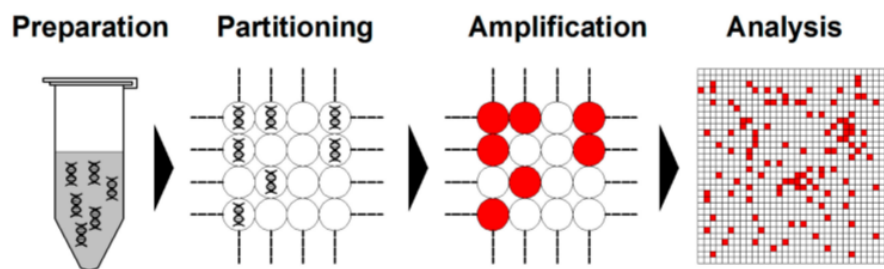


Figure I.14. Schemes of typical digital PCR (dPCR) workflow. Generally, dPCR is conducted following the steps of preparation, partitioning, amplification, and analysis [89].

I.3.1.4. qPCR detection of different targets

1). Genomic DNA

qPCR is the classical gold standard nucleic acid quantification method, which contains the basic processes of PCR (*see the section of I.3.1.1*) and real-time PCR (*see the section of I.3.1*). It is simpler than the qPCR of RNA because RNA requires a reverse transcription step at the initial stage, which is reverse transcribed into cDNA as a template for the subsequent qPCR processes.

2). Messenger RNA (mRNA)

Reverse transcription polymerase chain reaction (RT-PCR) is a universal technique for detecting coding RNAs (mRNA) and non-coding RNAs (microRNA). Before PCR, RNA must be transcribed into complementary DNA (cDNA) by an RNA-dependent DNA polymerase and used as a template for PCR amplification. This additional step results in a much more fragile and variable assay, moreover, the different types RNA structures have different reverse transcription procedure [90-92]. For the quantification of RNA, the reverse transcription step incorporates real-time PCR (RT-qPCR), then recording the fluorescence in each PCR cycle and monitoring the production of amplification products. Figure I.15 shows the RT-qPCR steps of

mRNA. With the advent of RT-qPCR technique, the sensitivity of mRNA detection has increased by several orders of magnitude, making the analysis of some extremely small amount of RNA samples possible.

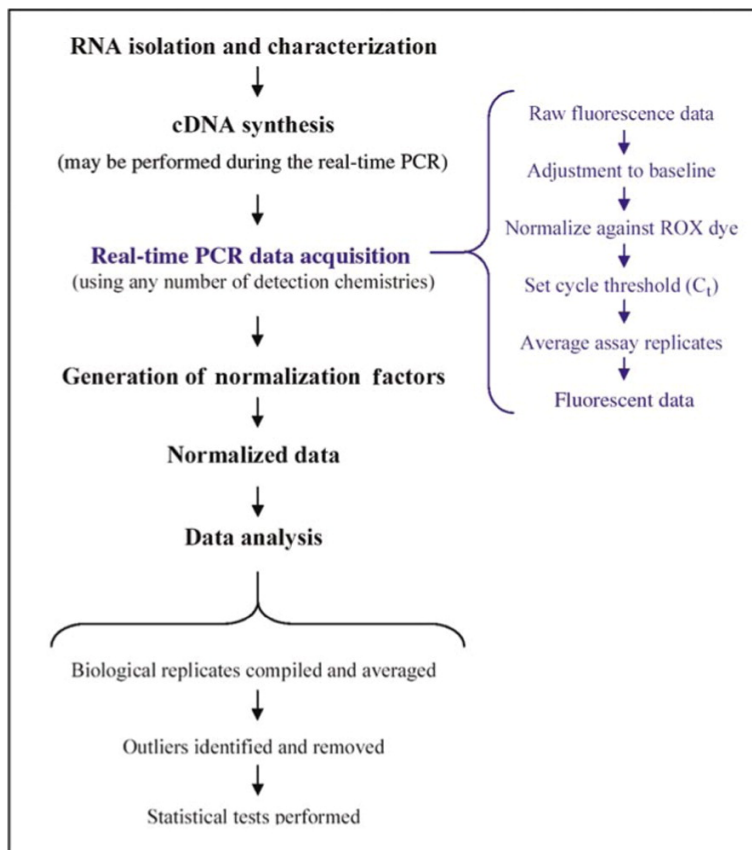


Figure I.15. Steps of mRNA real-time reverse transcription PCR [93].

For mRNA quantification, there are one-step and two-step RT-qPCR method.

a). One-Step RT-PCR

One-step RT-PCR, both the reverse transcription of mRNA and PCR are performed in the same single tube (Figure I.16), which contains mRNA templates and one-step RT-PCR kit containing designed primers. The kit is sufficient for the whole reaction and without adding additional reagents, it benefits to minimize the pipetting error and cross-contamination that affect the amplification efficiency of PCR. However, it contains some limitations, since the reverse

transcription and PCR step occur in the same tube, this prevents to optimized each individual reaction step and lead to low yield or efficiency in either step. Another one is that all the cDNA get from reverse transcription reaction is used up in subsequent PCR step, and cannot be used for further verification or experiments.

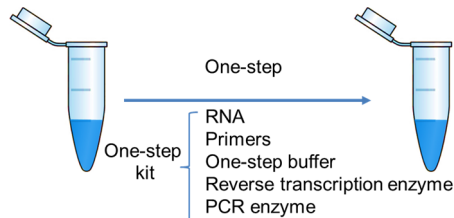


Figure I.16. One-Step RNA real-time reverse transcription PCR.

b). Two-Step RT-PCR

In the two-step RT-PCR, the reverse transcription reaction is separated from the PCR assay which occur in different reaction tubes (Figure I.17). First, RNA templates are reverse transcribed to cDNA, then the cDNA is diluted and transferred into a new reaction tube which contains PCR reagents to perform PCR. Two-step RT-PCR allows the reverse transcription reaction and PCR step to be optimized separately, so the two-step reaction can be more sensitive than one-step reaction.

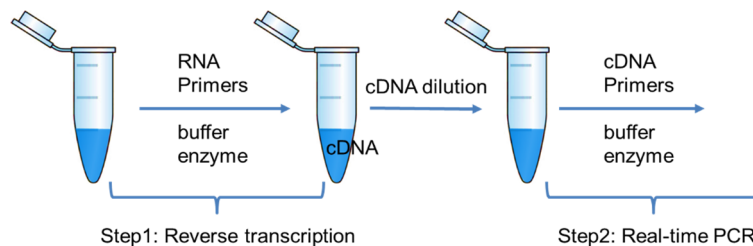


Figure I.17. Two-Step real-time reverse transcription PCR.

Since two-step RT-PCR involves transferring and diluting of cDNA, this is the source of errors and high contamination. Thus, the pipetting and diluting operation during the procedure must be carried out carefully to maximize the accuracy and reliability.

3). microRNA

Due to the microRNA precursor is a stable hairpin structure, and the mature miRNA is short (the average length is about 22nt), close to the standard PCR primers, so miRNAs are difficult to be detected by traditional RT-PCR. Therefore, a PCR method (TaqMan MicroRNA assays) suitable for miRNA was developed through extending the short mature miRNA. The TaqMan microRNA assay is similar to traditional TaqMan RT-PCR, there are two major approaches based on different extension ways of mature microRNA on the reverse transcription step. One is using the extended RT primer (Linear and stem-loop RT primer), the other is poly(A)-tailed RT-PCR method.

a). Approaches based on RT primers

The linear and stem-loop RT-PCR for mature microRNA assay are done both using two-step RT-PCR. During the RT step, the front portion of the primer can hybridize with the 3' end of miRNA template and then complete reverse transcription to cDNA with reverse transcriptase (Figure I.18). The two kinds of primers both obtain the extended sequence in the downstream of the cDNA, which through the stem-loop structure unfolds or directly obtains through linear primer during the annealing process. The extended cDNA provides the more suitable template for the followed step PCR. Next, the extended cDNA products are amplified and quantified using conventional TaqMan real-time PCR in the presence of the forward and reverse primer (Figure I.19) [94]. Finally, microRNA templates are analyzed based on the increasing fluorescence that comes from a dye-labeled TaqMan probes.



Figure I.18. Specificity of TaqMan miRNA assays between stem-loop and linear RT primers [94].

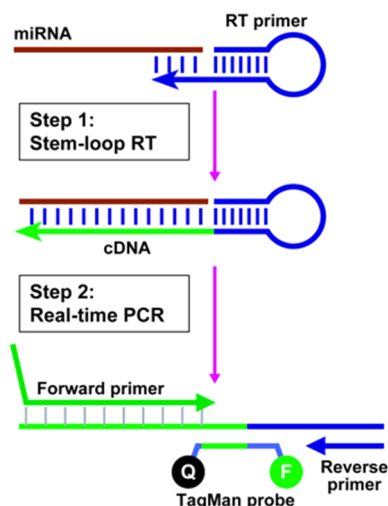


Figure I.19. Schematic description of TaqMan miRNA assays [94].

Caifu Chen et. observed the stem-loop PT-primer is specificity and sensitivity than the linear RT-primer, it is due to the base stacking of the stem enhances the stability of miRNA and DNA hetero-duplexes, improving the RT efficiency for relatively short RT primers [94, 95].

b). Approaches based on poly (A) polymerase

Han-Jiang Fu et al. established a simple method to amplify the mature miRNAs based on poly(A)-tailed RT-PCR called the TaqMan® advanced miRNA technique. First, microRNA template is extended by polyadenylating with poly(A) polymerase, and then cDNA was synthesized by a specific RT primer and reverse transcriptase using the poly(A)-tailed microRNA as templates [96-98]. On this basis, Kang Kang et al. optimized the primer structure of reverse transcription step that named S-Poly (T) primer. It consists of four segments (Figure I.20), from 5' to 3' direction is a universal reverse primer sequence, a universal TaqMan probe sequence and 17 dT bases complementary with tailed poly(A), followed by 5~7 specific bases that are complementary to the 3' end of a particular miRNA. This design greatly enhances the RT efficiency, and further improves the sensitivity and specificity in the miRNA assay, the limit of detection (LOD) for miR-21 can reach 0.1 pg of total RNA by using this method [99, 100].

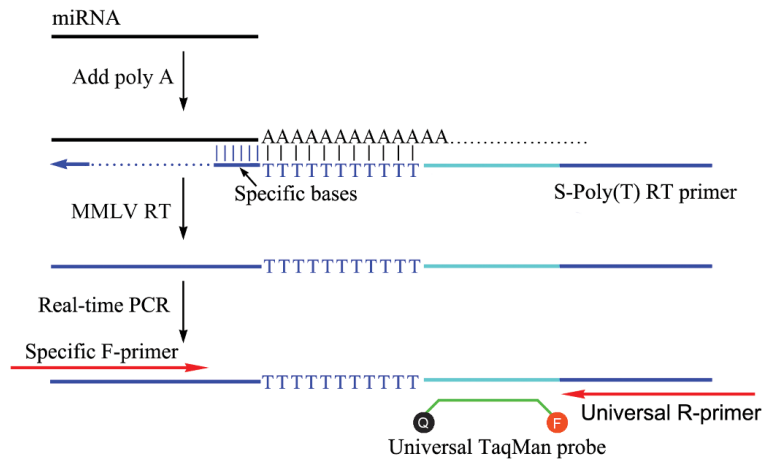


Figure I.20. Schematic representation of the S-Poly(T) Plus method for miRNA quantification [99].

I.3.2. Biosensors transduction techniques

The term “biosensor” is an abbreviation of “biological sensor”, Biosensors are defined by IUPAC as a device that uses specific biochemical reactions mediated by isolated enzymes, immunosystems, tissues, organelles or whole cells to detect chemical compounds usually by electrical, thermal or optical signals [101]. It can provide quantitative or semi-quantitative analysis information [102]. The basic device consisting of a biological recognition component (bioreceptor) which is made of immobilized biological sensitive materials as identification elements for the analyte of interest (enzymes, antibodies, antigens, microorganisms, cells, tissues, nucleic acids and other biologically active substances) [103], and a physicochemical detector (transducer) that can convert the biological response event from the interaction between bioreceptor and analyte into different measurable response signal, which are proportional to the concentration of target and finally displays the presence of the target. In other words, through a series of reactions, it can convert the analyte type, concentration and other properties into quantitative data that is easily accepted by people (Figure I.21). In addition, the signal can be further amplified by using nano materials, processed or stored for later analysis.

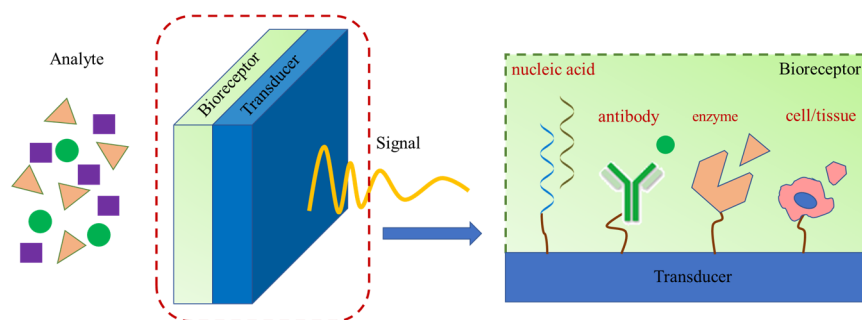


Figure I.21. General diagram of a biosensor.

There are various types of biosensors based on different classification methods. According to the bioreceptor, it can be divided into enzyme sensors, immunosensors, tissue sensors, microbial biosensors and nucleic acid biosensors etc. Here we focused on the nucleic acid biosensors that rely on nucleic acid hybridization.

The nucleic acid biosensors (DNA biosensor) are based on the properties of single-stranded nucleic acid molecule (probe), which is able to recognize the complementary nucleic acid strands by hybridization event [104]. DNA biosensors immobilized specific ssDNA sequences on the surface of solid supports and act as molecular recognition elements, then mainly use electrochemical, optical and piezoelectric sensors to measure their specific binding process with DNA targets [105].

I.3.2.1. Probe immobilization method

In order to construct a nucleic acid biosensor, the ssDNA probes were immobilized on the transducer component surface and act as bioreceptor component. Various immobilization strategies through physical, chemical or biological interaction have been developed to achieve 'greater sensitivity and selectivity.

1). Physical adsorption

The physical adsorption strategy of DNA probes is based on weak electrostatic or van der Waals interactions to immobilize the DNA probes on the substrate, which is the simplest method and

does not require any chemical modification for the DNA structure [106]. There are two types of physical adsorption: direct physical adsorption and electrochemical physical adsorption. The direct physical adsorption is carried out via electrostatic adsorption between negatively charged phosphate group of DNA and positively charged substrate surface (Figure I.22). Chitosan is usually used to modify the substrate surface to form a layer of positively charged polymer film due to the presence of free amines group (NH_3) [107]. Other cationic polymeric films have also been used as electrostatic adsorption immobilization strategies, such as poly-l-lysine (PLL) [108], polypyrrole (PPy) [109], polyaniline [109], polyethyleneimine [110].

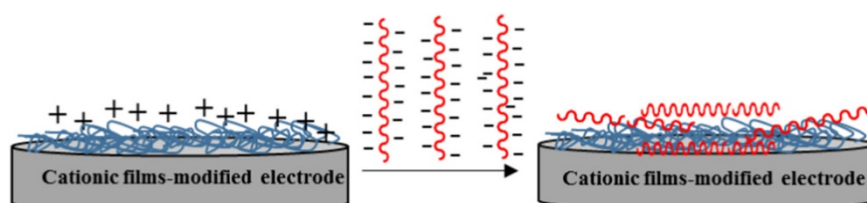


Figure I.22. The basic of electrostatic adsorption for immobilization of DNA probes [111].

Moreover, DNA probes also can be immobilized by electrochemical physical adsorption. By applying a positive electrochemical potential to the electrode and a positively charged surface is formed on the electrode, then immobilizes the negatively charged DNA. It can enhance and stabilize the DNA immobilization. Joseph et al. used a potential of + 1.7 V (vs. Ag/AgCl) applied to the smoothed carbon paste surface for 1 min to completed the pretreated and increase the roughness and hydrophilicity of carbon surface. Then electrochemical adsorption of ssDNA probe at a potential of +0.5 V (vs. Ag/AgCl) for a certain time [112]. In order to improve the efficiency and stability of immobilization, Velusamy et al. combined direct electrostatic and electrochemical adsorption. A gold electrode surface is coated with a layer of positively charged PPy film, and then applied a potential of + 0.8V for 10 min to immobilize DNA probes [113]. It must be noted that the applied potential must allow DNA to accumulate on the electrode surface without causing oxidation of deoxyribonucleic acid bases (such as guanine). The physical adsorption has the advantages of rapid, simple, and the probe do not chemical modification, however the immobilization is reversible and easy to dissociate from the

substrate surface due to the influence of temperature, pH buffer and ionic strength. In addition, the hybridization rate observed with this method is relatively low, because of the probe is randomly entangled on the surface with multiple sites [111].

2). Chemical adsorption

The chemical adsorption strategy is to immobilize DNA probes to the substrate surface via covalent binding to form the strong bonds, which has a good stability [111]. In this case, a chemical group thiols (SH) or amines (NH₂) was grafted on one end of the single stranded DNA probe, then covalently bonded to the bare substrate surface or the surface functionalized by specific group. This method allows DNA probes to immobilize on the electrode surface with high specificity and prevent non-specific binding. Furthermore, the DNA probe was immobilized on the substrate surface in a good vertical orientation, which can result in high DNA hybridization efficiency [114].

The Figure I.23 shows a number of DNA covalent binding methods on different electrochemical transducer surfaces. Millan et al. developed an immobilization way to covalently immobilized DNA on the glassy carbon surface via the coupling reaction between carboxyl group on the glassy carbon with amine group on the deoxyguanosine (dG) residues of DNA probe. Which the DNA probe can be a DNA that enriched with repetitive guanine bases or elongated by dG residues (Figure I.23a) [115]. The carboxyl group was activated by 1-(3-dimethylaminopropyl)-3-ethyl-carbodiimide (EDC) and N-hydroxysulfosuccinimide (NHS) into O-acylisourea intermediate that can bind easily with NH₂ group of DNA probe, where the carboxyl group on the glassy carbon was obtained by electrochemically oxidized in an acidic solution [115], and the carboxyl group on the carbon paste electrodes bulk were obtained by modifying either octadecylamine or stearic acid (Figure I.23b) [116]. In addition, a number of studies have developed immobilization approaches for covalently immobilizing amine grafted DNA probe on electrode surfaces modified with various functional groups, such as carboxyl [117], aldehyde [118], sulfonic [119], epoxy [120] and isothiocyanate [121], as summary in

Figure I.24. This type of covalently bound biosensor conferred the greater stability of the sensor, compared with physical adsorption, this path also allows a more homogeneous and regular coverage of the electrode surface. However, the immobilization process is more complex, lengthy, and requiring more steps.

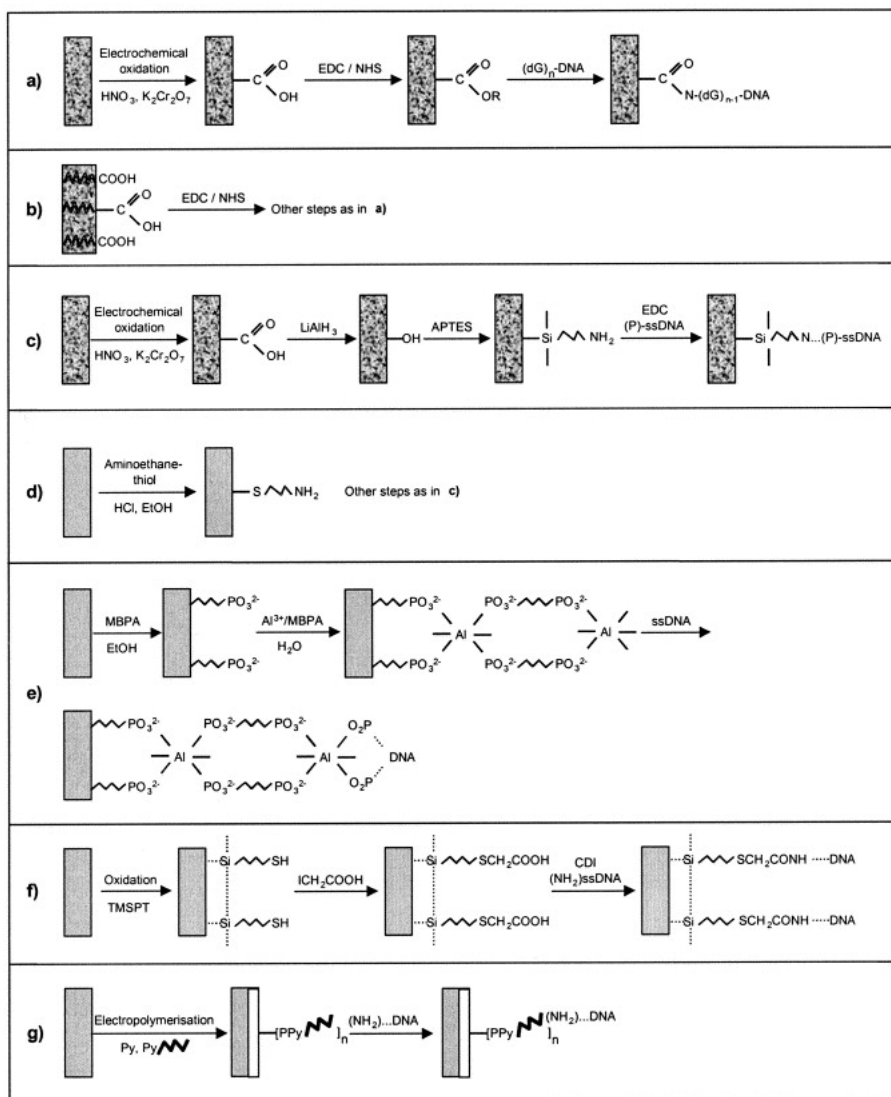


Figure I.23. Some common methods of DNA covalent binding on different electrochemical transducer surfaces [106].

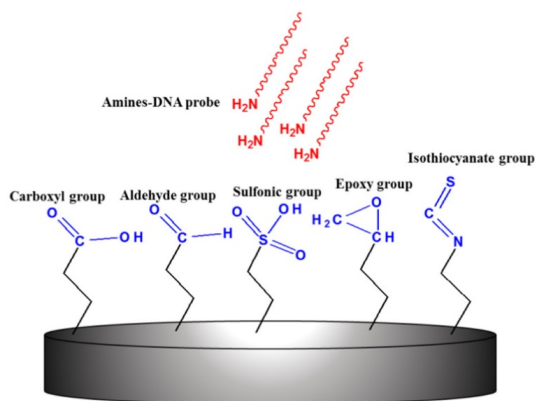


Figure I.24. The covalent immobilization methods of amine-labeled DNA probe on electrodes modified with different functional groups [111].

Gold electrode is an excellent and common electrode material due to its good conductivity. For nucleic acid biosensor, DNA probes were covalently immobilized on the gold electrode surface due to the strong affinity interaction between the thiol group and gold to form an Au-S covalent bond via chemisorption technique between thiol-modified DNA probes and gold (Au) surface (Figure I.25) [122]. Furthermore, 6-mercapto-1-hexanol (MCH) was introduced after DNA probes immobilization step to form the HS-ssDNA/MCH mixed monolayer and largely remove the nonspecific adsorption of DNA probes [123].

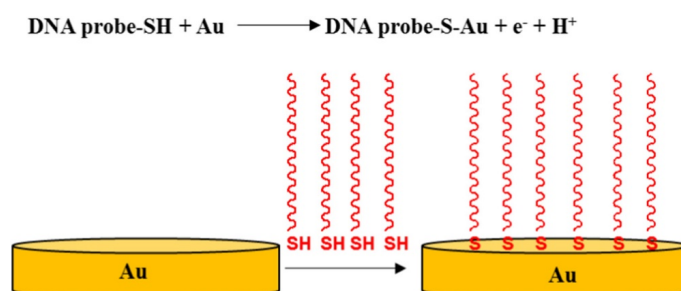


Figure I.25. DNA probes immobilization on the gold electrode surface via chemisorption technique due to the strong affinity interaction between the thiol group and gold [111].

3). Avidin/streptavidin–biotin complexation interaction

Another non-covalent immobilization strategy of DNA probe is used the affinity between the avidin/streptavidin and biotin that form a complex of avidin (streptavidin)-biotin. Avidin and

streptavidin are large tetrameric proteins (molecular weight = 2.44.31 g/mol) incorporating four identical binding sites, which can bind to small biotin molecules with high affinity, which is close to a covalent binding [124]. Arzum with co-workers designed a streptavidin modified carbon nanotube-based graphite electrode platform for DNA target detection, which all the process was depicted in Figure I.26 streptavidin was attached to the surface of multiwalled carbon nanotubes (MWCNTs) through the EDC and NHS coupling reaction between activated carboxyl group and avidin/streptavidin yield a stable amide linkage, the carboxylic acid groups on the MWCNTs were introduced through by acid treatment. Subsequently, biotinylated DNA probe was immobilized on the MWCNTs surface by the binding of biotin and streptavidin to construct DNA biosensor, then using electrochemical impedance spectroscopy to monitor hybridization event. The biosensor has been proven to have excellent selectivity and able to distinguish complementary sequences from a noncomplementary ones [125].

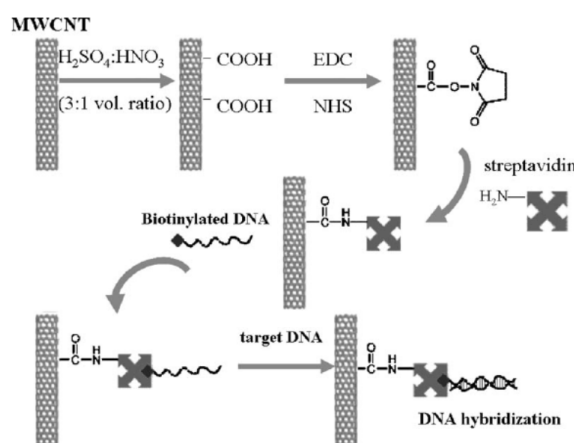


Figure I.26. The biotinylated HBV DNA probe immobilization process on the streptavidin modified MWCNT surface and the hybridization event [125].

I.3.2.2. The different type of Nucleic acid-based biosensor

The transducer is a key component of the biosensor, which converts the response of biochemical reaction into an easily measurable output signal. Based on the transduction and detection mechanisms, nucleic acid biosensors are divided into different types. Currently which being developed for the detection of nucleic acid hybridization are mostly based on optical,

surface acoustic wave, mass (mainly piezoelectric quartz crystal sensors), thermal and electrochemical transducer, etc. The transducer converts the signal that comes from nucleic acid hybridization event into a measurable response such as optical (light emission, absorption or reflectance), temperature change, mass change or current, potential change [126].

1). Optical biosensor

Optical sensors are one of the most widely used methods of DNA hybridization signal transduction modes, which the hybridization biological event of nucleic acids translated into optical signal, includes ultraviolet, visible and infrared spectrophotometry in transmission or reflectance modes (Figure I.27). It can be the emission or absorption of fluorescence, a change in color, luminescence or surface plasmon resonance (SPR) signal, which caused by the interaction of the probe with the target. This optical signal can then be translated and collected as an electrical signal for digital processing and exploited to monitor the biological recognition in biosensors [127].

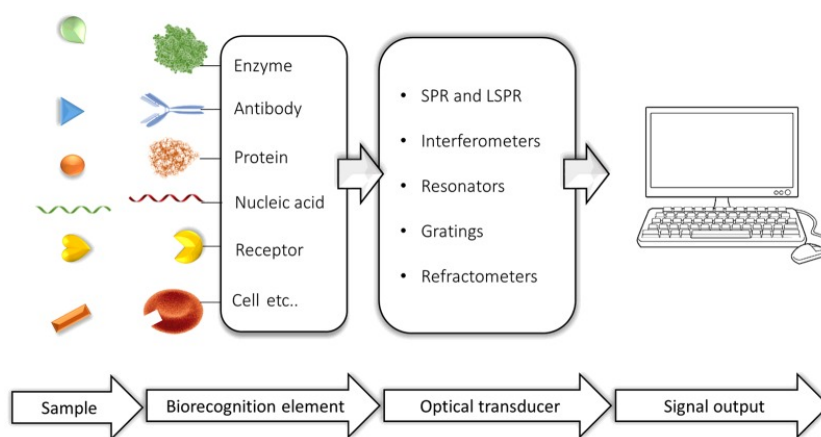


Figure I.27. The scheme of an optical biosensor, it is a compact analytical device containing a biorecognition sensing element integrated with an optical transducer system [128].

a). Fluorescence biosensor

Due to the fluorescent dyes for easy labeling of oligonucleotides and the availability of multiple fluorophores and quenchers, the fluorescence detection methods are widely used to identify nucleic acid hybridization events and then measure DNA targets. Finally, the fluorescence

signals from fluorescent molecules can be detected using fluorescence detection instrumentation, such as microscopy-coupled charge-coupled device (CCD) cameras, laser scanning fluorescence microscope, PMT detectors, confocal microscopes and a fiber sensor microarray. Several fluorescence strategies have been developed for DNA target, including in solution-based techniques and fiber optic detection formats with surface-bound probes.

i). Molecular beacons

Molecular beacons (MB) are a kind of stem-loop structure fluorescent signaling oligonucleotide probe that covalently links with a fluorophore at one end and a non-fluorescent quencher at the opposite end. The two ends sequence of the hairpin structure are complementary, such that in the absence of complementary target, the complementary sequences at two ends hybridize and cause the fluorophore and quencher to come within the requisite energy transfer distance, resulting in quenching of the fluorophore (Figure I.28a). Ideally the fluorophore should be completely quenched to ensure low background signals. The loop sequence includes the probe sequence that can be complementary to the target, which after combining with the complementary target and forming a longer and more stable rigid double helix, the conformational changes and the hairpin separates (denatures). The fluorophore and the quencher to move away from each other, the FRET effect reduces and thereby restoring fluorescence (as shown Figure I.28b), so the measurement of the change in fluorescence signal can estimate the amount of target. Molecular beacons can be employed either free in solution or fiber-optic detection by immobilizing to the surface [129, 130]. Moreover, molecular beacons can label with fluorescent dyes of different colors so that multiple targets can be detected simultaneously in the same reaction [131]. All differently colored molecular beacons can possess the same nonfluorescent quencher [132].

In addition, Taqman probe is another kind of special short nucleic acid strand with a fluorophore-quencher pair that based on FRET transduction mechanism are used in real-time PCR assay.

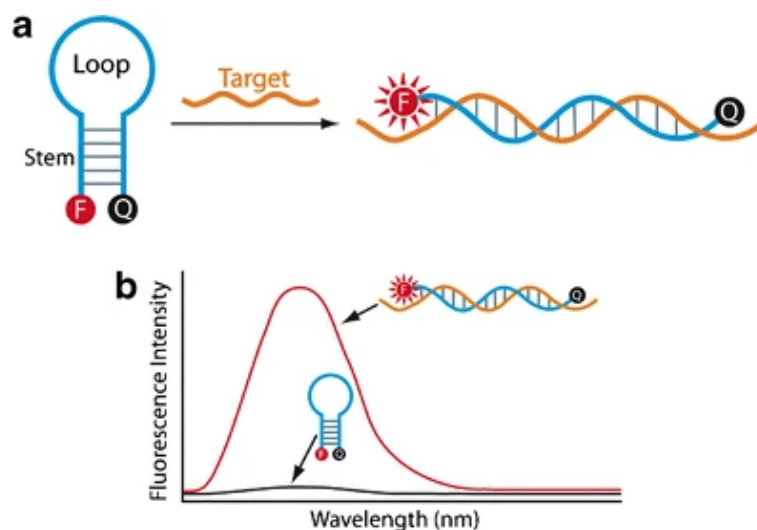


Figure I.28. a: Standard MB in its closed (left) and open (right) conformations. b: Representative fluorescence emission spectra of the closed MB (black) and the open MB (red) in the absence and presence of the target, respectively [133].

ii). Intercalating dyes

Fluorescent intercalating dye is a widely used fluorescent probe which can be reversibly inserted into double-stranded DNA, that provides an environment-dependent fluorescence enhancer. A larger increase in fluorescence signal is produced because of the dyes are activated for emission in presence of dsDNA compare with the free dye in solution [134]. The enhanced signal comes from the fluorescent intercalating dye provides a proportional response, that can be useful for selective detection of nucleic acid sequences and quantitative DNA hybridization measurements in biosensor. The intercalating dye is a planar polyaromatic compound that can reversibly bind to double-stranded DNA through three ways. *Electrostatic adsorption*: interactions with the anionic backbone of DNA by nonspecific electrostatic adsorption. *Groove binding*: interactions with the edges of base-pairs in either of the (major or minor) grooves of DNA. and *Intercalation*: intercalation of planar polyaromatic ring system between stacked base pairs on the DNA duplex. Figure I.29 shows some common planar polyaromatic compounds fluorescent intercalating dyes. Among them, ethidium bromide (EB) has been the most common labeling agent in the past and that was first discovered in the 1980's by Lee and co-

workers, but it has high carcinogenicity [135]. Now, more new fluorescent dyes that with high sensitivity and safety have been designed and synthesized, such as acridine orange (AO) [136, 137], proflavine [138], thiazole orange methoxy hydroxy ethyl (TOMEHE) and thiazole orange (TO), oxazole yellow (YO) series of asymmetric cyanine dyes [139-141]. SYBR Green is a nonspecific minor groove-binding molecule that already supplanted ethidium bromide in qPCR applications due to the brighter fluorescence and the low toxicity, mutagenicity [142].

DNA intercalating dyes are non-fluorescence in the unbound state, but after forming a high-fluorescence complexes with double-stranded DNA (dsDNA), the fluorescence intensity increases by more than 1000-fold [143]. The fluorescence intensity can increase by more than 3000 times, when combined with RNA. In addition, DNA intercalating dyes can also intercalate to nucleic acids that inside cells and it has more affinity for tumor cells than normal cells.

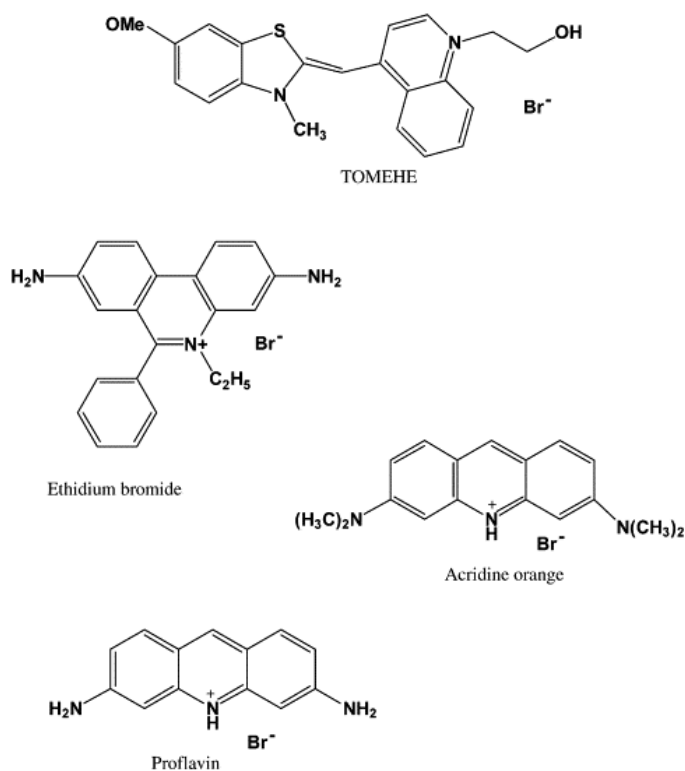


Figure I.29. Some common planar polyaromatic compounds fluorescent intercalating dyes, which can be widely used as fluorescent probes. They can be specifically inserted into double-stranded DNA and then activated for emission, thereby the fluorescence signal is enhanced [144].

iii). Fluorescent nanoparticles

Quantum dots (QDs) are a type of fluorescent nanoparticles used to label probe biomolecules, it is a colloidal core (*e.g.*, cadmium selenide (CdSe), cadmium sulfide, indium arsenide) that was encircled by one or more surface coatings. these nanometer-sized conjugates have excellent water solubility and biocompatibility. QDs can be excited for multicolor emission with a single light source, and the emission spectrum is directly related to their size which the larger the size, the longer the emission wavelength [145]. In addition, QDs have a broad absorption and narrow emission wavelengths, and have a relatively large Stokes shift, which makes the excitation spectrum can be far away from the emission spectrum and conducive to the detection of fluorescence spectrum [145, 146]. In comparison with organic dyes, due to the high quantum yields of QDs, the fluorescence intensity is brighter and more stable, and has a longer fluorescence lifetime, that is, QDs are highly stable against photobleaching. These novel optical properties make QDs to be the ideal fluorophores for using as biological labels.

Zhang et al. [147] developed an inorganic/organic hybrid biosensor based on FRET, that consist of a fluorescent-labelled reporter probe, a biotin-labelled capture probe, and a QD conjugated with several streptavidin, as shown in Figure I.30a. When the DNA target is present, it will both hybridize with capture and reporter probe in sandwich form, then which were captured by a single QD by the affinity between biotin and streptavidin. The resulting takes the fluorophore acceptors (Cy5) and the QD donor (CdSe–ZnS core–shell nanocrystals, 605QD) into close (Figure I.30b). Due to the effect of FRET, the fluorescence emission can be obtained from the acceptors, by illuminating the QDs donor, so that the target DNA can be quantitative by detecting of acceptor emission. In this system, QDs not only serve as energy donors for FRET, but also serve to capture and gather targets to be measured. The detection limit of this system is 100 times that of traditional fluorescent probe analysis methods, and without to amplify the target DNA in advance [148].

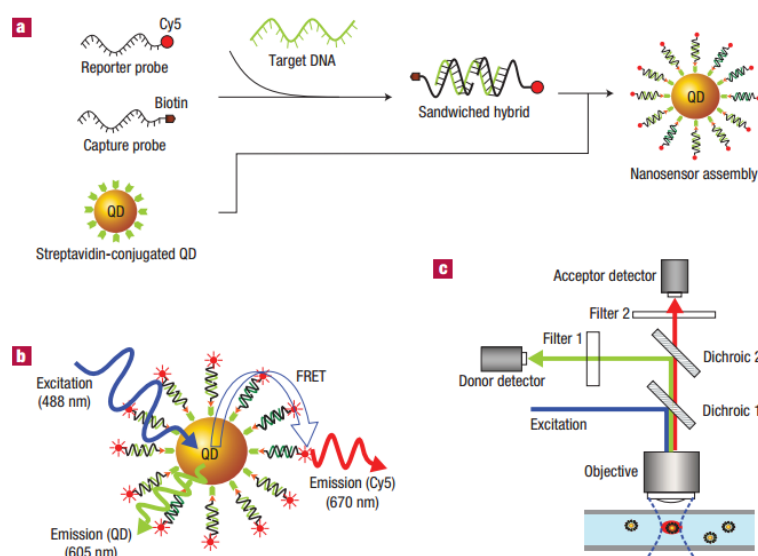


Figure I.30. Schematic of single-QD-based DNA nanosensors. a, Conceptual scheme showing the formation of a nanosensor assembly in the presence of targets. b, Fluorescence emission from Cy5 on illumination on QD caused by FRET between Cy5 acceptors and a QD donor in a nanosensor assembly. c, Experimental setup [147].

Among various detection strategies, the fluorescence method is the most widely used because of its many advantages, including high sensitivity, safety, and multiplexing capability. It also has some inherent shortcomings, such as the interference of fluorescent dyes with nucleic acid accumulation, background fluorescence and fluorescent photobleaching. In addition, it requires a large and expensive instrument to acquire the image data of the array. The demand for this instrument has seriously hampered the development of on-site or on-site nursing clinical applications of DNA based on fluorescence detection. However, the most limitation is that the probe nucleic acid must be labeled, which is time-consuming and expensive.

b). Chemiluminescence and Electrochemiluminescence

Chemiluminescence and electrochemiluminescence optic biosensor become hotspot in the field of bioanalysis because of the property of no-background signal and it is exempt from light source and avoids interference from light scattering. Chemiluminescence sensor use illumination generated by chemical reactions for trace analyze targets [149, 150]. Juru Miao et

al. developed a label-free chemiluminescence platform which can detect simultaneously three kinds of hepatitis B virus DNA target based on three kinds of special DNA immobilizing carriers with which water-soluble attributes (they are magnetic beads, polystyrene beads and PNIP). Which the chemiluminescence detection is generate by the instantaneous derivatization reaction between the 3,4,5-trimethoxyphenylglyoxal (TMPG) reagent and the guanine nucleotide-rich regions within the target DNA. The procedures are depicted in Figure I.31, and an excellent linearity was found in the range of 0.1 to 6.0 pmol with the lowest detection limit of 100 fmol [151].

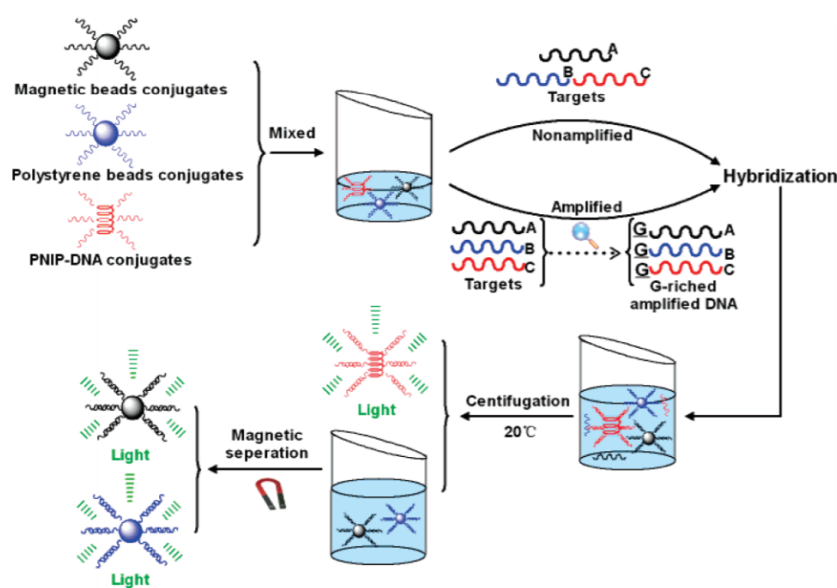


Figure I.31. Multitarget Label-Free chemiluminescence detection protocol based on different carrier vehicles [151].

Electrochemiluminescence is the electrogenerated chemiluminescence, is a kind of chemiluminescence that driven by electrochemical reaction, which has good controllability. The Figure I.32 illustrated an electrochemiluminescence biosensor to detect a single-strand DNA target by hybridized with the DNA probe immobilized on the gold electrode surface. The DNA probe is a hairpin structure which labeled with the thiol and on the other end tagged with signal-producing compound ruthenium complex. After hybridization with the target, the configuration of probe from hairpin structure converted into a linear double-helix configuration

and the ruthenium complex that labeled in the probe was far away from the electrode surface, the electrochemiluminescence signal decreased. It got a detection limit of 9×10^{-11} M for complementary DNA target and successfully detected single mismatch DNA target [152].

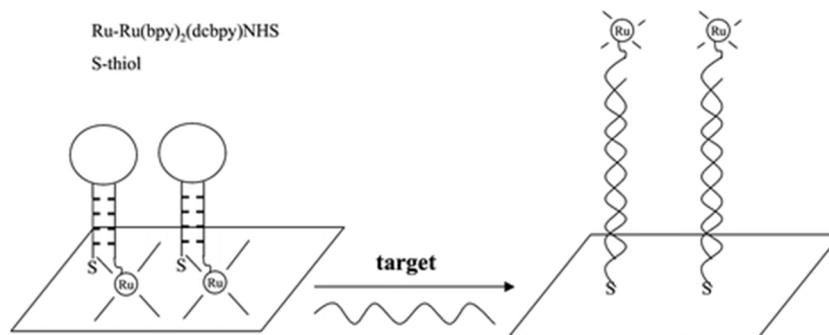


Figure I.32. Schematic diagram of the hairpin-DNA probe detection for DNA hybridization [152].

c). Colorimetry (Gold Nanoparticle)

Colorimetric biosensing based on gold nanoparticle (AuNP) is widely used in the analysis of nucleic acids, antibody, cell and other biological molecules due to their simplicity and versatility. The interaction of AuNPs and light is mainly affected by the environment, particle size, and then shows different colors. Which is associated with the coherent oscillation of AuNPs surface electrons (localized surface plasmon) induced by the incident electromagnetic field [153]. When visible light is irradiated on AuNPs, the light of resonant wavelength is absorbed by AuNPs, resulting in surface electron oscillation. The surface plasmon resonance phenomenon of small monodisperse AuNPs in diameter about 30nm can absorb the blue-green light (~ 450 nm) that in the visible light spectrum and then reflect the red light (~ 700 nm), thus solutions of AuNPs showing a red color. As the AuNPs size increases, the absorption band associated with the resonance of the plasma surface shifts to longer and closes to the red wavelengths. Therefore, the red light is absorbed and the blue light is reflected, then the AuNPs solution appears light blue or purple. In addition, the AuNPs surface charges become electrically neutral when excess salt is added to the AuNPs solution, which will causes AuNPs to aggregate and change from red to purple or blue, which arises from the interparticle plasmon coupling. And when the aggregated AuNPs are re-dispersed, the color changes from purple to

red. Thus, the AuNP-based colorimetric sensing platform is constructed to analysis the biological molecule or processes by controlling AuNP aggregation and dispersion, and observing the change in color. Dharanivasan and co-workers assembled AuNP-bifunctional oligonucleotide probes for colorimetric detection of tomato leaf curl virus DNA (ToLCNDV DNA), the AuNPs aggregated in absence of DNA target after salt treatment and caused color changes from red to blue (Figure I.33). Furthermore, there is no obvious change of color in the presence of DNA target that due to the hybridization and did not cause aggregation, which the change in optical absorbance property is related to the target concentration, finally got the limit of detection is 7.2ng [154].

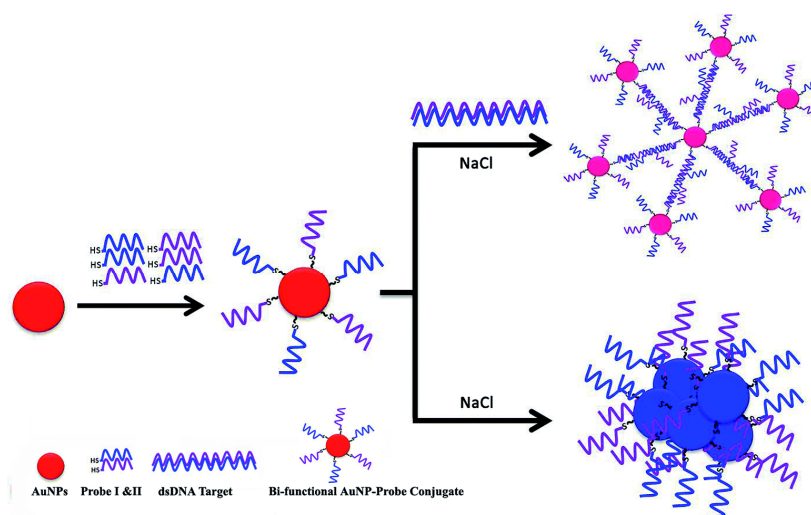


Figure I.33. Schematic representation of colorimetric detection of ToLCNDV DNA using AuNP conjugated bifunctional oligonucleotide probes and the self-assembly of gold clusters [154].

d). SPR and evanescent waves

In 1982, Liedberg et al. [155] have demonstrated the utility of surface plasmon resonance (SPR) as an optical biosensor and used for antigen-antibody interaction analysis first time. SPR is a physical optical phenomenon, it reflects the reflective index (RI) in the evanescent field on a metal. The SPR sensor is also an optical refractometer that can rely on monitoring a shift in resonance angle due to a change in the refractive index of the dielectric material on the surface

of SPR sensing resulting from the surface binding reaction. The variation in resonance angle for SPR is very sensitive and proportionally to the density of biological molecules that in the evanescent field (<500 nm) on the other surface of the metal (Figure I.34). Thus, SPR based-biosensors can detect the association and dissociation of biological molecules on a gold film surface in a real-time and without any labeling, which is also attributed to the function of evanescent waves. The changes in surface optical parameters caused by biochemical reactions, such as the affinity of antibody and antigen, receptor and ligand, and complementary DNA fragments in physiological conditions [156-159].

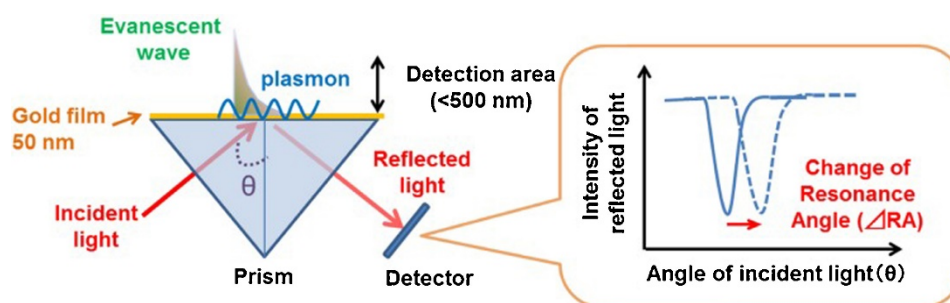


Figure I.34. Schematic description of SPR sensor [159].

Tatsuro Endo et al. developed a localized surface plasmon resonance (LSPR) based label-free optical biosensor based on a gold-capped nanoparticle layer substrate for monitoring the interaction of other biomolecules. The silica nanoparticles are modified with a silane coupling agent and immobilized on the surface of gold-deposited glass SPR substrate to form a silica nanoparticles layer. Through the affinity of biotin and streptavidin, the nucleic acid probe is immobilized on the surface as a biological receptor component to recognize the target DNA that associated with tumor necrosis factor. The LSPR biosensor assembly procedure is shown in Figure I.35. The optical properties of LSPR substrate were characterized through monitoring the changes in the absorbance strength that caused by the changes by surface modification and the hybridization of probe with DNA target. The limit of detection of target is 0.677pM by detecting the hybridization of PNA with target and PCR-amplified real samples DNA, and one base mismatch can be detected successfully.

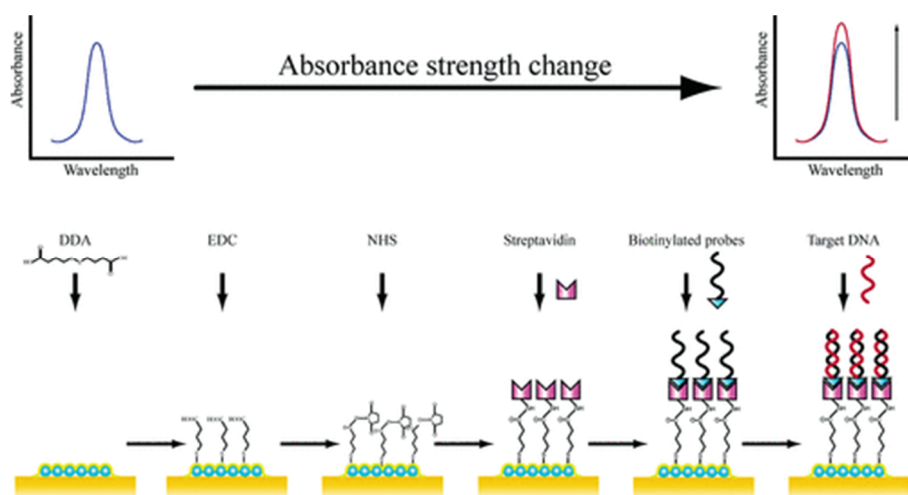


Figure I.35. Immobilization of probe oligonucleotides on SPR-based biosensor and the effect of hybridization on the absorbance values [160].

2). Mass-sensitive biosensor

Piezoelectric affinity biosensor is a kind of mass-sensitive biosensor, which are based on the coupling of the biological recognition element with a piezoelectric element (the gold electrode of a quartz crystal), it has the quartz crystal microbalance and the surface acoustic wave device two types [161]. For the DNA-based piezoelectric biosensors, it is based on the resonance frequency change of the crystal that caused by the interaction between the specific probe immobilized on the quartz crystal gold electrode and the complementary strand in the solution (the oscillation frequency decreases due to mass increases on the crystal structure caused by DNA hybridization). It can monitor the reaction on the surface of the gold electrode of a quartz crystal in real-time and label-free [162]. In 1993, Campbell et al. successfully detected the DNA hybridization by covalently immobilizing DNA probe on a polymer-modified piezoelectric crystal surface based on the quartz crystal microbalance principle. Compared with non-complementary target, A near 100 Hz frequency increased after hybridized with complementary target [163]. Silvia Storri et al. designed a DNA piezoelectric biosensor by immobilizing biotinylated 25-mer on a streptavidin-coated piezoelectric crystal, which able to distinguish the different length of DNA targets [164, 165].

3). Electrochemical biosensor

Electrochemical DNA biosensors commonly exploited the affinity of single-stranded DNA for a complementary strand of single-stranded DNA to detect specific sequences of DNA by detecting the changes in electrochemical signal in the presence or absence of complementary DNA. It can directly converse the DNA hybridization event into the electrical signal which greatly enhance the sensitivity compare with other detection ways (optical, mass). Figure I.36 demonstrated the basic design of electrochemical DNA biosensor, that single-stranded of DNA were immobilized on an electroactive surface (electrode) as the probe to construct a DNA hybridization biosensor, then the changes of electrical parameters (*e.g.*, current, potential, conductance, impedance and capacitance) caused by the hybridization event was measured. Commonly used electrochemical detection methods include Differential pulse voltammograms (DPV), Square wave voltammetry (SWV), Cyclic voltammograms (CV), electrochemical impedance spectroscopy (EIS), Amperometric detection, Linear sweep voltammetry (LSV), Chronocoulometry, Alternating current voltammetry (ACV), etc.

The commonly used DNA hybridization detection methods are label free and label-based electrochemical DNA methods, of which different types of transductions ways will be detailed in the subsequent section (section I.4) of the manuscript.

Electrochemical DNA biosensor has been rapidly developed in the field of DNA analysis in recent years due to the superior properties:

- i). The transduction is more direct because the biochemical process is transduced in an electrical response.
- ii). Label-free detection becomes possible which avoid to modify DNA sequence.
- iii). The electrochemical measurement protocol is also suitable for large-scale manufacturing of miniaturized devices.

Moreover, it with fast response, simplicity, sensitivity, good selectivity, experimental

convenience and low cost (disposability) compared to other nucleic acid detection methods [166].

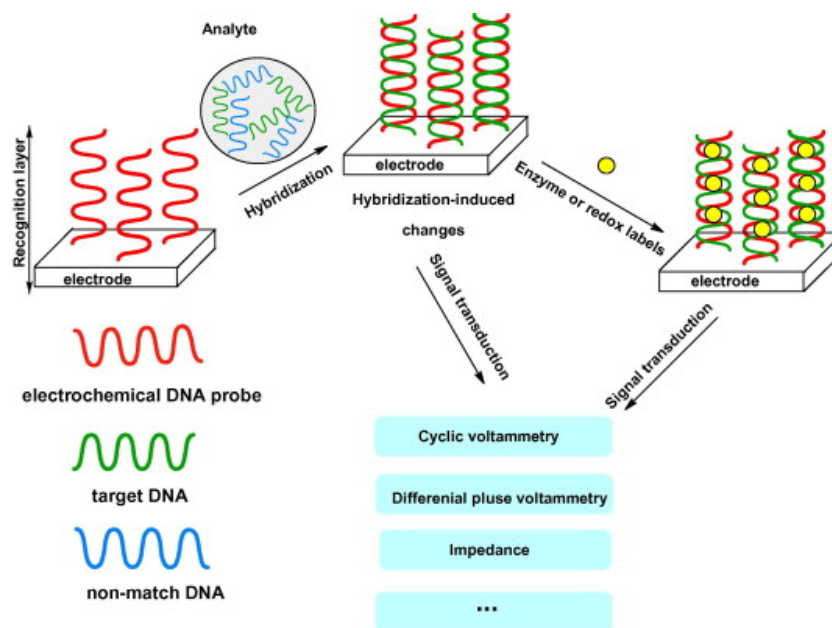


Figure I.36. General design of electrochemical DNA biosensor [167].

Conclusions

In recent years, the rapid development of biosensor research is inseparable from its unique functions and advantages. Different types sensors already can achieve femtomolar level detection (Table I.6), after long-term development. The advantages of biosensor mainly include: (1) Specificity and sensitivity: biosensors use biologically compounds as sensitive elements, which can specific recognition and binding of target molecules has high specificity, sensitivity and accuracy. (2) Fastly: the biosensor can directly and instantaneously measure the analyte, complete the analysis of the target substance, the response speed is fast, and the sample amount is small. (3) Convenience: The biosensor is mainly composed of sensitive elements and transducers integrated together to form a detection system, which avoids long and multi-step operations in the laboratory. Moreover, its small size, low cost, simple operation, generally does not require sample preparation, easy to carry and on-site inspection. (4) Continuity: The

biosensor can be regenerated, and the samples to be tested can be measured multiple times and continuously, enabling continuous detection and online analysis.

Different types of biosensors have their own unique advantages, but also have their own limitations. This is also the main reason for the limitation of application and commercialization of biosensors. For example, electrochemical biosensors have attracted the most attention because of their good selectivity, high sensitivity and accuracy, and easy miniaturization, but they are often interfered by electroactive substances. Optical sensors have a fast response speed, signal changes are not affected by electronic or magnetic interference, but it needs expensive equipment. Piezoelectric biosensors can dynamically evaluate the affinity reaction, the disadvantage is that the crystal needs to be calibrated and expensive equipment. There are still many important issues such as service life, long-term stability, reliability, mass production technology, etc., which are urgently to be solved in the research, application and industrialization of biosensors.

Table I.6. Performances of miRNA detection platforms and assays [168].

Detection Methode	detection platform	LOD	Target	Dynamic range	V _{target}	Biological specimen	Ref.
Fluorescence	EST2-ODN conjugates	2 pM	miR-141	1fM to 1nM	25µL/min	Human breast	[169]
			miR-16 / miR-21	0.002 nM to 200nM		adenocarcinoma cells	
	DSN amplification, pyrene excimer switching	0.58fM	let-7a/let-7b/let7c	1fM to 10nM	25µL	Human HeLa cells and blood samples	[170]
	QDs DSN amplification	42fM	miR-21/miR-148	0.1M to 10nM	30µL	Human breast cancer cells	[171]
Surface plasmon Resonance (SPR)	Streptavidin–oligonucleotide	1.7fM	miR-122/miR-29	0.1M to 100nM	5µL/min	Breast tumors	[172]
	Polymer brushes	0.35pM	miR-16/miR-181	0.1pM to 500pM	-	Erythrocyte lysate	[173]
	DNA super-sandwich assemblies and biotin–streptavidin amplification	9pM	miR-21, 1 or 2 base mismatch	10 pM to 1µM	-	Human breast adenocarcinoma cell	[174]
Electrochemiluminescence	PNA nanoporous metal–organic frameworks (MOFs)	10pM	miR-21/miR-96	0nM to 1000nM	60µL	Human breast cancer	[175]
Mass spectrometry (MS)	LDI–TOF-MS and nanoengineered microgold shell (1AuS)	0.1fM	miR-122	0.1fM to 1nM	-	Hepatocarcinoma cell line	[176]
Electrochemical	Amperometry, electrocatalytic nanoparticle tags	80fM	miR-106/let-7b/7c	0.3pM to 200 pM	5µL	Total RNA extracted from HeLa cells	[177]
	Electrochemical impedance spectroscopy (EIS)	2.0fM	let-7 family	5 M to 2.0 pM	5µL	Circulating miRNAs in the blood	[178]
	Cyclic voltammetry nafion, thionin (Thi), and Pd nanoparticles	1.87pM	miR-155 and noncomplementary sequence	5.6pM to 5.6×10 ⁻⁶ pM	20µL	Human blood serum	[179]

I.4. Electrochemical Nucleic Acids Biosensors transduction pathway

The electrochemical DNA biosensor immobilizes a single-stranded DNA probe on an electrode, and the electrode acts as a signal transducer to export the hybridization reaction that occurs on the surface. Since DNA is electrochemically inert, it is necessary to add electrochemically active recognition components in electrochemical detection. Usually these recognition components can selectively interact with single-stranded DNA or double-stranded DNA, so electrochemical DNA sensors usually detect the signals of these electrochemically active components to analyze hybridization reactions. There are many kinds of signal transduction pathway, such as based on variation of faradic resistance, long range electron transfer and catalyzed long-range electron transfer.

On the other hand, the hybridization reaction can be analyzed without detecting the signals of these electrochemically active components, which can base on direct DNA oxidation, the modification of the electrical properties of the electrode-solution interface due to hybridization (both electrical conductivity and capacity are changed), the measurement of the redox response of a DNA-probe labeled with an electroactive molecule, the redox charge variation of the polymer after hybridization.

This section introduces the different transduction pathway electrochemical nucleic acids biosensors. And analyzes the evolution of the detection limits of electrochemical nucleic acids biosensors, which is an update of these two reviews:

1. Lazerges, M., & Bedioui, F. (2013). *Analysis of the evolution of the detection limits of electrochemical DNA biosensors*. Analytical and bioanalytical chemistry, 405(11), 3705-3714.
2. Ho, T. H., Guillon, F. X., Bigey, P., Bedioui, F., & Lazerges, M. (2017). *Analysis of the evolution of the detection limits of electrochemical nucleic acid biosensors II*. Analytical and bioanalytical chemistry, 409(18), 4335-4352. Analysis of the evolution of the detection limits of electrochemical nucleic acid biosensors II

Analysis of the Evolution of the Detection Limits of Electrochemical Nucleic Acids Biosensors III

Y. Zhang¹, C. Slim¹, F.-X. Guillon¹, S. Griveau¹, F. Bedioui¹, M. Lazerges^{3,}*

¹ Institute of Chemistry for Life and Health Sciences, Synthesis, Electrochemistry, Imaging and Analytical Systems for Diagnosis Team, Paris-Sciences-et-Lettres, CNRS, Chimie ParisTech, 11 rue Pierre et Marie Curie, 75005 Paris, France.

² Faculté de Pharmacie de Paris, Faculté de Santé, Université de Paris, 4 avenue de l'Observatoire, 75006 Paris, France.

* mathieu.lazerges@parisdescartes.fr

Abstract. This review is focused on electrochemical nucleic acid biosensors that allowing direct detection after hybridization event. A classification founded on the nature of the electrochemical transduction pathway is established. It provides an overall picture of the detection limit evolution of the various sensor architectures developed during the last three decades and a critical report of recent strategies.

Keywords. Biosensors, electroanalytical methods, microelectrodes, nucleic acids.

Introduction

Nucleic acid biosensing for diagnosis is a major issue of life sciences, they are classically quantified by biological amplification (*i.e.* PCR) and subsequent fluorimetric detection. Electrochemical transduction offers two advantages versus classic assay: it does not require amplification and it permits direct transduction of a hybridization event on electric current. Nevertheless, the main limitation of electrochemical DNA-biosensors development is their high detection limit, which is beyond the PCR/fluorimetric assays one, and feeble reproducibility. Nevertheless, many works were performed to overcome these limitations and different approaches were reported [180, 181]. This review focuses electrochemical biosensors designed by grafting nucleic acids, DNA or PNA (peptide nucleic acid), grafted onto a solid electrode surface and direct hybridization with a non-labelled DNA-target, with or without redox indicator.

Acronyms

Electrode materials	
Au	Gold
C	Carbon
Fo	Foam
FTO	Fluorine doped Tin Oxide
GC	Glassy Carbon (sp ² carbon)
Gn	Graphene
Gr	Graphite
GO	Graphene Oxide
IDE	InterDigitated Electrode
ILE	Ionic Liquid Electrode
ITO	Indium Tin Oxide (InO ₂ /Sn ₂ O ₃ mixture)
MWNTs	Multi-Walled NanoTubes
NFs	NanoFibers
NGn	Nitrogen doped Graphene
NTs	NanoTubes
NWs	NanoWires
Pa	Paste
PA	Poly (Acrylonitrile)

Pe	Pencil
Pt	Platinum
PEDOT	Poly(3,4-EthyleneDiOxyThiophene)
PPy	Poly (Pyrrole)
PSS	Poly (Styrene Sulfonate)
PVF	Poly (Vinyl Ferrocene)
PVS	Poly (Vinyl Sulfonate)
SnO ₂	Tin Oxide
SPE	Screen-Printed Electrode

Electrochemical setups	
2E	2-electrode electrochemical cell
3E	3-electrode electrochemical cell
CMOS	Complementary Metal Oxide Semiconductor
FET	Field Effect Transistor
HEMT	High Electron Mobility Transistor

Electrochemical techniques	
CM	Capacity Measurement
CP	ChronoPotentiometry
CV	Cyclic Voltammetry
DPV	Differential Pulsed Voltammetry
EIS	Electrochemical Impedance Spectroscopy
LSV	Linear Sweep Voltammetry
SWV	Square Wave Voltammetry

I.4.1. Biosensors based on direct DNA oxidation

Hybridization can be transduced by guanine oxidation (Figure I.37).

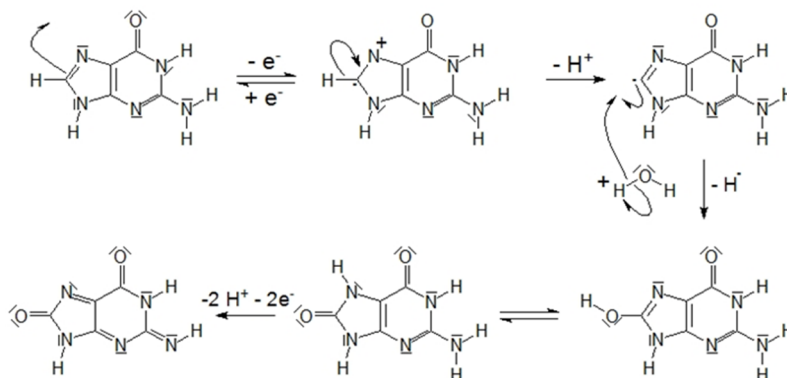


Figure I.37. Guanine oxidation mechanism.

The electrochemical oxidation signal increases after hybridization due to additional oxidation of the target guanine groups (Figure I.38).

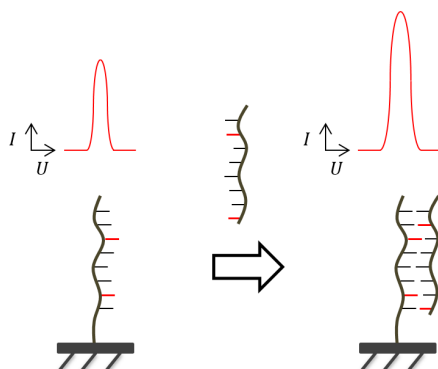


Figure I.38. Transduction based on electrochemical oxidation of guanine: before (left) and after (right) hybridization (guanine groups are red).

Guanine oxidation process is irreversible due to chemical reactions coupled to electron transfer.

The faradic oxidation charge $Q(\text{C})$ of guanine of adsorbed DNA is:

$$Q = \Gamma \cdot F \cdot A$$

$\Gamma(\text{mol}/\text{cm}^2)$ is the surface concentration of guanine, $F(\text{C}/\text{mol})$ the *Faraday* constant and $A(\text{cm}^2)$ the electrode area. An interesting strategy was then developed in order to increase signal/noise ratio by replacing guanine bases of an oligonucleotide probe by inosine ones (Figure I.39).

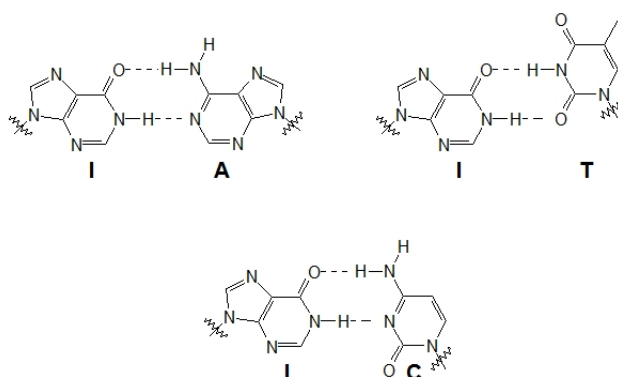


Figure I.39. Double hydrogen bonded complexes of inosine with A, T and C bases.

The inosine oxidation potential is higher than guanine one, thus the electrochemical response of the probe is silenced (Figure I.40).

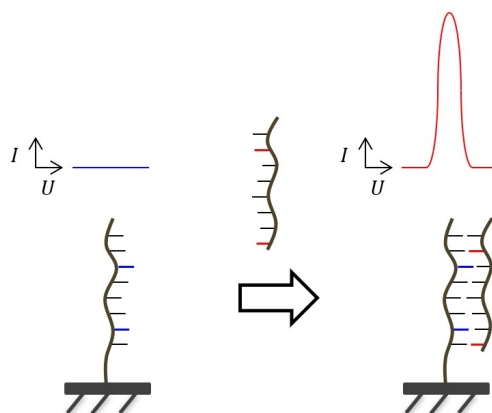


Figure I.40. Transduction based on electrochemical oxidation of guanine, Differential Pulsed Voltammetry (DPV) response before (blue) and after (red) hybridization. The signal before hybridization is silenced by substitution of guanine with inosine.

A decrease of the selectivity of the biosensor was not mentioned by the authors, but it can be expected as the inosine can form hydrogen bonded complexes with both A, T and C bases. Anyhow, this does not constitute a shortcoming as it is possible to restore this loss of selectivity by increasing the probe size by few bases. The performances of electrochemical DNA biosensors based on guanine oxidation are summarized in Table I.7.

Table I.7. DNA detection limits of biosensors based on guanine oxidation.

Electrode (Setup)	Measure	Target	PCR	Target Volume	LOD (M)	Year	Ref.
C-Pa (3-electrode)	CV	20-base DNA	No	10 μ L	$1.0 \cdot 10^{-6}$	1997	[182]
C-Pa (3-electrode)	CP	29-base DNA	No	-	$1.3 \cdot 10^{-8}$	1998	[183]
Gr-Pe (3-electrode)	CP	19-base DNA	No	200 μ L	$7.0 \cdot 10^{-8}$	2001	[184]
C-SPE (3-electrode)	SWV	244-base DNA	Yes	10 μ L	$4.0 \cdot 10^{-7}$	2002	[185]
C-Pa (3-electrode)	DPV	23-base DNA	Yes	10 μ L	$3.0 \cdot 10^{-9}$	2002	[186]
Gr-PE (3-electrode)	DPV	20-base DNA	Yes	-	$5.0 \cdot 10^{-10}$	2005	[187]
Gr-PE/C-NTs (3-electrode)	DPV	20-base DNA	No	20 μ L	$1.6 \cdot 10^{-8}$	2006	[188]
Pt/PPy/PVS (3-electrode)	DPV	25-base DNA (G ₂₅)	No	-	$1.0 \cdot 10^{-17}$	2007	[189]
Gr/SnO ₂ -NPs/PVF (3-electrode)	DPV	20-base DNA	No	-	$3.0 \cdot 10^{-7}$	2010	[190]
Gr-Pe (3-electrode)	DPV	121-base DNA	Yes	2.5 μ L	$1.0 \cdot 10^{-15}$	2011	[191]

Gr-Pe (3-electrode)	CV	500-base DNA	No	-	$3.9 \cdot 10^{-7}$	2014	[192]
Gr-Pe/C-MWNTs (3-electrode)	DPV	16-base DNA	Yes	30 μ L	$1.7 \cdot 10^{-8}$	2017	[193]
Gr-Pe/GO (3-electrode)	DPV	20-base DNA	No	1mL	$4.3 \cdot 10^{-11}$	2017	[194]
Gr-Pe/GO (3-electrode)	DPV	22-base miRNA	No	40 μ L	$1.1 \cdot 10^{-6}$	2017	[195]
Gr-Pe/PA-NFs (3-electrode)	DPV	18-base DNA	No	75 μ L	$3.7 \cdot 10^{-8}$	2018	[196]
Gr-Pe/GO (3-electrode)	DPV	22-base miRNA	No	100 μ L	$7.0 \cdot 10^{-7}$	2018	[197]
C-Pa/Ag-NPs (3-electrode)	EIS	22-base miRNA	No	-	$1.0 \cdot 10^{-18}$	2018	[198]
Gr-Pe (3-electrode)	DPV	28-base DNA	Yes	200 μ L	$2.1 \cdot 10^{-8}$	2018	[199]
C-SPE (3-electrode)	DPV	23-base DNA	Yes	10 μ L	$1.2 \cdot 10^{-6}$	2019	[200]
Gr-Pe (3-electrode)	DPV	22-base miRNA	No	40 μ L	$8.0 \cdot 10^{-8}$	2019	[201]
C-Pa/C-NTs/Au-NPs (3-electrode)	DPV	22-base miRNA	No	-	$4.7 \cdot 10^{-15}$	2019	[202]
GO/PEDOT/PSS (3-electrode)	DPV	21-base DNA	No	-	$1.5 \cdot 10^{-14}$	2020	[203]

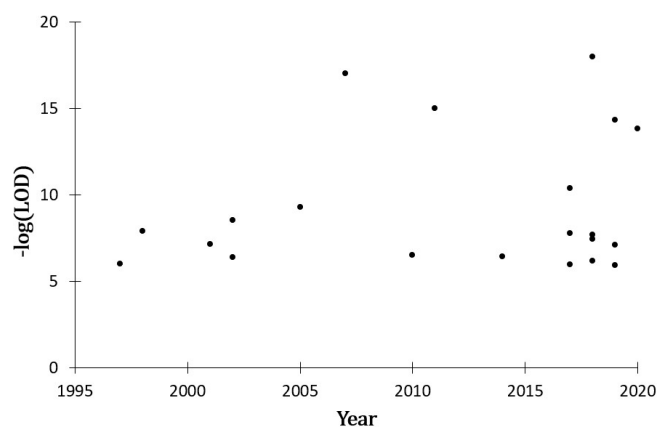


Figure I.41. LOD evolution of electrochemical DNA-biosensors based on guanine oxidation.

5 studies report a LOD in the femtomolar range and the lower reported LOD is equal to 10^{-18} M.

I.4.2. Biosensors based on electric properties of electrode-electrolyte interface

Transduction can be simply based on the modification of the electrical properties of the electrode-electrolyte interface due to hybridization: both electrical conductivity and capacity of the interface are changed during hybridization. This kind of transduction is interesting because it does not require redox species and because DNA -probe and -target are not damaged during the measurement, allowing repeating hybridization with the same biosensor. The variation of the interfacial capacity can be measured by non-transient electrochemical

techniques like electrochemical impedance spectroscopy (EIS) or linear sweep (LSV) and cyclic voltammetry (CV) (Figure I.42).

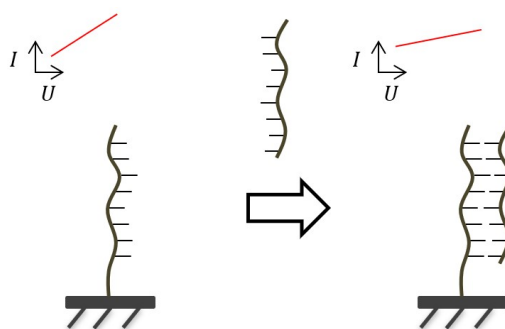


Figure I.42. Electrochemical transduction of DNA hybridization based on electric properties of electrode-electrolyte interface: linear sweep voltammetry response.

Non-transient electrochemical techniques permits separation of ohmic and capacitive responses of the interface. The LOD reported for this transduction pathway are summarized in (Table I.8) and presented on Figure I.43.

Table I.8. DNA detection limits of biosensors based on electric properties of electrode-electrolyte interface.

Electrode (setup)	Measure	Target	PCR	Target Volume	LOD (M)	Year	Ref.
Si/4-ABDMMS (3-electrode)	EIS	30-base DNA (A ₃₀)	Yes	50 μ L	$1.0 \cdot 10^{-10}$	2000	[204]
Au (3-electrode)	EIS	26-base DNA	No	-	$1.0 \cdot 10^{-9}$	2003	[205]
CdIn ₂ O ₄ semi-conductor (3-electrode)	EIS	20-base DNA	No	-	$1.3 \cdot 10^{-11}$	2006	[206]
Au (3-electrode)	EIS	27-base DNA	No	20 μ L	$1.0 \cdot 10^{-14}$	2008	[207]
Au/SDD-Co(II) (3-electrode)	EIS	21-base DNA	No	250 μ L	$3.4 \cdot 10^{-13}$	2010	[208]
Au/PAMAM/GaNNWs (3-electrode)	EIS	24-base DNA	No	-	$1.0 \cdot 10^{-19}$	2013	[209]
GC/AuNps/PPy (3-electrode)	EIS	20-base DNA	No	7 μ L	$8.4 \cdot 10^{-13}$	2014	[210]
RGO-FET (3-electrode)	CP	22-base DNA	No	-	$1.0 \cdot 10^{-13}$	2014	[211]
SiO ₂ - IDE CMOS (2-electrode)	CM	20-base DNA	No	-	$1.0 \cdot 10^{-17}$	2017	[212]
Au-IDE (2-electrode)	CM	24-base DNA	No	20 μ L	$1.5 \cdot 10^{-18}$	2017	[213]
Al-IDE (2-electrode)	EIS	28-base DNA	No	10 μ L	$1.0 \cdot 10^{-17}$	2017	[214]
Gr-FET (3-electrode)	CP	26-base DNA	No	-	$1.0 \cdot 10^{-11}$	2017	[215]
C-NTs-FET (3-electrode)	CA	24-base DNA	No	-	$1.0 \cdot 10^{-12}$	2017	[216]
CNT-FET (3-electrode)	CA	21-base DNA	No	-	$1.0 \cdot 10^{-12}$	2017	[217]

AAO-FET (3-electrode)	CP	10-base DNA	No	-	$1.0 \cdot 10^{-10}$	2017	[218]
Gr-FET (3-electrode)	CP	15-base DNA	No	-	$1.0 \cdot 10^{-13}$	2018	[219]
MoS ₂ -FET (3-electrode)	CA	22-base DNA	No	-	$6.0 \cdot 10^{-15}$	2018	[220]
NiO-FET (3-electrode)	CA	21-base DNA	No	20 μ L	$3.0 \cdot 10^{-19}$	2018	[221]
ITO NWs-FET (3-electrode)	CA	21-base DNA	No	6 μ L	$1.0 \cdot 10^{-15}$	2018	[222]
Gr-FET (3-electrode)	CP	15-base DNA	No	-	$1.0 \cdot 10^{-16}$	2018	[223]
MoS ₂ -FET (3-electrode)	CA	23-base miRNA	No	20 μ L	$3.0 \cdot 10^{-17}$	2018	[224]
Au/AuNPs (3-electrode)	EIS	22-base miRNA	No	-	$2.0 \cdot 10^{-12}$	2018	[225]
Al/p-Si/SiO ₂ /PAH EIS chip (2-electrode)	EIS	72-base DNA	Yes	50 μ L	$3.0 \cdot 10^{-10}$	2018	[226]
GaN /AlGaN-HEMT (3-electrode)	CA	22-base DNA	No	20 μ L	$1.0 \cdot 10^{-15}$	2018	[227]
Gr-FET (3-electrode)	CA	16-base DNA	No	50 μ L	$1.0 \cdot 10^{-15}$	2019	[228]
CeO ₂ NRs/Ppy NPs (3-electrode)	EIS	26-base DNA	No	-	$2.9 \cdot 10^{-7}$	2019	[229]
MoS ₂ -FET (3-electrode)	CA	30-base DNA	No	60 μ L	$1.0 \cdot 10^{-16}$	2019	[230]
Al/p-Si/SiO ₂ /PAH EIS chip (2-electrode)	EIS	72-base DNA	No	100 μ L	$1.0 \cdot 10^{-10}$	2019	[231]
Gr-FET (3-electrode)	CP	15-base DNA	No	-	$1.0 \cdot 10^{-19}$	2020	[232]
SiO ₂ -ISFET (3-electrode)	EIS	21-base DNA	No	-	$1.0 \cdot 10^{-10}$	2020	[233]
Gr-FET (3-electrode)	CP	20-base miRNA	No	1 μ L	$1.0 \cdot 10^{-14}$	2020	[234]
ITO/GA (3-electrode)	EIS	24-base DNA	No	10 μ L	$1.4 \cdot 10^{-15}$	2020	[235]

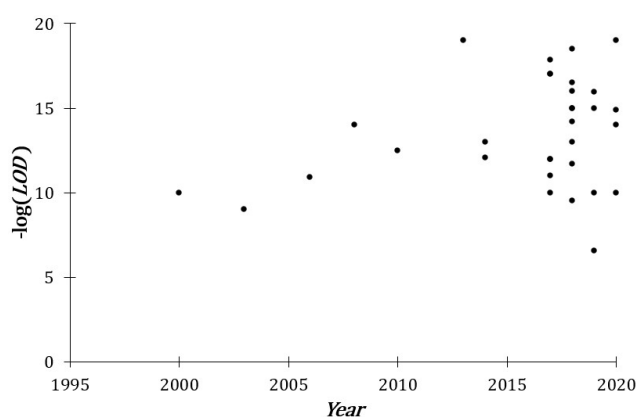


Figure I.43. LOD evolution of electrochemical DNA-biosensors based on electric properties of electrode-electrolyte interface.

10 studies report a LOD in the femtomolar range, 6 studies report a LOD in the attomolar range and the lower reported LOD is equal to 10^{-19} M.

I.4.3. Biosensors based on redox probe labeling

The principle of this transduction is based on the measurement of the redox response of a DNA-probe labeled with an electroactive molecule, in a classic or hairpin configurations (Figure I.44).

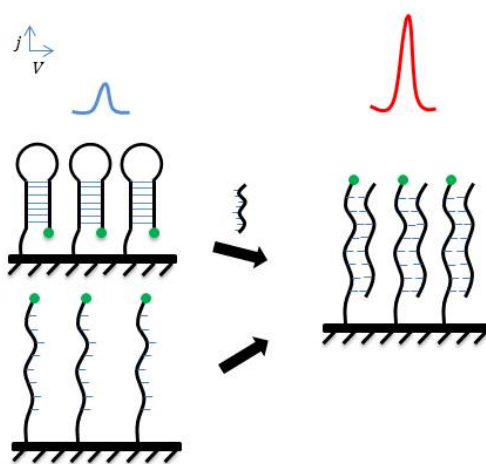


Figure I.44. Illustration of redox probe electrochemical transduction pathway with classic (left, bottom) and hairpin (left, top) DNA-probes tagged with redox groups (green circle symbols).

The electrochemical response is due to reversible oxidation of the redox probe:

$$Q = \Gamma \cdot F \cdot A$$

Γ (mol/cm²) is the surface concentration of redox probes onto electrode, F (C/mol) the *Faraday* constant and A (cm²) the electrode area. In the case of a hairpin configuration, the current can increase or decrease depending on the nature of the transduction and on the DNA-probe sequence. This transduction pathway allows single mismatch detection and is focused on detection of short DNA targets. The *LOD* reported for this transduction pathway are summarized in (Table I.9) and presented on Figure I.45. Tagging a DNA-probe with a redox

group adds one step more to the probe synthesis. Also, such probes are expensive to produce as they require two chemical modifications, for both surface anchoring and redox monitoring functions.

Table I.9. Detection limit of electrochemical DNA-biosensors based on redox probe labelling.

Electrode (setup)	Measure	Target	PCR	Target Volume	LOD (M)	Year	Ref.
GC/chitosan (3-electrode)	DPV	256-base DNA	No	1 mL	$2.0 \cdot 10^{-9}$	2001	[236]
Au (3-electrode)	CV	27-base DNA	No	500 μ L	$1.0 \cdot 10^{-11}$	2003	[237]
Au (3-electrode)	CV	24-base DNA	No	2 μ L	$1.0 \cdot 10^{-13}$	2006	[238]
Au (3-electrode)	CV	15-base DNA	No	5 μ L	$2.0 \cdot 10^{-10}$	2007	[239]
Au (3-electrode)	DPV	28-base DNA	No	12 μ L	$1.0 \cdot 10^{-9}$	2011	[240]
Au (3-electrode)	CV	17-base DNA	No	100 μ L	$2.0 \cdot 10^{-8}$	2014	[241]
Au (3-electrode)	DPV	27-base DNA	No	5 μ L	$7.4 \cdot 10^{-16}$	2015	[242]
Au (3-electrode)	CV	18-base DNA	No	-	$1.7 \cdot 10^{-18}$	2016	[243]
Au (3-electrode)	DPV	18-base DNA	No	20 μ L	$6.0 \cdot 10^{-14}$	2017	[244]
Au (3-electrode)	DPV	14-base DNA	No	-	$2.3 \cdot 10^{-12}$	2017	[245]
Au (3-electrode)	CV	25-base DNA	No	10 μ L	$5.0 \cdot 10^{-9}$	2017	[246]
C-SP/G-PANI (3-electrode)	SWV	14-base DNA	Yes	3 μ L	$2.3 \cdot 10^{-9}$	2017	[247]
Au (3-electrode)	DPV	21-base DNA	No	5 μ L	$7.0 \cdot 10^{-10}$	2017	[248]
GC/AuNPs (3-electrode)	LSV	22-base miRNA	No	50 μ L	$2.0 \cdot 10^{-17}$	2017	[249]
Au microchip array (3-electrode)	CV	27-base DNA	No	5 μ L	$2.5 \cdot 10^{-13}$	2017	[250]
ITO/PET (3-electrode)	DPV	22-base miRNA	No	3 μ L	$5.0 \cdot 10^{-9}$	2018	[251]
Au-Cys (3-electrode)	DPV	28-base DNA	Yes	2.5 μ L	$1.5 \cdot 10^{-10}$	2018	[252]
Gr-PE/CB/AuNPs (3-electrode)	DPV	22-base miRNA	No	100 μ L	$1.0 \cdot 10^{-15}$	2019	[253]
Au (3-electrode)	CV	22-base miRNA	No	200 μ L	$1.7 \cdot 10^{-16}$	2020	[254]

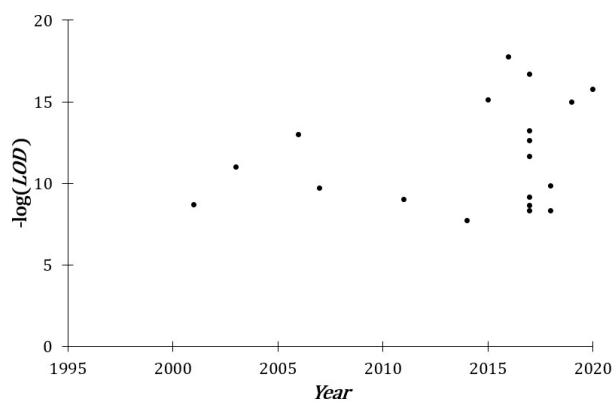


Figure I.45. LOD evolution of electrochemical DNA-biosensors based on redox probe labelling.

3 studies report a LOD in the femtomolar range, 2 studies report a LOD in the attomolar range and the lower reported LOD is equal to $1.7 \cdot 10^{-19}$ M.

I.4.4. Biosensors based on long range electron transfer

The most developed electrochemical biosensors are based on long-range electron transfer. The transduction is related to an increase of the electronic conductivity of DNA duplex subsequently to π -stacking of DNA bases along helix axis. The first generation of these biosensors was based on the electrochemical response of cationic redox species, such as tris(1,10-phenanthroline)cobalt(III) perchlorate (*i.e.* $[\text{Co}(\text{Phen})]^{3+}, 3\text{ClO}_4^-$) intercalated in the negatively charged DNA-probes (Figure I.46).

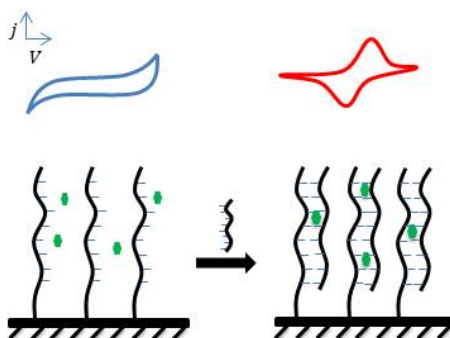


Figure I.46. Hybridization detection based on long-range electron transfer of cationic redox species and evolution of limit of detection.

The *LOD* reported for this transduction pathway are summarized in Table I.10 and presented on Figure I.47.

Table I.10. Detection limit of electrochemical DNA-biosensors based on long-range electron transfer.

Electrode (setup)	Measure	Target	PCR	Target Volume	LOD (M)	Year	Ref.
CPE (3-electrode)	DPV	20-base DNA	No	-	$9.0 \cdot 10^{-9}$	2010	[255]
GC/ZnONW/MWCNT/AuNP (3-electrode)	DPV	24-base DNA	No	4 μ L	$3.5 \cdot 10^{-14}$	2010	[256]
GC/graphene/ PANIw	DPV	24-base DNA	No	-	$3.3 \cdot 10^{-13}$	2011	[257]
GC/MP/AuNPs (3-electrode)	DPV	22-base DNA	No	-	$7.2 \cdot 10^{-11}$	2011	[258]
Au (3-electrode)	DPV	20-base DNA	No	-	$1.0 \cdot 10^{-10}$	2012	[259]
GC/GO (3-electrode)	DPV	18-base DNA	No	10 μ L	$3.2 \cdot 10^{-14}$	2012	[260]
Gold/Ni(en) ₃ Ag ₂ I ₄ (3-electrode)	SWV	18-base DNA	No	-	$5.0 \cdot 10^{-12}$	2013	[261]
GC/Fe@AuNPs/AETGO (3-electrode)	SWV	17-base DNA	No	-	$2.1 \cdot 10^{-15}$	2014	[262]
GC/ MWCNT-PAMAM	DPV	22-base miRNA	No	100 μ L	$5.0 \cdot 10^{-16}$	2015	[263]
Au/CS-MWCNTs/AuNPs	DPV	21-base DNA	Yes	4 μ L	$3.3 \cdot 10^{-16}$	2015	[264]
Au (3-electrode)	DPV	18-base DNA	No	2.5 μ L	$1.7 \cdot 10^{-10}$	2016	[265]
ITO/AuNPs (3-electrode)	SWV	22-base miRNA	No	-	$1.0 \cdot 10^{-15}$	2016	[266]
GC/IL/NrGO (3-electrode)	DPV	30-base DNA	No	5 μ L	$8.1 \cdot 10^{-9}$	2017	[267]
Au (3-electrode)	DPV	24-base miRNA	No	100 μ L	$1.0 \cdot 10^{-7}$	2017	[268]
Au (3-electrode)	DPV	24-base DNA	No	40 μ l	$1.2 \cdot 10^{-14}$	2017	[269]
GC/Pd-Au@CDs (3-electrode)	DPV	24-base DNA	No	200 μ L	$1.9 \cdot 10^{-17}$	2017	[270]
Au-SPE (3-electrode)	DPV	21-base DNA	No	2.5 μ L	$8.5 \cdot 10^{-12}$	2017	[271]
GC/PEG/PANI (3-electrode)	DPV	19-base DNA	No	1 mL	$3.8 \cdot 10^{-15}$	2017	[272]
CILE/AuNPs/RGO (3-electrode)	DPV	22-base DNA	Yes	10 μ L	$3.2 \cdot 10^{-14}$	2017	[273]
Gr-PE /Ppy (3-electrode)	DPV	22-base miRNA	No	100 μ L	$1.7 \cdot 10^{-10}$	2017	[274]
C-SP /GO/AuNWs (3-electrode)	DPV	23-base miRNA	No	2.5 μ L	$1.7 \cdot 10^{-15}$	2017	[275]
Au (3-electrode)	DPV	26-base DNA	No	-	$1.0 \cdot 10^{-9}$	2017	[276]
C-SP /AuNPs/AcMPs (3-electrode)	DPV	24-base DNA	Yes	300 μ L	$1.0 \cdot 10^{-18}$	2017	[277]
C-SP /AuNPs/PSA (3-electrode)	DPV	30-base DNA	No	-	$1.0 \cdot 10^{-21}$	2017	[278]
KC-PPy-SPE/AuNPs (3-electrode)	DPV	26-base DNA	Yes	350 μ L	$5.0 \cdot 10^{-18}$	2017	[279]
FTO/Pt-Pd/ZnO (3-electrode)	CV	34-base DNA	No	-	$4.3 \cdot 10^{-5}$	2017	[280]

GC/3D NG-Fe ₃ O ₄ (3-electrode)	DPV	25-base DNA	No	5 μ L	$3.6 \cdot 10^{-15}$	2017	[281]
3D-GF/AgNPs (3-electrode)	DPV	25-base DNA	Yes	5 μ L	$1.0 \cdot 10^{-14}$	2018	[282]
Au-SPE/CDs/AuSPEs (3-electrode)	DPV	25-base DNA	Yes	10 μ L	$1.6 \cdot 10^{-10}$	2018	[283]
AuNWEs (3-electrode)	SWV	22-base DNA	No	50 μ L	$4.8 \cdot 10^{-16}$	2018	[284]
GC/AuNPs (3-electrode)	DPV	22-base miRNA	No	200 μ L	$7.8 \cdot 10^{-17}$	2018	[285]
3D-NG (3-electrode)	DPV	25-base DNA	No	5 μ L	$2.4 \cdot 10^{-18}$	2018	[286]
Pt (3-electrode)	DPV	33-base DNA	No	200 μ L	$1.4 \cdot 10^{-18}$	2018	[287]
C-SPE/Au colloid/Si nanospheres (3-electrode)	DPV	30-base DNA	No	400 μ L	$1.0 \cdot 10^{-9}$	2018	[288]
Pt/PEDOT:PSS/PEDOT/AuNPs (3-electrode)	DPV	19-base DNA	Yes	-	$1.0 \cdot 10^{-12}$	2018	[289]
Au/ns-AuNPs (3-electrode)	DPV	26-base DNA	No	10 μ L	$2.0 \cdot 10^{-19}$	2018	[290]
C-SPE /AuNP/HSiSs (3-electrode)	DPV	17-base DNA	No	300 μ L	$8.2 \cdot 10^{-20}$	2018	[291]
GC/H ₂ N-GQD/GA (3-electrode)	DPV	22-base miRNA	No	5 μ L	$9.5 \cdot 10^{-11}$	2018	[292]
GC/PPy/PEG (3-electrode)	DPV	19-base RNA	No	-	$3.3 \cdot 10^{-14}$	2019	[293]
GC (3-electrode)	DPV	24-base DNA	No	10 μ L	$1.0 \cdot 10^{-16}$	2019	[294]
Au/Chitosan (3-electrode)	DPV	22-base miRNA	No	-	$8.0 \cdot 10^{-14}$	2019	[295]
Gr-PE (3-electrode)	DPV	22-base miRNA	No	100 μ L	$8.4 \cdot 10^{-8}$	2020	[296]
C-SPE/rGO/PPy/AuNPs (3-electrode)	DPV	22-base DNA	No	5 μ L	$4.0 \cdot 10^{-17}$	2020	[297]
GC/MWPPy/ZnO (3-electrode)	DPV	15-base DNA	No	20 μ L	$2.9 \cdot 10^{-11}$	2020	[298]
C-SPE /rGO-MWCNT/AuNPs (3-electrode)	DPV	14-base DNA	Yes	-	$5.0 \cdot 10^{-17}$	2020	[299]
CILE/3D-Gr (3-electrode)	DPV	22-base DNA	Yes	10 μ L	$3.3 \cdot 10^{-13}$	2020	[300]

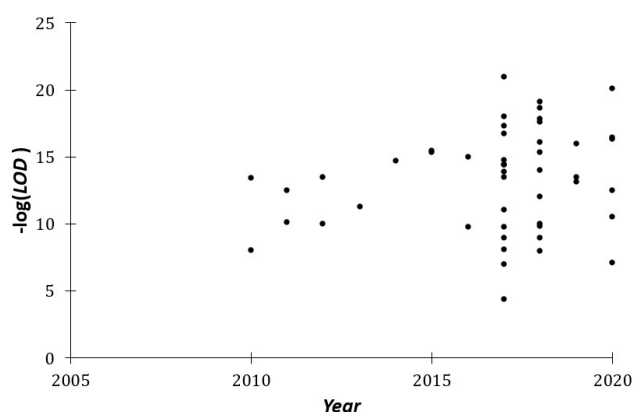


Figure I.47. LOD evolution of electrochemical DNA-biosensors based on long-range electron transfer.

15 studies report a LOD in the femtomolar range, 11 studies report a LOD in the attomolar range and the lower reported LOD is equal to $7.7 \cdot 10^{-21}$ M.

I.4.5. Biosensors based on catalyzed long-range electron transfer

A major breakthrough of biosensors based on long-range electron transfer was performed by using two redox systems, a redox intercalator (methylene blue) adsorbed in the DNA biological layer at a low concentration (10^{-6} M) and a negatively charged redox indicator ($[\text{Fe}(\text{CN})_6]^{2-}$) in bulk solution at a higher concentration (10^{-3} M). The diffusion of the redox indicator within the negatively charged DNA layer is prevented by electrostatic repulsions with negatively charged DNA phosphate backbones. Moreover, the concentration of the intercalator is very low, yielding to a very low current. The unique electrochemical response of this system is the redox signal of the indicator electrocatalyzed by long-range electron transfer enhanced by the redox intercalator (Figure I.48).

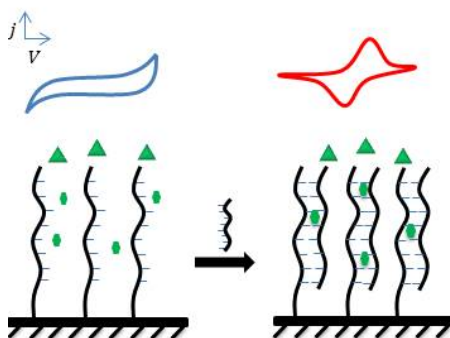


Figure I.48. Hybridization detection based on catalyzed long-range electron transfer (green triangles are redox indicators and green circles are redox intercalators).

This transduction pathway allows single mismatch detection and is focused on detection of short DNA targets. The detection limit of these biosensors is low, but there is not enough results in the bibliography to do a solid evaluation (Table I.11 and Figure I.49). This low detection limit is due to the fact that the faradic signal is not limited to the redox species adsorbed on the biosensor surface. Another advantage of this transduction pathway, over all other ones, is the possible detection of single mismatch at room temperature. Indeed, a single mismatched target

can be hybridized without heating but the mismatch induces a disrupting of axial π -stacking of DNA bases, yielding to a decrease of long-range electron transfer efficiency.

Table I.11. Detection limit of electrochemical DNA-biosensors based on catalyzed long-range electron transfer.

Electrode (setup)	Measure	Target	PCR	Target Volume	LOD (M)	Year	Ref.
Au wire (3-electrode)	CV	23-base DNA	No	7 μ L	$1.0 \cdot 10^{-11}$	2007	[301]
Au nanowire (3-electrode)	CV	20-base DNA	No	-	$1.0 \cdot 10^{-13}$	2009	[302]
GC/carbon nanofibre-chitosan (3-electrode)	DPV	17-base DNA	No	3 μ L	$8.8 \cdot 10^{-11}$	2012	[303]
Au (2-electrode)	CV	23-base DNA	No	50 μ L	$6.0 \cdot 10^{-8}$	2013	[304]
Au UMEs (2-electrode)	CA	22-base DNA	No	50 μ L	$1.0 \cdot 10^{-14}$	2016	[305]
Au UMEs (2-electrode)	CV	21-base miRNA	No	500 μ L	$1.0 \cdot 10^{-16}$	2016	[306]

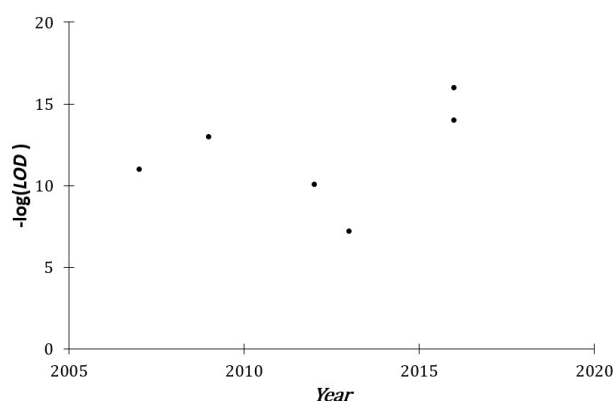


Figure I.49. LOD evolution of electrochemical DNA-biosensors based on catalyzed long-range electron transfer.

2 studies report a LOD in the femtomolar range and the lower reported LOD is equal to $1.0 \cdot 10^{-16}$ M.

I.4.6. Biosensors Based on Conducting polymers

Reversible oxidation of organic conjugated polymers, like polypyrrole, can be used to perform hybridization transduction (Figure I.50). The transduction is based on the redox charge variation of the polymer after hybridization.

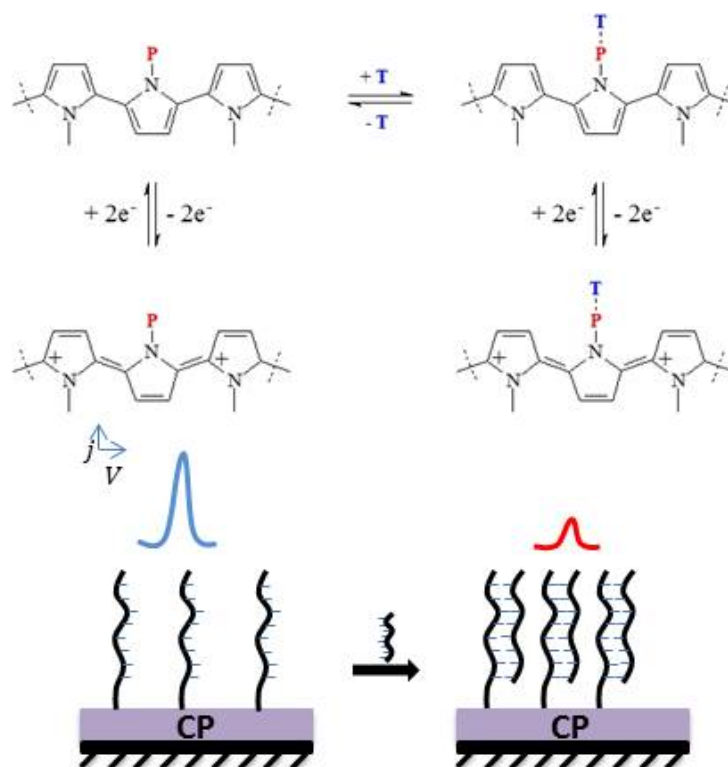


Figure I.50. Reversible pyrrole oxidation of polypyrrole response of probe (P) and probe-target (P-T) and evolution of limit of detection (red circle: single mismatched detection).

It should be noted that the oxidation of polypyrrole into a dication group (*i.e.* bipolaron) occurs at a low potential, preventing guanine oxidation. This transduction pathway allows single mismatch detection and is focused on detection of short DNA targets. In spite of the low detection limits in the fM range (10^{-15} M), this approach suffers from some major limitations. First, ss-DNA *vs* ds-DNA discrimination is feeble as the conducting polymer charge difference, before and after hybridization, is very low by comparison with the signal of the conducting polymer background (before hybridization). Also, aging of the conducting polymer is a major issue. Indeed, this is a key point which is generally poorly addressed in the reported studies. Indeed, conducting polymers are π -conjugated materials that can be irreversibly oxidized in air. This decreases the redox charge of the material and constitutes a severe limitation because each quantification requires a calibration curve. The *LOD* reported for this transduction pathway are summarized in Table I.12 and presented on Figure I.51.

Table I.12. Detection limit of electrochemical DNA-biosensors based on conducting polymers.

Electrode (setup)	Measure	Target	PCR	Target Volume	LOD (M)	Year	Ref.
Pt/PPy (3-electrode)	CV	15-base DNA	No	-	$1.0 \cdot 10^{-11}$	2001	[307]
Pt/PPy-Fc (3-electrode)	CV	25-base DNA	No	-	$1.0 \cdot 10^{-14}$	2002	[308]
Pt/PTAE (3-electrode)	CV	15-base DNA	No	-	$1.0 \cdot 10^{-9}$	2003	[309]
Pt/PPy (3-electrode)	CA	23-base DNA	Yes	50 μ L	$5.2 \cdot 10^{-11}$	2004	[310]
ITO/PPy (3-electrode)	CA	41-base DNA	No	5 μ L	$1.6 \cdot 10^{-15}$	2005	[311]
Au/PPy (3-electrode)	CA	20-base DNA	No	-	$7.2 \cdot 10^{-13}$	2006	[312]
Au/PPy (3-electrode)	CV	18-base DNA	No	10 μ L	$1.6 \cdot 10^{-16}$	2006	[313]
GC/poly(JUG-co-JUGA) (3-electrode)	SWV	10 to 30-bases DNA	No	-	$2.5 \cdot 10^{-8}$	2006	[314]
Gr-SPE/PPy-Fc (3-electrode)	CV	33-base DNA	No	33 μ L	$1.0 \cdot 10^{-10}$	2007	[315]
GC/PPy-co-PPA (3-electrode)	CV	18-bases DNA	No	40 μ L	$9.8 \cdot 10^{-10}$	2007	[316]
Au/PPy (3-electrode)	CV	24-base DNA	No	-	$1.0 \cdot 10^{-12}$	2008	[317]
GC/poly(JUG-co-JUGA) (3-electrode)	SWV	15-bases DNA	No	1 mL	$1.0 \cdot 10^{-8}$	2008	[318]
Au/JUG _{thio} (3-electrode)	SWV	20-bases DNA	No	50 μ L	$3.0 \cdot 10^{-10}$	2008	[319]
GC/Pin (3-electrode)	CV	18-bases DNA	No	3 mL	$5.8 \cdot 10^{-12}$	2009	[320]
Au/PPy-Fc (3-electrode)	CV	32-base DNA	No	50 μ L	$5.0 \cdot 10^{-17}$	2010	[321]
GC/poly(JUG-co-JUGA) (3-electrode)	SWV	22-base miRNA	No	500 μ L	$6.5 \cdot 10^{-13}$	2014	[322]
Pt/PPy (3-electrode)	DPV	40-base DNA	No	-	$1.0 \cdot 10^{-10}$	2014	[323]
Au/MWCNTs/PPy/PAMAM-Fc (3-electrode)	CV/SWV	15-base DNA	Yes	-	$3.0 \cdot 10^{-16}$	2015	[324]
Au/PEDOT (3-electrode)	DPV	21-base DNA	No	-	$1.3 \cdot 10^{-10}$	2015	[325]
GC/AuNPs/JUG-MHA (3-electrode)	SWV	23-base miRNA	No	500 μ L	$1.0 \cdot 10^{-13}$	2017	[326]
GC/PANI/PA (3-electrode)	DPV, CV	22-base miRNA	No	-	$3.4 \cdot 10^{-16}$	2020	[327]

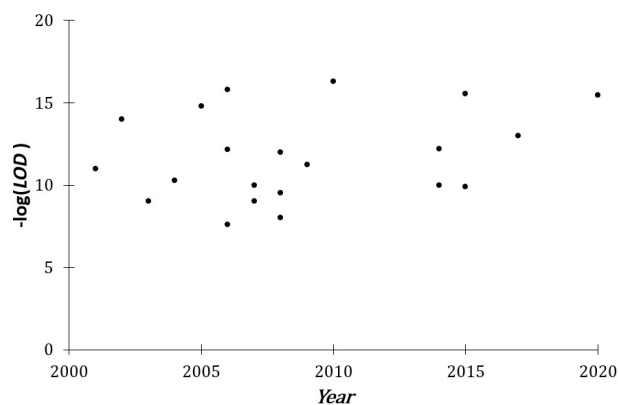


Figure I.51. LOD evolution of electrochemical DNA-biosensors based on conducting polymers.

6 studies report a LOD in the femtomolar range and the lower reported LOD is equal to $5.0 \cdot 10^{-17}$ M.

I.4.7. Biosensors based on variation of faradic resistance

The last transduction pathway is based on the decrease of faradic charge subsequent to hybridization. Both negative charge of the DNA layer and steric hindrance increase during hybridization process, inducing a decrease of the redox response of the indicators, in bulk solution or adsorbed on the surface (Figure I.52).

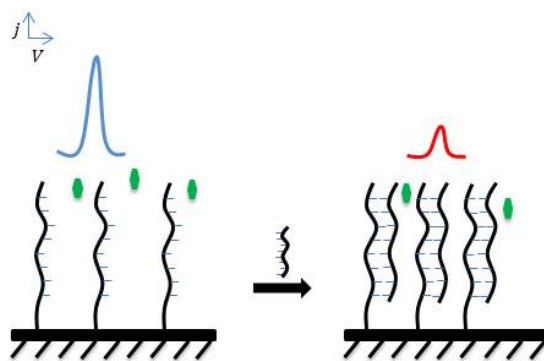


Figure I.52. Illustration of DNA biosensor variation of faradic resistance.

This transduction pathway allows single mismatch detection and is focused on detection of short DNA targets. The reported data show that low reproducible detection limits in the pM-fM range ($10^{-12}/10^{-15}$ M) can be reached (Table I.13), but this transduction pathway is not interesting by comparison with long range electron transfer. Indeed, the decrease of signal upon

hybridization is not convenient for analytical sciences, as the hybridization response is lower than the initial one. Also, detection of single mismatch is not possible at room temperature for the same reason, as both perfected matched and single mismatched DNA induce a decrease of the redox response. The *LOD* reported for this transduction pathway are summarized in (Table I.13) and presented on Figure I.53

Table I.13. Detection limit of electrochemical DNA-biosensors based on faradic resistance increase.

Electrode (setup)	Measure	Target	PCR	Target Volume	LOD (M)	Year	Ref.
Au (3-electrode)	DPV	24-base DNA	No	-	$1.0 \cdot 10^{-10}$	2004	[328]
GC/CeO ₂ /CHIT (3-electrode)	DPV	44-base DNA	No	10 μ L	$1.6 \cdot 10^{-11}$	2006	[329]
GC/PDC/SWNTs (3-electrode)	EIS	20-base DNA	Yes	10 μ L	$1.4 \cdot 10^{-12}$	2007	[330]
GC/PDC-SWNTs/PDDA (3-electrode)	DPV	20-base DNA	Yes	2 mL	$2.6 \cdot 10^{-12}$	2008	[331]
GC/EBT/NG (3-electrode)	DPV	18-base DNA	No	10 μ L	$1.0 \cdot 10^{-13}$	2010	[332]
Au/GG1PAMAM (3-electrode)	DPV	23-base DNA	No	5 μ L	$1.0 \cdot 10^{-12}$	2012	[333]
Au/ZrO ₂ -CeO ₂ /Chitosan (3-electrode)	DPV	20-base DNA	No	10 μ L	$3.0 \cdot 10^{-14}$	2012	[334]
GC/CuS-Gr/AuNPs (3-electrode)	DPV	18-base DNA	No	10 μ L	$1.0 \cdot 10^{-13}$	2014	[335]
GC/MWCNT (3-electrode)	DPV	22-base DNA	No	10 μ L	$1.0 \cdot 10^{-11}$	2016	[336]
Au nanotubes array (3-electrode)	DPV	21-base DNA	No	10 μ L	$7.7 \cdot 10^{-9}$	2016	[337]
GC/hemin-rGO/AuNPs (3-electrode)	DPV	22-base DNA	No	50 μ L	$1.4 \cdot 10^{-19}$	2017	[338]
PEG/CB (3-electrode)	EIS	24-base miRNA	No	100 μ L	$1.0 \cdot 10^{-11}$	2017	[339]
Au (3-electrode)	CV	18-base DNA	Yes	-	$2.0 \cdot 10^{-16}$	2017	[340]
C-SPE /ZnO/PSE-G (3-electrode)	EIS	25-base RNA	No	5 μ L	$4.3 \cdot 10^{-12}$	2017	[341]
Au (3-electrode)	DPV	18-base DNA	No	-	$7.6 \cdot 10^{-15}$	2017	[342]
Au (3-electrode)	EIS	25-base DNA	No	30 μ L	$1.5 \cdot 10^{-10}$	2017	[343]
GC/GO (3-electrode)	DPV	16-base DNA	No	10 μ L	$1.2 \cdot 10^{-9}$	2017	[344]
GC/MoS ₂ -Thi-AuNPs (3-electrode)	SWV	22-base miRNA	No	5 μ L	$2.6 \cdot 10^{-13}$	2017	[345]
GC/Cys-AuNPs (3-electrode)	EIS	22-base miRNA	No	30 μ L	$2.5 \cdot 10^{-13}$	2017	[346]
Au/Fc/PAMAM (3-electrode)	DPV	23-base DNA	No	-	$3.0 \cdot 10^{-10}$	2019	[347]

Gr-SPE/G/AuNPs (3-electrode)	DPV	15-base DNA	No	8 μ L	$3.6 \cdot 10^{-16}$	2017	[348]
GC (3-electrode)	EIS	25-base DNA	No	2 μ L	$1.5 \cdot 10^{-13}$	2017	[349]
Au (3-electrode)	EIS	38-base DNA	No	20 μ L	$1.0 \cdot 10^{-7}$	2017	[350]
GC/MNF (3-electrode)	CV/EIS/ DPV	28-base DNA	No	6 μ L	$1.2 \cdot 10^{-19}$	2017	[351]
GC/GO/CS (3-electrode)	EIS	21-base DNA	No	15 μ L	$3.6 \cdot 10^{-15}$	2017	[352]
ITO/NVTO/CHIT (3-electrode)	EIS	26-base DNA	No	10 μ L	$1.1 \cdot 10^{-16}$	2017	[353]
Au-NTs/PC (3-electrode)	EIS	25-base DNA	No	1 μ L	$1.0 \cdot 10^{-15}$	2018	[354]
Gr-SPE /AuNPs (3-electrode)	EIS	14-base DNA	No	15 μ L	$1.0 \cdot 10^{-7}$	2018	[355]
Au/AgNF/PPy (3-electrode)	CV	22-base miRNA	No	10 μ L	$2.0 \cdot 10^{-16}$	2018	[356]
Au (3-electrode)	CV	50-base DNA	Yes	20 μ L	$6.5 \cdot 10^{-13}$	2018	[357]
Au (3-electrode)	DPV	32-base DNA	No	40 μ L	$7.9 \cdot 10^{-12}$	2018	[358]
GC/Thi-rGO/AuNPs (3-electrode)	DPV	25-base DNA	No	5 μ L	$4.3 \cdot 10^{-19}$	2018	[359]
Carbon graphene ink/PAD (3-electrode)	EIS	15-base DNA	Yes	3 μ L	$1.2 \cdot 10^{-9}$	2018	[360]
Au/MNP-CNTs (3-electrode)	DPV	25-base DNA	No	40 μ L	$8.4 \cdot 10^{-12}$	2018	[361]
Gr-SPE/MoS ₂ (3-electrode)	CV, EIS	20-base DNA	No	3 μ L	$3.4 \cdot 10^{-9}$	2018	[362]
FTO/NFG/AgNPs/PANI (3-electrode)	DPV	22-base miRNA	No	-	$2.0 \cdot 10^{-16}$	2018	[363]
GC/poly (Py-co-PAA) (3-electrode)	EIS	25-base DNA	No	20 μ L	$2.9 \cdot 10^{-9}$	2018	[364]
Au (3-electrode)	DPV	22-base miRNA	No	5 μ L	$1.0 \cdot 10^{-12}$	2018	[365]
ITO-PET/P ₃ ANA/PU (3-electrode)	EIS	DNA	No	-	$1.0 \cdot 10^{-7}$	2018	[366]
PEG/GO (3-electrode)	EIS	22-base miRNA	No	100 μ L	$2.6 \cdot 10^{-7}$	2018	[367]
GC/GO/AgNPs (3-electrode)	EIS	23-base miRNA	No	10 mL	$4.5 \cdot 10^{-15}$	2018	[368]
GC/ERGO/PP ₃ CA (3-electrode)	EIS, DPV	19-base DNA	No	20 μ L	$3.0 \cdot 10^{-15}$	2018	[369]
GC/Gr (3-electrode)	EIS	15-base DNA	No	100 μ L	$1.0 \cdot 10^{-18}$	2018	[370]
Au/CeO ₂ NRs (3-electrode)	EIS	26-base DNA	No	30 μ L	$1.0 \cdot 10^{-8}$	2018	[371]
CPE/RCNFs – MWCNTs (3-electrode)	EIS	19-base DNA	No	10 μ L	$2.4 \cdot 10^{-12}$	2018	[372]
GC/Gr/Pol/AuNP (3-electrode)	DPV	18-base DNA	No	6 μ L	$1.0 \cdot 10^{-12}$	2018	[373]
Au/ AgNPs/CD/lipid/MPA (3-electrode)	EIS	30-base DNA	No	2 μ L	$1.0 \cdot 10^{-16}$	2019	[374]
ITO/c-GNF/APTMS-ZnO (3-electrode)	EIS	17-base DNA	No	20 μ L	$1.0 \cdot 10^{-16}$	2019	[375]

FTO/Gr microfiber/ZnO (3-electrode)	EIS	20-base DNA	No	-	$3.3 \cdot 10^{-15}$	2019	[376]
GC/ERGO/PABA/AuNPs (3-electrode)	EIS	20-base DNA	No	5 μ L	$3.7 \cdot 10^{-17}$	2019	[377]
Ti/AuNPs (3-electrode)	DPV	28-base DNA	Yes	20 μ L	$9.7 \cdot 10^{-16}$	2019	[378]
GC/AGr (3-electrode)	DPV	23-base miRNA	No	3 μ L	$1.3 \cdot 10^{-14}$	2019	[379]
GC/GN (3-electrode)	EIS	20-base DNA	No	5 μ L	$1.0 \cdot 10^{-16}$	2019	[380]
Si/Pt/ZnO (3-electrode)	EIS	36-base DNA	No	10 μ L	$2.8 \cdot 10^{-13}$	2019	[381]
GC/CHIT/CeO ₂ (3-electrode)	EIS/DPV	20-base DNA	No	5 μ L	$2.0 \cdot 10^{-15}$	2019	[382]
Au (3-electrode)	CV	17-base DNA	No	5 μ L	$1.0 \cdot 10^{-13}$	2019	[383]
C-SPE /G ₂ -PS (3-electrode)	EIS	22-base miRNA	No	35 μ L	$1.4 \cdot 10^{-7}$	2019	[384]
Paper/Graphene ink (3-electrode)	DPV	21-base DNA	No	2 μ L	$1.5 \cdot 10^{-12}$	2020	[385]
GC/ZnO/AuNPs (3-electrode)	DPV	19-base DNA	No	-	$1.8 \cdot 10^{-12}$	2020	[386]
GC/PA@Ni-MOF (3-electrode)	EIS	27-base DNA	No	10 μ L	$7.5 \cdot 10^{-16}$	2020	[387]
Au (3-electrode)	EIS	22-base DNA	No	200 μ L	$4.1 \cdot 10^{-11}$	2020	[388]

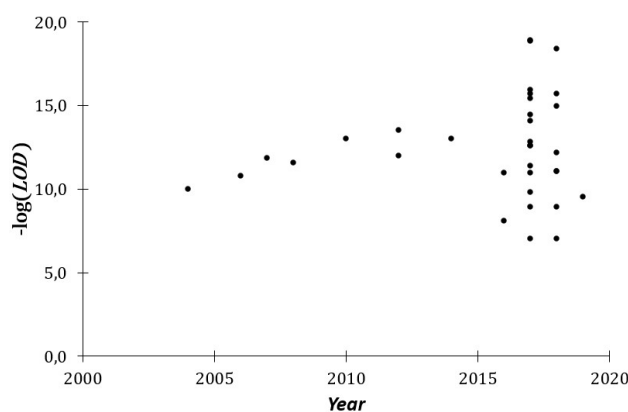


Figure I.53. LOD evolution of electrochemical DNA-biosensors based on faradic resistance increase.

Acknowledgements

YuanYuan Zhang acknowledges the *China Scholarship Council* for PhD grant.

Compliance with Ethical Standards

We certify compliance of this review and we do not have any conflict of interest to report.

I.5. Object of the Thesis

As we all know, cancer is difficult to detect at an early stage, so it is extremely necessary to find biomarkers for cancer diagnosis. miRNAs have been proposed as novel and promising biological fluid-based biomarkers, which the specific alterations in their expression profiles are associated with many diseases, including cancer. Mature miRNAs are very stable in biological fluids and highly specific in different cancer states, it allows be diagnosed non-invasively in the early stages of cancer, thereby improving the cure rate of cancer. miRNA-21 is one of the first miRNAs discovered, encoded by the MIR21 gene, located on the chromosomal positive strand 17q23.2. In the study of cancer, it found that miR-21 is an oncogenic miRNA, which is overexpressed in most cancer types analysis so far. Such as liver, lung, breast, stomach, prostate, colon and pancreas cancer.

The miRNA quantitative detection in the early stages of cancer can predict different cancers. Because of its low content in biological fluids (between 10^{-12} and 10^{-17} M), accurate quantification of its content is a prerequisite for clinical diagnosis. miRNAs quantification makes it possible to establish a diagnosis with a significantly lower number of analyzes than that based on the quantification of messenger-ribonucleic micro-acids (mRNAs). At present, in order to improve the sensitivity and detection ability of miRNA quantification method, which has grown to become a research field in its own right. There are contain RT-qPCR and different types of biosensor (optic, mass and electrochemical).

This doctorate presents the technological development of analytical tools allowing a direct detection of miRNAs: electrochemical and optical biosensors which target miRNA-21. The analytical performance of the biosensors developed as part of this doctorate is compared to that of PCR for the detection of miRNAs in blood samples of human origin.

RT-qPCR detection method is the gene (miRNA) gold standard quantitative detection, which is the most sensitive and effective one. Their detection is carried out conventionally by a preliminary step of reverse transcription and amplification of their concentration by polymerase

chain reaction (PCR) followed by a fluorescence measurement. The limits of this method are its high cost, its long analysis time and the error induced by their preliminary amplification step by PCR: miRNAs of different sequences may not be amplified in the same way under identical operating conditions.

The direct detection of miRNA, that is to say without prior amplification by PCR, constitutes a challenge in medical diagnosis, SPR and electrochemical are two techniques able to directly quantify miRNA. SPR is a physical optical phenomenon, it is also an optical refractometer that can rely on monitoring a shift in resonance angle due to a change in the refractive index of the dielectric material on the surface of SPR sensing resulting from the surface binding reaction. Thus, SPR based-biosensors can detect the association and dissociation of biological molecules on a gold film surface in a real-time and without any labeling.

Electrochemical DNA biosensor has been rapidly developed in the field of DNA analysis in recent years due to the superior properties. It can directly converse the DNA hybridization event into the electrical signal which greatly enhance the sensitivity compare with other detection ways (optical, mass). Moreover, it with fast response, simplicity, sensitivity, good selectivity, experimental convenience and low cost (disposability) compared to other nucleic acid detection method.

It is of great significance to establish a rapid, simple and efficient new technology for early diagnosis of miRNA cancer biomarkers. In this project, SPR and electrochemical miRNA biosensors are constructed to analyze miRNAs in human blood samples and evaluate their performance by comparing with PCR.

References

1. Bray F, Ferlay J, Soerjomataram I, Siegel RL, Torre LA, Jemal A. Global cancer statistics 2018: GLOBOCAN estimates of incidence and mortality worldwide for 36 cancers in 185 countries. *CA: a cancer journal for clinicians* 2018,**68**:394-424.
2. Organization WH. Geneva: *World Health Organization*. who.int/gho/database/en/. Accessed June 21, 2018.; 2018.
3. Institute NC. NCI Dictionary of Cancer Terms. In. <https://www.cancer.gov/publications/dictionaries/cancer-terms/def/cancer>; 2019.
4. Book G. Compendium of chemical terminology. *International Union of Pure and Applied Chemistry* 2014,**528**.
5. Herber RF, Duffus JH, Christensen JM, Olsen E, Park MV. Risk assessment for occupational exposure to chemicals. A review of current methodology (IUPAC Technical Report). *Pure and Applied Chemistry* 2001,**73**:993-1031.
6. Nordberg M, Duffus J, Templeton DM. Glossary of terms used in toxicokinetics (IUPAC Recommendations 2003). *Pure and Applied Chemistry* 2004,**76**:1033-1082.
7. Organization WH. *Biomarkers and Risk Assessment: Concepts and Principles-Environmental Health Criteria 155*; 1993.
8. Organization WH. International Programme on Chemical Safety. Biomarkers in Risk Assessment: Validity and Validation, 2001. In; 2018.
9. Carlomagno N, Incollingo P, Tammaro V, Peluso G, Rupealta N, Chiacchio G, *et al.* Diagnostic, predictive, prognostic, and therapeutic molecular biomarkers in third millennium: a breakthrough in gastric cancer. *BioMed research international* 2017,**2017**.
10. Osei E, Walters P, Masella O, Tennant Q, Fishwick A, Dadzie E, *et al.* A review of predictive, prognostic and diagnostic biomarkers for brain tumours: towards personalised and targeted cancer therapy. *Journal of Radiotherapy in Practice* 2019:1-16.
11. Seethala RR, Griffith CC. Molecular pathology: predictive, prognostic, and diagnostic markers in salivary gland tumors. *Surgical pathology clinics* 2016,**9**:339-352.
12. Misale S, Yaeger R, Hobor S, Scala E, Janakiraman M, Liska D, *et al.* Emergence of KRAS mutations and acquired resistance to anti-EGFR therapy in colorectal cancer. *Nature* 2012,**486**:532-536.
13. Silvestris N, Tommasi S, Santini D, Russo A, Simone G, Petriella D, *et al.* KRAS mutations and sensitivity to anti-EGFR monoclonal antibodies in metastatic colorectal carcinoma: an open issue. *Expert opinion on biological therapy* 2009,**9**:565-577.
14. Group F-NBW. BEST (Biomarkers, Endpoints, and other Tools) resource. 2016.
15. Group F-NBW. Understanding Prognostic versus Predictive Biomarkers. *Food and Drug Administration (US): Silver Spring, MD, USA* 2016.
16. Piro L, White C, Grillo-Lopez A, Janakiraman N, Saven A, Beck T, *et al.* Extended Rituximab (anti-CD20 monoclonal antibody) therapy for relapsed or refractory low-grade or follicular non-Hodgkin's lymphoma. *Annals of Oncology* 1999,**10**:655-661.
17. Zhang W-y, Wang Y, Guo Y-l, Dai H-r, Yang Q-m, Zhang Y-j, *et al.* Treatment of CD20-directed chimeric antigen receptor-modified T cells in patients with relapsed or refractory B-cell non-Hodgkin lymphoma: an early phase IIa trial report. *Signal transduction and targeted therapy* 2016,**1**:1-9.
18. Geneticist. THE INCREDIBLE MICRORNA'S. In. <https://www.geneticistinc.com/blog/microrna>; 2018.
19. Franklin RE, Gosling RG. Molecular configuration in sodium thymonucleate. *Nature* 1953,**171**:740-741.
20. Watson JD, Crick FH. Molecular structure of nucleic acids: a structure for deoxyribose nucleic acid. *Nature* 1953,**171**:737-738.
21. Choi JJ, Reich III CF, Pisetsky DS. The role of macrophages in the in vitro generation of extracellular DNA from apoptotic and necrotic cells. *Immunology* 2005,**115**:55-62.
22. Jahr S, Hentze H, Englisch S, Hardt D, Fackelmayer FO, Hesch R-D, *et al.* DNA fragments in the blood plasma of cancer patients: quantitations and evidence for their origin from apoptotic and necrotic cells. *Cancer research* 2001,**61**:1659-1665.
23. Lo YD. Circulating nucleic acids in plasma and serum: an overview. *Annals of the New York Academy of Sciences* 2001,**945**:1-7.
24. Chan K, Lo YD. Circulating nucleic acids as a tumor marker. *Histology and histopathology* 2002.
25. Rapisuwon S, Vietsch EE, Wellstein A. Circulating biomarkers to monitor cancer progression and

- treatment. *Computational and structural biotechnology journal* 2016,**14**:211-222.
26. Mandel P, Metais P. Les acides nucleiques du plasma sanguine chez l'homme. 1948.
 27. Wan JC, Massie C, Garcia-Corbacho J, Mouliere F, Brenton JD, Caldas C, *et al.* Liquid biopsies come of age: towards implementation of circulating tumour DNA. *Nature Reviews Cancer* 2017,**17**:223.
 28. Bettegowda C, Sausen M, Leary RJ, Kinde I, Wang Y, Agrawal N, *et al.* Detection of circulating tumor DNA in early-and late-stage human malignancies. *Science translational medicine* 2014,**6**:224ra224-224ra224.
 29. Diehl F, Schmidt K, Choti MA, Romans K, Goodman S, Li M, *et al.* Circulating mutant DNA to assess tumor dynamics. *Nature medicine* 2008,**14**:985.
 30. Lehmann-Werman R, Neiman D, Zemmour H, Moss J, Magenheim J, Vaknin-Dembinsky A, *et al.* Identification of tissue-specific cell death using methylation patterns of circulating DNA. *Proceedings of the National Academy of Sciences* 2016,**113**:E1826-E1834.
 31. Snyder MW, Kircher M, Hill AJ, Daza RM, Shendure J. Cell-free DNA comprises an in vivo nucleosome footprint that informs its tissues-of-origin. *Cell* 2016,**164**:57-68.
 32. Sun K, Jiang P, Chan KA, Wong J, Cheng YK, Liang RH, *et al.* Plasma DNA tissue mapping by genome-wide methylation sequencing for noninvasive prenatal, cancer, and transplantation assessments. *Proceedings of the National Academy of Sciences* 2015,**112**:E5503-E5512.
 33. Lecomte T, Berger A, Zinzindohoué F, Micard S, Landi B, Blons H, *et al.* Detection of free-circulating tumor-associated DNA in plasma of colorectal cancer patients and its association with prognosis. *International journal of cancer* 2002,**100**:542-548.
 34. Maire F, Micard S, Hammel P, Voitot H, Lévy P, Cugnenc P, *et al.* Differential diagnosis between chronic pancreatitis and pancreatic cancer: value of the detection of KRAS2 mutations in circulating DNA. *British journal of cancer* 2002,**87**:551-554.
 35. Joseph L. Circulating tumor cells and nucleic acids for tumor diagnosis. In: *Molecular Pathology of Neoplastic Gastrointestinal Diseases*: Springer; 2013. pp. 229-247.
 36. Liggett T, Melnikov A, Yi QI, Replogle C, Brand R, Kaul K, *et al.* Differential methylation of cell-free circulating DNA among patients with pancreatic cancer versus chronic pancreatitis. *Cancer: Interdisciplinary International Journal of the American Cancer Society* 2010,**116**:1674-1680.
 37. Hibi K, Robinson CR, Booker S, Wu L, Hamilton SR, Sidransky D, *et al.* Molecular detection of genetic alterations in the serum of colorectal cancer patients. *Cancer Research* 1998,**58**:1405-1407.
 38. Richardson M, Gunawan J, Hatton M, Seidlitz E, Hirte H, Singh G. Malignant ascites fluid (MAF), including ovarian-cancer-associated MAF, contains angiostatin and other factor (s) which inhibit angiogenesis. *Gynecologic oncology* 2002,**86**:279-287.
 39. Grady WM, Rajput A, Lutterbaugh JD, Markowitz SD. Detection of aberrantly methylated hMLH1 promoter DNA in the serum of patients with microsatellite unstable colon cancer. *Cancer research* 2001,**61**:900-902.
 40. Huang X-H, Sun L-H, Lu D-D, Sun Y, Ma L-J, Zhang X-R, *et al.* Codon 249 mutation in exon 7 of p53 gene in plasma DNA: maybe a new early diagnostic marker of hepatocellular carcinoma in Qidong risk area, China. *World journal of gastroenterology: WJG* 2003,**9**:692.
 41. Chang Y-C, Ho C-L, Chen HH, Chang T-T, Lai W-W, Dai Y, *et al.* Molecular diagnosis of primary liver cancer by microsatellite DNA analysis in the serum. *British journal of cancer* 2002,**87**:1449-1453.
 42. Wong IH, Lo YD, Yeo W, Lau WY, Johnson PJ. Frequent p15 promoter methylation in tumor and peripheral blood from hepatocellular carcinoma patients. *Clinical cancer research* 2000,**6**:3516-3521.
 43. Su Y-W, Huang Y-W, Chen S-H, Tzen C-Y. Quantitative analysis of plasma HBV DNA for early evaluation of the response to transcatheter arterial embolization for HBV-related hepatocellular carcinoma. *World Journal of Gastroenterology: WJG* 2005,**11**:6193.
 44. Silva JM, Silva J, Sanchez A, Garcia JM, Dominguez G, Provencio M, *et al.* Tumor DNA in plasma at diagnosis of breast cancer patients is a valuable predictor of disease-free survival. *Clinical Cancer Research* 2002,**8**:3761-3766.
 45. Chen Xq, Bonnefoi H, Diebold-Berger S, Lyautey J, Lederrey C, Faltin-Traub E, *et al.* Detecting tumor-related alterations in plasma or serum DNA of patients diagnosed with breast cancer. *Clinical cancer research: an official journal of the American Association for Cancer Research* 1999,**5**:2297-2303.
 46. Shaw JA, Page K, Blighe K, Hava N, Guttery D, Ward B, *et al.* Genomic analysis of circulating cell-free DNA infers breast cancer dormancy. *Genome research* 2012,**22**:220-231.
 47. Kohler C, Radpour R, Barekati Z, Asadollahi R, Bitzer J, Wight E, *et al.* Levels of plasma circulating cell free nuclear and mitochondrial DNA as potential biomarkers for breast tumors. *Molecular cancer*

- 2009,**8**:105.
48. Andriani F, Conte D, Mastrangelo T, Leon M, Ratcliffe C, Roz L, *et al.* Detecting lung cancer in plasma with the use of multiple genetic markers. *International journal of cancer* 2004,**108**:91-96.
 49. Allan JM, Hardie LJ, Briggs JA, Davidson LA, Watson JP, Pearson SB, *et al.* Genetic alterations in bronchial mucosa and plasma DNA from individuals at high risk of lung cancer. *International journal of cancer* 2001,**91**:359-365.
 50. Fujiwara K, Fujimoto N, Tabata M, Nishii K, Matsuo K, Hotta K, *et al.* Identification of epigenetic aberrant promoter methylation in serum DNA is useful for early detection of lung cancer. *Clinical Cancer Research* 2005,**11**:1219-1225.
 51. Jacob F, Monod J. Genetic regulatory mechanisms in the synthesis of proteins. *Journal of molecular biology* 1961,**3**:318-356.
 52. Jacob F, Monod J. On the regulation of gene activity. In: *Cold Spring Harbor Symposia on Quantitative Biology*: Cold Spring Harbor Laboratory Press; 1961. pp. 193-211.
 53. Brenner S, Jacob F, Meselson M. An unstable intermediate carrying information from genes to ribosomes for protein synthesis. *Nature* 1961,**190**:576-581.
 54. Blagden SP, Willis AE. The biological and therapeutic relevance of mRNA translation in cancer. *Nature reviews Clinical oncology* 2011,**8**:280.
 55. Kopreski MS, Benko FA, Gocke CD. Circulating RNA as a tumor marker: detection of 5T4 mRNA in breast and lung cancer patient serum. *Annals of the New York Academy of Sciences* 2001,**945**:172-178.
 56. Siddiqui N, Borden KL. mRNA export and cancer. *Wiley Interdisciplinary Reviews: RNA* 2012,**3**:13-25.
 57. Lee SY, Chang HN. High cell density cultivation of Escherichia coli W using sucrose as a carbon source. *Biotechnology letters* 1993,**15**:971-974.
 58. Hwa, Jin, Jung, Yousin, Suh. Regulation of IGF -1 signaling by microRNAs. *Frontiers in Genetics* 2015.
 59. Lee Y, Jeon K, Lee JT, Kim S, Kim VN. MicroRNA maturation: stepwise processing and subcellular localization. *The EMBO journal* 2002,**21**:4663-4670.
 60. Gromak N, Dienstbier M, Macias S, Plass M, Eyraas E, Cáceres JF, *et al.* Drosha regulates gene expression independently of RNA cleavage function. *Cell reports* 2013,**5**:1499-1510.
 61. Macias S, Plass M, Stajuda A, Michlewski G, Eyraas E, Cáceres JF. DGCR8 HITS-CLIP reveals novel functions for the Microprocessor. *Nature structural & molecular biology* 2012,**19**:760.
 62. Bohnsack MT, Czaplinski K, GÖRLICH D. Exportin 5 is a RanGTP-dependent dsRNA-binding protein that mediates nuclear export of pre-miRNAs. *Rna* 2004,**10**:185-191.
 63. Lund E, Güttinger S, Calado A, Dahlberg JE, Kutay U. Nuclear export of microRNA precursors. *science* 2004,**303**:95-98.
 64. Yi R, Qin Y, Macara IG, Cullen BR. Exportin-5 mediates the nuclear export of pre-microRNAs and short hairpin RNAs. *Genes & development* 2003,**17**:3011-3016.
 65. Price C, Chen J. MicroRNAs in cancer biology and therapy: Current status and perspectives. *Genes & Diseases* 2014,**1**:53-63.
 66. Wikipedia. MIRN21. In. <https://en.wikipedia.org/wiki/MIRN21>; 2019.
 67. Kleppe K, Ohtsuka E, Kleppe R, Molineux I, Khorana H. Studies on polynucleotides: XCVI. Repair replication of short synthetic DNA's as catalyzed by DNA polymerases. *Journal of molecular biology* 1971,**56**:341-361.
 68. Mullis K, Faloona F, Scharf S, Saiki R, Horn G, Erlich H. Specific enzymatic amplification of DNA in vitro: the polymerase chain reaction. In: *Cold Spring Harbor symposia on quantitative biology*: Cold Spring Harbor Laboratory Press; 1986. pp. 263-273.
 69. Mullis KB. The unusual origin of the polymerase chain reaction. *Scientific American* 1990,**262**:56-65.
 70. Mullis KB, Faloona FA. Specific synthesis of DNA in vitro via a polymerase-catalyzed chain reaction. In: *Recombinant DNA Methodology*: Elsevier; 1989. pp. 189-204.
 71. Vierstraete A. Principle of the PCR. *University of Ghent, Belgium* 1999.
 72. Lawyer FC, Stoffel S, Saiki RK, Myambo K, Drummond R, Gelfand DH. Isolation, characterization, and expression in Escherichia coli of the DNA polymerase gene from Thermus aquaticus. *Journal of Biological Chemistry* 1989,**264**:6427-6437.
 73. Westermeier R. Gel electrophoresis. *e LS* 2001.
 74. Higuchi R, Fockler C, Dollinger G, Watson R. Kinetic PCR analysis: real-time monitoring of DNA amplification reactions. *Bio/technology* 1993,**11**:1026-1030.
 75. Holden MJ, Wang L. Quantitative real-time PCR: fluorescent probe options and issues. In: *Standardization and quality assurance in fluorescence measurements II*: Springer; 2008. pp. 489-508.

76. Pfaffl MW. Quantification strategies in real-time polymerase chain reaction. *Quantitative real-time PCR. Appl Microbiol* 2012;53-62.
77. Svec D, Tichopad A, Novosadova V, Pfaffl MW, Kubista M. How good is a PCR efficiency estimate: Recommendations for precise and robust qPCR efficiency assessments. *Biomolecular detection and quantification* 2015;3:9-16.
78. Ståhlberg A, Håkansson J, Xian X, Semb H, Kubista M. Properties of the reverse transcription reaction in mRNA quantification. *Clinical chemistry* 2004;50:509-515.
79. Kontanis EJ, Reed FA. Evaluation of real-time PCR amplification efficiencies to detect PCR inhibitors. *Journal of forensic sciences* 2006;51:795-804.
80. Ruijter J, Ramakers C, Hoogaars W, Karlen Y, Bakker O, Van den Hoff M, *et al.* Amplification efficiency: linking baseline and bias in the analysis of quantitative PCR data. *Nucleic acids research* 2009;37:e45-e45.
81. Suslov O, Steindler DA. PCR inhibition by reverse transcriptase leads to an overestimation of amplification efficiency. *Nucleic acids research* 2005;33:e181-e181.
82. Vaerman J, Saussoy P, Ingargiola I. Evaluation of real-time PCR data. *Journal of biological regulators and homeostatic agents* 2004;18:212-214.
83. Formisano-Tréziny C, de San Feliciano M, Gabert J. Development of plasmid calibrators for absolute quantification of miRNAs by using real-time qPCR. *The Journal of Molecular Diagnostics* 2012;14:314-321.
84. Livak KJ, Schmittgen TD. Analysis of relative gene expression data using real-time quantitative PCR and the $2^{-\Delta\Delta CT}$ method. *methods* 2001;25:402-408.
85. Rao X, Huang X, Zhou Z, Lin X. An improvement of the $2^{-\Delta\Delta CT}$ method for quantitative real-time polymerase chain reaction data analysis. *Biostatistics, bioinformatics and biomathematics* 2013;3:71.
86. Schmittgen TD, Livak KJ. Analyzing real-time PCR data by the comparative C T method. *Nature protocols* 2008;3:1101.
87. Winer J, Jung CKS, Shackel I, Williams PM. Development and validation of real-time quantitative reverse transcriptase-polymerase chain reaction for monitoring gene expression in cardiac myocytes in vitro. *Analytical biochemistry* 1999;270:41-49.
88. Morley AA. Digital PCR: a brief history. *Biomolecular detection and quantification* 2014;1:1-2.
89. Cao Y, Yu M, Dong G, Chen B, Zhang B. Digital PCR as an Emerging Tool for Monitoring of Microbial Biodegradation. *Molecules* 2020;25:706.
90. Bustin S. INVITED REVIEW Quantification of mRNA using real-time reverse transcription PCR (RT-PCR): trends and problems. *Journal of molecular endocrinology* 2002;29:23-39.
91. Bustin SA, Mueller R. Real-time reverse transcription PCR (qRT-PCR) and its potential use in clinical diagnosis. *Clinical Science* 2005;109:365-379.
92. Bustin SA, Nolan T. Pitfalls of quantitative real-time reverse-transcription polymerase chain reaction. *Journal of biomolecular techniques: JBT* 2004;15:155.
93. Wong ML, Medrano JF. Real-time PCR for mRNA quantitation. *Biotechniques* 2005;39:75-85.
94. Chen C, Ridzon DA, Broomer AJ, Zhou Z, Lee DH, Nguyen JT, *et al.* Real-time quantification of microRNAs by stem-loop RT-PCR. *Nucleic acids research* 2005;33:e179-e179.
95. Schmittgen TD, Lee EJ, Jiang J, Sarkar A, Yang L, Elton TS, *et al.* Real-time PCR quantification of precursor and mature microRNA. *Methods* 2008;44:31-38.
96. Forero DA, González-Giraldo Y, Castro-Vega LJ, Barreto GE. qPCR-based methods for expression analysis of miRNAs. *BioTechniques* 2019;67:192-199.
97. Fu H-J, Zhu J, Yang M, Zhang Z-Y, Tie Y, Jiang H, *et al.* A novel method to monitor the expression of microRNAs. *Molecular biotechnology* 2006;32:197-204.
98. Shi R, Chiang VL. Facile means for quantifying microRNA expression by real-time PCR. *Biotechniques* 2005;39:519-525.
99. Kang K, Zhang X, Liu H, Wang Z, Zhong J, Huang Z, *et al.* A novel real-time PCR assay of microRNAs using S-Poly (T), a specific oligo (dT) reverse transcription primer with excellent sensitivity and specificity. *PloS one* 2012;7:e48536.
100. Niu Y, Zhang L, Qiu H, Wu Y, Wang Z, Zai Y, *et al.* An improved method for detecting circulating microRNAs with S-Poly (T) Plus real-time PCR. *Scientific reports* 2015;5:15100.
101. Nagel B, Dellweg H, Gierasch L. Glossary for chemists of terms used in biotechnology (IUPAC Recommendations 1992). *Pure and Applied Chemistry* 1992;64:143-168.

102. Turner A, Karube I, Wilson GS. *Biosensors: fundamentals and applications*: Oxford university press; 1987.
103. Sharma A, Rogers KR. Biosensors. *Measurement Science and Technology* 1994,**5**:461.
104. Wang J. DNA biosensors based on peptide nucleic acid (PNA) recognition layers. A review. *Biosensors and Bioelectronics* 1998,**13**:757-762.
105. Zhai J, Cui H, Yang R. DNA based biosensors. *Biotechnology advances* 1997,**15**:43-58.
106. Pividori M, Merkoci A, Alegret S. Electrochemical genosensor design: immobilisation of oligonucleotides onto transducer surfaces and detection methods. *Biosensors and Bioelectronics* 2000,**15**:291-303.
107. Taufik S, Yusof NA, Tee TW, Ramli I. Bismuth oxide nanoparticles/chitosan/modified electrode as biosensor for DNA hybridization. *Int. J. Electrochem. Sci* 2011,**6**:1880-1891.
108. Nascimento GA, Souza EV, Campos-Ferreira DS, Arruda MS, Castelletti CH, Wanderley MS, *et al.* Electrochemical DNA biosensor for bovine papillomavirus detection using polymeric film on screen-printed electrode. *Biosensors and Bioelectronics* 2012,**38**:61-66.
109. Saoudi B, Despas C, Chehimi MM, Jammul N, Delamar M, Bessière J, *et al.* Study of DNA adsorption on polypyrrole: interest of dielectric monitoring. *Sensors and Actuators B: Chemical* 2000,**62**:35-42.
110. Davis F, Hughes MA, Cossins AR, Higson SP. Single gene differentiation by DNA-modified carbon electrodes using an AC impedimetric approach. *Analytical chemistry* 2007,**79**:1153-1157.
111. Rashid JIA, Yusof NA. The strategies of DNA immobilization and hybridization detection mechanism in the construction of electrochemical DNA sensor: A review. *Sensing and bio-sensing research* 2017,**16**:19-31.
112. Wang J, Cai X, Jonsson C, Balakrishnan M. Adsorptive stripping potentiometry of DNA at electrochemically pretreated carbon paste electrodes. *Electroanalysis* 1996,**8**:20-24.
113. Velusamy V, Arshak K, Yang CF, Yu L, Korostynska O, Adley C. Comparison between DNA immobilization techniques on a redox polymer matrix. *American Journal of Analytical Chemistry* 2011,**2**:392.
114. Wang Q, Zhang B, Lin X, Weng W. Hybridization biosensor based on the covalent immobilization of probe DNA on chitosan–mutiwalled carbon nanotubes nanocomposite by using glutaraldehyde as an arm linker. *Sensors and Actuators B: Chemical* 2011,**156**:599-605.
115. Millan KM, Mikkelsen SR. Sequence-selective biosensor for DNA based on electroactive hybridization indicators. *Analytical Chemistry* 1993,**65**:2317-2323.
116. Millan KM, Saraullo A, Mikkelsen SR. Voltammetric DNA biosensor for cystic fibrosis based on a modified carbon paste electrode. *Analytical chemistry* 1994,**66**:2943-2948.
117. Zhang X, Gao F, Cai X, Zheng M, Gao F, Jiang S, *et al.* Application of graphene–pyrenebutyric acid nanocomposite as probe oligonucleotide immobilization platform in a DNA biosensor. *Materials Science and Engineering: C* 2013,**33**:3851-3857.
118. Xu B, Zheng D, Qiu W, Gao F, Jiang S, Wang Q. An ultrasensitive DNA biosensor based on covalent immobilization of probe DNA on fern leaf-like α -Fe₂O₃ and chitosan Hybrid film using terephthalaldehyde as arm-linker. *Biosensors and Bioelectronics* 2015,**72**:175-181.
119. Wang L, Liao X, Ding Y, Gao F, Wang Q. DNA biosensor based on a glassy carbon electrode modified with electropolymerized Eriochrome Black T. *Microchimica Acta* 2014,**181**:155-162.
120. Li F, Chen W, Zhang S. Development of DNA electrochemical biosensor based on covalent immobilization of probe DNA by direct coupling of sol–gel and self-assembly technologies. *Biosensors and Bioelectronics* 2008,**24**:781-786.
121. Tan S, Wang L, Yu J, Hou C, Jiang R, Li Y, *et al.* DNA-functionalized silicon nitride nanopores for sequence-specific recognition of DNA biosensor. *Nanoscale research letters* 2015,**10**:205.
122. Hashimoto K, Ito K, Ishimori Y. Sequence-specific gene detection with a gold electrode modified with DNA probes and an electrochemically active dye. *Analytical chemistry* 1994,**66**:3830-3833.
123. Herne TM, Tarlov MJ. Characterization of DNA probes immobilized on gold surfaces. *Journal of the American Chemical Society* 1997,**119**:8916-8920.
124. Masarik M, Kizek R, Kramer KJ, Billova S, Brazdova M, Vacek J, *et al.* Application of Avidin– Biotin Technology and Adsorptive Transfer Stripping Square-Wave Voltammetry for Detection of DNA Hybridization and Avidin in Transgenic Avidin Maize. *Analytical chemistry* 2003,**75**:2663-2669.
125. Erdem A, Papakonstantinou P, Murphy H, McMullan M, Karadeniz H, Sharma S. Streptavidin Modified Carbon Nanotube Based Graphite Electrode for Label-Free Sequence Specific DNA Detection. *Electroanalysis: An International Journal Devoted to Fundamental and Practical Aspects of*

- Electroanalysis* 2010,**22**:611-617.
126. Mulchandani A, Bassi AS. Principles and applications of biosensors for bioprocess monitoring and control. *Critical reviews in biotechnology* 1995,**15**:105-124.
 127. Leatherbarrow RJ, Edwards PR. Analysis of molecular recognition using optical biosensors. *Current opinion in chemical biology* 1999,**3**:544-547.
 128. Borisov SM, Wolfbeis OS. Optical biosensors. *Chemical reviews* 2008,**108**:423-461.
 129. Liu X, Tan W. A fiber-optic evanescent wave DNA biosensor based on novel molecular beacons. *Analytical Chemistry* 1999,**71**:5054-5059.
 130. Steemers FJ, Ferguson JA, Walt DR. Screening unlabeled DNA targets with randomly ordered fiber-optic gene arrays. *Nature biotechnology* 2000,**18**:91-94.
 131. Tyagi S, Bratu DP, Kramer FR. Multicolor molecular beacons for allele discrimination. *Nature biotechnology* 1998,**16**:49-53.
 132. Marras SA, Kramer FR, Tyagi S. Efficiencies of fluorescence resonance energy transfer and contact-mediated quenching in oligonucleotide probes. *Nucleic acids research* 2002,**30**:e122-e122.
 133. Guo J, Ju J, Turro NJ. Fluorescent hybridization probes for nucleic acid detection. *Analytical and bioanalytical chemistry* 2012,**402**:3115-3125.
 134. Piunno PA, Krull UJ, Hudson RH, Damha MJ, Cohen H. Fiber-optic DNA sensor for fluorometric nucleic acid determination. *Analytical chemistry* 1995,**67**:2635-2643.
 135. Prütz WA. Inhibition of DNA-ethidium bromide intercalation due to free radical attack upon DNA. *Radiation and environmental biophysics* 1984,**23**:7-18.
 136. Meng Y, Liu F, Han J, Sun S, Fan J, Song F, *et al.* Interaction study on DNA, single-wall carbon nanotubes and acridine orange. *Materials Science and Engineering: B* 2012,**177**:887-891.
 137. Patra D, Sleem F. Acridine orange and silica nanoparticles facilitated novel robust fluorescent hollow microcapsules toward DNA bio-sensor. *Colloids and Surfaces A: Physicochemical and Engineering Aspects* 2014,**443**:320-325.
 138. Qi L, Fan Y-Y, Wei H, Zhang D, Zhang Z-Q. Graphene oxide-enhanced and proflavine-probed fluorescence polarization biosensor for ligand-RNA interaction assay. *Sensors and Actuators B: Chemical* 2018,**257**:666-671.
 139. Fürstenberg A, Julliard MD, Deligeorgiev TG, Gadjev NI, Vasilev AA, Vauthey E. Ultrafast excited-state dynamics of DNA fluorescent intercalators: new insight into the fluorescence enhancement mechanism. *Journal of the American Chemical Society* 2006,**128**:7661-7669.
 140. Hanafi-Bagby D, Piunno PA, Wust CC, Krull UJ. Concentration dependence of a thiazole orange derivative that is used to determine nucleic acid hybridization by an optical biosensor. *Analytica chimica acta* 2000,**411**:19-30.
 141. Srinivasan K, Morris S, Girard J, Kline M, Reeder D. Enhanced detection of PCR products through use of TOTO and YOYO intercalating dyes with laser induced fluorescence--capillary electrophoresis. *Applied and theoretical electrophoresis: the official journal of the International Electrophoresis Society* 1993,**3**:235-239.
 142. Zipper H, Brunner H, Bernhagen J, Vitzthum F. Investigations on DNA intercalation and surface binding by SYBR Green I, its structure determination and methodological implications. *Nucleic acids research* 2004,**32**:e103-e103.
 143. Rye HS, Yue S, Wemmer DE, Quesada MA, Haugland RP, Mathies RA, *et al.* Stable fluorescent complexes of double-stranded DNA with bis-intercalating asymmetric cyanine dyes: properties and applications. *Nucleic acids research* 1992,**20**:2803-2812.
 144. Neidle S. Principles of Small Molecule-DNA Recognition. *Principles of Nucleic Acid Structure* 2008,**1**:132-203.
 145. Chan WC, Nie S. Quantum dot bioconjugates for ultrasensitive nonisotopic detection. *Science* 1998,**281**:2016-2018.
 146. Bruchez M, Moronne M, Gin P, Weiss S, Alivisatos AP. Semiconductor nanocrystals as fluorescent biological labels. *science* 1998,**281**:2013-2016.
 147. Zhang C-Y, Yeh H-C, Kuroki MT, Wang T-H. Single-quantum-dot-based DNA nanosensor. *Nature materials* 2005,**4**:826-831.
 148. Mattoussi H, Mauro JM, Goldman ER, Anderson GP, Sundar VC, Mikulec FV, *et al.* Self-assembly of CdSe- ZnS quantum dot bioconjugates using an engineered recombinant protein. *Journal of the American Chemical Society* 2000,**122**:12142-12150.
 149. Cai S, Tian X, Sun L, Hu H, Zheng S, Jiang H, *et al.* Platinum (II)-oligonucleotide coordination based

- aptasensor for simple and selective detection of platinum compounds. *Analytical chemistry* 2015,**87**:10542-10546.
150. Xiang W, Lv Q, Shi H, Xie B, Gao L. Aptamer-based biosensor for detecting carcinoembryonic antigen. *Talanta* 2020:120716.
151. Miao J, Cao Z, Zhou Y, Lau C, Lu J. Instantaneous derivatization technology for simultaneous and homogeneous determination of multiple DNA targets. *Analytical chemistry* 2008,**80**:1606-1613.
152. Zhang J, Qi H, Li Y, Yang J, Gao Q, Zhang C. Electrogenerated chemiluminescence DNA biosensor based on hairpin DNA probe labeled with ruthenium complex. *Analytical chemistry* 2008,**80**:2888-2894.
153. Zhao W, Brook MA, Li Y. Design of gold nanoparticle-based colorimetric biosensing assays. *ChemBioChem* 2008,**9**:2363-2371.
154. Dharanivasan G, Riyaz SM, Jesse DMI, Muthuramalingam TR, Rajendran G, Kathiravan K. DNA templated self-assembly of gold nanoparticle clusters in the colorimetric detection of plant viral DNA using a gold nanoparticle conjugated bifunctional oligonucleotide probe. *RSC advances* 2016,**6**:11773-11785.
155. Liedberg B, Nylander C, Lundström I. Biosensing with surface plasmon resonance—how it all started. *Biosensors and Bioelectronics* 1995,**10**:i-ix.
156. Homola J. Present and future of surface plasmon resonance biosensors. *Analytical and bioanalytical chemistry* 2003,**377**:528-539.
157. Homola J, Koudela I, Yee SS. Surface plasmon resonance sensors based on diffraction gratings and prism couplers: sensitivity comparison. *Sensors and Actuators B: Chemical* 1999,**54**:16-24.
158. Ritzefeld M, Sewald N. Real-time analysis of specific protein-DNA interactions with surface plasmon resonance. *Journal of amino acids* 2012,**2012**.
159. Yanase Y, Hiragun T, Ishii K, Kawaguchi T, Yanase T, Kawai M, *et al.* Surface plasmon resonance for cell-based clinical diagnosis. *Sensors* 2014,**14**:4948-4959.
160. Endo T, Kerman K, Nagatani N, Takamura Y, Tamiya E. Label-free detection of peptide nucleic acid–DNA hybridization using localized surface plasmon resonance based optical biosensor. *Analytical Chemistry* 2005,**77**:6976-6984.
161. Tombelli S, Minunni M, Mascini M. Piezoelectric biosensors: strategies for coupling nucleic acids to piezoelectric devices. *Methods* 2005,**37**:48-56.
162. Rahman M, Kumar P, Park D-S, Shim Y-B. Electrochemical sensors based on organic conjugated polymers. *Sensors* 2008,**8**:118-141.
163. Campbell N, Evans JA, Fawcett N. Detection of poly (U) hybridization using azido modified poly (A) coated piezoelectric crystals. *Biochemical and biophysical research communications* 1993,**196**:858-863.
164. Dolatabadi JEN, Mashinchian O, Ayoubi B, Jamali AA, Mobed A, Losic D, *et al.* Optical and electrochemical DNA nanobiosensors. *TrAC Trends in Analytical Chemistry* 2011,**30**:459-472.
165. Storri S, Santoni T, Mascini M. A piezoelectric biosensor for DNA hybridisation detection. *Analytical letters* 1998,**31**:1795-1808.
166. Zhang S, Wright G, Yang Y. Materials and techniques for electrochemical biosensor design and construction. *Biosensors and Bioelectronics* 2000,**15**:273-282.
167. Liu A, Wang K, Weng S, Lei Y, Lin L, Chen W, *et al.* Development of electrochemical DNA biosensors. *TrAC Trends in Analytical Chemistry* 2012,**37**:101-111.
168. D’Agata R, Spoto G. Advanced methods for microRNA biosensing: a problem-solving perspective. *Analytical and bioanalytical chemistry* 2019:1-20.
169. Pöhlmann C, Sprinzl M. Electrochemical detection of microRNAs via gap hybridization assay. *Analytical chemistry* 2010,**82**:4434-4440.
170. Ma F, Liu W-j, Zhang Q, Zhang C-y. Sensitive detection of microRNAs by duplex specific nuclease-assisted target recycling and pyrene excimer switching. *Chemical Communications* 2017,**53**:10596-10599.
171. Wang Y, Howes PD, Kim E, Spicer CD, Thomas MR, Lin Y, *et al.* Duplex-specific nuclease-amplified detection of MicroRNA using compact quantum dot–DNA conjugates. *ACS applied materials & interfaces* 2018,**10**:28290-28300.
172. Zhang D, Yan Y, Cheng W, Zhang W, Li Y, Ju H, *et al.* Streptavidin-enhanced surface plasmon resonance biosensor for highly sensitive and specific detection of microRNA. *Microchimica Acta* 2013,**180**:397-403.
173. Vaisocherová H, Šípová H, Višová I, Bocková M, Špringer T, Ermini ML, *et al.* Rapid and sensitive detection of multiple microRNAs in cell lysate by low-fouling surface plasmon resonance biosensor.

- Biosensors and Bioelectronics* 2015,**70**:226-231.
174. Qavi AJ, Kindt JT, Bailey RC. Sizing up the future of microRNA analysis. *Analytical and bioanalytical chemistry* 2010,**398**:2535-2549.
175. Wu Y, Han J, Xue P, Xu R, Kang Y. Nano metal–organic framework (NMOF)-based strategies for multiplexed microRNA detection in solution and living cancer cells. *Nanoscale* 2015,**7**:1753-1759.
176. D’Agata R, Spoto G. Surface plasmon resonance imaging for nucleic acid detection. *Analytical and bioanalytical chemistry* 2013,**405**:573-584.
177. Gao Z, Yang Z. Detection of microRNAs using electrocatalytic nanoparticle tags. *Analytical chemistry* 2006,**78**:1470-1477.
178. Gao Z, Deng H, Shen W, Ren Y. A label-free biosensor for electrochemical detection of femtomolar microRNAs. *Analytical chemistry* 2013,**85**:1624-1630.
179. Wu X, Chai Y, Yuan R, Su H, Han J. A novel label-free electrochemical microRNA biosensor using Pd nanoparticles as enhancer and linker. *Analyst* 2013,**138**:1060-1066.
180. Ho TH, Guillon FX, Bigey P, Bedioui F, Lazerges M. Analysis of the evolution of the detection limits of electrochemical nucleic acid biosensors II. *Anal Bioanal Chem* 2017,**409**:4335-4352.
181. Lazerges M, Bedioui F. Analysis of the evolution of the detection limits of electrochemical DNA biosensors. *Anal Bioanal Chem* 2013,**405**:3705-3714.
182. Cai X, Rivas G, Shirashi H, Farias P, Wang J, Tomschik M, *et al.* Electrochemical analysis of formation of polynucleotide complexes in solution and at electrode surfaces. *Analytica chimica acta* 1997,**344**:65-76.
183. Wang J, Rivas G, Fernandes JR, Paz JLL, Jiang M, Waymire R. Indicator-free electrochemical DNA hybridization biosensor. *Analytica chimica acta* 1998,**375**:197-203.
184. Wang J, Kawde A-N. Pencil-based renewable biosensor for label-free electrochemical detection of DNA hybridization. *Analytica Chimica Acta* 2001,**431**:219-224.
185. Lucarelli F, Marrazza G, Palchetti I, Cesaretti S, Mascini M. Coupling of an indicator-free electrochemical DNA biosensor with polymerase chain reaction for the detection of DNA sequences related to the apolipoprotein E. *Analytica Chimica Acta* 2002,**469**:93-99.
186. Ozkan D, Erdem A, Kara P, Kerman K, Meric B, Hassmann J, *et al.* Allele-specific genotype detection of factor V Leiden mutation from polymerase chain reaction amplicons based on label-free electrochemical genosensor. *Analytical chemistry* 2002,**74**:5931-5936.
187. Ariksoysal DO, Karadeniz H, Erdem A, Sengonul A, Sayiner AA, Ozsoz M. Label-free electrochemical hybridization genosensor for the detection of hepatitis B virus genotype on the development of lamivudine resistance. *Analytical chemistry* 2005,**77**:4908-4917.
188. Erdem A, Papakonstantinou P, Murphy H. Direct DNA hybridization at disposable graphite electrodes modified with carbon nanotubes. *Analytical Chemistry* 2006,**78**:6656-6659.
189. Arora K, Prabhakar N, Chand S, Malhotra B. Immobilization of single stranded DNA probe onto polypyrrole-polyvinyl sulfonate for application to DNA hybridization biosensor. *Sensors and Actuators B: Chemical* 2007,**126**:655-663.
190. Muti M, Kuralay F, Erdem A, Abaci S, Yumak T, Sinağ A. Tin oxide nanoparticles-polymer modified single-use sensors for electrochemical monitoring of label-free DNA hybridization. *Talanta* 2010,**82**:1680-1686.
191. Alipour E, Pournaghi-Azar MH, Parvizi M, Golabi SM, Hejazi MS. Electrochemical detection and discrimination of single copy gene target DNA in non-amplified genomic DNA. *Electrochimica acta* 2011,**56**:1925-1931.
192. Tajik S, Taher MA, Beitollahi H. Mangiferin DNA biosensor using double-stranded DNA modified pencil graphite electrode based on guanine and adenine signals. *Journal of Electroanalytical Chemistry* 2014,**720-721**:134-138.
193. Ozkan-Ariksoysal D, Kayran YU, Yilmaz FF, Ciucu AA, David IG, David V, *et al.* DNA-wrapped multi-walled carbon nanotube modified electrochemical biosensor for the detection of Escherichia coli from real samples. *Talanta* 2017,**166**:27-35.
194. Ahour F, Shamsi A. Electrochemical label-free and sensitive nanobiosensing of DNA hybridization by graphene oxide modified pencil graphite electrode. *Analytical Biochemistry* 2017,**532**:64-71.
195. Isin D, Eksin E, Erdem A. Graphene oxide modified single-use electrodes and their application for voltammetric miRNA analysis. *Materials Science and Engineering: C* 2017,**75**:1242-1249.
196. Tanik NA, Demirkan E, Aykut Y. Guanine oxidation signal enhancement in DNA via a polyacrylonitrile nanofiber-coated and cyclic voltammetry-treated pencil graphite electrode. *Journal of Physics and*

- Chemistry of Solids* 2018,**118**:73-79.
197. Eksin E, Erdem A. Electrochemical detection of microRNAs by graphene oxide modified disposable graphite electrodes. *Journal of Electroanalytical Chemistry* 2018,**810**:232-238.
 198. Elhakim HKA, Azab SM, Fekry AM. A novel simple biosensor containing silver nanoparticles/propolis (bee glue) for microRNA let-7a determination. *Mater Sci Eng C Mater Biol Appl* 2018,**92**:489-495.
 199. Subak H, Ozkan-Ariksoysal D. Label-free electrochemical biosensor for the detection of Influenza genes and the solution of guanine-based displaying problem of DNA hybridization. *Sensors and Actuators B: Chemical* 2018,**263**:196-207.
 200. Erdem A, Eksin E. Zip nucleic acid based single-use biosensor for electrochemical detection of Factor V Leiden mutation. *Sensors and Actuators B: Chemical* 2019,**288**:634-640.
 201. Yaralı E, Kanat E, Erac Y, Erdem A. Ionic Liquid Modified Single-use Electrode Developed for Voltammetric Detection of miRNA-34a and its Application to Real Samples. *Electroanalysis* 2020,**32**:384-393.
 202. Azab SM, Elhakim HK, Fekry AM. The strategy of nanoparticles and the flavone chrysin to quantify miRNA-let 7a in zepto-molar level: Its application as tumor marker. *Journal of Molecular Structure* 2019,**1196**:647-652.
 203. Dagi Kiransan K, Topçu E. Conducting Polymer-Reduced Graphene Oxide Sponge Electrode for Electrochemical Detection Based on DNA Hybridization. *ACS Applied Nano Materials*.
 204. Berney H, West J, Haeefe E, Alderman J, Lane W, Collins J. A DNA diagnostic biosensor: development, characterisation and performance. *Sensors and Actuators B: Chemical* 2000,**68**:100-108.
 205. Guiducci C. DNA detection by integrable electronics. *Biosensors and Bioelectronics* 2004,**19**:781-787.
 206. Zebda A, Stambouli V, Labeau M, Guiducci C, Diard JP, Le Gorrec B. Metallic oxide CdIn₂O₄ films for the label free electrochemical detection of DNA hybridization. *Biosens Bioelectron* 2006,**22**:178-184.
 207. Hassen WM, Chaix C, Abdelghani A, Bessueille F, Leonard D, Jaffrezic-Renault N. An impedimetric DNA sensor based on functionalized magnetic nanoparticles for HIV and HBV detection. *Sensors and Actuators B: Chemical* 2008,**134**:755-760.
 208. Martinovic J, van Wyk J, Mapolie S, Jahed N, Baker P, Iwuoha E. Electrochemical and spectroscopic properties of dendritic cobalto-salicylaldimine DNA biosensor. *Electrochimica Acta* 2010,**55**:4296-4302.
 209. Sahoo P, Suresh S, Dhara S, Saini G, Rangarajan S, Tyagi AK. Direct label free ultrasensitive impedimetric DNA biosensor using dendrimer functionalized GaN nanowires. *Biosens Bioelectron* 2013,**44**:164-170.
 210. Nowicka AM, Fau M, Rapecki T, Donten M. Polypyrrole-Au Nanoparticles Composite as Suitable Platform for DNA Biosensor with Electrochemical Impedance Spectroscopy Detection. *Electrochimica Acta* 2014,**140**:65-71.
 211. Cai B, Wang S, Huang L, Ning Y, Zhang Z, Zhang G-J. Ultrasensitive label-free detection of PNA-DNA hybridization by reduced graphene oxide field-effect transistor biosensor. *ACS nano* 2014,**8**:2632-2638.
 212. Chen C-M, Lu MS-C. A CMOS capacitive biosensor array for highly sensitive detection of pathogenic avian influenza DNA. In: *2017 19th International Conference on Solid-State Sensors, Actuators and Microsystems (TRANSDUCERS)*: IEEE; 2017. pp. 1632-1635.
 213. Wang L, Veselinovic M, Yang L, Geiss BJ, Dandy DS, Chen T. A sensitive DNA capacitive biosensor using interdigitated electrodes. *Biosensors and Bioelectronics* 2017,**87**:646-653.
 214. Cheng C, Oueslati R, Wu J, Chen J, Eda S. Capacitive DNA sensor for rapid and sensitive detection of whole genome human herpesvirus-1 dsDNA in serum. *Electrophoresis* 2017,**38**:1617-1623.
 215. Xu S, Zhan J, Man B, Jiang S, Yue W, Gao S, *et al.* Real-time reliable determination of binding kinetics of DNA hybridization using a multi-channel graphene biosensor. *Nature communications* 2017,**8**:14902.
 216. Tran TL, Nguyen TT, Tran TTH, Tran QT, Mai AT. Detection of influenza A virus using carbon nanotubes field effect transistor based DNA sensor. *Physica E: Low-dimensional Systems and Nanostructures* 2017,**93**:83-86.
 217. Xuan CT, Thuy NT, Luyen TT, Huyen TT, Tuan MA. Carbon nanotube field-effect transistor for DNA sensing. *Journal of electronic materials* 2017,**46**:3507-3511.
 218. Tao W, Lin P, Hu J, Ke S, Song J, Zeng X. A sensitive DNA sensor based on an organic electrochemical transistor using a peptide nucleic acid-modified nanoporous gold gate electrode. *RSC advances* 2017,**7**:52118-52124.
 219. Xu S, Jiang S, Zhang C, Yue W, Zou Y, Wang G, *et al.* Ultrasensitive label-free detection of DNA hybridization by sapphire-based graphene field-effect transistor biosensor. *Applied Surface Science* 2018,**427**:1114-1119.

220. Mei J, Li Y-T, Zhang H, Xiao M-M, Ning Y, Zhang Z-Y, *et al.* Molybdenum disulfide field-effect transistor biosensor for ultrasensitive detection of DNA by employing morpholino as probe. *Biosensors and Bioelectronics* 2018,**110**:71-77.
221. Majd SM, Salimi A, Astinchap B. The development of radio frequency magnetron sputtered p-type nickel oxide thin film field-effect transistor device combined with nucleic acid probe for ultrasensitive label-free HIV-1 gene detection. *Sensors and Actuators B: Chemical* 2018,**266**:178-186.
222. Shariati M. The field effect transistor DNA biosensor based on ITO nanowires in label-free hepatitis B virus detecting compatible with CMOS technology. *Biosensors and Bioelectronics* 2018,**105**:58-64.
223. Tian M, Xu S, Zhang J, Wang X, Li Z, Liu H, *et al.* RNA detection based on graphene field-effect transistor biosensor. *Advances in Condensed Matter Physics* 2018,**2018**.
224. Majd SM, Salimi A, Ghasemi F. An ultrasensitive detection of miRNA-155 in breast cancer via direct hybridization assay using two-dimensional molybdenum disulfide field-effect transistor biosensor. *Biosensors and Bioelectronics* 2018,**105**:6-13.
225. Peng J, He T, Sun Y, Liu Y, Cao Q, Wang Q, *et al.* An organic electrochemical transistor for determination of microRNA21 using gold nanoparticles and a capture DNA probe. *Microchimica Acta* 2018,**185**:408.
226. Bronder TS, Jessing MP, Poghossian A, Keusgen M, Schoning MJ. Detection of PCR-Amplified Tuberculosis DNA Fragments with Polyelectrolyte-Modified Field-Effect Sensors. *Anal Chem* 2018,**90**:7747-7753.
227. Chen Y-W, Tai T-Y, Hsu C-P, Sarangadharan I, Pulikkathodi AK, Wang H-L, *et al.* Direct detection of DNA using electrical double layer gated high electron mobility transistor in high ionic strength solution with high sensitivity and specificity. *Sensors and Actuators B: Chemical* 2018,**271**:110-117.
228. Li S, Huang K, Fan Q, Yang S, Shen T, Mei T, *et al.* Highly sensitive solution-gated graphene transistors for label-free DNA detection. *Biosensors and Bioelectronics* 2019,**136**:91-96.
229. Nguyet NT, Van Thu V, Lan H, Trung T, Le A-T, Pham V-H, *et al.* Simple Label-Free DNA Sensor Based on CeO₂ Nanorods Decorated with Ppy Nanoparticles. *Journal of Electronic Materials* 2019,**48**:6231-6239.
230. Liu J, Chen X, Wang Q, Xiao M, Zhong D, Sun W, *et al.* Ultrasensitive monolayer MoS₂ field-effect transistor based DNA sensors for screening of down syndrome. *Nano letters* 2019,**19**:1437-1444.
231. Bronder TS, Poghossian A, Jessing MP, Keusgen M, Schoning MJ. Surface regeneration and reusability of label-free DNA biosensors based on weak polyelectrolyte-modified capacitive field-effect structures. *Biosens Bioelectron* 2019,**126**:510-517.
232. Tian M, Qiao M, Shen C, Meng F, Frank LA, Krasitskaya VV, *et al.* Highly-sensitive graphene field effect transistor biosensor using PNA and DNA probes for RNA detection. *Applied Surface Science* 2020:146839.
233. Lee C, Lu MS-C. CMOS Ion Sensitive Field Effect Transistors for Detection of DNA Hybridization Under Debye Screen Effect. In: *2020 IEEE 33rd International Conference on Micro Electro Mechanical Systems (MEMS)*: IEEE; 2020. pp. 299-302.
234. Gao J, Gao Y, Han Y, Pang J, Wang C, Wang Y, *et al.* Ultrasensitive Label-free MiRNA Sensing Based on a Flexible Graphene Field-Effect Transistor without Functionalization. *ACS Applied Electronic Materials* 2020,**2**:1090-1098.
235. Deshmukh R, Prusty AK, Roy U, Bhand S. A capacitive DNA sensor for sensitive detection of Escherichia coli O157:H7 in potable water based on the z3276 genetic marker: fabrication and analytical performance. *Analyst* 2020,**145**:2267-2278.
236. Xu C, Cai H, He P, Fang Y. Electrochemical detection of sequence-specific DNA using a DNA probe labeled with aminoferrocene and chitosan modified electrode immobilized with ssDNA. *Analyst* 2001,**126**:62-65.
237. Fan C, Plaxco KW, Heeger AJ. Electrochemical interrogation of conformational changes as a reagentless method for the sequence-specific detection of DNA. *Proc Natl Acad Sci USA* 2003,**100**:9134-9137.
238. Jenkins DM, Chami B, Kreuzer M, Presting G, Alvarez AM, Liaw BY. Hybridization probe for femtomolar quantification of selected nucleic acid sequences on a disposable electrode. *Analytical chemistry* 2006,**78**:2314-2318.
239. Jin Y, Yao X, Liu Q, Li J. Hairpin DNA probe based electrochemical biosensor using methylene blue as hybridization indicator. *Biosens Bioelectron* 2007,**22**:1126-1130.
240. Farjami E, Clima L, Gothelf K, Ferapontova EE. "Off-on" electrochemical hairpin-DNA-based genosensor for cancer diagnostics. *Anal Chem* 2011,**83**:1594-1602.
241. Salamifar SE, Lai RY. Fabrication of electrochemical DNA sensors on gold-modified recessed platinum

- nanoelectrodes. *Anal Chem* 2014,**86**:2849-2852.
242. Qian Y, Tang D, Du L, Zhang Y, Zhang L, Gao F. A novel signal-on electrochemical DNA sensor based on target catalyzed hairpin assembly strategy. *Biosens Bioelectron* 2015,**64**:177-181.
243. Li S, Qiu W, Zhang X, Ni J, Gao F, Wang Q. A high-performance DNA biosensor based on the assembly of gold nanoparticles on the terminal of hairpin-structured probe DNA. *Sensors and Actuators B: Chemical* 2016,**223**:861-867.
244. Zhan F, Liao X, Gao F, Qiu W, Wang Q. Electroactive crown ester-Cu²⁺ complex with in-situ modification at molecular beacon probe serving as a facile electrochemical DNA biosensor for the detection of CaMV 35s. *Biosensors and Bioelectronics* 2017,**92**:589-595.
245. Hong N, Cheng L, Wei B, Chen C, He LL, Ceng J, *et al.* An electrochemical DNA sensor without electrode pre-modification. *Biosensors and Bioelectronics* 2017,**91**:110-114.
246. Lotfi Zadeh Zhad HR, Lai RY. Hexavalent chromium as an electrocatalyst in DNA sensing. *Analytical chemistry* 2017,**89**:13342-13348.
247. Teengam P, Siangproh W, Tuantranont A, Henry CS, Vilaivan T, Chailapakul O. Electrochemical paper-based peptide nucleic acid biosensor for detecting human papillomavirus. *Anal Chim Acta* 2017,**952**:32-40.
248. Li Q, Zhao C, Zheng Z, Weng S, Chen Q, Liu Q, *et al.* A signal-off double probes electrochemical DNA sensor for the simultaneous detection of Legionella and Legionella pneumophila. *Journal of Electroanalytical Chemistry* 2017,**788**:23-28.
249. Liu L, Chang Y, Xia N, Peng P, Zhang L, Jiang M, *et al.* Simple, sensitive and label-free electrochemical detection of microRNAs based on the in situ formation of silver nanoparticles aggregates for signal amplification. *Biosensors and Bioelectronics* 2017,**94**:235-242.
250. Pursey JP, Chen Y, Stulz E, Park MK, Kongsuphol P. Microfluidic electrochemical multiplex detection of bladder cancer DNA markers. *Sensors and Actuators B: Chemical* 2017,**251**:34-39.
251. Liu S, Su W, Li Y, Zhang L, Ding X. Manufacturing of an electrochemical biosensing platform based on hybrid DNA hydrogel: Taking lung cancer-specific miR-21 as an example. *Biosensors and Bioelectronics* 2018,**103**:1-5.
252. Jampasa S, Siangproh W, Laocharoensuk R, Yanatatsaneejit P, Vilaivan T, Chailapakul O. A new DNA sensor design for the simultaneous detection of HPV type 16 and 18 DNA. *Sensors and Actuators B: Chemical* 2018,**265**:514-521.
253. Yammouri G, Mohammadi H, Amine A. A highly sensitive electrochemical biosensor based on carbon black and gold nanoparticles modified pencil graphite electrode for microRNA-21 detection. *Chemistry Africa* 2019,**2**:291-300.
254. Chandra S, Adeloju S. A NEW SENSOR FOR DETECTING MICRORNA 133B (PARKINSON'S DISEASE BIOMARKER). *Sensors International* 2020:100005.
255. Hejazi MS, Raouf JB, Ojani R, Golabi SM, Asl EH. Brilliant cresyl blue as electroactive indicator in electrochemical DNA oligonucleotide sensors. *Bioelectrochemistry* 2010,**78**:141-146.
256. Wang J, Li S, Zhang Y. A sensitive DNA biosensor fabricated from gold nanoparticles, carbon nanotubes, and zinc oxide nanowires on a glassy carbon electrode. *Electrochimica Acta* 2010,**55**:4436-4440.
257. Bo Y, Yang H, Hu Y, Yao T, Huang S. A novel electrochemical DNA biosensor based on graphene and polyaniline nanowires. *Electrochimica Acta* 2011,**56**:2676-2681.
258. Li F, Feng Y, Dong P, Yang L, Tang B. Gold nanoparticles modified electrode via simple electrografting of in situ generated mercaptophenyl diazonium cations for development of DNA electrochemical biosensor. *Biosens Bioelectron* 2011,**26**:1947-1952.
259. Wang L, Wang X, Chen X, Liu J, Liu S, Zhao C. Development of an electrochemical DNA biosensor with the DNA immobilization based on in situ generation of dithiocarbamate ligands. *Bioelectrochemistry* 2012,**88**:30-35.
260. Du M, Yang T, Li X, Jiao K. Fabrication of DNA/graphene/polyaniline nanocomplex for label-free voltammetric detection of DNA hybridization. *Talanta* 2012,**88**:439-444.
261. Shi L, Chu Z, Dong X, Jin W, Dempsey E. A highly oriented hybrid microarray modified electrode fabricated by a template-free method for ultrasensitive electrochemical DNA recognition. *Nanoscale* 2013,**5**:10219-10225.
262. Yola ML, Eren T, Atar N. A novel and sensitive electrochemical DNA biosensor based on Fe@Au nanoparticles decorated graphene oxide. *Electrochimica Acta* 2014,**125**:38-47.
263. Li F, Peng J, Zheng Q, Guo X, Tang H, Yao S. Carbon nanotube-polyamidoamine dendrimer hybrid-modified electrodes for highly sensitive electrochemical detection of microRNA24. *Anal Chem*

- 2015,**87**:4806-4813.
264. Sun Y, He X, Ji J, Jia M, Wang Z, Sun X. A highly selective and sensitive electrochemical CS-MWCNTs/Au-NPs composite DNA biosensor for Staphylococcus aureus gene sequence detection. *Talanta* 2015,**141**:300-306.
265. Hajihosseini S, Nasirizadeh N, Hejazi MS, Yaghmaei P. An electrochemical DNA biosensor based on Oracet Blue as a label for detection of Helicobacter pylori. *Int J Biol Macromol* 2016,**91**:911-917.
266. Su S, Wu Y, Zhu D, Chao J, Liu X, Wan Y, *et al.* On-Electrode Synthesis of Shape-Controlled Hierarchical Flower-Like Gold Nanostructures for Efficient Interfacial DNA Assembly and Sensitive Electrochemical Sensing of MicroRNA. *Small* 2016,**12**:3794-3801.
267. Sukumaran P, Veettil VT, Rajappa S, Li C-Z, Alwarappan S. Ionic liquid modified N-doped graphene as a potential platform for the electrochemical discrimination of DNA sequences. *Sensors and Actuators B: Chemical* 2017,**247**:556-563.
268. Yi X, Lu Z, Kong Y, Chen Z. Label-Free Electrochemical Detection of MicroRNAs via Intercalation of Hemin into the DNA/RNA Hybridization. *Int. J. Electrochem. Sci* 2017,**12**:2813-2821.
269. Gaiji H, Jolly P, Ustuner S, Goggins S, Abderrabba M, Frost CG, *et al.* A Peptide Nucleic Acid (PNA)-DNA Ferrocenyl Intercalator for Electrochemical Sensing. *Electroanalysis* 2017,**29**:917-922.
270. Huang Q, Lin X, Zhu J-J, Tong Q-X. Pd-Au@ carbon dots nanocomposite: Facile synthesis and application as an ultrasensitive electrochemical biosensor for determination of colitoxin DNA in human serum. *Biosensors and Bioelectronics* 2017,**94**:507-512.
271. Aghaei F, Seifati SM, Nasirizadeh N. Development of a DNA biosensor for the detection of phenylketonuria based on a screen-printed gold electrode and hematoxylin. *Analytical Methods* 2017,**9**:966-973.
272. Hui N, Sun X, Niu S, Luo X. PEGylated polyaniline nanofibers: antifouling and conducting biomaterial for electrochemical DNA sensing. *ACS Applied Materials & Interfaces* 2017,**9**:2914-2923.
273. Niu X, Zheng W, Yin C, Weng W, Li G, Sun W, *et al.* Electrochemical DNA biosensor based on gold nanoparticles and partially reduced graphene oxide modified electrode for the detection of Listeria monocytogenes hly gene sequence. *Journal of Electroanalytical Chemistry* 2017,**806**:116-122.
274. Kaplan M, Kilic T, Guler G, Mandli J, Amine A, Ozsoz M. A novel method for sensitive microRNA detection: Electropolymerization based doping. *Biosensors and Bioelectronics* 2017,**92**:770-778.
275. Azimzadeh M, Nasirizadeh N, Rahaie M, Naderi-Manesh H. Early detection of Alzheimer's disease using a biosensor based on electrochemically-reduced graphene oxide and gold nanowires for the quantification of serum microRNA-137. *RSC advances* 2017,**7**:55709-55719.
276. Loo AH, Chua CK, Pumera M. DNA biosensing with 3D printing technology. *Analyst* 2017,**142**:279-283.
277. Rahman M, Heng LY, Futra D, Chiang CP, Rashid ZA, Ling TL. A highly sensitive electrochemical DNA biosensor from acrylic-gold nano-composite for the determination of arowana fish gender. *Nanoscale research letters* 2017,**12**:484.
278. Rahman M, Heng LY, Futra D, Ling TL. Ultrasensitive biosensor for the detection of Vibrio cholerae DNA with polystyrene-co-acrylic acid composite nanospheres. *Nanoscale research letters* 2017,**12**:474.
279. Esmaeili C, Heng LY, Chiang CP, Rashid ZA, Safitri E, Marugan RSPM. A DNA biosensor based on kappa-carrageenan-polypyrrole-gold nanoparticles composite for gender determination of Arowana fish (Scleropages formosus). *Sensors and Actuators B: Chemical* 2017,**242**:616-624.
280. Singhal C, Pundir C, Narang J. A genosensor for detection of consensus DNA sequence of Dengue virus using ZnO/Pt-Pd nanocomposites. *Biosensors and Bioelectronics* 2017,**97**:75-82.
281. Chen M, Su H, Mao L, Guo M, Tang J. Highly sensitive electrochemical DNA sensor based on the use of three-dimensional nitrogen-doped graphene. *Mikrochim Acta* 2017,**185**:51.
282. Chen M, Wang Y, Su H, Mao L, Jiang X, Zhang T, *et al.* Three-dimensional electrochemical DNA biosensor based on 3D graphene-Ag nanoparticles for sensitive detection of CYFRA21-1 in non-small cell lung cancer. *Sensors and Actuators B: Chemical* 2018,**255**:2910-2918.
283. García-Mendiola T, Bravo I, López-Moreno JM, Pariente F, Wannemacher R, Weber K, *et al.* Carbon nanodots based biosensors for gene mutation detection. *Sensors and Actuators B: Chemical* 2018,**256**:226-233.
284. Hua H, Liu Y, Guan X, Li Y. DNA nanosensors based on the use of single gold nanowire electrodes and methylene blue as an intercalator. *Microchimica Acta* 2018,**185**:152.
285. Tian L, Qian K, Qi J, Liu Q, Yao C, Song W, *et al.* Gold nanoparticles superlattices assembly for electrochemical biosensor detection of microRNA-21. *Biosens Bioelectron* 2018,**99**:564-570.

286. Chen M, Su H, Mao L, Guo M, Tang J. Highly sensitive electrochemical DNA sensor based on the use of three-dimensional nitrogen-doped graphene. *Microchimica Acta* 2018,**185**:51.
287. Yuan Y, Xun Z, Zhang B, Guan Y. Electrochemical Signal Enhancer Fabricated Using Lysine-rich Peptide for Ultrasensitive Electrochemical DNA Biosensor Analysis. *Electroanalysis* 2019,**31**:607-610.
288. Ling YP, Heng LY, Chee HY. A quantification strategy for DNA hybridization via measurement of adsorbed anthraquinone monosulphonic acid on silica nanospheres. *Measurement* 2019,**135**:640-650.
289. Gu Y, Tseng P-Y, Bi X, Yang JH. Quantification of DNA by a thermal-durable biosensor modified with conductive poly (3, 4-ethylenedioxythiophene). *Sensors* 2018,**18**:3684.
290. Nazari-Vanani R, Sattarahmady N, Yadegari H, Delshadi N, Hatam GR, Heli H. Electrochemical quantitation of *Leishmania infantum* based on detection of its kDNA genome and transduction of non-spherical gold nanoparticles. *Anal Chim Acta* 2018,**1041**:40-49.
291. Ariffin EY, Lee YH, Futra D, Tan LL, Abd Karim NH, Ibrahim NNN, *et al.* An ultrasensitive hollow-silica-based biosensor for pathogenic *Escherichia coli* DNA detection. *Analytical and bioanalytical chemistry* 2018,**410**:2363-2375.
292. Akbarnia A, Zare HR. A voltammetric assay for microRNA-25 based on the use of amino-functionalized graphene quantum dots and ss-and ds-DNAs as gene probes. *Microchimica Acta* 2018,**185**:503.
293. Wang J, Hui N. Electrochemical functionalization of polypyrrole nanowires for the development of ultrasensitive biosensors for detecting microRNA. *Sensors and Actuators B: Chemical* 2019,**281**:478-485.
294. Song J, Ni J, Wang Q, Chen H, Gao F, Lin Z, *et al.* A planar and uncharged copper(II)-picolinic acid chelate: Its intercalation to duplex DNA by experimental and theoretical studies and electrochemical sensing application. *Biosens Bioelectron* 2019,**141**:111405.
295. Han S, Liu W, Yang S, Wang R. Facile and Label-Free Electrochemical Biosensors for MicroRNA Detection Based on DNA Origami Nanostructures. *ACS Omega* 2019,**4**:11025-11031.
296. Erdem A, Eksin E, Kadikoylu G, Yildiz E. Voltammetric detection of miRNA hybridization based on electroactive indicator-cobalt phenanthroline. *Int J Biol Macromol* 2020,**158**:819-825.
297. Fani M, Rezayi M, Meshkat Z, Rezaee SA, Makvandi M, Angali KA. A Novel Electrochemical DNA Biosensor Based on a Gold Nanoparticles-Reduced Graphene Oxide-Polypyrrole Nanocomposite to detect Human T-Lymphotropic Virus-1. *IEEE Sensors Journal* 2020.
298. Ma W, Du H, Zhang M, Mori J, Ren X, Wang H, *et al.* One-Step Synthesis of Tunable Zinc-Based Nanohybrids as an Ultrasensitive DNA Signal Amplification Platform. *ACS Applied Materials & Interfaces* 2019,**12**:2983-2990.
299. Mahmoodi P, Rezayi M, Rasouli E, Avan A, Gholami M, Mobarhan MG, *et al.* Early-stage cervical cancer diagnosis based on an ultra-sensitive electrochemical DNA nanobiosensor for HPV-18 detection in real samples. *Journal of Nanobiotechnology* 2020,**18**:1-12.
300. Niu X, Chen W, Wang X, Men Y, Wang Q, Sun W, *et al.* A graphene modified carbon ionic liquid electrode for voltammetric analysis of the sequence of the *Staphylococcus aureus* nuc gene. *Microchimica Acta* 2018,**185**:167.
301. Dharuman V, Hahn JH. Label free electrochemical DNA hybridization discrimination effects at the binary and ternary mixed monolayers of single stranded DNA/diluent/s in presence of cationic intercalators. *Biosens Bioelectron* 2008,**23**:1250-1258.
302. Fang Z, Kelley SO. Direct electrocatalytic mRNA detection using PNA-nanowire sensors. *Analytical chemistry* 2009,**81**:612-617.
303. Wipawakarn P, Ju H, Wong DK. A label-free electrochemical DNA biosensor based on a Zr(IV)-coordinated DNA duplex immobilised on a carbon nanofibre|chitosan layer. *Anal Bioanal Chem* 2012,**402**:2817-2826.
304. Lazerges M, Tal VT, Bigey P, Scherman D, Bedioui F. Electrochemical DNA-biosensors: Two-electrode setup well adapted for miniaturized devices. *Sensors and Actuators B: Chemical* 2013,**182**:510-513.
305. Nassi A, Guillon FX, Amar A, Hainque B, Amriche S, Maugé D, *et al.* Electrochemical DNA-biosensors based on long-range electron transfer: optimization of the amperometric detection in the femtomolar range using two-electrode setup and ultramicroelectrode. *Electrochimica Acta* 2016,**209**:269-277.
306. Horny MC, Lazerges M, Siaugue JM, Pallandre A, Rose D, Bedioui F, *et al.* Electrochemical DNA biosensors based on long-range electron transfer: investigating the efficiency of a fluidic channel microelectrode compared to an ultramicroelectrode in a two-electrode setup. *Lab Chip* 2016,**16**:4373-4381.
307. Korri-Youssefi H, Yassar A. Electrochemical probing of DNA based on oligonucleotide-functionalized

- polypyrrole. *Biomacromolecules* 2001,**2**:58-64.
308. Korri-Yousoufi H, Makrouf B. Electrochemical biosensing of DNA hybridization by ferrocenyl groups functionalized polypyrrole. *Analytica Chimica Acta* 2002,**469**:85-92.
309. Cha J, Han JI, Choi Y, Yoon DS, Oh KW, Lim G. DNA hybridization electrochemical sensor using conducting polymer. *Biosensors and Bioelectronics* 2003,**18**:1241-1247.
310. Ramanaviciene A, Ramanavicius A. Pulsed amperometric detection of DNA with an ssDNA/polypyrrole-modified electrode. *Anal Bioanal Chem* 2004,**379**:287-293.
311. Komarova E, Aldissi M, Bogomolova A. Direct electrochemical sensor for fast reagent-free DNA detection. *Biosens Bioelectron* 2005,**21**:182-189.
312. Chen Y, Elling, Lee Y-l, Chong S-c. A Fast, Sensitive and Label Free Electrochemical DNA Sensor. *Journal of Physics: Conference Series* 2006,**34**:204-209.
313. dos Santos Riccardi C, Yamanaka H, Josowicz M, Kowalik J, Mizaikoff B, Kranz C. Label-free DNA detection based on modified conducting polypyrrole films at microelectrodes. *Analytical chemistry* 2006,**78**:1139-1145.
314. Reisberg S, Piro B, Noel V, Pham MC. Selectivity and sensitivity of a reagentless electrochemical DNA sensor studied by square wave voltammetry and fluorescence. *Bioelectrochemistry* 2006,**69**:172-179.
315. Bouchet A, Chaix C, Marquette CA, Blum LJ, Mandrand B. Cylinder-shaped conducting polypyrrole for labelless electrochemical multidetection of DNA. *Biosens Bioelectron* 2007,**23**:735-740.
316. Peng H, Soeller C, Vigar NA, Caprio V, Travas-Sejdic J. Label-free detection of DNA hybridization based on a novel functionalized conducting polymer. *Biosens Bioelectron* 2007,**22**:1868-1873.
317. Tlili C, Jaffrezic-Renault NJ, Martelet C, Korri-Yousoufi H. Direct electrochemical probing of DNA hybridization on oligonucleotide-functionalized polypyrrole. *Materials Science and Engineering: C* 2008,**28**:848-854.
318. Reisberg S, Dang LA, Nguyen QA, Piro B, Noel V, Nielsen PE, *et al.* Label-free DNA electrochemical sensor based on a PNA-functionalized conductive polymer. *Talanta* 2008,**76**:206-210.
319. March G, Noël V, Piro Bt, Reisberg S, Pham M-C. Nanometric layers for direct, signal-on, selective, and sensitive electrochemical detection of oligonucleotides hybridization. *Journal of the American Chemical Society* 2008,**130**:15752-15753.
320. Nie G, Zhang Y, Guo Q, Zhang S. Label-free DNA detection based on a novel nanostructured conducting poly(indole-6-carboxylic acid) films. *Sensors and Actuators B: Chemical* 2009,**139**:592-597.
321. Le HQ, Chebil S, Makrouf B, Sauriat-Dorizon H, Mandrand B, Korri-Yousoufi H. Effect of the size of electrode on electrochemical properties of ferrocene-functionalized polypyrrole towards DNA sensing. *Talanta* 2010,**81**:1250-1257.
322. Tran HV, Piro B, Reisberg S, Anquetin G, Duc HT, Pham MC. An innovative strategy for direct electrochemical detection of microRNA biomarkers. *Anal Bioanal Chem* 2014,**406**:1241-1244.
323. Bouffier L, Wang BS, Roget A, Livache T, Demeunynck M, Mailley P. Electrochemical transduction of DNA hybridization at modified electrodes by using an electroactive pyridoacridone intercalator. *Anal Bioanal Chem* 2014,**406**:1163-1172.
324. Miodek A, Mejri N, Gomgnimbou M, Sola C, Korri-Yousoufi H. E-DNA sensor of Mycobacterium tuberculosis based on electrochemical assembly of nanomaterials (MWCNTs/PPy/PAMAM). *Anal Chem* 2015,**87**:9257-9264.
325. Galan T, Prieto-Simon B, Alvira M, Eritja R, Gotz G, Bauerle P, *et al.* Label-free electrochemical DNA sensor using "click"-functionalized PEDOT electrodes. *Biosens Bioelectron* 2015,**74**:751-756.
326. Tran HV, Nguyen ND, Piro B, Tran LT. Fabrication of a quinone containing layer on gold nanoparticles directed to a label-free and reagentless electrochemical miRNA sensor. *Analytical Methods* 2017,**9**:2696-2702.
327. Yang L, Wang H, Lü H, Hui N. Phytic Acid Functionalized Antifouling Conducting Polymer Hydrogel for Electrochemical Detection of MicroRNA. *Analytica Chimica Acta* 2020.
328. Zhu N, Zhang A, Wang Q, He P, Fang Y. Electrochemical detection of DNA hybridization using methylene blue and electro-deposited zirconia thin films on gold electrodes. *Analytica Chimica Acta* 2004,**510**:163-168.
329. Feng KJ, Yang YH, Wang ZJ, Jiang JH, Shen GL, Yu RQ. A nano-porous CeO(2)/Chitosan composite film as the immobilization matrix for colorectal cancer DNA sequence-selective electrochemical biosensor. *Talanta* 2006,**70**:561-565.
330. Yang J, Jiao K, Yang T. A DNA electrochemical sensor prepared by electrodepositing zirconia on composite films of single-walled carbon nanotubes and poly(2,6-pyridinedicarboxylic acid), and its

- application to detection of the PAT gene fragment. *Anal Bioanal Chem* 2007,**389**:913-921.
331. Yang T, Zhang W, Du M, Jiao K. A PDDA/poly(2,6-pyridinedicarboxylic acid)-CNTs composite film DNA electrochemical sensor and its application for the detection of specific sequences related to PAT gene and NOS gene. *Talanta* 2008,**75**:987-994.
332. Lin L, Chen J, Lin Q, Chen W, Chen J, Yao H, *et al.* Electrochemical biosensor based on nanogold-modified poly-eriochrome black T film for BCR/ABL fusion gene assay by using hairpin LNA probe. *Talanta* 2010,**80**:2113-2119.
333. Jayakumar K, Rajesh R, Dharuman V, Venkatasan R, Hahn JH, Pandian SK. Gold nano particle decorated graphene core first generation PAMAM dendrimer for label free electrochemical DNA hybridization sensing. *Biosens Bioelectron* 2012,**31**:406-412.
334. Wang Q, Gao F, Zhang X, Zhang B, Li S, Hu Z, *et al.* Electrochemical characterization and DNA sensing application of a sphere-like CeO₂-ZrO₂ and chitosan nanocomposite formed on a gold electrode by one-step electrodeposition. *Electrochimica Acta* 2012,**62**:250-255.
335. Xu CX, Zhai QG, Liu YJ, Huang KJ, Lu L, Li KX. A novel electrochemical DNA biosensor construction based on layered CuS-graphene composite and Au nanoparticles. *Anal Bioanal Chem* 2014,**406**:6943-6951.
336. Shahrokhian S, Salimian R, Kalhor HR. A simple label-free electrochemical DNA biosensor based on carbon nanotube-DNA interaction. *RSC advances* 2016,**6**:15592-15598.
337. Torati SR, Reddy V, Yoon SS, Kim C. Electrochemical biosensor for Mycobacterium tuberculosis DNA detection based on gold nanotubes array electrode platform. *Biosens Bioelectron* 2016,**78**:483-488.
338. Ye Y, Gao J, Zhuang H, Zheng H, Sun H, Ye Y, *et al.* Electrochemical gene sensor based on a glassy carbon electrode modified with hemin-functionalized reduced graphene oxide and gold nanoparticle-immobilized probe DNA. *Microchimica Acta* 2017,**184**:245-252.
339. Yammouri G, Mandli J, Mohammadi H, Amine A. Development of an electrochemical label-free biosensor for microRNA-125a detection using pencil graphite electrode modified with different carbon nanomaterials. *Journal of Electroanalytical Chemistry* 2017,**806**:75-81.
340. Bizid S, Blili S, Mlika R, Haj Said A, Korri-Youssoufi H. Direct Electrochemical DNA Sensor based on a new redox oligomer modified with ferrocene and carboxylic acid: Application to the detection of Mycobacterium tuberculosis mutant strain. *Anal Chim Acta* 2017,**994**:10-18.
341. Low SS, Loh HS, Boey JS, Khiew PS, Chiu WS, Tan MTT. Sensitivity enhancement of graphene/zinc oxide nanocomposite-based electrochemical impedance genosensor for single stranded RNA detection. *Biosens Bioelectron* 2017,**94**:365-373.
342. Gao N, Gao F, He S, Zhu Q, Huang J, Tanaka H, *et al.* Graphene oxide directed in-situ deposition of electroactive silver nanoparticles and its electrochemical sensing application for DNA analysis. *Anal Chim Acta* 2017,**951**:58-67.
343. Ribovski L, Zucolotto V, Janegitz BC. A label-free electrochemical DNA sensor to identify breast cancer susceptibility. *Microchemical Journal* 2017,**133**:37-42.
344. Kocak I, Şanal T, Hazer B. An electrochemical biosensor for direct detection of DNA using polystyrene-g-soya oil-g-imidazole graft copolymer. *Journal of Solid State Electrochemistry* 2017,**21**:1397-1405.
345. Zhu D, Liu W, Zhao D, Hao Q, Li J, Huang J, *et al.* Label-free electrochemical sensing platform for microRNA-21 detection using thionine and gold nanoparticles co-functionalized MoS₂ nanosheet. *ACS applied materials & interfaces* 2017,**9**:35597-35603.
346. Asadzadeh-Firouzabadi A, Zare HR. Application of cysteamine-capped gold nanoparticles for early detection of lung cancer-specific miRNA (miR-25) in human blood plasma. *Analytical Methods* 2017,**9**:3852-3861.
347. Senel M, Dervisevic M, Kokkokoğlu F. Electrochemical DNA biosensors for label-free breast cancer gene marker detection. *Analytical and bioanalytical chemistry* 2019,**411**:2925-2935.
348. Mousavisani SZ, Raoof JB, Ojani R, Valiollahi R. Rapid detection of single nucleotide mutation in p53 gene based on gold nanoparticles decorated on graphene nanosheets. *Journal of Chemical Sciences* 2017,**129**:131-139.
349. Karimizefreh A, Mahyari FA, VaezJalali M, Mohammadpour R, Sasanpour P. Impedimetric biosensor for the DNA of the human papilloma virus based on the use of gold nanosheets. *Microchimica Acta* 2017,**184**:1729-1737.
350. Falcone N, She Z, Chen C, Dong B, Yi D, Kraatz H-B. Demonstration of a tailorable and PCR-free detection of Enterococcus DNA isolated from soil samples. *Analytical Methods* 2017,**9**:1643-1649.
351. Tripathy S, Vanjari SRK, Singh V, Swaminathan S, Singh SG. Electrospun manganese (III) oxide

- nanofiber based electrochemical DNA-nanobiosensor for zeptomolar detection of dengue consensus primer. *Biosensors and Bioelectronics* 2017,**90**:378-387.
352. Xu S, Zhang Y, Dong K, Wen J, Zheng C, Zhao S. Electrochemical DNA biosensor based on graphene oxide-chitosan hybrid nanocomposites for detection of Escherichia coli O157: H7. *Int. J. Electrochem. Sci* 2017,**12**:3443-3458.
353. Wang Y, Huang X, Li H, Guo L. Sensitive impedimetric DNA biosensor based on (Nb, V) codoped TiO₂ for breast cancer susceptible gene detection. *Materials Science and Engineering: C* 2017,**77**:867-873.
354. Shariati M, Ghorbani M, Sasanpour P, Karimizefreh A. An ultrasensitive label free human papilloma virus DNA biosensor using gold nanotubes based on nanoporous polycarbonate in electrical alignment. *Analytica Chimica Acta* 2019,**1048**:31-41.
355. Khater M, de la Escosura-Muñiz A, Quesada-González D, Merkoçi A. Electrochemical detection of plant virus using gold nanoparticle-modified electrodes. *Analytica chimica acta* 2019,**1046**:123-131.
356. Kangkamano T, Numnuam A, Limbut W, Kanatharana P, Vilaivan T, Thavarungkul P. Pyrrolidinyl PNA polypyrrole/silver nanofoam electrode as a novel label-free electrochemical miRNA-21 biosensor. *Biosensors and Bioelectronics* 2018,**102**:217-225.
357. Manzano M, Viezzi S, Mazerat S, Marks RS, Vidic J. Rapid and label-free electrochemical DNA biosensor for detecting hepatitis A virus. *Biosens Bioelectron* 2018,**100**:89-95.
358. Hong SA, Kim YJ, Kim SJ, Yang S. Electrochemical detection of methylated DNA on a microfluidic chip with nanoelectrokinetic pre-concentration. *Biosens Bioelectron* 2018,**107**:103-110.
359. Ye Y, Xie J, Ye Y, Cao X, Zheng H, Xu X, *et al.* A label-free electrochemical DNA biosensor based on thionine functionalized reduced graphene oxide. *Carbon* 2018,**129**:730-737.
360. Teengam P, Siangproh W, Tuantranont A, Vilaivan T, Chailapakul O, Henry CS. Electrochemical impedance-based DNA sensor using pyrrolidinyl peptide nucleic acids for tuberculosis detection. *Analytica Chimica Acta* 2018,**1044**:102-109.
361. Lee J, Morita M, Takemura K, Park EY. A multi-functional gold/iron-oxide nanoparticle-CNT hybrid nanomaterial as virus DNA sensing platform. *Biosensors and Bioelectronics* 2018,**102**:425-431.
362. Singhal C, Khanuja M, Chaudhary N, Pundir C, Narang J. Detection of chikungunya virus DNA using two-dimensional MoS₂ nanosheets based disposable biosensor. *Scientific reports* 2018,**8**:1-11.
363. Salahandish R, Ghaffarinejad A, Omidinia E, Zargartalebi H, Majidzadeh AK, Naghib SM, *et al.* Label-free ultrasensitive detection of breast cancer miRNA-21 biomarker employing electrochemical nanogenosensor based on sandwiched AgNPs in PANI and N-doped graphene. *Biosens Bioelectron* 2018,**120**:129-136.
364. Zhu B, Travas-Sejdic J. PNA versus DNA in electrochemical gene sensing based on conducting polymers: study of charge and surface blocking effects on the sensor signal. *Analyst* 2018,**143**:687-694.
365. Boriachek K, Umer M, Islam MN, Gopalan V, Lam AK, Nguyen N-T, *et al.* An amplification-free electrochemical detection of exosomal miRNA-21 in serum samples. *Analyst* 2018,**143**:1662-1669.
366. Gokce ZG, Akalın P, Kok FN, Sarac AS. Impedimetric DNA biosensor based on polyurethane/poly (m-anthranilic acid) nanofibers. *Sensors and Actuators B: Chemical* 2018,**254**:719-726.
367. Congur G, Eksin E, Erdem A. Impedimetric detection of miRNA-34a using graphene oxide modified chemically activated graphite electrodes. *Sensors and Actuators A: Physical* 2018,**279**:493-500.
368. Ebrahimi A, Nikokar I, Zokaei M, Bozorgzadeh E. Design, development and evaluation of microRNA-199a-5p detecting electrochemical nanobiosensor with diagnostic application in Triple Negative Breast Cancer. *Talanta* 2018,**189**:592-598.
369. Shahrokhian S, Salimian R. Ultrasensitive detection of cancer biomarkers using conducting polymer/electrochemically reduced graphene oxide-based biosensor: Application toward BRCA1 sensing. *Sensors and Actuators B: Chemical* 2018,**266**:160-169.
370. Benvidi A, Saucedo NM, Ramnani P, Villarreal C, Mulchandani A, Tezerjani MD, *et al.* Electro-oxidized Monolayer CVD Graphene Film Transducer for Ultrasensitive Impedimetric DNA Biosensor. *Electroanalysis* 2018,**30**:1791-1800.
371. Nguyet NT, Van Thu V, Trung T, Vuong PH, Tam PD. Highly sensitive DNA sensors based on cerium oxide nanorods. *Journal of Physics and Chemistry of Solids* 2018,**115**:18-25.
372. Ehzari H, Safari M, Shahlaei M. A simple and label-free genosensor for BRCA1 related sequence based on electrospun ribbon conductive nanofibers. *Microchemical Journal* 2018,**143**:118-126.
373. Mazloum-Ardakani M, Barazesh B, Khoshroo A, Moshtaghian M, Sheikhha MH. A new composite consisting of electrosynthesized conducting polymers, graphene sheets and biosynthesized gold nanoparticles for biosensing acute lymphoblastic leukemia. *Bioelectrochemistry* 2018,**121**:38-45.

374. Divya KP, Karthikeyan R, Sinduja B, Grace AA, John SA, Hahn JH, *et al.* Carbon dots stabilized silver–lipid nano hybrids for sensitive label free DNA detection. *Biosensors and Bioelectronics* 2019,**133**:48-54.
375. Jaiswal N, Pandey CM, Solanki S, Tiwari I, Malhotra BD. An impedimetric biosensor based on electrophoretically assembled ZnO nanorods and carboxylated graphene nanoflakes on an indium tin oxide electrode for detection of the DNA of Escherichia coli O157: H7. *Microchimica Acta* 2020,**187**:1.
376. Zhang J, Han D, Yang R, Ji Y, Liu J, Yu X. Electrochemical detection of DNA hybridization based on three-dimensional ZnO nanowires/graphite hybrid microfiber structure. *Bioelectrochemistry* 2019,**128**:126-132.
377. Shamsipur M, Samandari L, Taherpour AA, Pashabadi A. Sub-femtomolar detection of HIV-1 gene using DNA immobilized on composite platform reinforced by a conductive polymer sandwiched between two nanostructured layers: a solid signal-amplification strategy. *Analytica chimica acta* 2019,**1055**:7-16.
378. Tripathy S, Joseph J, Pothuneedi S, Das D, Vanjari SRK, Rao AN, *et al.* A miniaturized electrochemical platform with an integrated PDMS reservoir for label-free DNA hybridization detection using nanostructured Au electrodes. *Analyst* 2019,**144**:6953-6961.
379. Salimi A, Kavosi B, Navaee A. Amine-functionalized graphene as an effective electrochemical platform toward easily miRNA hybridization detection. *Measurement* 2019,**143**:191-198.
380. Gong Q, Han H, Yang H, Zhang M, Sun X, Liang Y, *et al.* Sensitive electrochemical DNA sensor for the detection of HIV based on a polyaniline/graphene nanocomposite. *Journal of Materiomics* 2019,**5**:313-319.
381. Xia J, Qing J, Liu J. A sensitive electrochemical impedance DNA biosensor based on ZnO nanorod electrodes for BCR/ABL fusion gene detection. *Int. J. Electrochem. Sci* 2019,**14**:4271-4279.
382. Qian X, Qu Q, Li L, Ran X, Zuo L, Huang R, *et al.* Ultrasensitive electrochemical detection of Clostridium perfringens DNA based morphology-dependent DNA adsorption properties of CeO₂ nanorods in dairy products. *Sensors* 2018,**18**:1878.
383. Kumari P, Adeloju SB. Fabrication of a novel DNA affinity biosensor based on hybridisation induced current by electrostatic repulsion of silicotungstic acid as a redox indicator. *Talanta* 2019,**194**:127-133.
384. Congur G, Erdem A. PAMAM dendrimer modified screen printed electrodes for impedimetric detection of miRNA-34a. *Microchemical Journal* 2019,**148**:748-758.
385. Srisomwat C, Teengam P, Chuaypen N, Tangkijvanich P, Vilaivan T, Chailapakul O. Pop-up paper electrochemical device for label-free hepatitis B virus DNA detection. *Sensors and Actuators B: Chemical* 2020:128077.
386. Hatami Z, Ragheb E, Jalali F, Tabrizi MA, Shamsipur M. Zinc oxide-gold nanocomposite as a proper platform for label-free DNA biosensor. *Bioelectrochemistry* 2020,**133**:107458.
387. Sheta SM, El-Sheikh SM, Osman DI, Salem AM, Ali O, Harraz FA, *et al.* A novel HCV electrochemical biosensor based on a Polyaniline@ Ni-MOF nanocomposite. *Dalton Transactions* 2020.
388. Kang SJ, Kim S, Lee K, Shin I-S, Kim Y-R. Tunable Electrochemical Grafting of Diazonium for Highly Sensitive Impedimetric DNA Sensor. *Journal of The Electrochemical Society* 2020,**167**:087504.

CHAPTER II: Experimental Results

— miRNA Quantification by Optical techniques

Contents

CHAPTER II: Experimental Results.....	132
— miRNA Quantification by Optical techniques	132
LIST OF FIGURES	135
LIST OF TABLES	136
II.1. DNA hybridization studies	137
II.1.1. Ultraviolet method.....	137
II.1.2. The <i>Qubit</i> [®] dsDNA BR Assay	140
References.....	142
II.2. miRNA-21 quantification by RT- qPCR	143
miRNA-21 quantitative detection by Reverse Transcription Realtime Polymerase chain reaction (RT-qPCR): Stem-loop primer RT-qPCR vs Poly (A)-tail extension RT-qPCR	144
Abstract.....	144
Keywords	144
II.2.1. Introduction	145
II.2.2. Experimental	147
II.2.2.1. Material and methods	147
II.2.2.2. cDNA synthesis by stem-loop primer reverse transcription assay or Poly (A)-tail extension reverse transcription assay	147
II.2.2.3. miRNA purification from plasma.....	149
II.2.2.4. Real-time PCR (qPCR) using TaqMan probe	149
II.2.2.5. Absolute quantification of miRNA-21	151
II.2.3. Results and Discussion.....	152
II.2.3.1. Evaluation of the performances of two methods by analyzing miRNA-21 standard solutions in nuclease free water.....	152
II.2.3.2 Analysis of miRNA-21 standard solutions in plasma	158
Conclusions.....	160
References.....	160
Supplementary Information	162
II.3. miRNA-21 quantification by SPR	165
Label-free graphene oxide based-SPR genosensor for the quantification of microRNA21 ..	166
Abstract.....	166

Keywords	166
II.3.1. Introduction	167
II.3.2. Experimental	169
II.3.2.1. Material and methods	169
II.3.2.2. Construction of the biosensing platform	170
II.3.3. Results and Discussion.....	171
II.3.3.1. Construction and characterization of genosensor.....	171
II.3.3.2. Analytical performance of the genosensor	175
Conclusions.....	177
Acknowledgements.....	177
Compliance with ethical standards	177
References.....	178
Conclusion of the Chapter II	180

LIST OF FIGURES

Figure II.1. The ultraviolet absorption spectroscopy of single-stranded and double-stranded DNA (same concentration) [2].....	138
Figure II.2. Ultraviolet absorbance spectrum of different single-stranded DNA and after them mixing. a: DNA probe and DNA target (complementary); b: DNA probe and miRNA-21; c: DNA probe and mismatch DNA target (one base); d: DNA probe and Random DNA target. Detection range is between 225 and 450 nm and resolution set at 1 nm.	139
Figure II.3. the dsDNA concentration in different sample solution varying with time.	141
Figure II.4. Schematic description of TaqMan probe qPCR.	150
Figure II.5. The manuscript protocol for miRNA-21 calibration curve (a) and the protocol for qPCR amplification efficiency curve (b).....	152
Figure II.6. qPCR amplification efficiency curve of stem-loop primer RT-qPCR (a) and poly (A)-tail extension RT-qPCR (b): The logarithm values of serial dilution factor of cDNA versus the corresponding C_t value.....	153
Figure II.7. qPCR calibration curve of different concentration miRNA sample by stem-loop primer RT-qPCR (a) and poly (A)-tail extension RT-qPCR (b). The serial dilution concentration of miRNA-21 (10^{-5} mol L ⁻¹ to 10^{-18} mol L ⁻¹) Log value vs the corresponding C_t value, each point was repeated at least 6 times.	155
Figure II.8. The qPCR amplification efficiency curve (a) and qPCR calibration curve of different concentration miRNA-21 sample in plasma (b) of poly (A)-tail extension RT-qPCR.....	158
Figure II.9. The C_t value of different samples measured by poly (A)-tail extension RT-qPCR.....	159
Figure II.10. Schematic diagram and data analysis of reverse transcription real-time PCR workflow of microRNA using the two methods.	162
Figure II.11. Schematic diagram of two microRNA reverse transcription (RT) methods.....	162
Figure II.12. qPCR amplification efficiency curve of Poly (A)-tail extension RT-qPCR: The logarithm values of serial dilution factor of cDNA that obtained from HCT116 cell line reverse transcription versus the corresponding C_t value, the amplification efficiency was 104.89%.....	163
Figure II.13. qPCR amplification efficiency curve of Poly (A)-tail extension RT-qPCR: The logarithm values of serial dilution factor of cDNA that obtained from plasma A reverse transcription versus the corresponding C_t value, the amplification efficiency is near 0. The plasma was purified by the miRNA purification kit Human Panel A to keep the miRNA-21 in plasma and named plasma A.	163
Figure II.14. The fluorescence amplification plot of miRNA-21 at serial concentration dilutions (from 10^{-8} M to 10^{-16} M) and no template control (NTC), that carried out Poly (A)-tail extension RT-qPCR.....	164
Figure II.15. Scheme for the different steps during the building of the plasmonic microRNA-21 genosensor.	170
Figure II.16. a) Bars plot for the variation of total R_{ct} during the self-assembling of 1.00 mg mL ⁻¹ PDDA (red) and 0.50 mg mL ⁻¹ GO (blue) at Au/MPS platform. The inset shows the Nyquist plots for the two layers of PDDA and two layers of GO as well as the corresponding equivalent circuit. Redox marker, 2.0×10^{-3} M hydroquinone/benzoquinone; EIS parameters: amplitude, 0.010 V, frequency range, 1.0×10^{-2} to 1.0×10^6 Hz; working potential, 0.200 V. b) $\Delta\theta_{SPR}$ calculated from the sensorgram obtained during the consecutive self-assembling of 4 bilayers of 1.00 mg mL ⁻¹ PDDA (red) and 0.50 mg mL ⁻¹ GO (blue). Rinsing solutions:	

0.050 M phosphate buffer solution pH 7.40 before and after self-assembling of PDDA; and 0.100 M NaOH before and after the immobilization of GO.....172

Figure II.17. a) SPR sensorgram obtained during the building of microRNA-21 genosensor: immobilization of MPS at Au (black arrow), PDDA at Au/MPS (red arrow), GO at Au/MPS/PDDA (blue arrow), activation of Au/MPS/(PDDA/GO)₂ with EDC/NHS (green arrow), covalent attachment of DNA probe (pink arrow), quenching with Et (orange arrow), and interaction with microRNA-21 (violet arrow). The inset shows the $\Delta\theta_{\text{SPR}}$ obtained after addition of microRNA-21, used as the analytical signal. b) $\Delta\theta_{\text{SPR}}$ calculated from the sensorgram obtained in a).174

Figure II.18. Calibration plot for microRNA-21 quantification. Each point is an average of three different experiments.175

LIST OF TABLES

Table II.1. DNA and miRNA sample sequences.138

Table II.2. The percentage reduction after hybridization in UV absorbance.139

Table II.3. Comparison of the performance of two miRNA-21 RT-qPCR detection methods.....157

Table II.4. Comparison of the analytical characteristics of the proposed biosensor with the most relevant SPR-based microRNA-21 biosensors reported in the last years.176

II.1. DNA hybridization studies

Nucleic acid molecule hybridization is one of the most basic experimental techniques in nucleic acid research. The process of complementary nucleotide sequences (DNA or RNA) forming a stable hybrid double-stranded DNA molecule through Watson-Crick base pairing is called hybridization. The hybridization process is highly specific, and specific target sequences can be detected based on the known sequences of the probes used. Therefore, hybridization technology has been widely used in the field of molecular biology for the screening of cloned genes, the characterization of specific gene sequences in the genome, quantitative detection, and clinic diagnosis. In this part, we used Ultraviolet method, Qubit® dsDNA BR assay and Qubit® microRNA assay to detect the complementarity of nucleotide sequences probe and target sample (DNA and miRNA-21), ensure that the analysis performance of the genetic biosensors designed subsequently can be truly evaluated.

II.1.1. Ultraviolet method

The ultraviolet absorption spectroscopy is the traditional classical method for quantification oligonucleotide, and one of the most widely used methods to determine the concentration composition (purity) and structure of DNAs and RNAs. Nucleic acids absorb in the ultraviolet region of the spectrum due to the conjugated double bond and ring systems of the constituent purines and pyrimidines. The maximum absorbance of nucleic acids is at the wavelength of 260 nm, so the absorbance of DNAs and RNAs at 260nm is measured, and then use it to determine the concentration of nucleotides by using the Beer–Lambert law ($A = \epsilon \cdot C \cdot l$) in conjunction with the molar extinction coefficient (ϵ) of constituent nucleotides. Where A is absorbance, l is the path length, and C is the analyte concentration.

Double-stranded DNA (dsDNA) absorbs less UV light than denatured single-stranded (ssDNA) DNA due to the stacking interactions between the bases, it is called the hypochromic effect which is attributed to the hydrogen bonds between the paired bases in the double helix limits the resonance behavior of the aromatic ring of the bases which results in decrease in the UV

absorbance of dsDNA [1]. In this part, the absorbance of ssDNA and dsDNA is measured by ultraviolet spectrophotometry to evaluate the complementarity degree between the probe and the target (Figure II.1), which the dsDNA is obtained by mixing the same concentration of ssDNA probe with different single-stranded targets (T, miRNA-21, mT and rT, Table II.1) thus provide evidence for subsequent electrochemical detection.

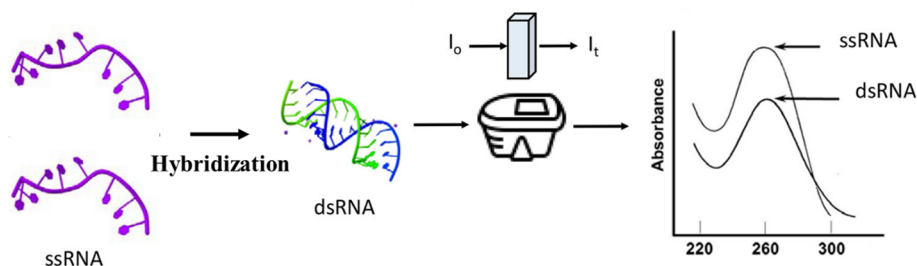


Figure II.1. The ultraviolet absorption spectroscopy of single-stranded and double-stranded DNA (same concentration) [2].

Table II.1. DNA and miRNA sample sequences.

Name	Sequence
DNA probe (P)	1-DTPA-5' TCA ACA TCA GTC TGA TAA GCT A 3'
DNA target (T)	5' TAG CTT ATC AGA CTG ATG TTG A 3'
miRNA-21	5' UAG CUU AUC AGA CUG AUG UUG A 3'
mismatch DNA target (mT)	5' TAG CTT ATC A CA CTG ATG TTG A 3'
Random DNA target (rT)	5' CAG TCG TAA GCT CTG AGT CTA T 3'

Prepare $3.0 \times 10^{-6}M$ and $6.0 \times 10^{-6}M$ with two different concentrations of single-stranded DNA probe (P), DNA target (T), miRNA-21, mismatch DNA target (mT) and random DNA target (rT) in 0.5M NaCl. Then, the UV absorption of four kinds of single-stranded DNA with a concentration of $3.0 \times 10^{-6}M$ from 225nm to 400nm was recorded. In addition, 300 μL of the probe with a concentration of $5.52 \times 10^{-6}M$ was mixed with 300 μL of different targets with a concentration of $5.52 \times 10^{-6}M$, and then statically reacted for 30 minutes before UV measurement. The measurement results are shown in the Figure II.2.

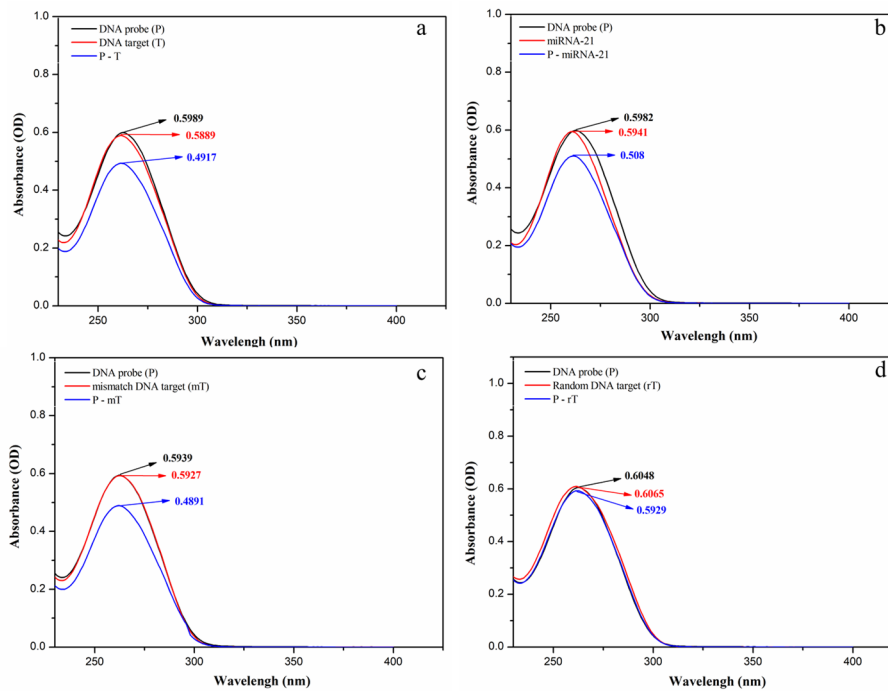


Figure II.2. Ultraviolet absorbance spectrum of different single-stranded DNA and after them mixing. a: DNA probe and DNA target (complementary); b: DNA probe and miRNA-21; c: DNA probe and mismatch DNA target (one base); d: DNA probe and Random DNA target. Detection range is between 225 and 450 nm and resolution set at 1 nm.

Table II.2. The percentage reduction after hybridization in UV absorbance.

Sample (Targets)	The percentage reduction of after hybridization in UV absorbance	
	$1 - (A_{\text{after hybridization}} / [(A_{\text{ss-DNAp}} + A_{\text{ss-DNAt}}) / 2])$	
DNA target (T) (Complementary)	17.2%	
miRNA-21	14.79%	
mismatch DNA target (mT) (one mismatch)	17.56%	
Random DNA target (rT)	2.11%	

According to the hypochromic effect, the UV absorbance of double stranded DNA (or RNA) is lower than the single stranded shape, it also means that this property was allowed to judge the hybridization of two single-stranded DNA. The Figure II.2 shows ultraviolet absorption spectroscopy of single-stranded DNA probe (P), different kinds of single-stranded DNA target (T, miRNA-21, mT and rT) and the mixture products of DNA probe with different all kinds of DNA targets.

For the comparison, all samples are measured at the same concentration. Compared with the single-stranded DNA probe and target, the UV absorbance spectra are basically the same, when the target are the DNA target (T) (Figure II.2a), miRNA-21 (Figure II.2b) and mismatch DNA target (mT) (Figure II.2c), the UV absorption reduced after they were mixed with DNA probe. This phenomenon indicates that a hybrid event has occurred. From the Figure II.2d, when the target is random DNA (rT), there is almost no change in UV absorbance after mixing. It is further proved that the previous three targets mixed with probe have hybridization events and can use to establish and evaluate the electrochemical gene sensor platform. Table II.2 shows the percentage reduction of after mixing different target with probe in UV absorbance. The percentage decrease in UV absorbance when the target is miRNA-21 was lower than the other two targets, it may be due to the instability of miRNA, which is partially hydrolyzed. Moreover, the reduce percentage in UV absorbance was basically same when the target both are complementary DNA target and one mismatch DNA target, which illustrates that the UV spectrophotometry method cannot distinguish one mismatched DNA target.

Although The ultraviolet absorption spectroscopy is commonly used but it is not selective and cannot distinguish DNA, RNA, or protein. Values are easily affected by other contaminants (e.g. free nucleotides, salts, and organic compounds) and variation in base composition. In addition, the sensitivity of spectrophotometry is often inadequate, prohibiting quantitation of DNA and RNA at low concentrations. For overcoming these shortcomings, the fluorescence method has become another commonly used method, it distinguishes single-stranded and double-stranded DNA and RNA more sensitively and specifically, based on the specific binding of fluorescent dyes to double-stranded DNA or RNA. Therefore, we used commercial fluorescent kits to monitor the hybridization process of DNA probe with different targets (T, miRNA-21, mT, rT).

II.1.2. The *Qubit*[®] dsDNA BR Assay

The *Qubit*[®] dsDNA (broad range) BR Assay Kits (*ThermoFisher, life technologies, Q32850*) containing fluorescent dyes that bind selectively to double-stranded DNA is used to monitor

the hybridization process of DNA probe with different types of DNA targets respectively. The fluorescence value was recorded by using *Qubit*[®] 2.0 Fluorometer (*ThermoFisher, life technologies*, Q32866), which the fluorescence can convert to dsDNA concentration then recorded directly. For each assay, the new calibration should be run by using standard#1 and standard#2 solution which were prepared according to the instruction. Then use *Qubit*[®] Assay buffer to diluted all single-stranded DNA, miRNA-21 to 1 μ g/mL, and prepared different mixed solutions with 1 μ g/mL DNA probe and different 1 μ g/mL different targets in different tubes. Then recorded the concentration of dsDNA every 10 minutes, and its concentration is directly converted from fluorescence value by *Qubit*[®] 2.0 Fluorometer.

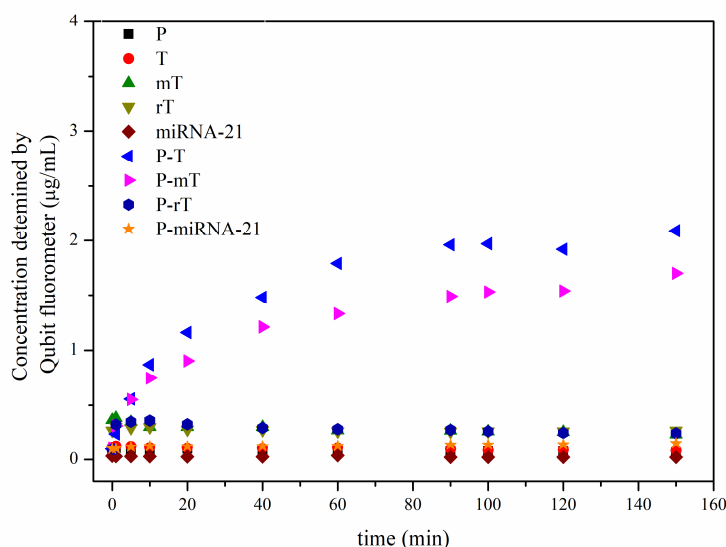


Figure II.3. the dsDNA concentration in different sample solution varying with time.

Figure II.3 shows the dsDNA concentration in different sample solution varying with time. The value of only contain ssDNA or ssmiRNA-21 solution is basically 0 and does not change with time. However, for different mixed samples the value also does not change with time, except for the mixed solution of DNA probe with complementary DNA target and DNA probe with mismatch DNA probe. The value reached the plateau when the hybridization time reaches 90 minutes. This indicates that in the two mixed solutions, dsDNA derived from the crossover event was produced. Because fluorescent dyes can selectively bind to double-stranded DNA,

fluorescence increases with the amount of double-stranded DNA.

An interesting phenomenon is that when the target is mismatch DNA (one base), the fluorescence was lower than when the target is complementary DNA at the same time. And when the target is the random DNA there is no hybridization took place because of the fluorescence almost near 0 and never changed.

References

1. HISATOME M, MARUYAMAN, IKEDA K, FURUTERA T, ISHIKAWA T, YAMAKAWA K. Synthesis and some spectroscopic properties of porphyrin derivatives connected with nucleobases (adenine, thymine, guanine and cytosine) by alkanamide chains. *Chemical and pharmaceutical bulletin* 1996,**44**:1801-1811.
2. Nwokeoji AO, Kilby PM, Portwood DE, Dickman MJ. Accurate quantification of nucleic acids using hypochromicity measurements in conjunction with UV spectrophotometry. *Analytical chemistry* 2017,**89**:13567-13574.

II.2. miRNA-21 quantification by RT- qPCR

RT-qPCR detection method is the gene (miRNA) gold standard quantitative detection, the detection is carried out conventionally by a preliminary step of reverse transcription and amplification of their concentration by polymerase chain reaction (PCR) followed by a fluorescence measurement to quantify. The principle is to add a fluorescent dye or fluorescent molecule-labeled oligonucleotide chain (TaqMan probe) to the PCR system. Then recording fluorescence signal to monitor the amount of the target gene, and infer the initial amount of the target gene based on this. It has the advantages of real-time monitoring of the number of nucleic acid and high sensitivity.

This section presented the method of quantifying miRNA-21 using reverse transcription real-time polymerase chain reaction (RT-qPCR) method to quantify miRNA-21, and discussed and compared the performance of two RT-qPCR methods for miRNA-21 analysis. One is stem-loop primer reverse transcription, and the other is poly(A)-tail extension method.

I contributed the experiment of this section which carried out in the Equipe labellisée Ligue Nationale Contre le Cancer, Paris Descartes University, Paris University, France

I wrote the first draft of all parts which was discussed and revised with the supervisors.

Thanks to the guidance and help from *Philippe Nizard* and *Valérie Taly* for this section experiment.

miRNA-21 quantitative detection by Reverse Transcription Real-time Polymerase chain reaction (RT-qPCR): Stem-loop primer RT-qPCR vs Poly (A)-tail extension RT-qPCR

Y. Zhang^a, P. Nizard^b, S. Griveau^a, V. Taly^b, F. Bedioui^{a,}, M. Lazerges^c, C. Slim^a*

^a Institute of Chemistry for Life and Health Sciences, Synthesis, Electrochemistry, Imaging and Analytical Systems for Diagnosis Team, Paris-Sciences-et-Lettres, CNRS, Chimie ParisTech, 11 rue Pierre et Marie Curie, 75005 Paris, France.

^b Faculté des Sciences Fondamentales et Biomédicales, Université de Paris, Translational Research & Microfluidics, UMRS1147 CNRS, 12 rue de l'Ecole de Médecine, 75006 Paris, France.

^c Faculté de Pharmacie de Paris, Faculté de Santé, Université de Paris, 4 avenue de l'Observatoire, 75006 Paris, France.

Abstract

Level of expression of miRNAs in tissues indicates a variety of diseases and their progressions. Although different methods have been developed to quantify miRNAs. Quantitative PCR remain the classic method, regarded as the reference for validating other methods. In this work, sensitive and selective miRNA-21 detection was evaluated using two methods: stem-loop primer RT-qPCR and poly (A)-tail extension RT-qPCR. Purified plasma was used to simulate the real biological environment in order to generate a calibration curve for miRNA-21: the dynamic range was between 10^{-8} M and 10^{-16} M, the LOD and LOQ were respectively 0.87aM and 1.85aM. Finally, the expression level of mature miRNA-21 was profiled using the human colon cancer 116 cell line.

Keywords

Diagnosis, miRNA-21, RT-qPCR, Stem-loop, Poly(A) tail, colon cancer

II.2.1. Introduction

microRNAs (miRNAs) are a class of endogenous non-coding RNAs found in eukaryotes with regulatory functions. They are approximately 20 nucleotides in length. Since *Lee et al.* have discovered first the miRNA gene *lin-4* in 1993 by studying the developmental timing of nematode [1], many research has focused on miRNAs. Mature miRNAs are produced by a series of long primary transcripts through a series of nuclease cleavage processing, and then assembled into RNA-induced silencing complex (RISC) which recognizes the target mRNA through base complementation and guide the silencing complex to degrade the target mRNA or inhibit the translation of the target mRNAs to direct important cellular processes based on the extent of base pairing [2]. They are involved in almost all physiological processes, such as development proliferation, apoptosis, differentiation, immune responses and metabolism.

Recent numerous researches have established that miRNA is a promising biomarker in the treatment of cancer, diagnosis and prognosis, it regulates gene expression at the post-translational level. miRNAs are abnormally expressed in tissues and serum of patients with different types of malignant tumors. Although the majority of miRNAs are found intracellularly, a significant number of miRNAs are found to be stable outside the cell, including in serum and other various body fluids [3-6]: secreted miRNAs are packaged in lipid vesicles or a complexes with RNA-binding protein, which prevent miRNAs degradation [7, 8]. In addition, the plasma, serum and body fluids are easy to access allowing noninvasive clinical diagnosis [9]. It has been demonstrated that miRNA-21 is a carcinogenic miRNA, it is encoded by a single gene which is mapped to chromosome 17q23.2 [10]. Unlike some other selectively expressed miRNAs, miRNA-21 is universally expressed in mammal organ systems such as the heart, the spleen, the small intestine and the colon [10]. Tumors occur as a result of downregulation of cancer suppressor genes and overexpression of oncogenes [11]. Many studies have identified that miRNA-21 can control the occurrence and progression of cancer by upregulating its expression in various types of tumors [11]. It exhibits high expression levels in solid tumors, including head and neck neoplasms, esophageal, gastric, pancreatic, lung, liver, breast and

prostatic cancer [12-14].

RT-qPCR is the classical quantitative method for miRNAs detection and quantification. It is regarded as a gold standard of nucleic acid quantification and widely used in clinical diagnosis due to the high specificity and sensitivity [15-17], which mainly contains two step: reverse transcription (RT) and real-time PCR (qPCR). One of the key aspects is to synthesize cDNA through the reverse transcription step to obtain a stable qPCR step template. However, the miRNA fragment is too short to bind properly to the primer, so it is necessary to extend the cDNA product sequence to perform the qPCR step. Currently, there are two techniques for cDNA extension: stem-loop primer reverse transcription assay and poly (A)-tail extension reverse transcription assay.

Stem-loop primer reverse transcription assay uses a specific stem-loop primer to extend the 3' end of the target miRNA to produce an extension cDNA template [18-20]. The front portion of the primer can be hybridized with the 3' end of miRNA target and then the complete reverse transcription to cDNA with reverse transcriptase, then, during the annealing process, the stem-loop structure unfolds to obtain the increased sequence downstream of the miRNA [21, 22]. The poly (A)-tail extension reverse transcription assay extends the miRNA by adding an adenosine tail to the 3' end of the target miRNA under the action of poly (A) polymerase, then using a universal primer to bind to the 3' poly (A) tail and perform reverse transcription with the participation of reverse transcriptase to generate a cDNA template [23-25]. Finally, the cDNA obtained from both stem-loop primer reverse transcription or poly (A)-tail extension method is amplified by a specific couple of forward and reverse primers in the presence of a specific dye-labeled probe.

At present, no literature has studied the application of these two methods for the detection of miRNA-21, nor their analytical performances. In this study, RT-qPCR analysis based on stem-loop primer reverse transcription assay and poly (A)-tail extension reverse transcription assay were first compared, the technique with lower LOD and the larger dynamic range was then use to analyze the expression level of miRNA-21 in the human colon cancer 116 cell line.

II.2.2. Experimental

II.2.2.1. Material and methods

Synthetic miRNA-21 (Thermo Fisher Scientific, France), miRNA purification kit Human Panel A (Thermo Fisher Scientific, France, TaqMan[®], #4473087), miRNA purification kit Human Panel B (Thermo Fisher Scientific, France, TaqMan[®], #4473088), microRNA reverse transcription kit (Thermo Fisher Scientific, France, TaqMan[®], #4366596), stem-loop reverse transcription primer (Thermo Fisher Scientific, France, TaqMan[®] microRNA assay, #4427975), universal master mix II (No UNG, Thermo Fisher Scientific, France, TaqMan[™], # 4440043), microRNA forward PCR primer, reverse PCR primer and TaqMan[®] MGB probe mixture comes from TaqMan[®] microRNA assay (Thermo Fisher Scientific, France, #4427975) and TaqMan[®] advanced microRNA assay (Thermo Fisher Scientific, France, #A25576), advanced miRNA cDNA synthesis kit (Thermo Fisher Scientific, France, TaqMan[®], #A28007), Fast Advanced Master Mix (Thermo Fisher Scientific, France, TaqMan[®], 4444556), plasma sample (healthy donor from Etablissement Français du Sang), human colon cancer 116 cell line from Translational Research & Microfluidics team (Université de Paris).

II.2.2.2. cDNA synthesis by stem-loop primer reverse transcription assay or Poly (A)-tail extension reverse transcription assay.

Both stem-loop primer reverse transcription assay and poly (A)-tail extension reverse transcription assay were used to perform the reverse transcription of miRNA-21. Reactions were performed on a thermal cycler (*CI1000touch*, Thermo Fisher Scientific, BIORAD, France) according to the manufacturer's instructions, then the converted cDNA was used to perform qPCR. The rest of the cDNA was stored at -20 °C.

Preparation of miRNA samples. The miRNA-21 sample was serially diluted in nuclease-free water by 10-fold from 10^{-5} mol L⁻¹ to 10^{-18} mol L⁻¹. The diluted miRNA-21 solutions and non-template control (NTC) solutions were submitted to reverse transcription by a stem-loop primer reverse transcription assay and poly (A)-tail extension reverse transcription assay. The qPCR

assays were carried out in triplicate with all the cDNA sample and blank to quantify miRNA-21.

Stem-loop primer reverse transcription assay. MicroRNA reverse transcription kit are for use with the stem-loop primer reverse transcription primer to convert miRNA-21 to cDNA. The 15 μ L total volume of each RT reaction contains 5 μ L different known concentration miRNA-21 template, 0.15 μ L dNTPs with dTTP (100 mmol L⁻¹), 1 μ L multiscribeTM reverse transcriptase (50 units/ μ L), 1.5 μ L reverse transcription buffer (10X), 0.19 μ L RNase inhibitor (20 units/ μ L), 4.16 μ L Nuclease-free water and 3 μ L stem-loop RT primer (5X). The RT reactions carried out in the thermal cycler at 16 °C for 30 minutes to anneal primers, followed at 42 °C for 30 minutes for the extension phase, then at 85 °C for 5 minutes to block the activity of the reverse transcriptase. All RT reactions included different concentration miRNA-21 template and non-template controls (NTC).

Poly (A)-tail extension reverse transcription assay. Advanced miRNA cDNA synthesis kit is used to extend the length of miRNA through poly (A)-tail extension reverse transcription assay. Each reaction tube contains 2 μ L different known concentration miRNA-21 template, 0.5 μ L poly (A) buffer (10X), 0.5 μ L ATP, 0.3 μ L poly (A) enzyme and 1.7 μ L nuclease free water. The poly (A) tailing reaction performs in the thermal cycler at 37 °C for 45 minutes to add a 3'-adenosine tail to the miRNA by poly (A) polymerase then increased the temperature to 65 °C for 10 minutes to stop the reaction. Followed modifying the 5' end of miRNA with adding adaptor, added 4.5 μ L PEG 8000 (50%), 0.6 μ L ligation adaptor (25X), 1.5 μ L RNA ligase, 3 μ L DNA ligase buffer (5X) and 0.4 μ L nuclease free water to each reaction tube containing the miRNA that with poly (A) tail and undergoes adaptor ligation at the 16 °C for 60 minutes, the adaptor acts as the forward-primer binding site for the miR-Amp reaction. The modified miRNA with the addition of a poly (A) tail on the 3' end and an adaptor on the 5' end was used for reverse transcription (RT) reaction, transferred the RT reaction mix containing 1.2 μ L dNTP Mix, 1.5 μ L universal RT primer (20X), 3 μ L RT enzyme mix (10X), 6 μ L RT buffer (5X) and 3.3 μ L nuclease free water to each reaction tube containing the adaptor ligation

reaction product, the mixture solution performed the reverse transcription reaction step at 42 °C for 15 minutes, a universal RT primer binds to the 3' poly (A) tail and the modified miRNA is reverse transcribed under the action of RT enzyme, then at 85 °C for 5 minutes to stop the RT reaction. The miR-Amp reaction was followed to increase the number of cDNA molecules, 5 µL of the RT reaction products transferred to the miR-Amp reaction mix that contains 25 µL miR-Amp master mix (2X), 2.5 µL miR-Amp primer mix (20X) and 17.5 µL nuclease free water, placed the tubes into the thermal cycle and incubated at 95 °C for 5 minutes to activate the enzyme, followed by running amplification of 14 cycles at 95 °C for 3 seconds, 60 °C for 30 seconds, in the end at 99 °C for 10 minutes to stop the reaction. The miR-Amp reaction product proceed to performing the real-time PCR and the rest were stored at -20 °C.

II.2.2.3. miRNA purification from plasma

miRNAs from healthy donor plasma were purified by the miRNA ABC purification kit, this kit allowed to purify miRNA from plasma using functionalized magnetic beads which were functionalized with complementary sequences to catch specific miRNAs. There are two kinds of kits: Human panel A and Human panel B, each panel can catch more than 300 different miRNAs. Human Panel A allows to purify the miRNA-21 from plasma and named plasma A. While, Human Panel B is contrary of Panel A, and can purify another part of miRNAs, which does not contain miRNA-21. The plasma that purified with Panel B was named plasma B, which is used as the real biological environment and the miRNA-21 templates of different concentrations are added to make a calibration curve of miRNA-21 in plasma by RT-qPCR.

II.2.2.4. Real-time PCR (qPCR) using TaqMan probe

All the qPCRs of both the stem-loop primer RT-qPCR and poly (A)-tail extension RT-qPCR were carried out on the 7500 fast real-time PCR system (Applied Bioscience), cDNA samples obtained by reverse transcription of all miRNA templates were amplified by qPCR and quantitative fluorescence analysis by using *TaqMan*[®] MGB probe (Figure II.4). *TaqMan*[®] MGB probe complementary to miRNA sequence for specific detection, the 5' end of the probe linked

a reporter dye (FAM™ dye) and the 3' end of the probe linked a nonfluorescent quencher (NFQ) and a minor groove binder (MGB). MGB group modified probe increases the melting temperature without increase probe length, which allows the design of shorter probes. In addition, the fluorescence of reporter dye is quenched by the NFQ dye when the probe is intact, but during PCR, the DNA polymerase cleaves probe that hybridized to the cDNA and separates the reporter dye and NFQ dye results in increased fluorescence of the reporter which monitor each PCR cycle and quantified cDNA.

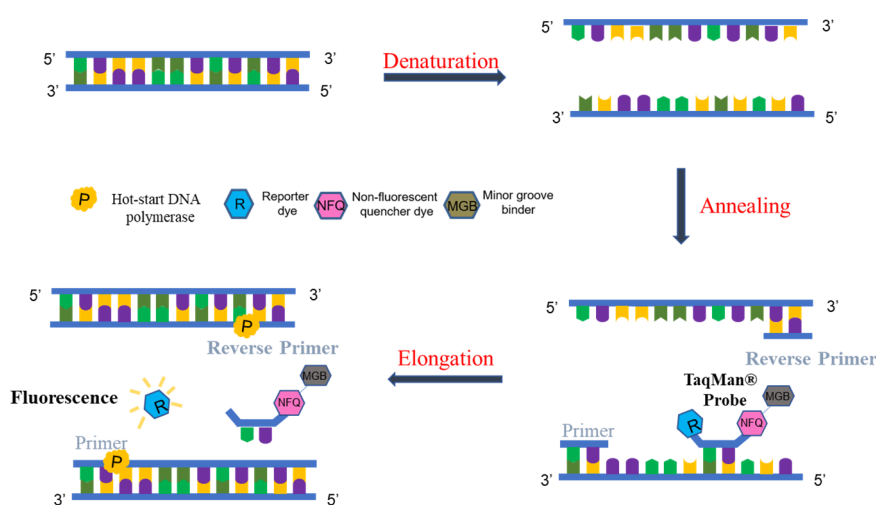


Figure II.4. Schematic description of TaqMan probe qPCR.

For qPCR of stem-loop primer RT-qPCR, the final qPCR reaction volume was 20 μL consisting of 1.33 μL RT products cDNA, 1 μL microRNA forward PCR primer, reverse PCR primer and TaqMan® MGB probe mixture (20X) comes from the TaqMan® microRNA assay components, 10 μL universal master mix II (2X, no UNG) and 7.67 μL nuclease free water, the reaction plate was loaded into the qPCR instrument with an initial enzyme activation step at the 95 °C for 2 minutes, followed by 40 cycles of 95 °C for 15 seconds to denature, at 60 °C for 60 seconds to anneal and elongate.

For qPCR of poly (A)-tail extension RT-qPCR, a final reaction volume of 20 μL consisting of 10 μL fast advanced master mix (2X), 1 μL microRNA forward PCR primer, reverse PCR primer and TaqMan® MGB probe mixture (20X) comes from the *TaqMan*® advanced

microRNA assay, 4 μL nuclease free water and 5 μL RT products of 1:10 dilution, placed the plate into the qPCR instrument with the following conditions: one enzyme activation step at 95 $^{\circ}\text{C}$ for 20 seconds, followed by running 40 cycles consisting of denaturing at 95 $^{\circ}\text{C}$ for 3 seconds and annealing and elongation at 60 $^{\circ}\text{C}$ for 30 seconds.

Fluorescence amplification curves recorded from the *TaqMan*[®] microRNA assays and *TaqMan*[®] advanced microRNA assays were analyzed using SDS 2.4 software.

II.2.2.5. Absolute quantification of miRNA-21

Absolute quantification determines the actual concentration of miRNA-21 target by relating the threshold cycle (C_t) value to a calibration curve based on the miRNA-21 dilution and not cDNA dilution (Figure II.5a). The miRNA-21 template was serially diluted in nuclease-free water by 10-fold (from 10^{-5} to 10^{-18} mol L^{-1} and a non-template control (NTC)) and all dilution points were carried out reverse transcription separately to cDNA before qPCR by both stem-loop primer RT-qPCR and poly (A)-tail extension RT-qPCR. During the qPCR procedure, the amplification efficiency is important in absolute quantification, which determined from the cDNA calibration curve from a serial dilution of a single RT product (Figure II.5b). In the protocol, the cDNA obtained from the reverse transcription of 10^{-9} mol L^{-1} miRNA was selected for 10-fold serial dilution and then run a qPCR. cDNA calibration curve was generated by plotting the logarithm values of serial dilution factor of cDNA on the X-axis and the corresponding C_t values on the Y-axis, C_t values in each dilution were measured in triplicate. From the slope of each calibration curve, PCR amplification efficiency (E) was calculated according to the Equation [26, 27]:

$$E = 10^{(-1/\text{slope})} - 1 \quad (1)$$

The calibration curve of miRNA-21 of the two methods and was obtained by plotting the C_t values (on the Y-axis) as a function of the logarithm values of serial dilution concentrations of

miRNA-21 template (on the X-axis). C_t values in each dilution were measured in triplicate. Theoretically, the PCR amplification efficiency should be 100% (the slope of calibration curve is -3.3) during the exponential phase in the amplification curve, meaning that polymerase enzyme is working at maximum capacity and that all the target sequence double during each replication cycle reference.

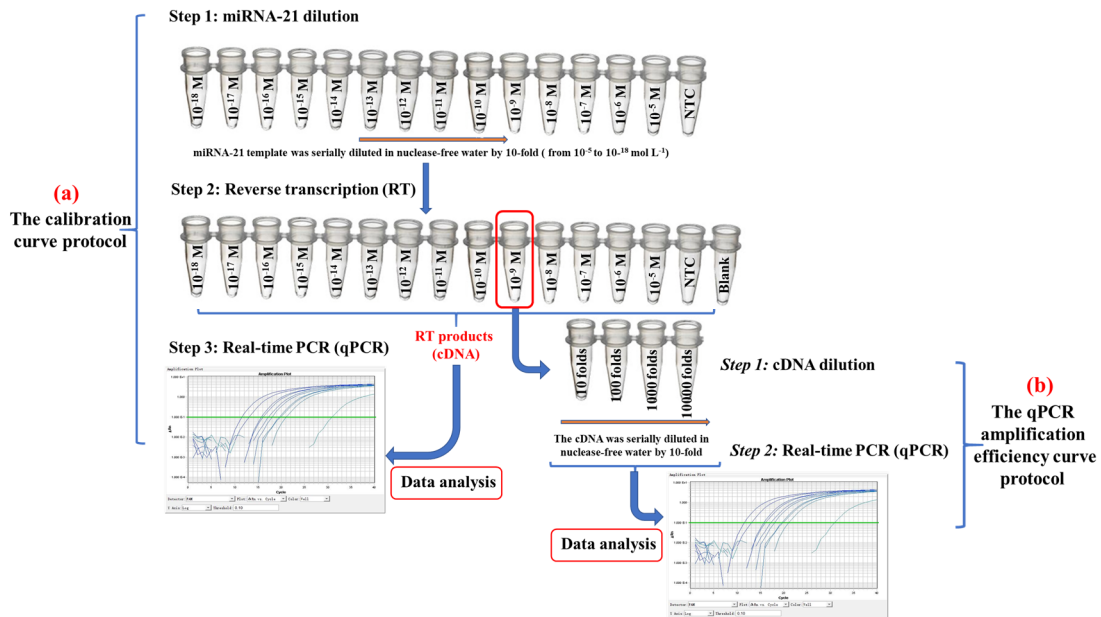


Figure II.5. The manuscript protocol for miRNA-21 calibration curve (a) and the protocol for qPCR amplification efficiency curve (b).

II.2.3. Results and Discussion

II.2.3.1. Evaluation of the performances of two methods by analyzing miRNA-21 standard solutions in water

The sensitivity of miRNA-21 quantification by using stem-loop primer RT-qPCR and poly (A)-tail extension RT-qPCR (Figure II.) were evaluated by establishing calibration curve of miRNA-21. In our manuscript protocol, the calibration curve was based on miRNA-21 dilution and not cDNA, all dilution miRNA points were reverse transcribed separately before being amplified for each miRNA (Figure II.5a). The amplification efficiency of qPCR step was

determined from the calibration curve, which result from a serial dilution of one RT product, during our protocol, the concentration of 10^{-9} mol L⁻¹ was chosen to dilute (Figure II.5b). The amplification efficiency of the calibration curve does not only reflect the specificity of qPCR primers but also the efficiency of the RT to convert RNA into cDNA.

1). PCR amplification efficiency for stem-loop primer RT-qPCR and poly (A)-tail extension RT-qPCR.

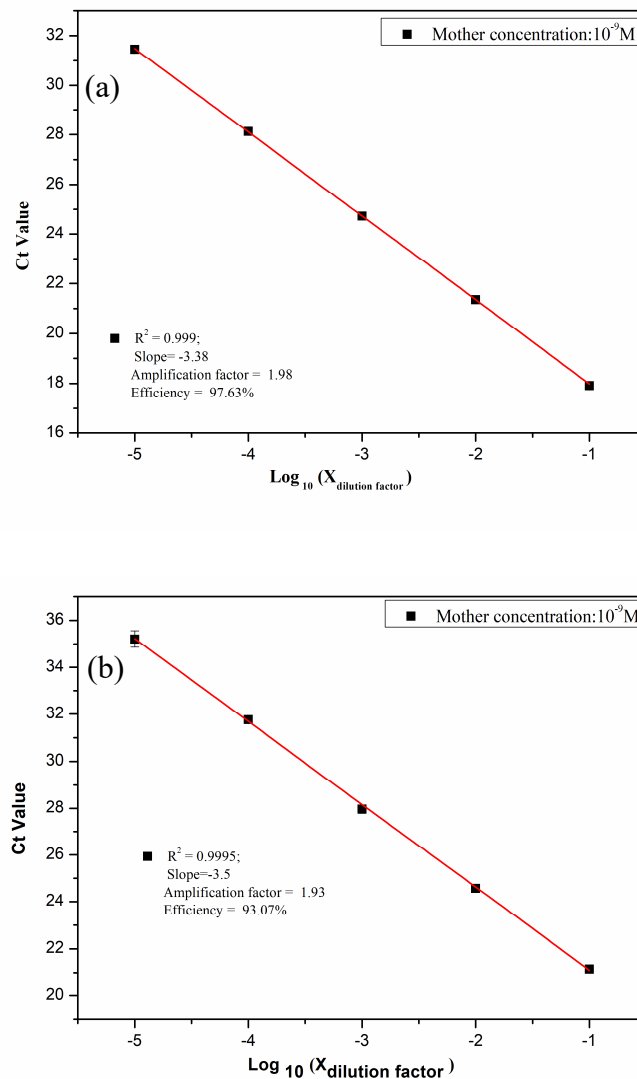


Figure II.6. qPCR amplification efficiency curve of stem-loop primer RT-qPCR (a) and poly (A)-tail extension RT-qPCR (b): The logarithm values of serial dilution factor of cDNA versus the corresponding

C_t value.

In order to ensure the effectiveness of amplification of cDNA by reverse transcription of miRNA-21 in the qPCR step, the cDNA obtained by reverse transcription of miRNA-21 with a concentration of 10^{-9} mol L⁻¹ was serially diluted 5 points with a 10-fold dilution gradient to generate the calibration curve of qPCR amplification efficiency. Then the qPCR reaction was carried out together with cDNA of different concentrations obtained by reverse transcription of other miRNA-21 with different concentrations. Figure II.6. shows the calibration curve of qPCR amplification efficiency, in *TaqMan*[®] microRNA assays (Figure II.6a) and in *TaqMan*[®] advanced microRNA assays (Figure II.6b), with the logarithmic value of the dilution factor as the X-axis, and the corresponding C_t value plotted on the Y-axis. From the Figure II.7. The linear relationship of the two curves are excellent and the correlation coefficient (R^2) are 0.999 and 0.9995 respectively. According to equation (1), from the slope -3.38 and -3.5 of the two calibration curves, PCR amplification efficiency (E) is 98% and 93% and the amplification factor is 1.98 and 1.93. The amplification efficiency (E) falls in the desired range of amplification efficiencies of PCR (90% to 110%) which is close to the exponential amplification. It means that polymerase enzyme is working at maximum capacity and all the target sequence doubled during each replication cycle, that all templates qPCR amplification using stem-loop primer RT-qPCR and poly (A)-tail extension RT-qPCR were effective and can be used to analyze the expression of miRNA-21.

2). qPCR Calibration curve for stem-loop primer RT-qPCR and poly (A)-tail extension RT-qPCR.

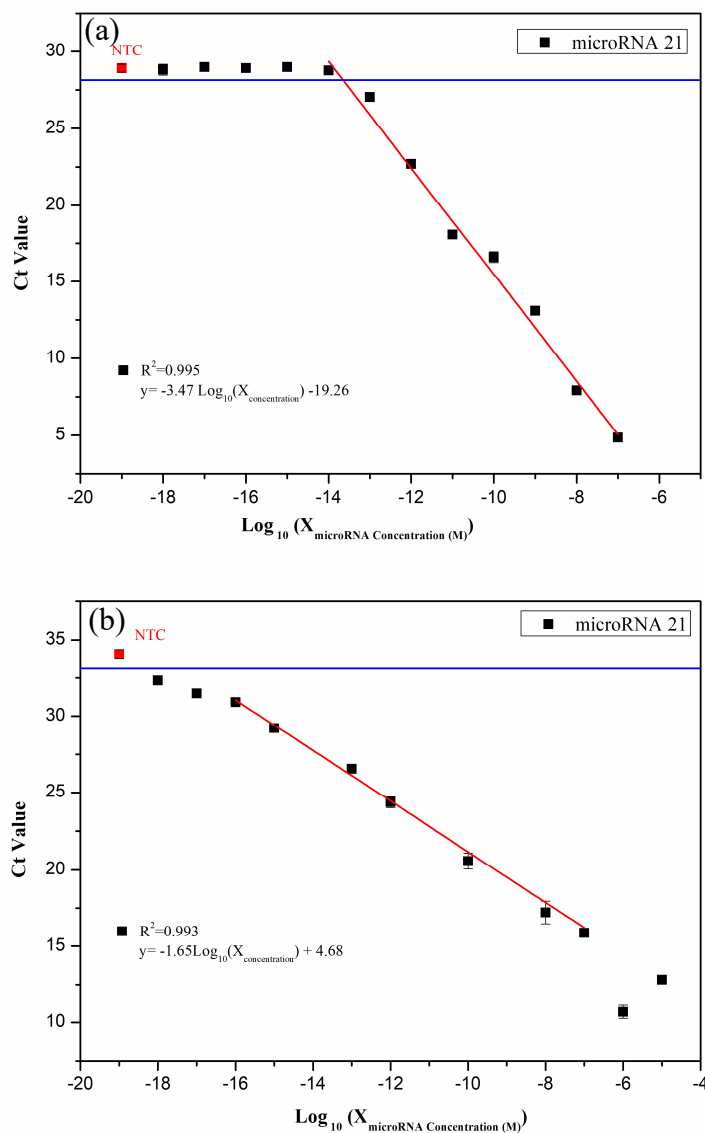


Figure II.7. qPCR calibration curve of different concentration miRNA sample by *TaqMan*® microRNA assays (a) and *TaqMan*® advanced microRNA assays (b). The serial dilution concentration of miRNA-21 ($10^{-5} \text{ mol L}^{-1}$ to $10^{-18} \text{ mol L}^{-1}$) Log value vs the corresponding C_t value, each point was repeated at least 6 times.

The absolute quantification of miRNA-21 is by establishing a calibration curve, which a standard miRNA-21 of known concentration was used as a template. Serially diluted in nuclease-free water by 10-fold (from 10^{-5} to 10^{-18} M) and all dilution points were performed

reverse transcription separately to cDNA then qPCR. Because the qPCR of miRNA used a two-step method, in order to evaluate the first step reverse transcription, a non-template control (NTC) performed RT reaction and qPCR simultaneously with other concentration miRNA-21 templates. The calibration curve was plotted by the logarithmic values of the serially diluted concentration of standard miRNA-21 and the corresponding C_t values using qPCR, on the X-axis and Y-axis respectively. Figure II. shows the calibration curve of miRNA-21 using stem-loop primer RT-qPCR (a) and poly (A)-tail extension RT-qPCR (b). For the calibration curve of stem-loop primer RT-qPCR, the logarithm of the standard miRNA-21 concentration has a linear relationship with the corresponding C_t in the concentration range of 10^{-7} mol L⁻¹ to 10^{-14} mol L⁻¹, with a correlation coefficient R^2 of 0.995. When the template's concentration is below 10^{-14} mol L⁻¹, the C_t entered the plateau, which is the background (approximately equal to 29), and when the template's concentration is 0 mol L⁻¹ (NTC), the C_t is also on the plateau.

Currently, there are several approaches that can be used to determine the limit of detection (LOD), and all are acceptable, depending on whether the procedure is non-instrumental or instrumental. LOD is the lowest amount or concentration of analyte in a sample, which can be reliably detected but not necessarily quantified [28]. For the LOD of qPCR, there are several methods are used to determined, due to in the blank control, generally no data can be detected or typically have values equal to the highest cycle number used in the PCR reaction, so the researchers think that the most commonly used method based on the standard deviation of the response and the slope is unsuitable for estimating qPCR LOD. Then they proposed a method that LOD is the measurand concentration that produces at least 95% positive replicates, in other word, during the experiment, methods should detect the presence of the analyte at least 95% of the times at the LOD, ensuring $\leq 5\%$ false negative results [29, 30]. However, this method of LOD should analyze with 60 replicates experiment per each point that means need huge workload, moreover, it is mainly to evaluate the LOD of qPCR of DNA. This study, miRNA analysis was performed by two-step, the first step was reverse transcription (RT) of miRNA, and the second step was qPCR. In the RT step we added a non-template control (NTC), which

accompanies all RT and qPCR processes, so in the next qPCR its data is used to evaluate LOD that was estimated by taking the intersection between the linear part of the experimental data and 3-fold of the SD line of NTC (background) can be used in the study [31], thus can be evaluated affected by noise contributed to by sampling, extraction, reverse transcription, and qPCR. Which the LOD of miRNA-21 using stem-loop primer RT-qPCR is 22 fmol L⁻¹ and the limit of quantitation (LOQ) is 31 fmol L⁻¹ based on the intersection between the linear section of the experimental data and 5-fold of the background SD line. Moreover, a control (blank with no cDNA) was run for each qPCR to eliminate reagents or surfaces cross contaminations. No amplification curves were observed for any blank, while other concentration miRNA-21 assays were successfully amplified suggesting the absence of non-specific interactions. For the calibration curve of poly (A)-tail extension RT-qPCR, the dynamic range is from 10⁻⁷ mol L⁻¹ to 10⁻¹⁶ mol L⁻¹ and the logarithm of the standard miRNA-21 concentration in this interval has a linear relationship with the corresponding C_t and the R² is 0.995. The LOD and LOQ is 6.11 amol L⁻¹ and 15.1 amol L⁻¹. The obtained both stem-loop primer RT-qPCR and poly (A)-tail extension RT-qPCR experimental performances are summarized in Table II.3, it shows the poly (A)-tail extension reverse transcription assay is better in the detection of miRNA-21 expression, thus, in the following, it was used to measure miRNA-21 in plasma.

Table II.3. Comparison of the performance of two miRNA-21 RT-qPCR detection methods.

Method	Dynamic range	LOD	LOQ
Stem-loop primer RT-qPCR	10 ⁻⁷ M to 10 ⁻¹⁴ M	22 fM	31 fM
Poly (A)-tail extension RT-qPCR	10 ⁻⁷ M to 10 ⁻¹⁶ M	6 aM	15 aM

II.2.3.2 Analysis of miRNA-21 standard solutions in plasma

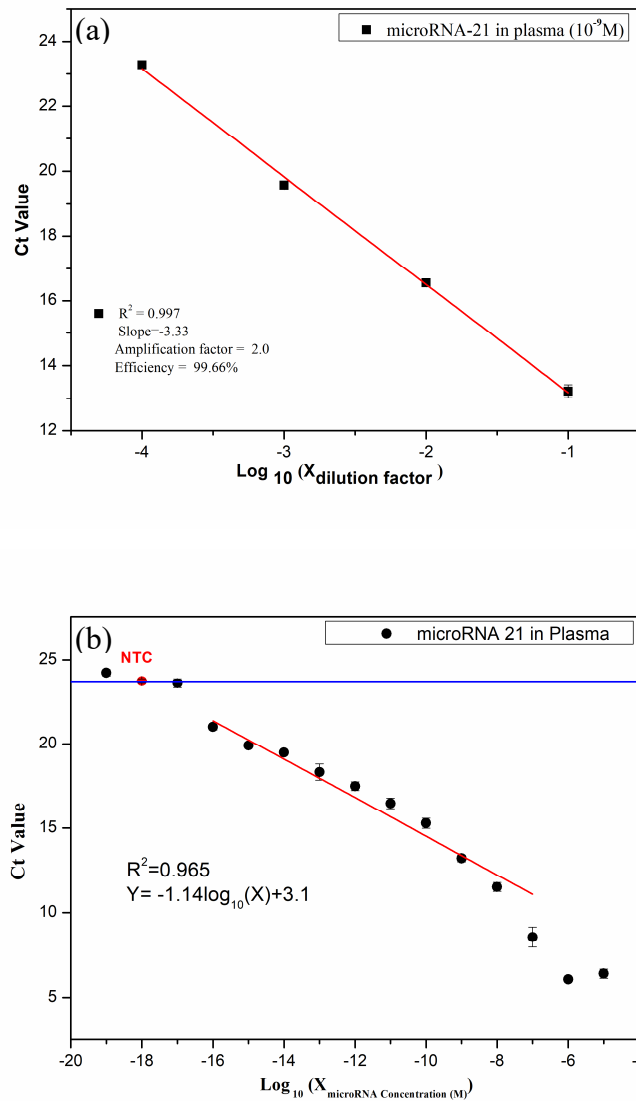


Figure II.8. The qPCR amplification efficiency curve (a) and qPCR calibration curve of different concentration miRNA-21 sample in plasma (b) of poly (A)-tail extension RT-qPCR.

For studying the actual conditions for microRNA-21 detection and the specificity and sensitivity of the poly (A)-tail extension RT-qPCR method for miRNA-21 detection in the presence of multiple miRNA, we choose to dilute the standard miRNA-21 into purified plasma solutions containing no miRNA-21. Our aim was to construct a calibration curve in the plasma matrix. Before the introduction of miRNA21, the plasma was purified by the miRNA purification kit

Human Panel B to remove miRNA-21. Then, this purified plasma was used to serially dilute standard miRNA-21 with a 10-fold (from 10^{-5} to 10^{-18} mol L⁻¹, a non-template control (NTC) and blank). Then we carried out the poly (A)-tail extension RT-qPCR. Figure II.a corresponds to the qPCR amplification efficiency curve, with a slope of -3.33 and R² is 0.997. The calculated PCR amplification efficiency (E) is 99.66%. Figure II.b shows the qPCR calibration curve of different miRNA-21 concentrations in purified plasma, which has a dynamic range between 10^{-8} mol L⁻¹ and 10^{-16} mol L⁻¹, the linear equation is:

$$C_t = 1.14 \times \log(X_{miRNA-21 \text{ concentration}}) + 3.1 \quad (2)$$

LOD and LOQ are respectively 0.87 amol L⁻¹ and 1.85 amol L⁻¹.

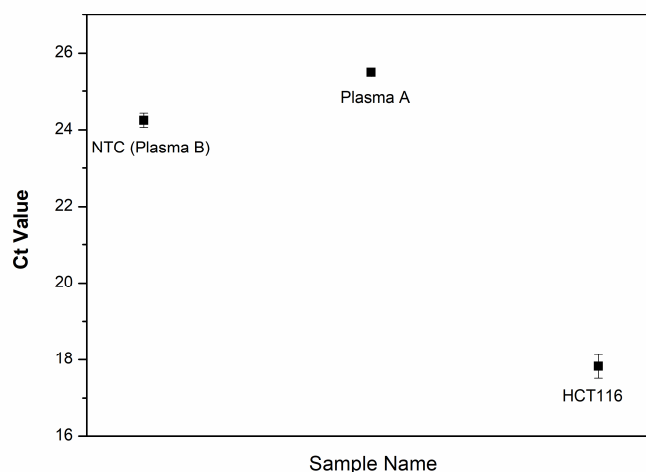


Figure II.9. The Ct value of different samples measured by poly (A)-tail extension RT-qPCR.

HCT116 is a human colon cancer cell line, a study has demonstrated that the upregulation of miR-21 is associated with colorectal cancer (CRC) [32], the detection of miRNA-21 expression level in HCT116 cell line can predict cancer. We used the total RNA of HCT116 cell line carried out the poly (A)-tail extension RT-qPCR to detect the expression level of miRNA-21. The amplification efficiency is 105% (supplementary information Figure II.). Figure II.9 shows the Ct values of plasma B, plasma A and HCT116 cell line (see Material and Methods), the Ct of

HCT116 cell line is 17.82 which is less than the C_t (24.2) of non-template control (plasma B), that shows there is a certain amount of miRNA-21 in this HCT116 cell line. According to the linear equation of calibration curve of miRNA-21 sample in plasma, the expression of miRNA-21 is calculated to be $1.22 \times 10^{-13} \text{ mol L}^{-1}$. The C_t of plasma A (the healthy donor plasma) is 25.5 which is near the value of plasma B (NTC), and the amplification efficiency of Plasma A is near 0 (Supplementary Information Figure II.). Both showed that no or few miRNA-21 was present in the healthy donor plasma, which was difficult to detect, but was detected in a sample from a cell line HCT116 which is known to express miRNA-21. It also shows the poly (A)-tail extension RT-qPCR has excellent selectivity and specificity for miRNA-21 detection.

Conclusions

In this work, the quantification of miRNA-21 by PT-qPCR based on the standard curve approach, the stem-loop primer RT-qPCR and poly (A)-tail extension RT-qPCR was evaluated to compare both approaches and to detect the expression level of miRNA-21. Even though the stem-loop primer RT-qPCR is more time-saving, less-step than poly (A)-tail extension RT-qPCR, the latter one is more sensitive and specific that can be used to detect low expression of miRNA-21 in plasma, with a dynamic range between 10^{-8} M and 10^{-16} M , and LOD and LOQ of 0.87 amol L^{-1} and 1.85 amol L^{-1} , respectively.

References

1. Lee RC, Feinbaum RL, Ambros V. The *C. elegans* heterochronic gene *lin-4* encodes small RNAs with antisense complementarity to *lin-14*. *cell* 1993,**75**:843-854.
2. Fabian MR, Sonenberg N, Filipowicz W. Regulation of mRNA translation and stability by microRNAs. *Annual review of biochemistry* 2010,**79**:351-379.
3. Hanson EK, Lubenow H, Ballantyne J. Identification of forensically relevant body fluids using a panel of differentially expressed microRNAs. *Analytical biochemistry* 2009,**387**:303-314.
4. Wang K, Zhang S, Weber J, Baxter D, Galas DJ. Export of microRNAs and microRNA-protective protein by mammalian cells. *Nucleic acids research* 2010,**38**:7248-7259.
5. Zen K, Zhang CY. Circulating microRNAs: a novel class of biomarkers to diagnose and monitor human cancers. *Medicinal research reviews* 2012,**32**:326-348.
6. Zubakov D, Boersma AW, Choi Y, van Kuijk PF, Wiemer EA, Kayser M. MicroRNA markers for forensic body fluid identification obtained from microarray screening and quantitative RT-PCR confirmation. *International journal of legal medicine* 2010,**124**:217-226.
7. Gibbings DJ, Ciaudo C, Erhardt M, Voinnet O. Multivesicular bodies associate with components of miRNA effector complexes and modulate miRNA activity. *Nature cell biology* 2009,**11**:1143-1149.
8. Valadi H, Ekström K, Bossios A, Sjöstrand M, Lee JJ, Lötvall JO. Exosome-mediated transfer of mRNAs and microRNAs is a novel mechanism of genetic exchange between cells. *Nature cell biology*

- 2007,**9**:654-659.
9. Allegra A, Alonci A, Campo S, Penna G, Petrunaro A, Gerace D, *et al.* Circulating microRNAs: new biomarkers in diagnosis, prognosis and treatment of cancer. *International journal of oncology* 2012,**41**:1897-1912.
 10. Cheng Y, Zhang C. MicroRNA-21 in cardiovascular disease. *Journal of cardiovascular translational research* 2010,**3**:251-255.
 11. Zhu W, Xu B. MicroRNA-21 identified as predictor of cancer outcome: a meta-analysis. *PloS one* 2014,**9**.
 12. Lü Y, Han B, Yu H, Cui Z, Li Z, Wang J. Berberine regulates the microRNA-21-ITGB4-PDCD4 axis and inhibits colon cancer viability. *Oncology letters* 2018,**15**:5971-5976.
 13. Ribas J, Lupold SE. The transcriptional regulation of miR-21, its multiple transcripts and their implication in prostate cancer. *Cell cycle* 2010,**9**:923-929.
 14. Young MR, Santhanam AN, Yoshikawa N, Colburn NH. Have tumor suppressor PDCD4 and its counteragent oncogenic miR-21 gone rogue? *Molecular interventions* 2010,**10**:76.
 15. Burgos J, Ramírez C, Tenorio R, Sastre I, Bullido M. Influence of reagents formulation on real-time PCR parameters. *Molecular and cellular probes* 2002,**16**:257-260.
 16. Ferre F. Quantitative or semi-quantitative PCR: reality versus myth. *Genome Research* 1992,**2**:1-9.
 17. Klein D. Quantification using real-time PCR technology: applications and limitations. *Trends in molecular medicine* 2002,**8**:257-260.
 18. Hurley J, Roberts D, Bond A, Keys D, Chen C. Stem-loop RT-qPCR for microRNA expression profiling. In: *Next-generation microRNA expression profiling technology*: Springer; 2012. pp. 33-52.
 19. Kramer MF. Stem-loop RT-qPCR for miRNAs. *Current protocols in molecular biology* 2011,**95**:15.10. 11-15.10. 15.
 20. Varkonyi-Gasic E, Hellens RP. Quantitative stem-loop RT-PCR for detection of microRNAs. In: *RNAi and Plant Gene Function Analysis*: Springer; 2011. pp. 145-157.
 21. Schmittgen TD, Lee EJ, Jiang J, Sarkar A, Yang L, Elton TS, *et al.* Real-time PCR quantification of precursor and mature microRNA. *Methods* 2008,**44**:31-38.
 22. Varkonyi-Gasic E, Wu R, Wood M, Walton EF, Hellens RP. Protocol: a highly sensitive RT-PCR method for detection and quantification of microRNAs. *Plant methods* 2007,**3**:12.
 23. Forero DA, González-Giraldo Y, Castro-Vega LJ, Barreto GE. qPCR-based methods for expression analysis of miRNAs. *BioTechniques* 2019,**67**:192-199.
 24. Niu Y, Zhang L, Qiu H, Wu Y, Wang Z, Zai Y, *et al.* An improved method for detecting circulating microRNAs with S-Poly (T) Plus real-time PCR. *Scientific reports* 2015,**5**:15100.
 25. Vautrot V, Behm-Ansmant I. Enhanced Probe-Based RT-qPCR Quantification of MicroRNAs Using Poly (A) Tailing and 5' Adaptor Ligation. In: *Quantitative Real-Time PCR*: Springer; 2020. pp. 39-54.
 26. Lee C, Kim J, Shin SG, Hwang S. Absolute and relative QPCR quantification of plasmid copy number in Escherichia coli. *Journal of biotechnology* 2006,**123**:273-280.
 27. Rasmussen R. Quantification on the LightCycler. In: *Rapid cycle real-time PCR*: Springer; 2001. pp. 21-34.
 28. Guideline IHT. Validation of analytical procedures: text and methodology Q2 (R1). In: *International conference on harmonization, Geneva, Switzerland*; 2005.
 29. Bustin SA, Benes V, Garson JA, Hellemans J, Huggett J, Kubista M, *et al.* The MIQE Guidelines: Minimum Information for Publication of Quantitative Real-Time PCR Experiments. In: Oxford University Press; 2009.
 30. Forootan A, Sjöback R, Björkman J, Sjögreen B, Linz L, Kubista M. Methods to determine limit of detection and limit of quantification in quantitative real-time PCR (qPCR). *Biomolecular detection and quantification* 2017,**12**:1-6.
 31. Schwarz G, Bäumler S, Block A, Felsenstein FG, Wenzel G. Determination of detection and quantification limits for SNP allele frequency estimation in DNA pools using real time PCR. *Nucleic Acids Research* 2004,**32**:e24-e24.
 32. Mercado-Pimentel ME, Onyeagucha BC, Li Q, Pimentel AC, Jandova J, Nelson MA. The S100P/RAGE signaling pathway regulates expression of microRNA-21 in colon cancer cells. *FEBS letters* 2015,**589**:2388-2393.

Supplementary Information

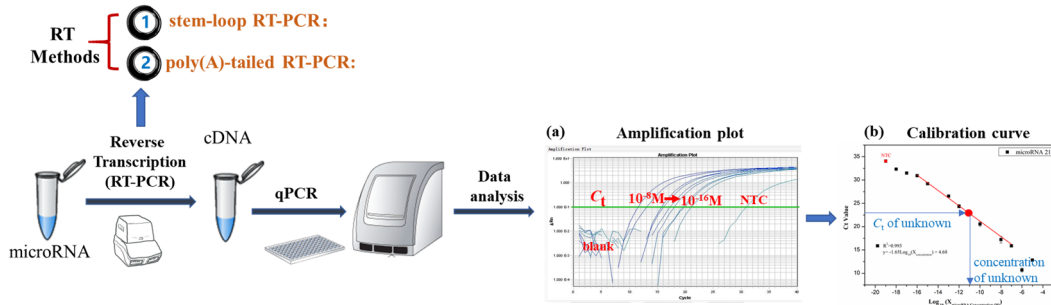


Figure II.10. Schematic diagram and data analysis of reverse transcription real-time PCR workflow of microRNA using the two methods.

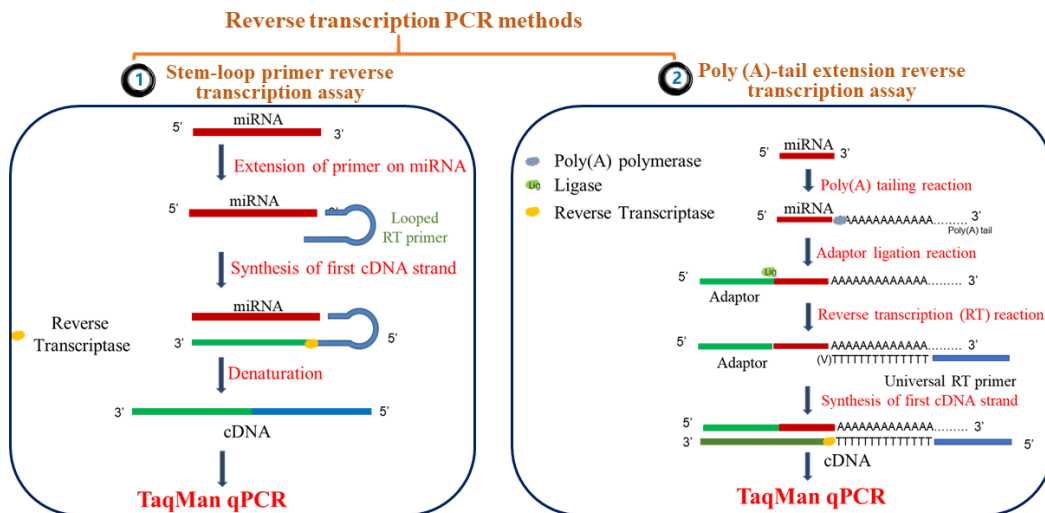


Figure II.11. Schematic diagram of two microRNA reverse transcription PCR methods.

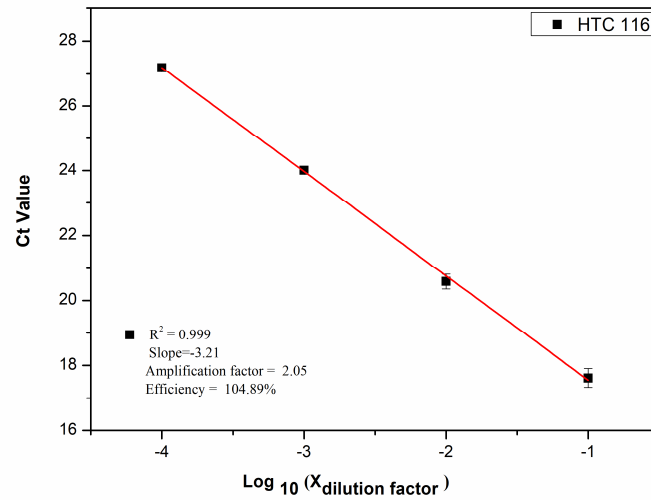


Figure II.12. qPCR amplification efficiency curve of Poly (A)-tail extension RT-qPCR: The logarithm values of serial dilution factor of cDNA that obtained from HCT116 cell line reverse transcription versus the corresponding Ct value, the amplification efficiency was 104.89%.

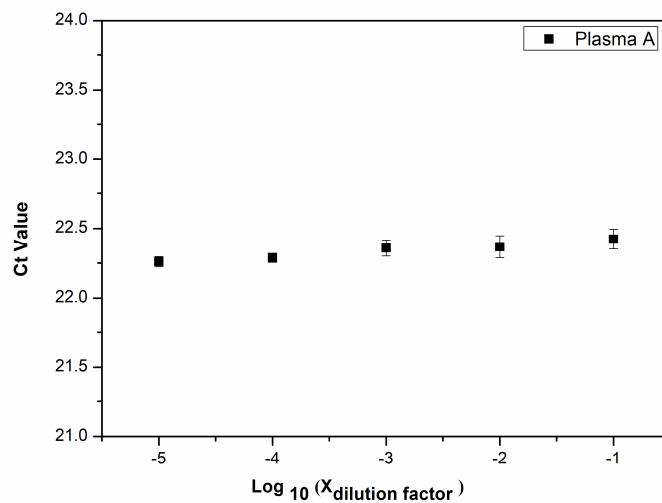


Figure II.13. qPCR amplification efficiency curve of Poly (A)-tail extension RT-qPCR: The logarithm values of serial dilution factor of cDNA that obtained from plasma A reverse transcription versus the corresponding C_t value, the amplification efficiency is near 0. The plasma was purified by the miRNA purification kit Human Panel A to keep the miRNA-21 in plasma and named plasma A.

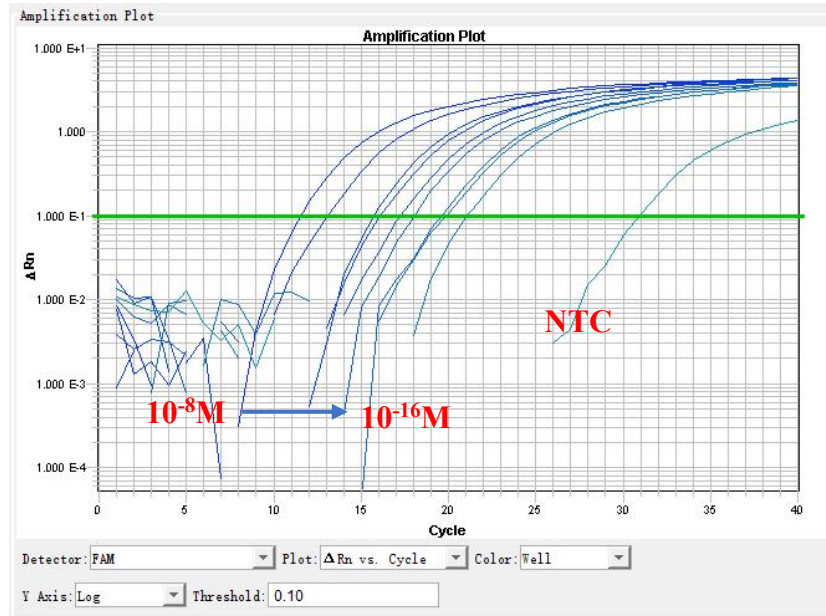


Figure II.14. The fluorescence amplification plot of miRNA-21 at serial concentration dilutions (from 10^{-8} M to 10^{-16} M) and no template control (NTC), that carried out Poly (A)-tail extension RT-qPCR.

II.3. miRNA-21 quantification by SPR

SPR sensor is an optical refractometer that can rely on monitoring a shift in resonance angle due to a change in the refractive index of the dielectric material on the surface of SPR sensing resulting from the surface binding reaction. Compared with the traditional fluorescence monitoring technology, the SPR biosensor can dynamically monitor the whole process of the interaction of biomolecules on the substrate surface in real time and without labeling. The detection process is convenient, quick, and with the high sensitivity. In most cases, the sample does not need to be processed. Moreover, since SPR is based on measuring reflected light, it can be performed in turbid or even opaque samples.

This section presented the development of a genosensor for microRNA-21 quantification using *Surface Plasmon Resonance (SPR)*. Which had been published in “*Analytical and Bioanalytical Chemistry*”.

I and Michael López Mujica completed the experiment and data analysis part together.

This part of the experiment was conducted in the departamento de Fisicoquímica at the facultad de Ciencias Químicas, Nacional de Córdoba, Argentina.

Thanks to Gustavo Rivas and Fabiana Gutiérrez for the guidance and help of this part of the experiment, and Michael López Mujica for helping me in the experiment part. Thanks to Gustavo Rivas, Fabiana Gutiérrez, Michael López Mujica, and other colleagues for helping me of my life in Argentina

Thanks to the financial support from CONICET, ANPCyT, and SECyT-UNC (Argentina) and ECOS-SUD program (A16E02).

Thankfully acknowledges LabEx MICHEM for supporting my living expenses in UNC Argentina.

Label-free graphene oxide based-SPR genosensor for the quantification of microRNA21

Michael López Mujica¹, Yuanyuan Zhang², Féthi Bédioui^{2,*}, Fabiana Gutiérrez^{1,*}, Gustavo Rivas^{1,*}

¹INFIQC-CONICET, Departamento de Fisicoquímica, Facultad de Ciencias Químicas, Universidad Nacional de Córdoba, Ciudad Universitaria. 5000 Córdoba, Argentina.

²Chimie ParisTech, PSL University, CNRS 2027, Institute of Chemistry for Life and Health Sciences, SEISAD 75005 Paris, France.

Abstract

This work is focused on the development of a genosensor for microRNA-21 quantification using Surface Plasmon Resonance (SPR) to transduce the hybridization event. The biosensing platform was built by self-assembling two bilayers of poly (diallyldimethylammonium chloride) (PDDA) and graphene oxide (GO) at a gold surface modified with 3-mercaptopropene sulfonate (MPS), followed by the covalent attachment of the DNA probe. GO was used in two directions, to allow the anchoring of the probe DNA and to increase the sensitivity of the biosensing event due to its field enhancer effect. The new bioanalytical platform represents an interesting alternative for the label-free biosensing of microRNA-21, with a linear range between 1.0fM and 10nM, a sensitivity of $(5.1 \pm 0.1) \text{ m}^{\circ}\text{M}^{-1}$ and a detection limit of 0.3fM. The proposed sensing strategy was successfully used for the quantification of microRNA-21 in enriched urine samples.

Keywords

microRNA-21, Genosensor, SPR, Graphene oxide, Cancer biomarker, Layer-by-layer self-assembly

II.3.1. Introduction

The microRNAs (miRNAs) are short endogenous and non-coding RNAs that have an important effect on the expression of a large number of proteins and, consequently on different molecular pathways [1]. They are present in several body fluids, such as serum, blood, urine, saliva and tears, thereby enabling minimally invasive detection [2]. Since the dysregulation in microRNAs-expression is an initial event in tumorigenesis, these microRNAs are very important biomarkers for early diagnosis of cancer and represent a good promise to reduce the worldwide health problem of this pathology [3, 4]. The advantages of miRNAs as biomarkers are connected with their high stability, their presence in several biological materials and the significant differences on their expression in healthy and pathological individuals [5].

microRNA-21 is an oncogenic microRNA that has been connected with different diseases, especially cancer. It has been found in patients with cervical cancer and has demonstrated to be useful for the prognosis and therapeutic application [6]. A critical study about the connection between dysregulated miRNAs and prostate cancer showed that miRNA-21 is one of the four microRNAs that give relevant information for the detection, prognosis and evaluation of the therapy [7]. microRNA-21 is also involved in the growth, metastasis and apoptosis of non-small cell lung cancer and is a promising biomarker for its diagnosis and prognosis [8]. Kura et al. [9] also showed that some biologically active nutrients like polyunsaturated fatty acids, vitamins E and D, dietary fiber, or selenium affect the expression of many miRNAs, connected with cardiovascular diseases, like miRNA-21, -30 family, -34, -155, or -199.

The determination of miRNAs is very complex due to their short sequence, low levels and high similarity between them. The current gold standard technique for miRNA detection is quantitative real-time polymerase chain reaction (qPCR) where the quantification of miRNAs extracted from body fluids is achieved through reverse transcription of miRNA and labeling with fluorescent probes [10]. Other common methods used in miRNA detection are surface enhanced Raman scattering, microarrays and Northern blot [11-13]; however, they present important limitations like requirement of specialized personnel and need of centralized

laboratories with expensive instrumentation [14]. Electrochemical biosensors have also demonstrated to be a very useful tool for the sensitive and selective quantification of microRNAs [15-17].

SPR biosensing strategies have made possible the real-time and label-free detection of different bioanalytes, providing additional useful information about binding kinetics and bioaffinity interactions. Q. Wang et al. [18] reported the selective femtomolar SPR detection of microRNA-21 by taking advantage of the electronic coupling between Au nanoparticles (AuNPs)-localized plasmon and Au surface plasmon, and the refractive index enhancement of the medium next to Au film caused by the hybrid generated between the DNA-linked AuNPs on the Au film surface and the terminus of capture DNA. A similar strategy was proposed by Liu et al. [19] for the sub-fM detection of microRNA-21 and cancer cells based on a multiple signal amplification strategy using a thiol-modified hairpin probe immobilized on a gold film with silver NPs deposited after the formation of the DNA supersandwich structure. Xue et al. [20] reported the use of antimonene for the specific label-free and aM detection of miRNA-21 and miRNA-155 due to the substantially stronger interaction of antimonene with ssDNA compared to DNA-RNA heteroduplex and the use of Au nanorods to amplify the SPR signal. Sipova et al. [21] presented a sensitive miRNA quantification strategy using a high-performance portable SPR sensor for spectroscopy of surface plasmons based on a special diffraction grating functionalized with the probe DNA and disperser (SPRCD) and the use of an antibody able to recognize the DNA-RNA duplex. The sensor was used to quantify miRNA from mouse liver tissues. Gayatri et al. [22] described a regenerative, solid-state localized SPR (LSPR) sensor based on gold nanoprisms that circumvent the need for labels or amplification, and enabled the detection of sub-fM microRNA-21 and microRNA-10b in human plasma of pancreatic cancer patients. SPR was also used for the quantification of microRNA-10b at attomolar level [23] and microRNA-93 at picomolar level [24]. Feng et al. [25] reported a surface plasmon-enhanced electrochemiluminescence with Ag nanoclusters deposited at DNA as electrochemiluminescence emitters and AuNPs deposited at glassy carbon electrode (GCE) as localized surface plasmon resonance source in combination with a catalytic hairpin assembly

amplification that allowed to reach a detection limit of 0.96 aM and a successful determination of miRNA-21 in enriched diluted serum samples.

Here, we are proposing a bioanalytical platform for the detection of microRNA-21 with SPR transduction based on the use of a gold disk modified with 3-mercaptopropene-1-sulfonate (MPS) followed by the self-assembling of poly(diallyldimethylammonium) chloride (PDDA) and graphene oxide (GO) and the covalent attachment of capture DNA. In the following sections we discuss the influence of the number of PDDA/GO bilayers on the plasmonic response of the resulting platform; the optimization of the amount of DNA probe immobilized at the surface and the hybridization time on the detection of the hybridization event; and the analytical performance of the biosensor.

II.3.2. Experimental

II.3.2.1. Material and methods

1). Chemicals and reagents

Sodium 3-mercapto-1-propanesulfonate (MPS), N-hydroxysuccinimide (NHS), Poly (diallyldimethylammonium chloride) (PDDA), N-(3-dimethylaminopropyl)-N'-ethylcarbodiimide hydrochloride (EDC), ethanolamine (Et), benzoquinone, hydroquinone, and poly(acrylic acid) (PAA) were purchased from Sigma-Aldrich. Ethanol, sulfuric acid (98%) and sodium hydroxide were provided by J. T. Baker. Graphene oxide (GO) was obtained from Graphenea. Other chemicals were reagent grade and used without further purification.

The DNA and RNA sequences (Invitrogen Life Technologies), are the following:

Sequence DNA probe: 5'-NH₂-TCA-ACA-TCA-GTC-TGA-TAA-GCT-A-3'

miRNA-21: 5'-UAG-CUU-AUC-AGA-CUG-AUG-UUG-A-3'

Single base mismatch: 5'-UAG-CUU-AUC-ACA-CUG-AUG-UUG-A-3'

Non-complementary sequence: 5'-GGG-GGG-GGG-GGG-GGG-GGG-GGG-3'

Ultrapure water (UW, $\rho = 18.2 \text{ M}\Omega \text{ cm}$) from a Millipore-MilliQ system was used for preparing all the solutions.

2). Apparatus

A platinum wire and Ag/AgCl, 3 M NaCl were used as counter and reference electrodes, respectively. All potentials are referred to the latter. Electrochemical Impedance Spectroscopy (EIS) measurements were performed with an Autolab PGSTAT30 potentiostat (Metrohm). The experiments were carried out in a 0.050 M phosphate buffer solution pH 7.40, using 2.0×10^{-3} M benzoquinone/hydroquinone as redox indicators. The EIS parameters were the following, amplitude: 0.010 V, frequency range: 1.0×10^{-2} to 1.0×10^6 Hz and working potential: 0.200 V. The impedance spectra were analyzed and fitted by using the Z-view program.

Surface Plasmon Resonance (SPR) measurements were performed using a single channel Autolab E-SPR SPRINGLE instrument (Eco Chemie). A standard gold disk (BK-7 Eco Chemie), mounted on a hemicylindrical lens through index-matching oil was used to build the platform. Sample solutions were injected manually and the measurements were carried out under batch conditions at 25 °C. The analytical signal was obtained from the change in the SPR minimum angle ($\Delta\theta_{\text{SPR}}$).

UV-Vis experiments were carried out with a Shimadzu UV1601 spectrophotometer and a quartz cuvette of 0.1 cm path length.

II.3.2.2. Construction of the biosensing platform

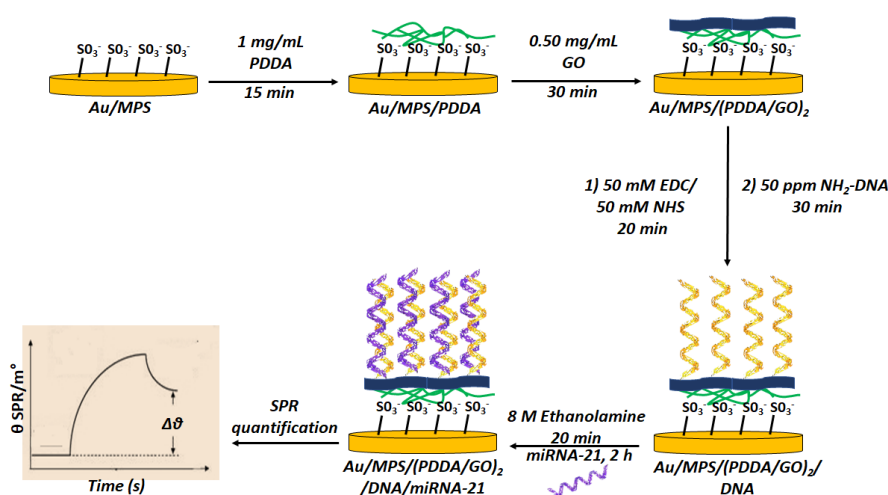


Figure.II.15. Scheme for the different steps during the building of the plasmonic microRNA-21 genosensor.

Figure.II.15 displays a scheme with the different steps during the construction of the biosensing platform. The gold disk was modified in-situ using a 2.00×10^{-2} M MPS solution (prepared in 1.60×10^{-3} M H_2SO_4) for 60 min. After washing the surface, it was allowed to interact with PDDA (1.00 mg mL^{-1} , prepared in 0.050 M phosphate buffer solution pH 7.40) for 15 min and after that, with GO (0.50 mg mL^{-1} GO solution prepared in 0.10 M NaOH) for 30 min. This procedure was repeated twice to obtain the required platform $\text{Au/MPS}/(\text{PDDA/GO})_2$. The carboxylate residues of GO were activated with an EDC/NHS mixture (0.100 M prepared in 0.050 M phosphate buffer solution pH 7.40) for 20 min and after that it was allowed to interact with a 50 ppm DNA probe solution (prepared in 0.050 M phosphate buffer pH 7.40 + 0.500 M NaCl) for 30 min. The unreacted GO carboxylate groups were quenched by adding 1.0 M Et solution (pH 8.30) for 15 min. The hybridization event was performed at $\text{Au/MPS}/(\text{PDDA/GO})_2/\text{DNA}$ by interacting with miRNA-21 (prepared in 0.050 M phosphate buffer solution pH 7.40 + 0.500 M NaCl) for 120 min. The surface of the modified gold-disk was carefully washed between the different steps. In fact, it was washed with the medium used to prepare the solution that interacted with the surface in the previous step, and then, for three times, with the medium used to prepare the solution that will interact with the platform in the next step. To obtain additional information, the platform $\text{Au/MPS}/(\text{PDDA/GO})_2$ was also interrogated by EIS using gold electrodes (CH Instruments, 3 mm diameter) prepared under the same experimental conditions as the SPR sensor.

II.3.3. Results and Discussion

II.3.3.1. Construction and characterization of genosensor

One interesting alternative to improve the sensitivity of SPR determinations is the incorporation of plasmonic nanostructures to SPR substrates due to the coupled field increments [26]. The high transmittance of the graphene-sheet and the high confinement and propagation of the surface plasmonic polaritons make graphenaceous materials very useful elements for the construction of SPR biosensors [27-29]. Therefore, taking into account the importance of GO to improve the sensitivity of SPR determinations, we evaluated the effect of

the number of GO layers immobilized at the gold disk by EIS, through the variations of the total charge transfer resistance (R_{ct}), and by SPR, through the changes in the plasmon angle.

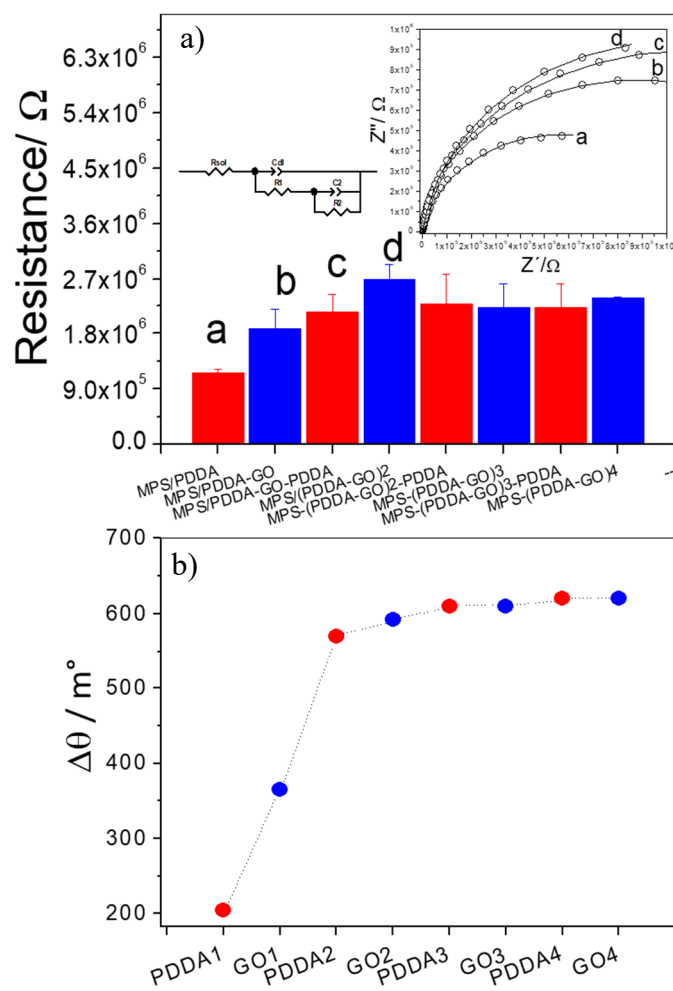


Figure II.8. a) Bars plot for the variation of total R_{ct} during the self-assembling of 1.00 mg mL^{-1} PDDA (red) and 0.50 mg mL^{-1} GO (blue) at Au/MPS platform. The inset shows the Nyquist plots for the two layers of PDDA and two layers of GO as well as the corresponding equivalent circuit. Redox marker, $2.0 \times 10^{-3} \text{ M}$ hydroquinone/benzoquinone; EIS parameters: amplitude, 0.010 V , frequency range, 1.0×10^{-2} to $1.0 \times 10^6 \text{ Hz}$; working potential, 0.200 V . b) $\Delta\theta_{SPR}$ calculated from the sensorgram obtained during the consecutive self-assembling of 4 bilayers of 1.00 mg mL^{-1} PDDA (red) and 0.50 mg mL^{-1} GO (blue). Rinsing solutions: 0.050 M phosphate buffer solution pH 7.40 before and after self-assembling of PDDA; and 0.100 M NaOH before and after the immobilization of GO.

Figure II.8a shows the changes in the total R_{ct} obtained after the assembling of several layers of PDDA and GO at Au/MPS using hydroquinone/benzoquinone as redox markers. The inset shows the Nyquist plots corresponding to the first two PDDA/GO bilayers, where the circles are the experimental points and the solid lines correspond to the fitting of these results with the equivalent circuit. The adsorption of GO at Au/MPS/PDDA produces an increment in the R_{ct} due to the poor conductivity of GO. The assembling of the next layer of PDDA produced a new increment in R_{ct} due to the blockage effect, to increase even more after the immobilization of the second layer of GO. Further immobilization of GO or PDDA does not produce significant changes, indicating that after the second PDDA/GO bilayer there is no substantial increment in the thickness of the multilayers system due to a poor accumulation either of GO or PDDA. The system was fitted with a double time constant equivalent circuit (also shown in the inset) based on the capillary membrane model, which has been used to evaluate the charge transport through multilayers of polyelectrolytes, to demonstrate the existence of possible defects in these multilayers systems [30, 31]. This model assumes that the electrode is not fully covered during the construction of the supramolecular architecture defining areas more accessible for the charge transfer of the redox mediator. The Nyquist plots present wide semicircles, product of the combination of two times constants, indicating the existence of areas with two different heterogeneous rate constants for hydroquinone/benzoquinone charge transfer [32]. Therefore, the results presented in Figure II.8a suggest that after the assembling of GO there is not full coverage of the PDDA layer, with the consequent existence of regions with different GO coverage and incomplete charge reversion of PDDA.

The platform was also evaluated by SPR. Figure II.8b depicts the changes in $\Delta\theta_{SPR}$ during the assembling of the different PDDA and GO layers. $\Delta\theta_{SPR}$ increases after each immobilization step up to the second (PDDA/GO) bilayer, in agreement with the EIS results, indicating that there is an effective immobilization of PDDA and GO up to the second bilayer. Further adsorption of GO or PDDA produces almost no change in θ_{SPR} . Therefore, two (GO/PDDA) bilayers were selected as the optimum platform for building the biosensor.

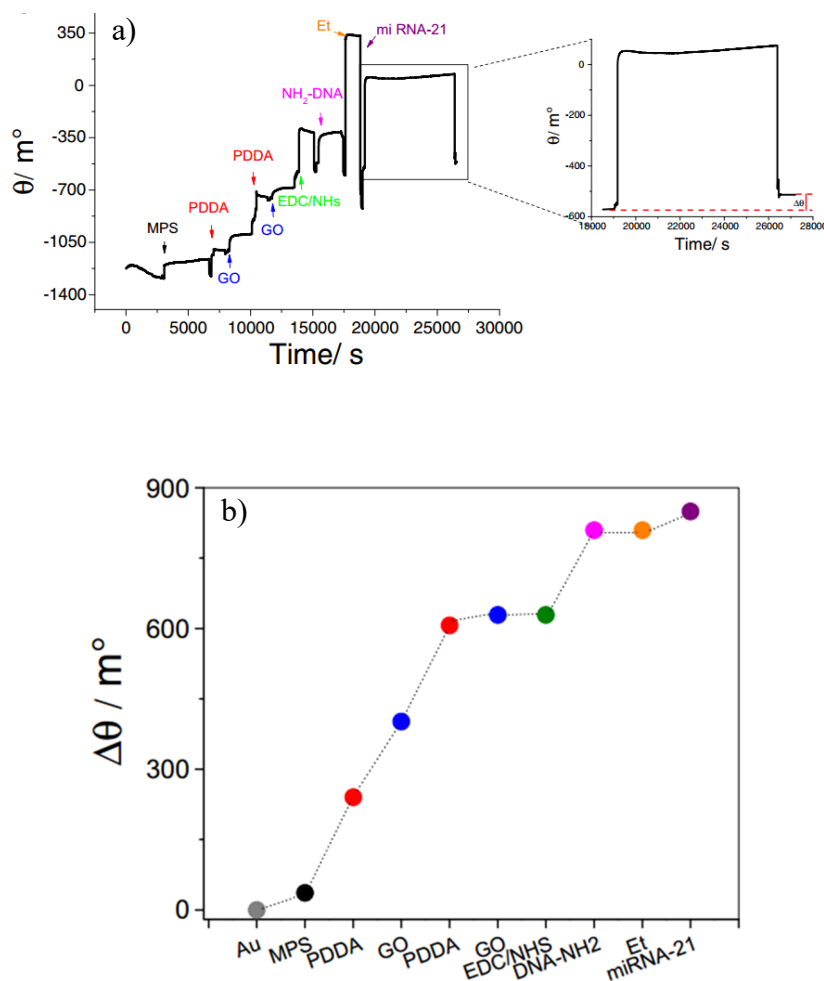


Figure II.9. a) SPR sensorgram obtained during the building of microRNA-21 genosensor: immobilization of MPS at Au (black arrow), PDDA at Au/MPS (red arrow), GO at Au/MPS/PDDA (blue arrow), activation of Au/MPS/(PDDA/GO)₂ with EDC/NHS (green arrow), covalent attachment of DNA probe (pink arrow), quenching with Et (orange arrow), and interaction with microRNA-21 (violet arrow). The inset shows the $\Delta\theta_{\text{SPR}}$ obtained after addition of microRNA-21, used as the analytical signal. b) $\Delta\theta_{\text{SPR}}$ calculated from the sensorgram obtained in a).

One of the main advantages of SPR-based biosensors is the capability to follow in real time the different steps during the construction of the bioanalytical platform and the detection of the biosensing event. Figure II.9a shows the SPR profiles obtained during the building of the whole bioanalytical platform (Au/MPS/(PDDA/GO)₂/DNA) and the target recognition. The analytical signal in the presence of microRNA-21 was obtained from the change in θ_{SPR} before and after the target addition and rinsing with Tween + buffer solution (inset of Figure II.9a). To evaluate

more clearly these changes, Figure II.9b displays the increment of $\Delta\theta_{\text{SPR}}$ after the incorporation of each layer of the biosensing platform and after the hybridization with microRNA-21.

The effect of the hybridization time was studied for 1.0×10^{-8} M microRNA-21. The SPR angle increases with the hybridization time from 60 to 120 min (13.9, 20.9 and 42.5 $\text{m}^\circ\text{M}^{-1}$ for 60, 90 and 120 min, respectively) and we selected 120 min as the best compromise between assay time and sensitivity. The effect of the amount of DNA probe covalently attached at Au/MPS/(PDDA/GO)₂ through the EDC/NHS chemistry, was also investigated by SPR. No significant changes in θ_{SPR} were observed for 50, 100 and 300 ppm DNA probe; therefore, we selected 50 ppm for further work. To demonstrate the advantages of GO on the SPR response, we built another supramolecular architecture by using PAA as negatively charged polymer instead of GO. $\Delta\theta_{\text{SPR}}$ increases during the assembling of the two (PDDA/PAA) bilayers although after the covalent attachment of the DNA probe and further hybridization with microRNA-21, the changes in the SPR angle were very small, indicating that the presence of GO is really necessary to obtain a sensitive SPR response (not shown).

II.3.3.2. Analytical performance of the genosensor

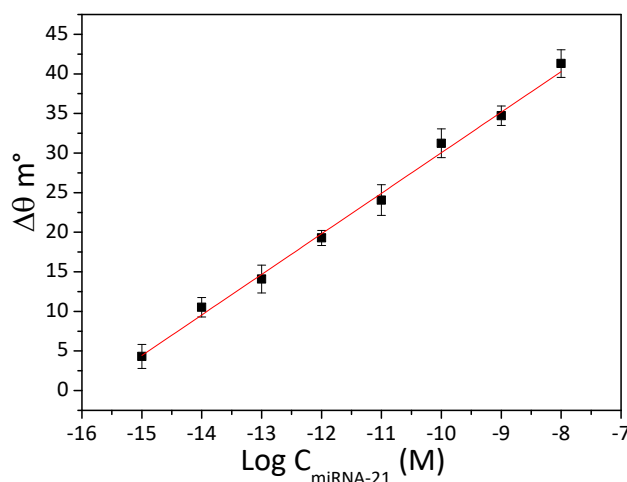


Figure II.10. Calibration plot for microRNA-21 quantification. Each point is an average of three different experiments.

Figure II.10 displays the plot of $\Delta\theta_{\text{SPR}}$ as a function of microRNA-21 concentration. There is a

linear dependence between 1.0 fM and 10 nM, with a sensitivity of $(5.1 \pm 0.1) \text{ m}^{\circ}\text{M}^{-1}$ and a detection limit of 0.3 fM (calculated as $3 \times \text{SD}/s$ where SD is the standard deviation of the blank signal and s , the sensitivity). The reproducibility, obtained from the determination of 10^{-10} M with three different biosensors was 5.8%. Table II.4 compares the analytical characteristics of our biosensor with the most relevant SPR-based microRNA-21 biosensors reported in the last years. The bioanalytical platform reported here presents detection limits lower or comparable to most of the biosensors reported in the Table II.4 and higher than the one obtained using an amplification signal based on the use of antimonene and AuNRs [20]. Therefore, the proposed strategy demonstrated to be competitive compared to the SPR-based microRNA21 biosensors already reported since it presents very good analytical performance using a simple scheme without the need of amplification steps. The selectivity of the biosensor was examined through the interaction of the biosensor with two non-complementary sequences, a fully non-complementary one and a one-base mismatch sequence. The response of the biosensor in both cases is considerably smaller than the one for microRNA-21. In fact, the analytical signal for the fully non-complementary was 0% while for a one-base mismatched sequence, it was only 40% of the one obtained in the presence of microRNA-21.

Table II.4. Comparison of the analytical characteristics of the proposed biosensor with the most relevant SPR-based microRNA-21 biosensors reported in the last years.

Target	Technique used for detection	Signal amplification strategy	DL	Linear range (μM)	Real sample	Ref.
miRNA-21	SPR	Gold nanoparticles (AuNPs) coupled with DNA supersandwich	8 fM	Up to 150 pM	Human serum	[18]
miRNA-21	SPR	DNA-linked AuNPs, DNA supersandwich structure, and positively charged silver nanoparticles (AgNPs)	0.6 fM	Up to 10 pM	–	[19]
miRNA-21 miRNA-55	SPR	Au nanorods connected to amplify SPR signal and antimonene for discriminating ssDNA and DNA-RNA heteroduplex	10 aM	10^{-17} to 10^{-11} M	–	[20]
miRNA-21 miR-10b	LSPR	–	23 – 35 fM	0.01–100 nM	Plasma	[21]
miRNA-21	SPR	[PDDA-GO] ₂	0.3 fM	1.0×10^{-15} to 1.0×10^{-6} M	Urine	This work

LSPR solid-state localized surface plasmon resonance

To evaluate the usefulness of Au/MPS/(PDDA/GO)₂/DNA biosensing platform for further

analytical applications, we quantify microRNA-21 in a 1:10 diluted urine sample enriched with 1.0×10^{-10} M microRNA-21, being the recovery 91.3 and 87.0 %. These results indicate that the proposed biosensor could be used for practical applications.

Conclusions

In summary, we reported a SPR biosensor for the femtomolar quantification of microRNA-21 using a simple scheme based on a supramolecular architecture built at a thiolated gold platform containing GO with successful application for the quantification of microRNA-21 in enriched urine samples. The incorporation of GO in the multistructure facilitates the covalent attachment of the NH₂-DNA probe and makes possible the enhancement of the SPR analytical signal, eliminating, in this way, the need for additional amplification scheme. The proposed strategy opens the door to the development of other biosensors by anchoring the corresponding biorecognition molecule at Au/MPS/(PDDA/GO)₂.

Acknowledgements

Financial support from CONICET, ANPCyT, SECyT-UNC (Argentina) and ECOS-SUD program (A16E02). M. L.-M. thankfully acknowledges CONICET for the PhD fellowship. Y. Zhang thanks Chinese Scholarship Council for providing a 3-year scholarship for her stay in France and LabEx MICHEM for supporting her living expenses in UNC Argentina.

Compliance with ethical standards

Conflict of interest The authors declare that they have no conflicts of interest.

References

1. Mazumder S, Datta S, Ray JG, Chaudhuri K, Chatterjee R. Liquid biopsy: miRNA as a potential biomarker in oral cancer. *Cancer Epidemiology* 2019,**58**:137-145.
2. Zhu C-s, Zhu L, Tan D-a, Qiu X-y, Liu C-y, Xie S-s, *et al.* Avenues toward microRNA detection in vitro: a review of technical advances and challenges. *Computational and Structural Biotechnology Journal* 2019,**17**:904-916.
3. Hayes J, Peruzzi PP, Lawler S. MicroRNAs in cancer: biomarkers, functions and therapy. *Trends in molecular medicine* 2014,**20**:460-469.
4. Shajari E, Mollasalehi H. Ribonucleic-acid-biomarker candidates for early-phase group detection of common cancers. *Genomics* 2020,**112**:163-168.
5. Peng Y, Croce CM. The role of MicroRNAs in human cancer. *Signal transduction and targeted therapy* 2016,**1**:1-9.
6. Hasanzadeh M, Movahedi M, Rejali M, Maleki F, Moetamani-Ahmadi M, Seifi S, *et al.* The potential prognostic and therapeutic application of tissue and circulating microRNAs in cervical cancer. *Journal of cellular physiology* 2019,**234**:1289-1294.
7. Sharma N, Baruah MM. The microRNA signatures: aberrantly expressed miRNAs in prostate cancer. *Clinical and translational oncology* 2019,**21**:126-144.
8. Zheng W, Zhao J, Tao Y, Guo M, Ya Z, Chen C, *et al.* MicroRNA-21: A promising biomarker for the prognosis and diagnosis of non-small cell lung cancer. *Oncology letters* 2018,**16**:2777-2782.
9. Kura B, Parikh M, Slezak J, Pierce GN. The influence of diet on microRNAs that impact cardiovascular disease. *Molecules* 2019,**24**:1509.
10. Varkonyi-Gasic E, Wu R, Wood M, Walton EF, Hellens RP. Protocol: a highly sensitive RT-PCR method for detection and quantification of microRNAs. *Plant methods* 2007,**3**:1-12.
11. Lee I, Ajay SS, Chen H, Maruyama A, Wang N, McInnis MG, *et al.* Discriminating single-base difference miRNA expressions using microarray Probe Design Guru (ProDeG). *Nucleic acids research* 2008,**36**:e27.
12. Li P, Long F, Chen W, Chen J, Chu PK, Wang H. Fundamentals and applications of surface-enhanced Raman spectroscopy-based biosensors. *Current Opinion in Biomedical Engineering* 2020,**13**:51-59.
13. Várallyay E, Burgyán J, Havelda Z. MicroRNA detection by northern blotting using locked nucleic acid probes. *Nature protocols* 2008,**3**:190-196.
14. Liu L, Song C, Zhang Z, Yang J, Zhou L, Zhang X, *et al.* Ultrasensitive electrochemical detection of microRNA-21 combining layered nanostructure of oxidized single-walled carbon nanotubes and nanodiamonds by hybridization chain reaction. *Biosensors and Bioelectronics* 2015,**70**:351-357.
15. Jirakova L, Hrstka R, Campuzano S, Pingarrón JM, Bartosik M. Multiplexed immunosensing platform coupled to hybridization chain reaction for electrochemical determination of microRNAs in clinical samples. *Electroanalysis* 2019,**31**:293-302.
16. Kutluk H, Bruch R, Urban GA, Dincer C. Impact of assay format on miRNA sensing: Electrochemical microfluidic biosensor for miRNA-197 detection. *Biosensors and Bioelectronics* 2020,**148**:111824.
17. Zouari M, Campuzano S, Pingarrón JM, Raouafi N. Femtomolar direct voltammetric determination of circulating miRNAs in sera of cancer patients using an enzymeless biosensor. *Analytica Chimica Acta* 2020,**1104**:188-198.
18. Wang Q, Liu R, Yang X, Wang K, Zhu J, He L, *et al.* Surface plasmon resonance biosensor for enzyme-free amplified microRNA detection based on gold nanoparticles and DNA supersandwich. *Sensors and Actuators B: Chemical* 2016,**223**:613-620.
19. Liu R, Wang Q, Li Q, Yang X, Wang K, Nie W. Surface plasmon resonance biosensor for sensitive detection of microRNA and cancer cell using multiple signal amplification strategy. *Biosensors and Bioelectronics* 2017,**87**:433-438.
20. Xue T, Liang W, Li Y, Sun Y, Xiang Y, Zhang Y, *et al.* Ultrasensitive detection of miRNA with an antimonene-based surface plasmon resonance sensor. *Nature communications* 2019,**10**:1-9.
21. Šířpová H, Zhang S, Dudley AeM, Galas D, Wang K, Homola Ji. Surface plasmon resonance biosensor for rapid label-free detection of microribonucleic acid at subfemtomole level. *Analytical chemistry* 2010,**82**:10110-10115.
22. Joshi GK, Deitz-McElyea S, Johnson M, Mali S, Korc M, Sardar R. Highly specific plasmonic biosensors for ultrasensitive microRNA detection in plasma from pancreatic cancer patients. *Nano letters* 2014,**14**:6955-6963.

23. Joshi GK, Deitz-McElyea S, Liyanage T, Lawrence K, Mali S, Sardar R, *et al.* Label-free nanoplasmonic-based short noncoding RNA sensing at attomolar concentrations allows for quantitative and highly specific assay of microRNA-10b in biological fluids and circulating exosomes. *ACS nano* 2015,**9**:11075-11089.
24. Schmieder S, Weißpflog J, Danz N, Klotzbach U, Sonntag F. Detection of miRNA using a surface plasmon resonance biosensor and antibody amplification. *Current Directions in Biomedical Engineering* 2016,**2**:135-138.
25. Feng X, Han T, Xiong Y, Wang S, Dai T, Chen J, *et al.* Plasmon-Enhanced Electrochemiluminescence of Silver Nanoclusters for microRNA Detection. *ACS sensors* 2019,**4**:1633-1640.
26. Zeng S, Baillargeat D, Ho H-P, Yong K-T. Nanomaterials enhanced surface plasmon resonance for biological and chemical sensing applications. *Chemical Society Reviews* 2014,**43**:3426-3452.
27. Grigorenko A, Polini M, Novoselov K. Graphene plasmonics. *Nature photonics* 2012,**6**:749-758.
28. Jung I, Rhyee J-S, Son JY, Ruoff RS, Rhee K-Y. Colors of graphene and graphene-oxide multilayers on various substrates. *Nanotechnology* 2011,**23**:025708.
29. Primo EN, Kogan MJ, Verdejo HE, Bollo S, Rubianes MD, Rivas GA. Label-free graphene oxide-based surface plasmon resonance immunosensor for the quantification of galectin-3, a novel cardiac biomarker. *ACS applied materials & interfaces* 2018,**10**:23501-23508.
30. Barreira SV, García-Morales V, Pereira CM, Manzanares JA, Silva F. Electrochemical impedance spectroscopy of polyelectrolyte multilayer modified electrodes. *The Journal of Physical Chemistry B* 2004,**108**:17973-17982.
31. Fernández-Sánchez C, McNeil CJ, Rawson K. Electrochemical impedance spectroscopy studies of polymer degradation: application to biosensor development. *TrAC Trends in Analytical Chemistry* 2005,**24**:37-48.
32. Chirea M, García-Morales V, Manzanares JA, Pereira C, Gulaboski R, Silva F. Electrochemical characterization of polyelectrolyte/gold nanoparticle multilayers self-assembled on gold electrodes. *The Journal of Physical Chemistry B* 2005,**109**:21808-21817.

Conclusion of the Chapter II

Optical technique is one of the most widely used DNA detection technique to translate the DNA hybridization biological event into optical signal (the emission or absorption of fluorescence, a change in color, luminescence or surface plasmon resonance (SPR) signal). Then this optical signal can then be translated and collected as electrical signal for digital processing for monitoring the biological recognition and quantification. In this chapter, we used two optical techniques to quantify miRNA-21 in plasma or other biological fluids of human, one is the RT-qPCR method, the other is SPR.

RT-qPCR is the gold standard quantitative detection method of gene (miRNA). Here, two methods, stem-loop primer reverse transcription and poly(A)-tail extension are used, and then the samples are amplified by polymerase chain reaction (PCR) while monitoring the fluorescence of the TaqMan probe. The latter is more sensitive and specific, and can be used to detect the attomole of miRNA-21 in plasma. The limitation of this method are high cost and long analysis time. In addition, more operation steps and PCR amplification step are easy to induce errors. Therefore, in order to overcome these limitations, a DNA biosensor that can directly detect DNA without amplification has developed.

SPR based-biosensor is another optical biosensor can monitor the association and dissociation of biological molecules on a gold film surface in a real-time and without any labeling. Here, we reported a SPR biosensor for the femtomolar quantification of microRNA-21 using a simple scheme based on a supramolecular architecture built at a thiolated gold platform containing GO. SPR can dynamically monitor the whole process of biomolecular interaction in real time, however, errors caused by indirect signal transduction, huge detection equipment and high cost limit the development of SPR biosensor.

CHAPTER III: Experimental Results

—miRNA Quantification by Electrochemistry

Contents

CHAPTER III: Experimental Results	181
—miRNA Quantification by Electrochemistry	181
LIST OF FIGURES	184
LIST OF TABLES	185
III.1. miRNA-21 quantification by EIS.....	186
Non-amplified impedimetric genosensor for quantification of miRNA-21 based on the use of reduced graphene oxide modified with chitosan	187
Abstract	187
Keywords	188
III.1.1. Introduction.....	188
III.1.2. Experimental	191
III.1.2.1. Reagents	191
III.1.2.2. Apparatus	191
III.1.2.3. Synthesis of RGO-CHIT	192
III.1.2.4. Construction of the biosensing platform.....	193
III.1.3. Results and discussion	194
Conclusions.....	201
Acknowledgements.....	201
Declaration of Conflict of Interest	201
References.....	201
Supplementary information	204
III.2. miRNA-21 quantification by Chronoamperometry	205
Electrochemical and reverse transcriptase real-time PCR analysis of miRNA-21	206
Abstract.....	206
Keywords	207
III.2.1. Introduction.....	207
III.2.2. Experimental section.....	209
III.2.2.1. Chemicals and biochemical compounds	209
III.2.2.2. Instruments.....	210
III.2.2.3. Plasma purification and RT-qPCR.....	210
III.2.2.4. Gold UME array fabrication and two-electrodes setup	211

III.2.2.5. Electrochemical measurements.....	212
III.2.2.6. Pretreatment of the gold ultramicroelectrodes (UME) array	213
III.2.2.7. Immobilization of DNA-probe self-assembled monolayer.....	213
III.2.2.8. Interfacial target oligonucleotide hybridization.....	214
III.2.3. Results and Discussion.....	215
III.2.3.1. Electrochemical response of gold UME array	215
III.2.3.2. Pretreatment of gold UME array.....	217
III.2.3.3. Calibration curve.....	221
III.2.3.4. Quantification of miRNA-21 in plasma based on RT-qPCR.....	222
III.2.3.5. The comparison between electrochemistry and RT-qPCR.....	223
Conclusions.....	223
References.....	224
Supplementary information	226
Conclusion of the Chapter III.....	230

LIST OF FIGURES

Figure III.1. Schematic representation of the different steps during the building of the miRNA-21 genosensor.	194
Figure III.2. (A) Nyquist plots obtained during the construction of biosensor. Inset: Equivalent circuit used to fit the experimental results (B) Charge transfer resistance after each step during the construction of the biosensing layer and after the hybridization with 1.0×10^{-8} M miRNA-21. Redox marker: 1.0×10^{-3} M $[\text{Fe}(\text{CN})_6]^{3-}/[\text{Fe}(\text{CN})_6]^{4-}$; Frequency range: 10 KHz to 10 mHz; Potential perturbation: 10 mV; Working potential: 0.200 V. Supporting electrolyte: 0.05 M phosphate buffer solution pH 7.40 with 0.5 M NaCl..	194
Figure III.3. (A) Nyquist plots for 1.0×10^{-3} M $[\text{Fe}(\text{CN})_6]^{3-}/[\text{Fe}(\text{CN})_6]^{4-}$ obtained at Au/MPS/RGO-CHIT/DNA for different concentrations of miRNA-21. Other conditions as in Figure III.2. (B) Calibration plot obtained from the impedimetric response shown in (A).....	196
Figure III.4. Charge transfer resistances obtained at GCE/MPS/RGO-CHIT/Alb/DNA in the presence of 1.0×10^{-9} M miRNA-21, 1-base-mismatch and fully non-complementary sequences. Hybridization time: 75 min. Other conditions as in Figure III.2.....	197
Figure III.5. UV-vis spectra corresponding to GO-CHIT (-) and RGO-CHIT (-).....	204
Figure III.6. Effect of the hybridization time of miRNA-21 at Au/MPS/RGO-CHIT/DNA on the R_{ct} in the presence of 50 ppm NH_2 -DNA. Concentration miRNA-21: 1.0×10^{-9} M. Redox marker: 1.0×10^{-3} M $[\text{Fe}(\text{CN})_6]^{3-}/[\text{Fe}(\text{CN})_6]^{4-}$; Frequency range: 10 KHz to 10 mHz; Potential perturbation: 10 mV; Working potential: 0.200 V. Supporting electrolyte: 0.050 M phosphate buffer solution pH 7.40 with 0.5 M NaCl.	204
Figure III.7. Schematic illustration of research in this article. (A) Real-time polymerase chain reaction (RT-qPCR) analysis and (B) label-free electrochemical quantification of the microRNAs.....	209
Figure III.8. Schematic illustration of the 10-band gold UME array platform and microdevice, a) 10-band gold UME array. b) PDMS well. c) gold band UME array platform. d) Cross section view of gold UME showing the layers and dimensions.....	211
Figure III.9. Chemical activation of the disulfide, immobilization of the DNA-probe and hybridization of the miRNA-target.	214
Figure III.10. Chronoamperometry responses of gold UME array (5 bands) measured at various potentials that from -0.3V to +0.3V in 0.5 M NaCl, 5 mM $[\text{Fe}(\text{III})(\text{CN})_6]^{3-} / [\text{Fe}(\text{II})(\text{CN})_6]^{4-}$: each circle corresponds to the chronoamperometric current measured 30 seconds after application of a constant potential difference ΔE complexes.	215
Figure III.11. Chronoamperometry response of bare Au UME array (5 gold bands) (red) and after DNA probe immobilization (blue) in 0.5 M NaCl, 5 mM $[\text{Fe}(\text{III})(\text{CN})_6]^{3-}$, 5 mM $[\text{Fe}(\text{II})(\text{CN})_6]^{4-}$, 5 μM MB solution with different treatment: acid chemical (H_2SO_4), basic chemical (KOH), electrochemical pretreatment (+ 1.2 V) and plasma (Ar).	218
Figure III.12. Blocking efficiency of long-range electron transfer for three saline buffer solutions.	219
Figure III.13. Chronoamperometry, Electrochemical response before hybridization (blue) and Electrochemical response after hybridization (red) of microelectrode array (10 bands). $\Delta E = 0.05\text{V}$, $\Delta I =$	

NaH₂PO₄ 0.3 M + [Fe (III)(CN)₆]³⁻/ [Fe (II)(CN)₆]⁴⁻ 5 mM and presence (full line) or absence of (dotted line) MB 5 μM by different activation methods: flame (a), chemical activation (b), electrochemical activation (c). The percentage of change current after hybridization by different activation methods and in different electrolyte that presence or absence of MB (d).....220

Figure III.14. The calibration curve of different concentrations of miRNA-21 in the buffer obtained at gold UME array by chronoamperometry.221

Figure III.15. The qPCR calibration curve of different concentration miRNA-21 sample in plasma of *TaqMan*[®] advanced microRNA assays.222

Figure III. 16. The vertical section of two-electrode setup of 10-gold bands UME array device.226

Figure III.17. Cyclic voltammograms of gold UME array (10 bands) in 5 mM [Fe (III)(CN)₆]³⁻ and 5mM [Fe (II)(CN)₆]⁴⁻ (red) with 0.5 M NaCl, and in NaCl 0.5 M (blue). The potential was swept from -0.3 V to +0.3 V at a scan rate of 50 mV/s.228

Figure III.18. The current of each single band UME vs average current of each band in the UME array which measured in 0.5M NaCl presence of 5 mM [Fe (III)(CN)₆]³⁻ and 5 mM [Fe (II)(CN)₆]⁴⁻ by cyclical voltammetry (a) and chronoamperometry (b).....229

LIST OF TABLES

Table III.1. Comparison of the analytical parameters for the most relevant miRNA-21 electrochemical biosensors reported in the last two years.199

Table III.2. The sequences of the oligonucleotides.210

Table III.3. The low detection limit of miRNA-21 by chronoamperometry and RT-qPCR.223

III.1. miRNA-21 quantification by EIS

Impedance technology is an effective tool for studying electrode processes. It is widely used in the field of electrochemical research. It can obtain more kinetic information and electrode interface structure information than other electrochemical methods, such as electron transfer resistance, double electricity Layer capacitance, etc. It should be noted that data from impedance experiments contain more information than from voltammetric experiments.

This section presented the *impedimetric genosensor* for non-amplified quantification of miRNA-21 based on the use of reduced graphene oxide modified with chitosan.

I and Michael López Mujica completed the experiment and data analysis part together. This part of the experiment was conducted in the departamento de Fisicoquímica at the facultad de Ciencias Químicas, Nacional de Córdoba, Argentina.

This section had been published in “*Microchemical Journal*”.

Thanks to Gustavo Rivas and Fabiana Gutiérrez for the guidance and help of this part of the experiment, and Michael López Mujica for helping me in the experiment part. Thanks to Gustavo Rivas, Fabiana Gutiérrez, Michael López Mujica, and other colleagues for helping me of my life in Argentina

Thanks to the financial support from CONICET, ANPCyT, and SECyT-UNC (Argentina) and ECOS-SUD program (A16E02).

Thankfully acknowledges LabEx MICHEM for supporting my living expenses in UNC Argentina.

Non-amplified impedimetric genosensor for quantification of miRNA-21 based on the use of reduced graphene oxide modified with chitosan

Michael López Mujica¹, Yuanyuan Zhang², Fabiana Gutiérrez^{1,*}, Féthi Bédioui^{2,*}, Gustavo Rivas^{1,*}

¹INFIQC-CONICET, Departamento de Fisicoquímica, Facultad de Ciencias Químicas, Universidad Nacional de Córdoba, Ciudad Universitaria. 5000 Córdoba, Argentina.

²Chimie ParisTech, PSL University, CNRS 2027, Institute of Chemistry for Life and Health Sciences, SEISAD 75005 Paris, France.

*Corresponding authors

*Email: fabigutierrez@gmail.com; fethi.bedioui@chimieparistech.psl.eu; grivas@fcq.edu.ar

Phone number: +54-351-5353866; Fax number: +54-351-4334188.

Abstract

We report here an impedimetric genosensor for the quantification of microRNA-21 using $[\text{Fe}(\text{CN})_6]^{3-/4-}$ as redox probe to transduce the hybridization event. The biosensing platform was built at a thiolated-gold electrode by covalent bond of reduced graphene oxide (RGO) modified with chitosan (CHIT) and further covalent attachment of the aminated DNA probe. GO was used to provide the carboxylic groups for the covalent attachment of CHIT and, once reduced, to improve the electroactivity of the resulting platform, while CHIT served as a bridge between the thiol and the aminated probe DNA. The proposed bioanalytical platform allows the label-free, non-amplified, simple and fast biosensing of microRNA-21, with a linear range between 1.0×10^{-12} M and 1.0×10^{-8} M, a sensitivity of $(134 \pm 4) \Omega\text{M}^{-1}$ ($r^2 = 0.996$), a detection limit

of 300 fM, and a reproducibility of 5.9 % for 1.0×10^{-12} M miRNA-21 and 2.2 % for 1.0×10^{-9} M miRNA-21. The genosensor was successfully used for the quantification of microRNA-21 in enriched human blood serum, urine and saliva samples.

Keywords

microRNA-21; Impedimetric biosensor; Biomarker; Graphene oxide; Chitosan.

III.1.1. Introduction

MicroRNAs (miRNAs) are non-coding RNAs of 19-25 nucleotides in length, that can be present in intergenic or intragenic regions of the genome and are involved in the post-transcriptional regulation of gene expression [1]. A dysregulation can be associated with cancer, dementia, and cardiovascular diseases, among other pathologies. miRNAs can have the role of tumor suppression or oncogenic function in cancer and have been connected with processes associated with cancer, such as apoptosis, invasion, metastasis, and proliferation [1]. Therefore, the development of highly sensitive and selective methodologies to quantify miRNAs, is highly required. Their low abundance, short length and high sequence-similarity with other family members, make the quantification of miRNAs a big challenge. In the last years there has been an increasing interest for the design of biosensors that allow the sensitive, selective and friendly quantification of miRNAs [2-4]. In this sense, the electrochemical ones have demonstrated to be very efficient [5].

miRNA-21 was one of the first mammalian miRNAs identified [6] and has been proposed as diagnostic and prognostic biomarker, and even as therapeutic target for several types of cancer [7]. The upregulation of miRNA-21 in breast, pancreatic, prostate, and colorectal cancers, makes miRNA-21 a non-invasive diagnostic biomarker. Therefore, as it is upregulated in several types of cancer, is convenient to use miRNA-21 as part of a panel of biomarkers instead of a specific biomarker for one type of cancer [1].

Most of the electrochemical miRNA-21 biosensors reported in the last couple of years have

been mainly based on the use of different amplification strategies. Zhang H. et al. [8] reported the use of a hairpin DNA modified-Au electrode associated with the action of a duplex specific nuclease (DSN), and the incorporation of a biotinylated signaling DNA/streptavidin-modified Au-nanoparticles(NPs)/biotinylated-horseradish peroxidase (HRP) to generate an enhanced analytical signal in the presence of hydrogen peroxide and 3,3',5,5'-tetramethylbenzidine (TMB). A signal amplification mediated by PdNPs accumulated at a guanine-rich ssDNA generated through rolling circle amplification (RCA) was also proposed [9]. Guo et al. [10] described the sub-fM biosensing by combination of a dual signal amplification strategy using hybridization chain reaction (HCR) and enzyme induced metallization (EIS). Tian et al. [11] described the use of a hairpin capture probe immobilized at Fe₃O₄, which is opened after interacting with miRNA-21, to allow the amplification by HCR and the synergized catalytic reduction of hydrogen peroxide/TMB system in the presence of a Cu(II) planar complex. Liang et al. [12] presented the pM detection of miRNA-21 using an amplification scheme based on HCR in connection with different strategies to transduce the hybridization event. An impedimetric quantification of miRNA-21, reported by Zhang et al. [13], was based on the use of glassy carbon electrode (GCE) modified with ZrO₂, graphene oxide (GO) and polyacrylic acid (PAA) containing the cyclically generated dsDNA from the hairpin unfolded after hybridization. The electrostatically accumulated [Ru(NH)₆]³⁺ (RuHex) at different platforms following diverse schemes was used to generate the analytical signal either with or without the catalytic effect of [Fe(CN)₆]³⁻ [14-16]. Feng et al. [17] proposed the voltammetric (SWV) quantification of miRNA-21 from the molybdophosphate generated through the facilitated accumulation of molybdate at the phosphate residues of the resulting DNA using HCR. Chen et al. [18] described a biosensor based on the SWV signal of the methylene blue (MB) released from mesoporous silica nanospheres-hairpin H1 and intercalated within the dsDNA generated at the gold electrode/capture DNA as a consequence of CHR after H1-miRNA-21 hybridization and CHA in the presence of the hairpin H2. A ratiometric scheme based on the different currents ratio of two redox markers before and after hybridization through mismatched catalytic hairpin

assembly (CHA) amplification and generation of stable “Y”-shaped DNA complexes, was reported by Li et al. [19]. Pingarrón’s group [20] reported an innovative alternative for the sub-pM detection of miRNA-21 using streptavidin-modified magnetic beads in connection with geno- and immunoassays and the detection at a magneto SPE through the use of anti DNA-RNA antibody modified with HRP. A highly sensitive DPV-detection of miRNA-21 through the sandwich hybridization with a thiolated capture probe-AuNPs-modified GCE and a MWCNTs-thionin-signaling probe, was also reported [21].

Although the non-amplified miRNA-21 electrochemical biosensors are not very frequent, some interesting alternatives have been also reported. Luo et al. [22] proposed the fM ratiometric detection of exosomal miRNA-21 using two redox markers located in a Y shape-like structure before and after hybridization. Ghazizadeh et al. [23] presented an original strategy by modifying SPE with MCFexosomes and the protein p19. Kaugkamano et al. [24] described the fM detection of miRNA-21 through the decrease of Ag oxidation signal at Au modified with polypyrrol/Ag and pyrrolidinyl PNA. Bharti et al. [25] proposed the use of fluorine tin oxide (FTO) properly modified to support the biotinylated probe and the , with transduction of the hybridization event through the decrease of the DPV signal of $[\text{Fe}(\text{CN})_6]^{3-/4-}$. The sub-pM detection of miRNA-21 based on the decrease of the SWV-thionin-redox signal at GCE/MoS₂-thionine-AuNPs was described by Zhu et al. [26]. Azzouzi et al. [27] proposed the impedimetric detection of miRNA-21 through the increment of the charge transfer resistance of a redox mediator produced by the anchoring of the complex biotin-molecular beacon-AuNPs-hybrid at the GCE/neutravidin.

The present work is focused on the development of a non-amplified impedimetric biosensor for miRNA-21 quantification taking advantage of the unique properties of graphenaceous materials in a double role of anchoring support to covalently immobilize the amine-rich polymer chitosan (CHIT) as graphene oxide (GO) and, as reduced graphene oxide (RGO), to improve to electroactivity of the resulting platform. The biosensing supramolecular

architecture was built at 3-mercapto-1-propanesulfonate-modified gold electrode by self-assembling of RGO-CHIT and covalent attachment of NH₂-DNA probe. The transduction of the hybridization event was obtained from the change of the charge transfer resistance (R_{ct}) using [Fe(CN)₆]^{3-/4-} as redox marker. In the following sections we discuss the characterization of the biosensing platform and the analytical performance of the resulting genosensor.

III.1.2. Experimental

III.1.2.1. Reagents

Sodium 3-mercapto-1-propanesulfonate (MPS), glutaraldehyde (glu), chitosan (CHIT), N-(3-dimethylaminopropyl)-N'-ethylcarbodiimide hydrochloride (EDC), N-hydroxy-succinimide (NHS), and bovin serum albumin (Alb) were purchased from Sigma. Potassium ferrocyanide was obtained from Merck and potassium ferricyanide from Biopack. Ethanol, sulfuric acid (98%) and sodium hydroxide were provided by J. T. Baker. Graphene oxide (GO, aqueous dispersion 4.0 mg mL⁻¹) was obtained from Graphenea. Other chemicals were reagent grade and used without further purification. DNA and RNA sequences, obtained from Invitrogen Life Technologies, are the following:

DNA probe: 5'-NH₂-TCA-ACA-TCA-GTC-TGA-TAA-GCT-A-3'

miRNA-21: 5'-UAG-CUU-AUC-AGA-CUG-AUG-UUG-A-3'

Single-base mismatch: 5'-UAG-CUU-AUC-ACA-CUG-AUG-UUG-A-3'

Non-complementary sequence: 5'-GGG-GGG-GGG-GGG-GGG-GGG-GGG-3'

Ultrapure water ($\rho = 18.2 \text{ M}\Omega \text{ cm}$) from a Millipore-MilliQ system was used for preparing all the solutions.

III.1.2.2. Apparatus

A platinum wire and Ag/AgCl, 3 M NaCl (BAS) were used as counter and reference electrodes,

respectively. All potentials are referred to the latter. Gold disk electrodes were used for preparing the biosensor. The gold working electrodes were cleaned before each experiment by successive mechanical, chemical and electrochemical treatment. The mechanical treatment consisted in polishing with 0.05 μm alumina for 6 min, followed by sonication in deionized water for 5 min. Chemical treatment was performed by immersion in “Piranha” solution (1:3 v/v $\text{H}_2\text{O}_2/\text{H}_2\text{SO}_4$) for 5 min, followed by sonication for 10 seconds in ultrasonic bath and rinsing with ultrapure water. During the electrochemical treatment, the surfaces were stabilized in 0.500 M H_2SO_4 solution by applying two consecutive step potentials of 2.0 V and -1.0 V for 2 and 4 seconds, respectively. The state of the surface after the pretreatment was evaluated by cyclic voltammetry at 0.100 Vs^{-1} in a 0.500 M H_2SO_4 solution.

Electrochemical Impedance Spectroscopy (EIS) measurements were performed with an PGSTAT30 potentiostat (Methrom). The redox probes were 1.0×10^{-3} M $[\text{Fe}(\text{CN})_6]^{3-}/[\text{Fe}(\text{CN})_6]^{4-}$ and the experiments were carried out in a 0.050 M phosphate buffer solution pH 7.40. EIS parameters were the following, amplitude: 0.010 V, frequency range: between 1.0×10^{-2} and 1.0×10^6 Hz, and working potential: 0.200 V. The impedance spectra were analyzed and fitted by using the Z-view program.

UV-Vis experiments were carried out with a Shimadzu UV1601 spectrophotometer and a quartz cuvette of 0.1 cm path length.

III.1.2.3. Synthesis of RGO-CHIT

A volume of 3.125 mL of 4.0 mg mL^{-1} GO solution was mixed with 6.875 mL of a 2.00 mg mL^{-1} CHIT previously prepared in a 2-(N-morpholino) ethanesulfonic acid (MES) 0.100 M pH 5.00 by sonicating for 2 h in ultrasonic bath. The resulting GO-CHIT mixture was sonicated in ultrasonic bath for 2 h to obtain a homogeneous dispersion. After that, the carboxylate groups of GO were activated with 0.100 M EDC and 0.100 M NHS by sonication for 2 hours and overnight reaction until completeness under stirring conditions. The purification of GO-CHIT

was carried out by centrifugation for 60 min at 3500 rpm and further resuspension of the pellet in a 0.15 M MES buffer pH 5.00. This process was repeated 4 times to eliminate the excess of CHIT. Subsequently, RGO-CHIT was chemically reduced by adding excess of NaBH₄ and stirring for 24 h. The resulting RGO-CHIT was washed following the same procedure as indicated before for washing GO-CHIT. The characterization of the synthesis was carried out by UV-vis spectroscopy, following the displacement of the GO extinction band at 234 nm (Figure III.5).

III.1.2.4. Construction of the biosensing platform

Figure III.1 presents a schematic illustration of the different steps followed to build the biosensing platform. The gold electrode was modified with a 2.00×10^{-2} M MPS solution (prepared in 1.60×10^{-3} M H₂SO₄) for 60 min. After washing the surface with the sulphuric acid solution and water, RGO-CHIT was electrostatically adsorbed for 60 min. Once the RGO-CHIT was immobilized at the electrode surface and after washing with MES, the amine residues were activated with 1.0 % v/v glutaraldehyde (prepared in 1% v/v CH₃COOH). Previous washing of the surface with 0.050 M phosphate buffer solution pH 7.40, the probe was covalently attached by depositing 20 μ L of 50 ppm NH₂-DNA probe solution (prepared in 0.050 M phosphate buffer pH 7.40 + 0.500 M NaCl) at the electrode surface for 30 min. After this step, the surface was washed with 0.050 M phosphate buffer pH 7.40 + 0.500 M NaCl and before performing the hybridization, the surface was blocked with 2.0 % w/v albumin for 30 min to avoid non-specific adsorptions. The hybridization was performed at the resulting Au/MPS/RGO-CHIT/DNA_{probe} biosensing platform by dropping the 20 μ L of miRNA-21 solution (prepared in 0.050 M phosphate buffer solution pH 7.40 + 0.500 M NaCl) for 75 min.

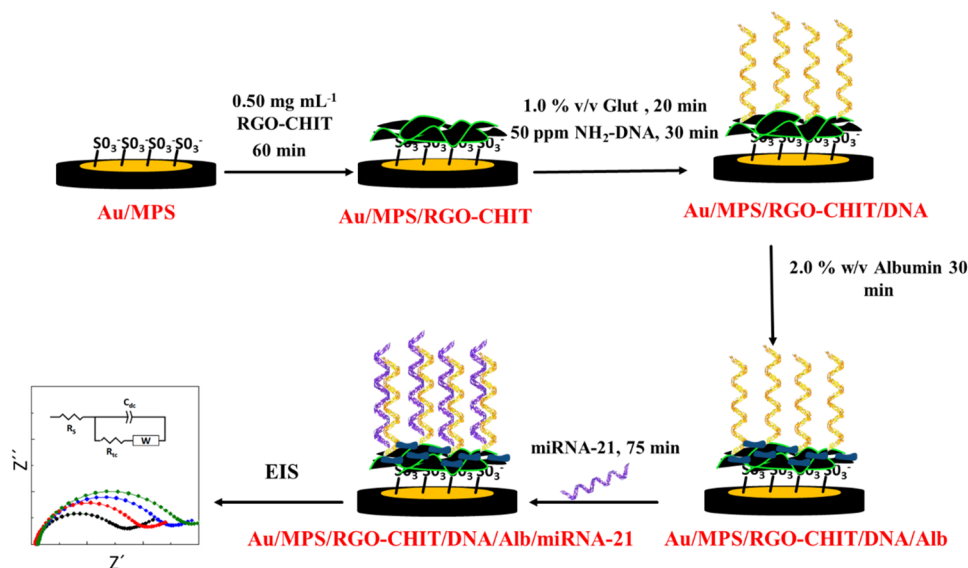


Figure III.1. Schematic representation of the different steps during the building of the miRNA-21 genosensor.

III.1.3. Results and discussion

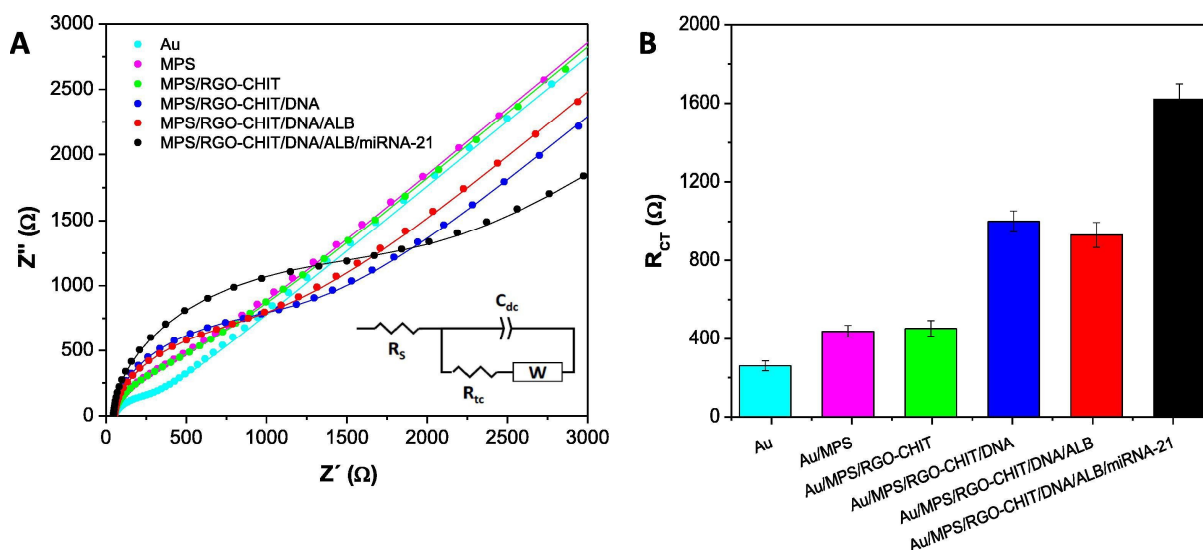


Figure III.2. (A) Nyquist plots obtained during the construction of biosensor. Inset: Equivalent circuit used to fit the experimental results (B) Charge transfer resistance after each step during the construction of the biosensing layer and after the hybridization with 1.0×10^{-8} M miRNA-21. Redox marker: 1.0×10^{-3} M

$[\text{Fe}(\text{CN})_6]^{3-}/[\text{Fe}(\text{CN})_6]^{4-}$; Frequency range: 10 KHz to 10 mHz; Potential perturbation: 10 mV; Working potential: 0.200 V. Supporting electrolyte: 0.05 M phosphate buffer solution pH 7.40 with 0.5 M NaCl.

Figure III.2A shows the Nyquist plots obtained after each step during the construction of the biosensing supramolecular architecture (Au, Au/MPS, Au/MPS/RGO-CHIT, Au/MPS/RGO-CHIT/DNA_{probe}, Au/MPS/RGOCHIT/DNA_{probe}/Alb) and after the hybridization event (Au/MPS/RGOCHIT/DNA_{probe}/miRNA-21) using 1.0×10^{-3} M $[\text{Fe}(\text{CN})_6]^{3-}/[\text{Fe}(\text{CN})_6]^{4-}$ as redox probe. The circles correspond to the experimental points while the solid lines represent the fitting with the model,

in this case a Randles circuit, where R_s is the solution resistance, R_{ct} is the charge transfer resistance, C_{dl} the capacitance of the double-layer and W , the Warburg impedance (Inset of Figure III.2A). Figure III.2B depicts the variation of the charge transfer resistance (R_{ct}) obtained from the Nyquist plots shown in Figure III.2A. The attachment of MPS at Au produced the expected increment of R_{ct} due to the blocking effect of the thiol and the electrostatic repulsion with the redox marker. The adsorption of RGO-CHIT does not produce a significant change in R_{ct} due to the compensation of different effects: the facilitated electrostatic interaction between CHIT and $[\text{Fe}(\text{CN})_6]^{3-}/[\text{Fe}(\text{CN})_6]^{4-}$ and the conductive nature of RGO that would facilitate the charge transfer, and the blocking effect of CHIT that would make more difficult the charge transfer of the redox probe. Once the DNA probe is immobilized at Au/MPS/RGO-CHIT, R_{ct} increases due to the blocking effect of the nonconductive nucleic acid layer and the electrostatic repulsion of the redox marker with the negatively charge ribose-phosphate backbone of DNA. The incorporation of Alb, to avoid the non-specific adsorption, produces a small decrease of R_{ct} mainly due to the shielding of the negative charges of DNA probe that compensates the blocking effect of the non-conductive protein. Once the hybridization with 1.0×10^{-8} M miRNA-21 takes place, there is an important increment of R_{ct} due to the increase of the electrostatic repulsion between the redox probe and the higher negative charge density as a consequence of the surface heteroduplex formation.

The effect of the hybridization time was evaluated from similar experiments performed with 1.0×10^{-9} M miRNA-21. There was an increment in the R_{ct} with the hybridization time from 30 to 75 min mainly due to the increase of the electrostatic repulsion between the redox marker and the enhanced negative charge density resulting from the formation of a higher amount of DNA-miRNA-21 with the hybridization time, to slightly decrease thereafter (Figure III.6). We selected 75 min as the best compromise between sensitivity, reproducibility and assay time.

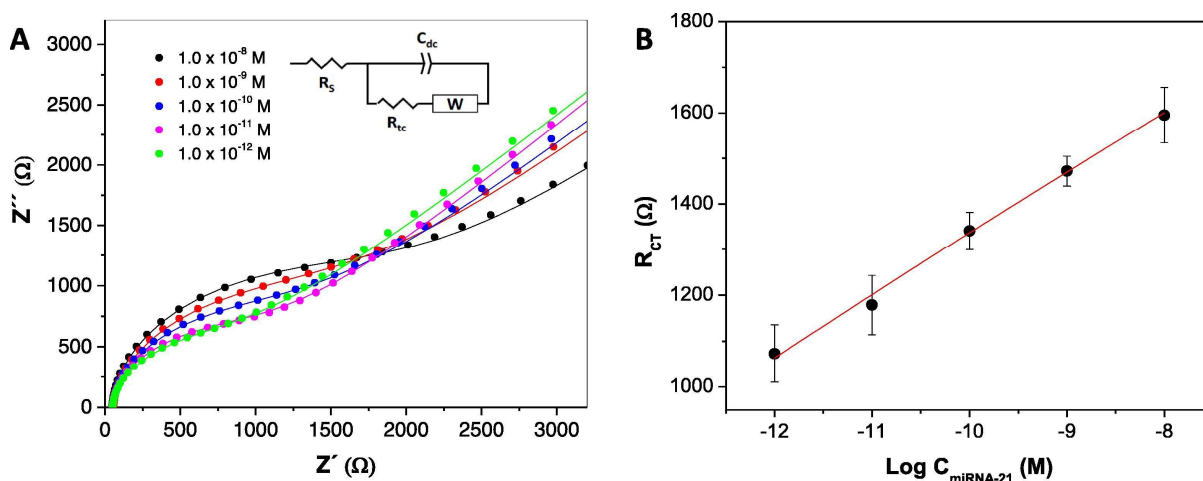


Figure III.3. (A) Nyquist plots for 1.0×10^{-3} M $[\text{Fe}(\text{CN})_6]^{3-}/[\text{Fe}(\text{CN})_6]^{4-}$ obtained at Au/MPS/RGO-CHIT/DNA_{probe} for different concentrations of miRNA-21. Redox marker: 1.0×10^{-3} M $[\text{Fe}(\text{CN})_6]^{3-}/[\text{Fe}(\text{CN})_6]^{4-}$; Other conditions as in Figure III.2. (B) Calibration plot obtained from the impedimetric response shown in (A).

Figure III.3A depicts the Nyquist plots obtained for Au/MPS/RGO-CHIT/DNA/Alb in the presence of different concentrations of miRNA-21 from 1.0×10^{-12} M to 1.0×10^{-8} M. Figure III.3B shows the plot of R_{ct} as a function of miRNA-21 concentration. There is a linear dependence for the whole range between 1.0×10^{-12} M and 1.0×10^{-8} M miRNA-21, with a sensitivity of $(134 \pm 4) \Omega\text{M}^{-1}$ ($r^2 = 0.996$) and a detection limit of 300 fM (calculated as $3 \times \text{SD}/s$ where SD is the standard deviation of the blank signal and s , the sensitivity). The reproducibility, obtained from the determination of 1.0×10^{-12} M miRNA-21 was 5.9 % while for 1.0×10^{-9} M miRNA-21, it was 2.2 %.

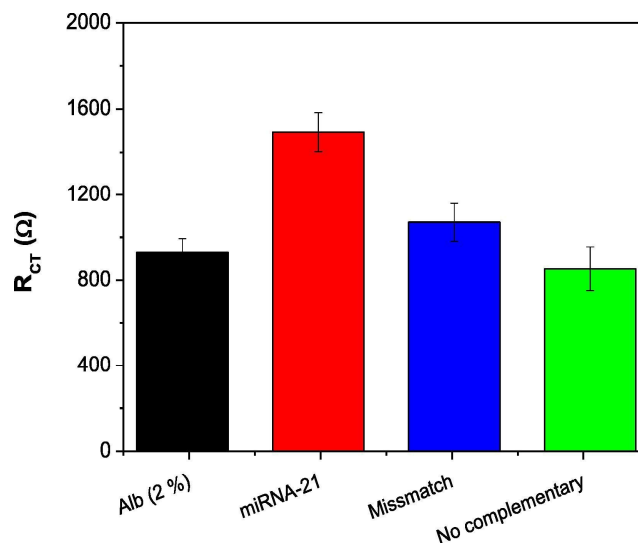


Figure III.4. Charge transfer resistances obtained at GCE/MPS/RGO-CHIT/Alb/DNA in the presence of 1.0×10^{-9} M miRNA-21, 1-base-mismatch and fully non-complementary sequences. Hybridization time: 75 min. Other conditions as in Figure III.2.

Figure III.4 shows the study of the selectivity of the biosensor. The plot shows the bars plot for the R_{ct} of the redox marker obtained at Au/MPS/RGO-CHIT/DNA/Alb in the presence of 1.0×10^{-9} M miRNA-21, one-base mismatch sequence and a fully non-complementary sequence, to evaluate the selectivity of the genosensor. No response was observed in the case of the fully noncomplementary sequence compared to the blank while for the one-base mismatch sequence, the R_{ct} is only 24.2 % of the complementary one, clearly indicating that the genosensor is able to discriminate non-complementary and even one-base mismatch sequences.

Considering that miRNA-21 can be found in different biological fluids and that, depending on the nature of the cancer, it is relevant to use one or the other fluid, we challenge our biosensor using several real samples: saliva, urine and reconstituted human serum samples diluted (1:10 (saliva and urine) and 1:1000 (serum samples)), with 0.050 M phosphate buffer solution pH 7.40 + 0.500 M NaCl) and enriched with 1.0×10^{-9} M miRNA-21. The recovery values were $(96 \pm 3) \%$, $(90 \pm 2) \%$, and $(98 \pm 3) \%$ for urine, saliva and serum, respectively. It is important

that analogue experiments performed with the diluted samples without miRNA-21, did not show any matrix effect, with interferences in R_{ct} of 1.9%, 2.3 % and 1,0 % for reconstituted serum, urine and saliva, respectively. These results indicate that the proposed genosensor can be successfully used for practical applications in different biological fluids.

Table III.1 compares the analytical performance of our biosensor with the most relevant miRNA-21 electrochemical biosensors reported in the last couple of years. Among them, most of the electrochemical biosensors based on the use of amplification schemes detection limits (femtomolar to attomolar) than our biosensor (300 fM) [8-11, 13-19, 25] while few of the amplified biosensors present higher detection limits than the proposed biosensing platform [12, 20]. Regarding the nonamplified detection, our biosensor presents better detection limits than the strategies reported in references [26, 27] and higher than those described in references [23, 24]. In summary, even when our biosensor does not present better detection limits than most of the biosensors reported in the Table 1, it is still competitive since it is possible to quantify miRNA-21 even at fM levels in a simple and fast way, without using amplification strategies involving labelling enzymes/redox markers, endonucleases, special isothermal amplification schemes, different nanomaterials, oligonucleotides with particular structures, and DNA analogues [8-11, 13-19, 25] or non-amplified strategies based on the use of expensive noble metal nanoparticles [21, 24, 25].

Table 1. Comparison of the analytical parameters for the most relevant miRNA-21 electrochemical biosensors reported in the last two years.

Technique	Electrode	Platform and detection	DL	LR	Real sample	Ref.
Amperometry	Au	Hairpin DNA modified-gold electrode, DSN-assisted target recycling, biotinylated signaling DNA/streptavidin-AuNPs to anchor the biotinylated HRP.	43 aM	0.1 fM to 100 pM	Tumor cells	[8]
DPV	Au	G-rich long ssDNAs generated by RCA to facilitate the in situ synthesis of PdNPs .	8.6 aM	50 aM to 100 fM	Human serum	[9]
DPV	Au	Integration of a dual signal amplification strategy of HCR and EIM, using capture probe (CP H1) modified magnetic nanobeads.	0.84 fM	1.0×10^{-15} M to 1.0×10^{-8} M	Human serum	[10]
DPV	MGCE	Capture hairpin immobilized at Fe ₃ O ₄ , amplification using HCR and detection from the synergistic reduction of hydrogen peroxide/ TMB system in the presence of a Cu(II) planar complex.	33 aM	100 aM to 100 nM	Human serum	[11]
DPV	Au	Amplification scheme based on HCR, which leads to extended growth of DNA chains and higher amplification efficiency through MB intercalation.	11 pM	30 pM to 7.0 nM	Human serum	[12]
EIS	GCE	ZrO ₂ /rGO/modified electrode coupled with CHA signal amplification strategy and detection through the change of charge transfer resistance of [Fe(CN) ₆] ^{3-/4-} .	4.3×10^{-15} M	1.0×10^{-14} M to 1.0×10^{-10} M	MCF7 cells and human embryonic kidney cells	[13]
Chronocoulometry	Au	Triple signal amplification based on target-triggered cyclic duplex specific nuclease digestion and bridge DNA/AuNPs; detection from the preconcentrated [Ru(NH ₃) ₆] ³⁺ .	6.8 aM	1.0×10^{-17} M to 1.0×10^{-11} M	Human serum	[14]
Chronocoulometry	SPE	MoS ₂ @AuNPs/capture DNA and detection through the [Ru(NH ₃) ₆] ³⁺ electrostatically bond to the surface hybrid.	100 aM	10 fM to 10 pM	-	[15]
Chronocoulometry	SPCE	GO-loaded iron oxide and detection from [Ru(NH ₃) ₆] ³⁺ catalyzed by [Fe(CN) ₆] ³⁻ .	1.0 fM	1.0 fM to 1.0 nM	Ovarian cancer and normal non-cancerous cells	[16]
SWV	Au	Thiol-modified hairpin capture probe immobilized at Au, detection carried out through the molybdophosphate accumulated at the ribose-phosphate backbone of the resulting duplex.	0.5 fM	1.0 fM to 1.0 nM	Human serum	[17]

SWV	Au	Mesoporous silica nanospheres-hairpin H1, CHA and HCR enzyme-free amplification, and detection from the nanospheres-released MB.	0.037 fM	0.1 fM to 5.0 pM	Liverhepatocellular cells	[18]
SWV	Au	SWV Au Ratiometric scheme based on target driven CHA mismatched using three hairpins. Detection from the currents ratio of two redox markers before and after hybridization.	1.1 fM	5.0 fM to 0.1 nM	Cell extraction samples from the MCF7	[19]
Amperometry	SPCE	Geno- and immunoassay using anti DNA-RNA antibody and detection from the bacterial protein A conjugated with poly-HRP40/hydrogen peroxide.	0.4 pM	1.0 pM to 100 pM	Cancer cells and tumor tissues	[20]
DPV	GCE	DNA-AuNPs, miRNA-21 and MWCNTs modified with a signaling DNA and labeled with thionine.	0.032 pM	0.1 pM to 12000 pM	-	[21]
DPV	GCE	LNA-modified “Y” shape-like structure and detection of exosomal miRNA-21 based on the distance-sensitive currents ratio of two redox markers.	2.3 fM	10 fM-70 fM	Exosomes samples	[22]
DPV	SPE	Immobilized p19 protein with MCF-exosome biomarkers and subsequent detection due activation of the system by target addition.	1.0 aM	1.0 pM to 100 nm	-	[23]
CV	Au	Electrode modified with polypyrrol/Ag and pyrrolidiny PNA and detection through the decrease of Ag oxidation signal.	10 fM	1.0×10^{-13} M to 1.0×10^{-8} M	Human plasma	[24]
DPV	FTO	CGO/Au-PtBNPs/SA/CP using $[\text{Fe}(\text{CN})_6]^{3-/4-}$ as redox probe.	1.0 fM	1.0 fM to 1.0 μM	Human serum	[25]
SWV	GCE	MoS ₂ -Thi-AuNPs nanohybrid as a signaling molecule to monitor DNA-RNA hybridization. Detection from the decrease in the electrochemical signal of Thi.	0.26 pM	1.0 pM to 10 nM	Human serum	[26]
EIS	GCE	Neutravidin and a highly specific biotinylated DNA/LNA molecular beacon probe conjugated with AuNPs and detection by increment of the charge transfer resistance of a redox probe.	0.3 pM	1.0 pM to 1000 pM	Human serum	[27]

DL: detection limit; LR: linear range; DSN: duplex-specific nuclease; AuNPs: gold nanoparticles; HRP: horseradish peroxidase; DPV: differential pulse voltammetry; ssDNA: single-stranded DNA; RCA: rolling circle amplification; PdNPs: palladium nanoparticles; HCR: hybridization chain reaction; EIM: enzyme-induced metallization; MGCE: magnetic glassy carbon electrode; TMB: 3,3',5,5'-tetramethylbenzidine; MB: methylene blue; EIS: electrochemical impedance spectroscopy; GCE: glassy carbon electrodes; rGO: reduced graphene oxide; CHA: catalytic hairpin assembly; MCF7: human breast cancer cell lines; SPE: screen-printed electrode; SPCE: screen-printed carbon electrode; GO: graphene oxide; SWV: square wave voltammetry; MWCNTs: multi-walled carbon nanotubes; LNA: locked nucleic acid; p19: RNA silencing suppressor; CV: cyclic voltammetry; PNA: peptide nucleic acid; FTO: fluorine tin oxide; CGO: carboxylated graphene oxide; Au-PtBNPs: Au-Pt bimetallic nanoparticles; SA: streptavidin; CP: capture probe; Thi: thionine.

Conclusions

This work reported the label-free and non-amplified impedimetric genosensing of miRNA-21 using a bioanalytical platform rationally built by taking advantage of the carboxylic groups of GO to support CHIT, the conductive properties of RGO to improve the electroactivity of the platform, and the high density of the amine groups of chitosan to work as bridge between MPS and the aminated capture probe. The resulting genosensor allowed the sensitive (femtomolar), selective, simple and fast quantification of miRNA-21 without any additional amplification step and successful application in different biological fluids.

In addition to these advantages for the quantification of miRNA-21, that make Au/MPS/RGO-CHIT/DNA highly competitive, it is a versatile bioanalytical platform that opens new horizons for multiple biosensing applications just selecting the most appropriate biorecognition element.

Acknowledgements

Financial support from CONICET, ANPCyT, SECyT-UNC (Argentina) and ECOS-SUD program (A16E02). M. L.-M. thankfully acknowledges CONICET for the PhD fellowship. Y. Zhang thanks Chinese Scholarchip Council for providing a three-year scholarship for her stay in France and LabEx MICHEM for supporting her living expenses in Argentina

Declaration of Conflict of Interest

No authors have any conflicts of interest to disclose.

References

1. D. Bautista-Sánchez, C. Arriaga-Canon, A. Pedroza-Torres, A. De La Rosa Velázquez, R. González-Barrios, L. Contreras-Espinosa, R. Montiel Manríquez, C. Castro-Hernández, V. Fragoso-Ontiveros, R. María Álvarez Gómez, L.A. Herrera, The Promising Role of miR-21 as a Cancer Biomarker and Its Importance in RNA-Based Therapeutics, *Molec. Ther.: Nuc. Aci.* 20 (2020) 409-420.
2. M.K. Masud, M. Umer, M.S.A. Hossain, Y. Yamauchi, N.T. Nguyen, M.J.A. Shiddiky, Nanoarchitecture Frameworks for Electrochemical miRNA Detection, *Trends Biochem. Sci.* 44 (2019) 433-452.
3. P. Gillespie, S. Ladame, D. O'Hare, Molecular methods in electrochemical microRNA detection, *Analyst* 144 (2019) 114-129.
4. M. López Mujica, Y. Zhang, F. Bédioui, F. Gutiérrez, G. Rivas, Label-free graphene oxide-based SPR genosensor for the quantification of microRNA21, *Anal. Bioanal. Chem.* 412 (2020) 3539–3546.

5. H. Mohammadi, G. Yammouri, A. Amine, Current advances in electrochemical genosensors for detecting microRNA cancer markers, *Curr. Opin. Electroche.* 16 (2019) 96-105.
6. M. Lagos-Quintana, R. Rauhut, W. Lendeckel, T. Tuschl, Identification of novel genes coding for small expressed RNAs, *Science* 294 (2001) 853-858.
7. R. Rupaimoole, F. Slack, MicroRNA therapeutics: towards a new era for the management of cancer and other diseases, *Nat. Rev. Drug Discov.* 6 (2017) 203–222.
8. H. Zhang, M. Fan, J. Jiang, Q. Shen, C. Cai, J. Shen, Sensitive electrochemical biosensor for MicroRNAs based on duplex-specific nuclease-assisted target recycling followed with gold nanoparticles and enzymatic signal amplification, *Anal. Chim. Acta.* 1064 (2019) 33-39.
9. C. Zhang, D. Li, D. Li, K. Wen, X. Yang, Y. Zhu, Rolling circle amplification-mediated: In situ synthesis of palladium nanoparticles for the ultrasensitive electrochemical detection of microRNA, *Analyst* 144 (12) (2019) 3817-3825.
10. W.J. Guo, Z. Wu, X.Y. Yang, D.W. Pang, Z.L. Zhang, Ultrasensitive electrochemical detection of microRNA-21 with wide linear dynamic range based on dual signal amplification, *Biosens. Bioelectron.* 131 (2019) 267-273.
11. L. Tian, J. Qi, O. Oderinde, C. Yao, W. Song, Y. Wang, Planar intercalated copper (II) complex molecule as small molecule enzyme mimic combined with Fe₃O₄ nanozyme for bienzyme synergistic catalysis applied to the microRNA biosensor, *Biosens. Bioelectron.* 110 (2018) 110-117.
12. M. Liang, M. Pan, J. Hu, F. Wang, X. Liu, Electrochemical Biosensor for MicroRNA Detection Based on Cascade Hybridization Chain Reaction, *ChemElectroChem.* 5 (2018) 1380-1386.
13. K. Zhang, N. Zhang, L. Zhang, H. Wang, H. Shi, Q. Liu, Label-free impedimetric sensing platform for microRNA-21 based on ZrO₂-reduced graphene oxide nanohybrids coupled with catalytic hairpin assembly amplification, *RSC Adv.* 8 (2018) 16146-16151.
14. B. Bo, T. Zhang, Y. Jiang, H. Cui, P. Miao, Triple Signal Amplification Strategy for Ultrasensitive Determination of miRNA Based on Duplex Specific Nuclease and Bridge DNA-Gold Nanoparticles, *Anal. Chem.* 20 (2018) 2395-2400.
15. A. Ganguly, J. Benson, P. Papakonstantinou, Sensitive chronocoulometric detection of miRNA at screen-printed electrodes modified by gold-decorated MoS₂ nanosheets, *ACS Appl. Bio Mater.* 1 (2018) 1184-1194.
16. M.N. Islam, L. Gorgannezhad, M.K. Masud, S. Tanaka, M.S.A. Hossain, Y. Yamauchi, N.T. Nguyen, M.A. Shiddiky, Graphene-Oxide-Loaded Superparamagnetic Iron Oxide Nanoparticles for Ultrasensitive Electrocatalytic Detection of MicroRNA, *ChemElectroChem.* 5 (2018) 2488-2495.
17. K. Feng, J. Liu, L. Deng, H. Yu, M. Yang, Amperometric detection of microRNA based on DNA-controlled current of a molybdophosphate redox probe and amplification via hybridization chain reaction, *Microchim. Acta* 185 (2018) 185:28.
18. H. Cheng, W. Li, S. Duan, J. Peng, J. Liu, W. Ma, H. Wang, X. He, K. Wang, Mesoporous Silica Containers and Programmed Catalytic Hairpin Assembly/Hybridization Chain Reaction Based Electrochemical Sensing Platform for MicroRNA Ultrasensitive Detection with Low Background, *Anal. Chem.* 91 (2019) 10672-10678.
19. X. Li, B. Dou, R. Yuan, Y. Xiang, Mismatched catalytic hairpin assembly and ratiometric strategy for highly sensitive electrochemical detection of microRNA from tumor cells, *Sensor Actuat. B-Chem.* 286 (2019) 191-197.
20. E. Vargas, R.M. Torrente-Rodríguez, V.R.V. Montiel, E. Povedano, M. Pedrero, J.J. Montoya, S. Campuzano, J.M. Pingarrón, Magnetic beads-based sensor with tailored sensitivity for rapid and single-step amperometric determination of miRNAs, *Int. J. Mol. Sci.* 18 (2017) 2151.
21. K. Deng, X. Liu, C. Li, H. Huang, Sensitive electrochemical sensing platform for microRNAs detection based on shortened multi-walled carbon nanotubes with high-loaded thionin, *Biosens. Bioelectron.* 117 (2018) 168-174.
22. L. Luo, L. Wang, L. Zeng, Y. Wang, Y. Weng, Y. Liao, T. Chen, Y. Xia, J. Zhang, J. Chen, A ratiometric electrochemical DNA biosensor for detection of exosomal MicroRNA, *Talanta* 207 (2020) 120298.
23. E. Ghazizadeh, Z. Naseri, M.R. Jaafari, M. Forozandeh-Moghadam, S. Hosseinkhani, A fires novel report of exosomal electrochemical sensor for sensing micro RNAs by using multi covalent attachment p19 with high sensitivity, *Biosens. Bioelectron.* 113 (2018) 74-81.
24. T. Kangkamano, A. Numnuam, W. Limbut, P. Kanatharana, T. Vilaivan, P. Thavarungkul, Pyrrolidinyl PNA polypyrrole/silver nanofoam electrode as a novel label-free electrochemical miRNA-21 biosensor,

- Biosens. Bioelectron. 102 (2018) 217-225.
25. A. Bharti, N. Agnihotri, N. Prabhakar, A voltammetric hybridization assay for microRNA-21 using carboxylated graphene oxide decorated with goldplatinum bimetallic nanoparticles, *Microchim. Acta* 186 (2019) 185.
26. D. Zhu, W. Liu, D. Zhao, Q. Hao, J. Li, J. Huang, J. Shi, J. Chao, S. Su, L. Wang, Label-Free Electrochemical Sensing Platform for MicroRNA-21 Detection Using Thionine and Gold Nanoparticles Co-Functionalized MoS₂ Nanosheet, *ACS Appl. Mater. Inter.* 9 (2017) 35597-35603.
27. S. Azzouzi, W.C. Mak, K. Kor, A.P.F. Turner, M.B. Ali, V. Beni V, An integrated dual functional recognition/amplification bio-label for the one-step impedimetric detection of Micro-RNA-21, *Biosens. Bioelectron.* 92 (2017) 154-161.

Supplementary information

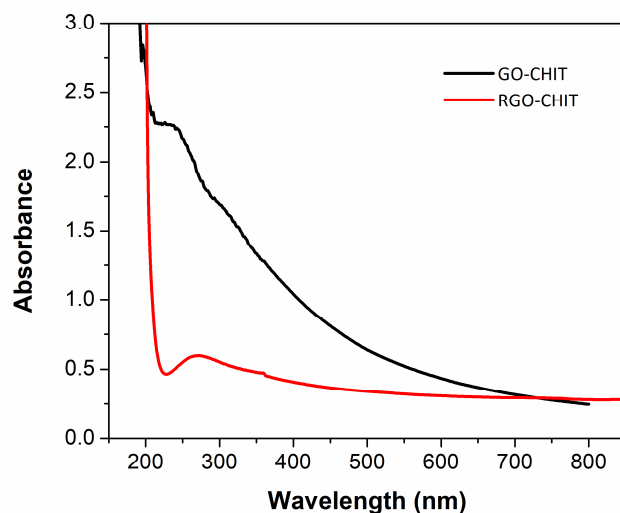


Figure III.5. UV-vis spectra corresponding to GO-CHIT (-) and RGO-CHIT (-).

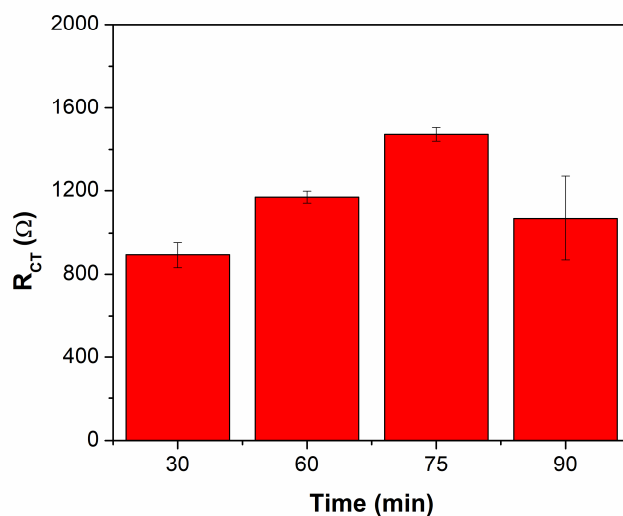


Figure III.6. Effect of the hybridization time of miRNA-21 at Au/MPS/RGO-CHIT/DNA on the R_{ct} in the presence of 50 ppm NH_2 -DNA. Concentration miRNA-21: 1.0×10^{-9} M. Redox marker: 1.0×10^{-3} M $[\text{Fe}(\text{CN})_6]^{3-}/[\text{Fe}(\text{CN})_6]^{4-}$; Frequency range: 10 KHz to 10 mHz; Potential perturbation: 10 mV; Working potential: 0.200 V. Supporting electrolyte: 0.050 M phosphate buffer solution pH 7.40 with 0.5 M NaCl.

III.2. miRNA-21 quantification by Chronoamperometry

This section presented the Label-free electrochemical analysis of miRNA-21 using *Chronoamperometry* based on ultramicroelectrode array.

I contributed all the experiment section and first draft, which was discussed and revised with all supervisors.

The electrochemical experiment part of this section was conducted in the *Laboratoire Synthèse Electrochimie Imagerie et Systèmes Analytiques (SEISAD)* of institute of Chemistry for Life & Health Sciences (*i-CLeHS*), *Chimie ParisTech, Université PSL, Paris*

The microfabrication of band microelectrodes array was carried out in *the département de chimie of École normale supérieure (ENS)* and *the Plateau of Institut Pierre-Gilles de Gennes (IPGG), Université PSL, Paris,*

Thanks to the help in microfabrication of Eric aït-Yahiatène and Laurent Thouin. Thanks to Mathieu Lazerges, Fethi Bedioui, Cyrine Slim and Sophie Griveau for their guidance and help in my experiment and life in the past three years in France, and the help in the early stage of this section of experiment from François-Xavier GUILLON

Electrochemical and reverse transcriptase real-time PCR analysis of miRNA-21

Y. Zhang^a, P. Nizard^b, S. Griveau^a, V. Taly^b, F. Bedioui^{a,*}, M. Lazerges^c, C. Slim^a

^a Institute of Chemistry for Life and Health Sciences, Synthesis, Electrochemistry, Imaging and Analytical Systems for Diagnosis Team, Paris-Sciences-et-Lettres, CNRS, Chimie ParisTech, 11 rue Pierre et Marie Curie, 75005 Paris, France.

^b Faculté des Sciences Fondamentales et Biomédicales, Université de Paris, Translational Research & Microfluidics, UMRS1147 CNRS, 12 rue de l'Ecole de Médecine, 75006 Paris, France.

^c Faculté de Pharmacie de Paris, Faculté de Santé, Université de Paris, 4 avenue de l'Observatoire, 75006 Paris, France.

Abstract

MicroRNAs (miRNAs) are small highly conserved non-coding RNA molecules in ~22 nucleotide length and regulate gene expression at the post-transcriptional level by silencing target transcripts through base-pair complementation with mRNA. The abnormal expression of miRNA is closely related to the occurrence of disease, and there is a certain disease specificity. reverse transcription real-time PCR (RT-qPCR) is a gold standard miRNA quantitation method, however, due to the cumbersome steps, the long time, and the error caused by the amplification step, other various quantitation methods for miRNA have been rapidly developed. Among them, the electrochemical conduction can directly convert biological recognition events into detectable electrical signals, which has become a promising quantitative method of miRNAs. In this paper developed a gold band ultramicroelectrodes (UMEs) array to construct a new electrochemical miRNA platform based on a label-free simple electrochemical detection method and compared with the RT-qPCR detection method that based on poly(A) tailing-based *TaqMan*® advanced microRNA assays. The miRNA-21 was chosen as a sample to evaluate the performance of two quantification methods, for the UME array, there is a linear relationship

between 1.0×10^{-18} mol L⁻¹ to 1.0×10^{-12} mol L⁻¹ and the LOD is 3 amol L⁻¹, for RT-qPCR, the dynamic range was between 10^{-16} mol L⁻¹ and 10^{-8} mol L⁻¹ and the LOD is 0.87 amol L⁻¹.

Keywords

Biosensor, electrochemical, microelectrode, miRNA, PCR

III.2.1. Introduction

MicroRNAs (miRNAs) are short non-coding, single-stranded RNA molecules, approximately 19–23 nucleotides length, that were first discovered in a transparent circle worm specie, *Caenorhabditis Elegans* in 1993 [1]. miRNA biological function is gene regulation by interaction with partially complementary RNA messengers (mRNA) to guide the silencing complex to degrade the target mRNA or inhibit the translation of the target mRNAs to direct important cellular processes [2, 3]. Recent studies indicate that circulating miRNAs may serve as novel and sensitive biomarkers, specific alterations in their expression profiles are associated with many diseases, including cancer, in line with *IUPAC*'s definition of biomarkers: which can indicator signalling an event or condition in a biological system or sample and giving a measure of exposure, effect, or susceptibility. The indicator may be a measurable chemical, biochemical, physiological, behavioral, or other alteration within an organism [4, 5]. miRNA discover constitutes a breakthrough in diagnosis as the analysis is simplified to the study of a hundred miRNA *versus* thousands mRNA targets.

In addition, studies found that miRNA exist in body fluids including blood, saliva and urine in a stable form and which are promising biomarker candidates [6, 7]. Circulating miRNAs have been proposed as potential blood-based biomarkers for disease detection since they offer the advantage of their non-invasive extraction [8, 9]. For the use of miRNAs as biomarkers in clinic practice, it is necessary to detect their expression level. The development of methods for detecting miRNAs has grown to become a research field in its own right. Traditional methods for detecting miRNAs include northern blotting, RT-qPCR, microarrays, electrochemical and

others; however, each of these methods has its own individual limitations [10-13].

RT-qPCR is the classical quantitative method for detecting miRNAs. It is regarded as a gold standard and is widely used for clinical diagnosis due to the high specificity and sensitivity [14-16]. However, there are severe limitations of diagnosis using a PCR: it is time-consuming and slight change of experimental amplifications conditions can induce important errors. Moreover, in the case of identical experimental conditions, two different sequences can be amplified in a different fashion [10].

Developing a method that can directly detect miRNA in human fluids (*i.e.* without amplification) is a hotspot in disease diagnosis in order to avoid these shortcomings. Electrochemistry is the only pathway allowing direct transduction of a biological event (*i.e.* hybridization) in an electrical signal [11, 17]. For other biosensors based on optical, surface acoustic wave, and mass transducers, it must convert the light, acoustic wave, and mass change signals caused by biological events into electrical signals for analysis, this supplemental conversion step complicates device design. Moreover, the technology of addressed wires circuits can be used to design addressing electrode networks, which is extremely useful for high-density screening required for genetic diagnosis [18]. Therefore, electrochemical technology has received more and more attention in genetic diagnosis. However, developing more reliable and efficient electrochemical biosensors to detect trace miRNA in biological samples is still a huge challenge.

Accordingly, we designed a gold band UMEs array to construct a new electrochemical device for miRNA detection based on a label-free simple electrochemical detection method. A platform is a complete and automatized system of analysis, ready to use, that can be used by a technician. miRNA-21 was used as the target biomarker to evaluate the detection performance of the electrochemical UMEs array, and compared with RT-qPCR detection method (Figure III.7).

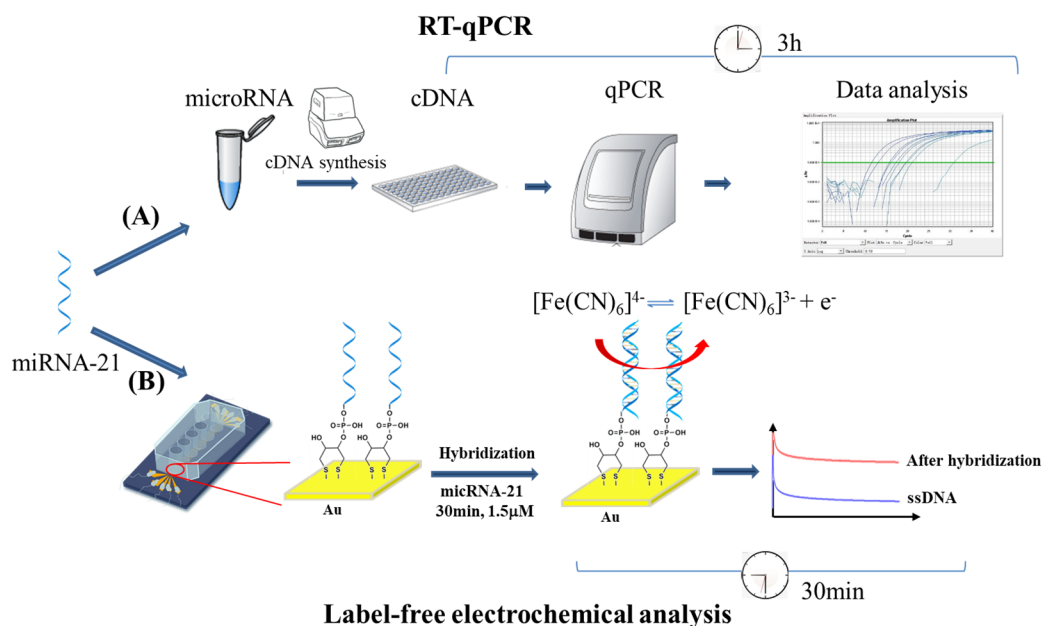


Figure III.7. Schematic illustration of research in this article. (A) Real-time polymerase chain reaction (RT-qPCR) analysis and (B) label-free electrochemical quantification of the microRNAs.

III.2.2. Experimental section

III.2.2.1. Chemicals and biochemical compounds

All solutions were prepared using deionized water (18.2 MΩ·cm). Sodium chloride (NaCl, 99.8%) was ordered from *Riedel-de Haën (France)*. Potassium ferricyanide ($\text{K}_3[\text{Fe}(\text{CN})_6]$), potassium ferrocyanide ($\text{K}_4\text{Fe}(\text{CN})_6(\text{H}_2\text{O})_3$), tris (2-carboxyethyl) phosphine hydrochloride (TCEP-HCl) were ordered from *Fisher Chemical (France)*. Sodium hydroxide (NaOH, analytical grade) was purchased from *Prolabo*, potassium hydroxide (KOH), H_2O_2 , sulfuric acid (H_2SO_4), sodium phosphate monobasic (NaH_2PO_4), $\text{Na}_3\text{O}_4\text{P} \cdot 12\text{H}_2\text{O}$, Na_2SO_4 , H_3PO_4 (37%), Methylene blue (MB), sulfuric acid (H_2SO_4) were purchased from *Sigma-Aldrich*. *TaqMan*[®] miRNA ABC purification kit – Human Panel B (#4473088), *TaqMan*[®] Advanced miRNA cDNA Synthesis Kit (#A28007) and *TaqMan*[®] Advanced miRNA Assays (#A25576) were purchased from *Thermo Fisher Scientific*, plasma sample (healthy donor, from *Etablissement Français du Sang*), human colon cancer cell line HCT116 from *Translational*

Research & Microfluidics team (Université de Paris).

The custom DTPA labeled DNA probe was synthesized by *Friz Biochem*, the other oligonucleotides were purchased from *Eurogentec* and all their purification was processed by high performance liquid chromatography (*HPLC*). The sequences of the oligonucleotides were as follows (Table III.):

Table III.2. The sequences of the oligonucleotides.

Name	Sequence
DNA probe (P)	1-DTPA-5' TCA ACA TCA GTC TGA TAA GCT A 3'
DNA target (T)	5' TAG CTT ATC AGA CTG ATG TTG A 3'
miRNA-21	5' UAG CUU AUC AGA CUG AUG UUG A 3'
mismatch DNA target (mT)	5' TAG CTT ATC A CA CTG ATG TTG A 3'
Random DNA target (rT)	5' CAG TCG TAA GCT CTG AGT CTA T 3'

III.2.2.2. Instruments

The electrochemical measurements were performed on a *Galvonastat Model 263 A* potentiostat galvanostat (*EGG INSTRUMENTS, Princeton Applied Research*) controlled by *VoltaMaster 4* software. Reverse transcription was performed using a *C1000touch* Thermal cycler (*Bio-Rad Laboratories*). The qPCR analyses were performed on a *7500 Fast Real-Time PCR* system (*Applied Bioscience*)

III.2.2.3. Plasma purification and RT-qPCR

The plasma was purified by the *TaqMan® miRNA ABC purification kit – Human Panel B* (*Thermo Fisher Scientific*) according to the manufacturer's instructions to remove the miRNAs. miRNA-21 templates of different concentrations are added to make a calibration curve in plasma using RT-qPCR.

For miRNA analysis, 2µL of miRNA-21 was reverse transcribed using *TaqMan® advanced miRNA reverse transcription kit* and *TaqMan® advanced microRNA assays*. The length of miRNA-21 was extended with a poly(A) sequence and specific reverse transcription was then

performed. Real-time PCR (qPCR) was performed with *TaqMan*® *Small RNA Assay* (20X), *TaqMan*® *Universal PCR Master Mix II* (2X, no UNG[‡]). The fluorescence of *TaqMan* probe was used to monitor the amplification of miRNA-21 with an *SDS 2.4 software*.

III.2.2.4. Gold UME array fabrication and two-electrodes setup

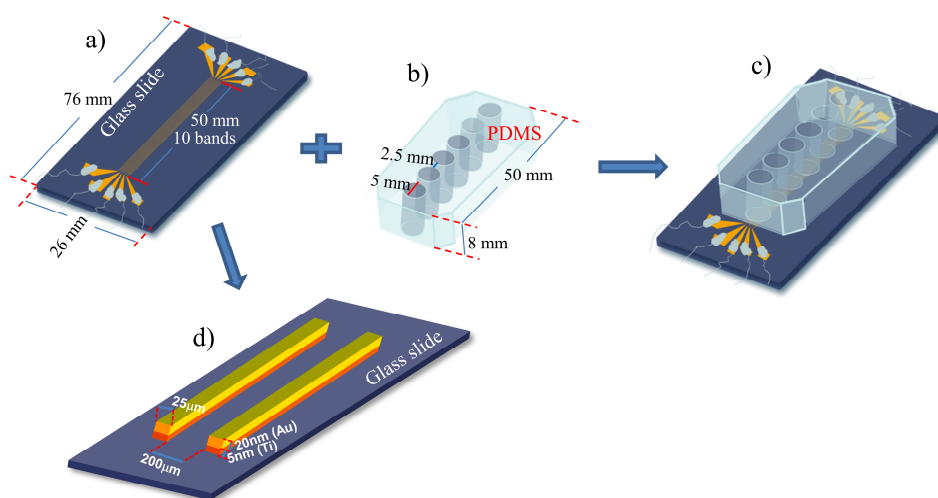


Figure III.8. Schematic illustration of the 10-band gold UME array platform and microdevice, a) 10-band gold UME array. b) PDMS well. c) gold band UME array platform. d) Cross section view of gold UME showing the layers and dimensions.

The working electrode was a 10 gold bands (5 mm length, 25 μm width) with a 200 μm gap (Figure III.8) fabricated on a glass slide by photolithography. The glass slides were first rinsed with acetone and isopropanol, then immersed in the piranha solution for 15 minutes, then rinsed with deionized water and treated with oxygen plasma (50w, 100sccm) for 5 minutes for treatment. Then *AZ-5214E* reversal photoresist was used to form pattern based on the shape of the mask, using twice UV exposure. A layer of titanium (Ti) 5 nm thick was directly deposited on the patterned developed glass substrate to increase the adhesion of the gold to the device using the sputtering technique in a vacuum chamber of K675X Turbo Large Chromium Coater

8 instrument, next deposited a thin gold layer with a thickness of 20 nm. Finally, the gold UME array is obtained after lift-off step (Figure III.8d). The final product forms a uniform layer of gold with high reproducibility, allowing large-scale manufacturing.

The PolyDiMethylSiloxane (PDMS) is classically use for fluidic applications due to its low cost and its excellents physical properties and biocompatibility. This easy to mold material is transparent and resists to oxidation. PDMS insulator layer was separated into numbers of small cylindrical hole with a diameter of 5 mm (Figure III.8b), and fixed it on the gold UME array sensing platform by simple manual pressure: the gold UME array was placed in the middle of the PDMS cylindrical hole (Figure III.8c), each cylindrical hole constitute an electrochemical compartment.

A two-electrode system (Figure III.16) was used: the gold bands array (10 bands) was the working electrode. 10 external wires were connected to each gold band by conductive epoxy. The counter electrode is an Au wire (1 mm diameter) dipped in the electrolyte of a cylindrical hole. It is considered as a pseudo-reference electrode, because its surface area is very large compared to the ultramicroelectrode one. In addition, since both electrodes of two-electrode setup are made of the same metal and immersed in the same electrolyte, the equilibrium potential is equal to 0 V. In other word the ΔI - ΔE response is centered on 0 V: such response is interesting in analytical sciences because it avoids to search equilibrium potential between each measure [19, 20]. Moreover, This configuration is well-adapted for architecture of electrochemical sensors integrated in microfluidics devices [20-22].

III.2.2.5. Electrochemical measurements

The experiments were performed in a 60 μ L of electrolyte: $[\text{Fe (III)(CN)}_6]^{3-}/[\text{Fe (II)(CN)}_6]^{4-}$ (5mM each) and methylene blue (5 μ M) in NaCl (0.5 M) or NaH_2PO_4 (0.3 M). The measurements were carried out after immersing electrodes 5 min in electrolyte. The two-electrode system was connected to the *Model 263 A* potentiostat (*EGG INSTRUMENTS, Princeton Applied Research*) controlled by *VoltaMaster 4* software. Cyclic voltammetry (CV)

and chronoamperometry (CA) were used to study electrochemical response of biosensors. For CV, the potential was swept from -0.3 V to +0.3 V at a scan rate of 50 mV/s. For CA, a 0 V potential difference was first applied during 10 s, then a potential chosen in the -0.3 V to +0.3 V range was applied for 30 s and the current was measured at the end of the potential pulse.

III.2.2.6. Pretreatment of the gold ultramicroelectrodes (UME) array

Five different pretreatment methods were applied to the gold ultramicroelectrodes array before DNA probe immobilization: chemical (acid and base), electrochemical (acid), plasma and flame heat. Efficiency of each pretreatment was evaluated by CV. Two protocols were used for chemical cleaning:

i. chemical pretreatment with 60 μL of 1M H_2SO_4 at different times from 1min to 68 min.

ii. chemical pretreatment with 60 μL of KOH (50mM) mixed with H_2O_2 (25% weight) during 40 min.

iii. Electrochemical pretreatment was performed by applying a constant + 1.2 V potential in 0.05M sulfuric acid until got the maximum peak current by cyclic voltammetry.

iv. For plasma pretreatment, the array was placed inside a plasma cleaner (*PDC-32G Harrick plasma*) during 5 min under 50 sccm Ar flow at 1 W power.

v. Heat pretreatment was performed by heating 5 times each side of the gold ultramicroelectrodes array substrate with a flame gun.

The efficiency each pretreatment method was evaluated by cyclic voltammetry, which carried out in electrolyte that contains 5 mM $[\text{Fe}(\text{III})(\text{CN})_6]^{3-}/[\text{Fe}(\text{II})(\text{CN})_6]^{4-}$ in 0.5 M NaCl.

III.2.2.7. Immobilization of DNA-probe self-assembled monolayer

A label-free biosensor of miRNA-21 was fabricated by immobilization of the complementary

DNA probe on the gold UME array (working electrode, Figure III.9). The DNA probe (40 μL) labeled with a DTPA group (disulfide ring) was grafted on the gold surface by immersing the UME array one night at room temperature (25 $^{\circ}\text{C}$) in a binding buffer: 20 μM DNA-probe, 0.19 M NaH_2PO_4 , 0.23 M Na_3PO_4 , 0.5M Na_2SO_4 , 10 mM TCEP-HCl adjust PH to 7 with 37% weight H_3PO_4 . TCEP-HCl was used to reduce the disulfide bond of DTPA in order to improve chemical binding of the DNA-probe onto the gold array. UME array was then washed with deionized water in order to remove unbinding DNA-probes.

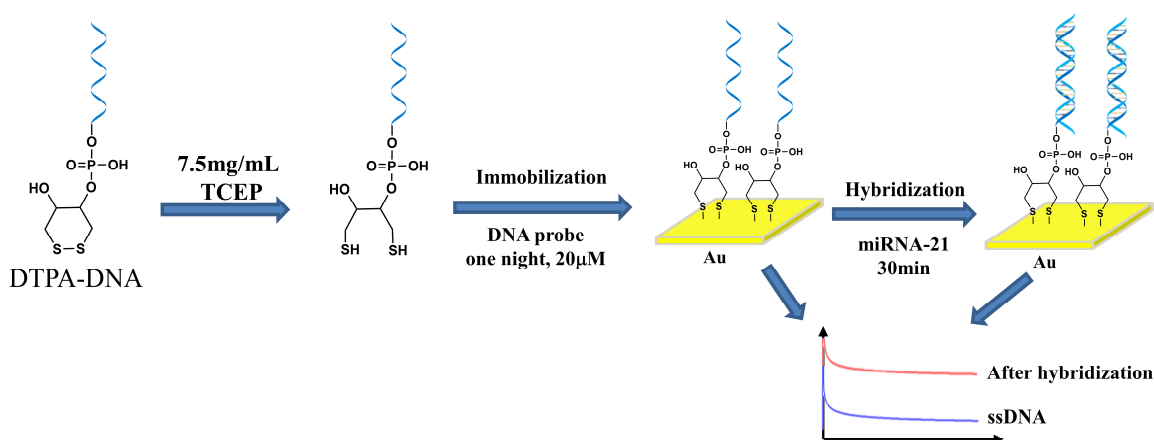


Figure III.9. Chemical activation of the disulfide, immobilization of the DNA-probe and hybridization of the miRNA-target.

III.2.2.8. Interfacial target oligonucleotide hybridization

Hybridization of different kinds of oligonucleotide targets with DNA probes grafted on the gold UME array surface was carried out by placing 40 μL of nucleic acid target solution in 0.3 M NaH_2PO_4 (pH 7) and waiting 30 min at room temperature (25 $^{\circ}\text{C}$). Afterwards, the gold UME array was rinsed with NaH_2PO_4 (0.3 M, pH 7) buffer.

Calibration curves of miRNA-21 diluted in buffer and purified plasma were established for concentration range from 10 aM to 1 nM concentration. Moreover miRNA-21 of the H116 cell line was then quantified to evaluate the biosensor performances. The concentration of cell line was calculated based on the calibration curve from qPCR experiment was used to compare

the value that measured by electrochemical.

III.2.3. Results and Discussion

III.2.3.1. Electrochemical response of gold UME array

The chronoamperometric response of a 5-band UME array is presented on Figure III.10.

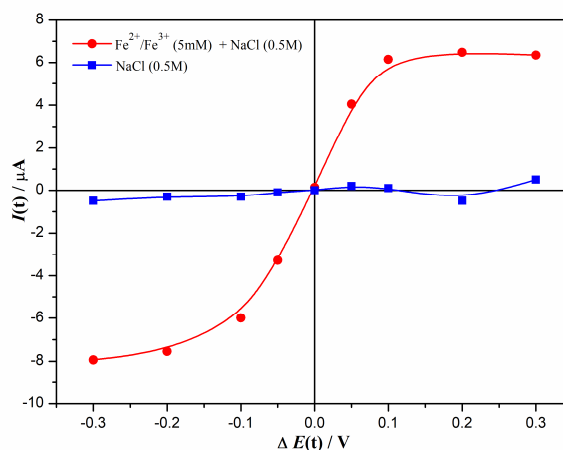
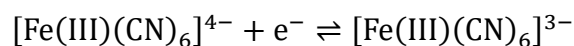


Figure III.10. Chronoamperometry responses of gold UME array (5 bands) measured at various potentials that from -0.3V to +0.3V in 0.5 M NaCl, 5 mM $[\text{Fe(III)(CN)}_6]^{3-} / [\text{Fe(II)(CN)}_6]^{4-}$: each circle corresponds to the chronoamperometric current measured 30 seconds after application of a constant potential difference ΔE complexes.

The CA curve corresponds to the redox reversible behavior of iron complexes:



For feeble polarizations ($|\Delta E| < 0.1 \text{ V}$), the $I-\Delta E$ response is mainly linear, the kinetics is limited by electronic transfer. For high polarizations ($|\Delta E| > 0.1 \text{ V}$), the $I-\Delta E$ response is mainly horizontal, the kinetics is limited by mass transfer (*i.e.* Fick diffusion). The limit current of an

array of N UME bands is [23]:

$$|I_L| = \frac{N \cdot I_1}{\ln\left(\frac{t}{\tau}\right)} \quad (1)$$

$$I_1 = 2 \cdot \pi \cdot F \cdot D \cdot C \cdot L \cdot w \quad (2)$$

$$\tau = \frac{w^2}{64 \cdot D} \quad (3)$$

Where the number of bands $N = 5$, the Faraday constant $F = 96845$ C/mol [24], the mean value of oxidation and reduction iron complexes diffusion coefficient $D = 6.4 \cdot 10^{-10}$ m².s⁻¹ [25], the concentration of iron complexes $C = 5$ mM, the electrodes length $L = 0.5$ cm and the electrodes width $w = 25$ μm. The limit current I_L calculated with these values is:

$$|I_L|_{(\mu A)} = \frac{48.5}{\ln\left(\frac{t(s)}{0.0153}\right)} \quad (4)$$

The limit current I_L calculated for 30 seconds is:

$$\left| I_{L, \text{calculated}}(30 \text{ s}) \right| = 6.4 \mu\text{A}$$

The variation of this limit current calculated with the derivative is negligible:

$$\frac{d \left| I_{L, \text{calculated}}(30 \text{ s}) \right|}{dt} = 4.3 \cdot 10^{-4} \mu\text{A/s}$$

The average redox value of experimental limit current I_L measured for 30 seconds is:

$$\left| I_{L, \text{measured}(30\text{ s})} \right| = 7.0 \mu\text{A}$$

The measured limit current is close to the theoretical current of 5 independent electrodes. This result demonstrates that 200 nm gap between electrodes of the array is enough to avoid overlap of the electrodes diffusion cylinders. In other words, electrochemical response of each electrode does not depend on other electrodes responses. The interest of the network is to increase the signal/noise ratio which is proportional of the measures number N square root:

$$\frac{I_{\text{signal}}}{I_{\text{noise}}} \propto N^{\frac{1}{2}} \quad (5)$$

III.2.3.2. Pretreatment of gold UME array

In order to optimize the performance of the gold UME array before DNA probe grafting, different surface treatments were compared (*cf.* part III.2.2.6.):

- i. acid chemical pretreatment (H_2SO_4);
- ii. basic chemical pretreatment (KOH);
- iii. Electrochemical pretreatment (+ 1.2 V; H_2SO_4);
- iv. Plasma pretreatment (Ar);
- v. Heat pretreatment (flame).

Blocking efficiency after pretreatment (methods i to iv) of long-range electron transfer through single-stranded DNA probe monolayer was calculated with I_{Au} steady state current before and I_{ss} after formation of the monolayer (Figure III.11):

$$1 - \frac{I_{ss}}{I_{Au}} \quad (6)$$

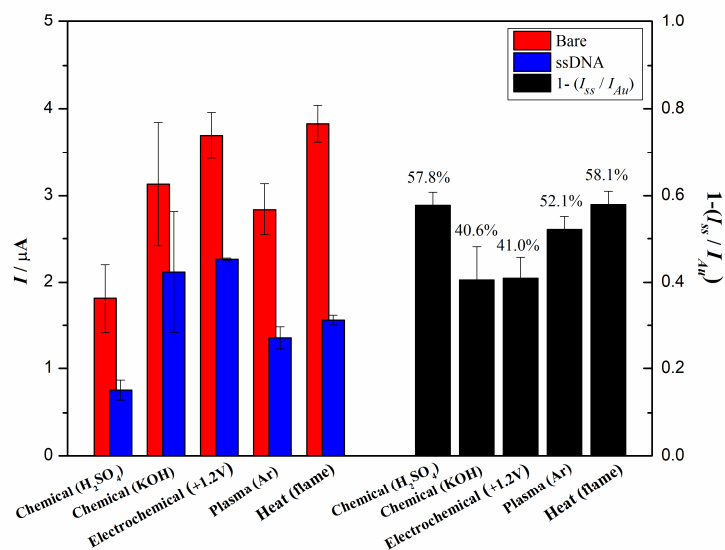


Figure III.11. Chronoamperometry response of bare Au UME array (5 gold bands) (red) and after DNA probe immobilization (blue) in 0.5 M NaCl, 5 mM [Fe(III)(CN)₆]³⁻, 5 mM [Fe(II)(CN)₆]⁴⁻, 5 μM MB solution with different treatment: acid chemical (H₂SO₄), basic chemical (KOH), electrochemical pretreatment (+ 1.2 V) and plasma (Ar).

The value of blocking current is close to 50% for the treatment methods (i) to (iv). Blocking efficiency was studied with three immobilization buffers (Figure III.12): NaCl, NaHCO₃ and NaH₂PO₄ (Figure III.12).

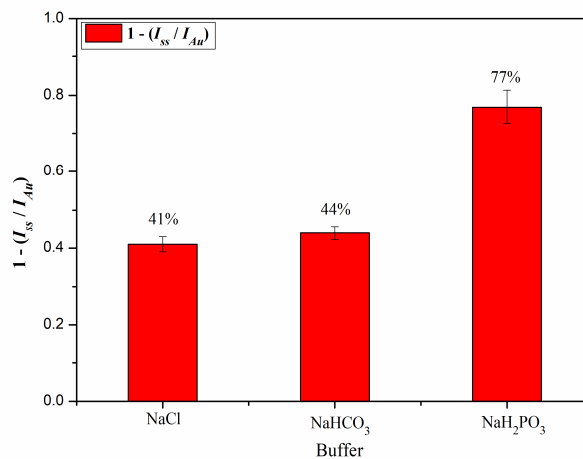


Figure III.12. Blocking efficiency of long-range electron transfer for three saline buffer solutions.

From Figure III.12, Blocking efficiency of long-range electron transfer was higher in NaH₂PO₃ solution, was chosen to replace NaCl, as chloride anions may corrode gold surfaces:



Hybridization efficiency of the nucleic acid target was calculated with I_{ss} steady state current before and I_{ds} after hybridization (Figure III.13):

$$\frac{I_{ds}}{I_{ss}} - 1 \quad (7)$$

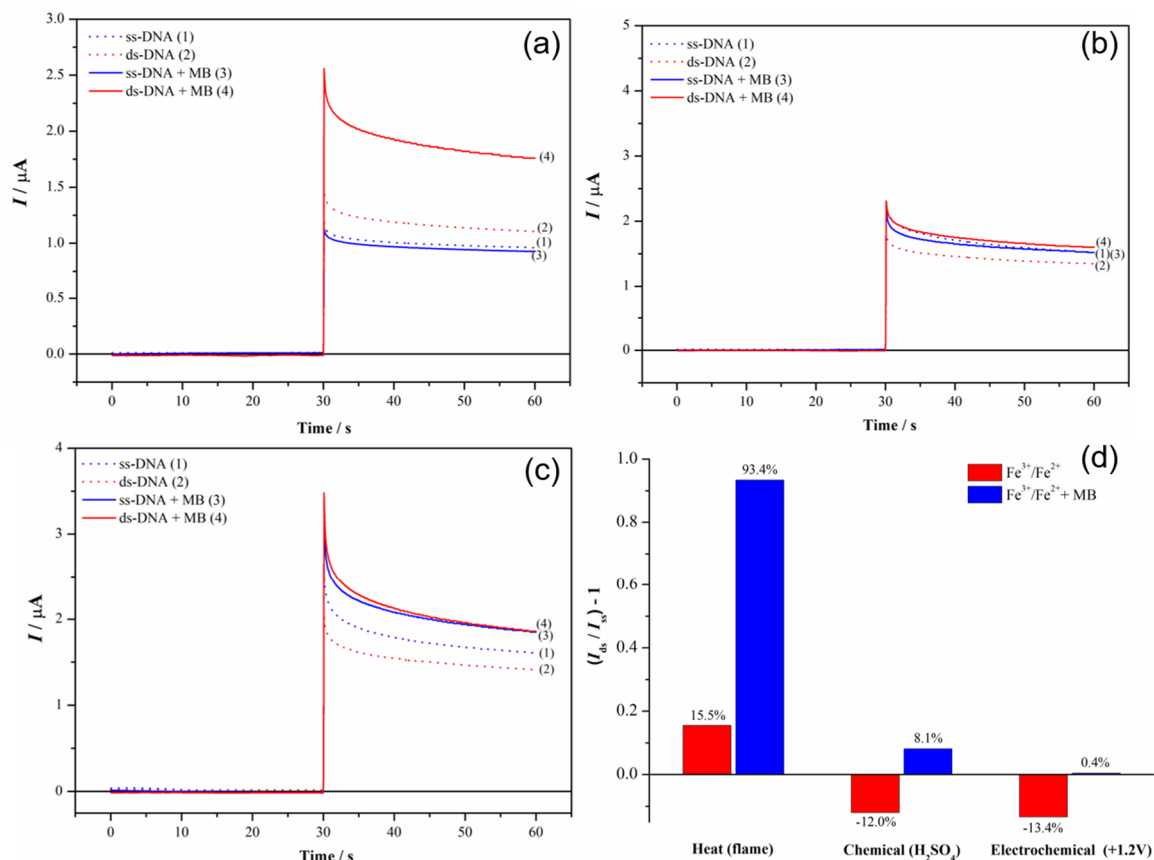


Figure III.13. Chronoamperometry, Electrochemical response before hybridization (blue) and Electrochemical response after hybridization (red) of microelectrode array (10 bands). $\Delta E = 0.05\text{V}$, $\Delta I = \text{NaH}_2\text{PO}_4$ 0.3 M + $[\text{Fe}(\text{III})(\text{CN})_6]^{3-}/[\text{Fe}(\text{II})(\text{CN})_6]^{4-}$ 5 mM and presence (full line) or absence of (dotted line) MB 5 μM by different activation methods: flame (a), chemical activation (b), electrochemical activation (c). The percentage of change current after hybridization by different activation methods and in different electrolyte that presence or absence of MB (d).

Figure III.13 shows the CA response in the electrolyte solution that presence and absence of MB after the formation of a self-assembled DNA probe monolayer and hybridized with 1.5 μM DNA target (T), the UME array surface was treated by three methods: flame (Figure III.13a), chemistry (Figure III.13b), and electrochemical (Figure III.13c), the Figure III.13d is the corresponding column graph. As shown, the current after hybridization has increased, which is due to the long-range electron transfer in double-stranded DNA increasing the conductivity.

Moreover, interestingly the amount of increasing current is higher when electrolyte presence of MB than absence MB, it proved that MB as a role of catalyzed in increase current and amplifies the increase in current. Furthermore, Hybridization efficiency is highest for the flame treatment. It was therefore chosen to prepare gold array of UME for further experiments.

III.2.3.3. Calibration curve

Figure III.14 shows the calibration curve of different concentrations of miRNA-21 in the buffer obtained at gold UME array by chronoamperometry. The signal is the difference after (I_{ds}) and before (I_{ss}) hybridization. There is a linear relationship between 1.0×10^{-18} mol L⁻¹ to 1.0×10^{-8} mol L⁻¹ miRNA-21, and the function is:

$$y = 0.1 \log(C_{miRNA-21}) + 1.95$$

The low detection limit is 5.7×10^{-18} mol L⁻¹ (calculated as 3-fold of the SD, where SD is the standard deviation of the blank signal) R^2 is 0.985.

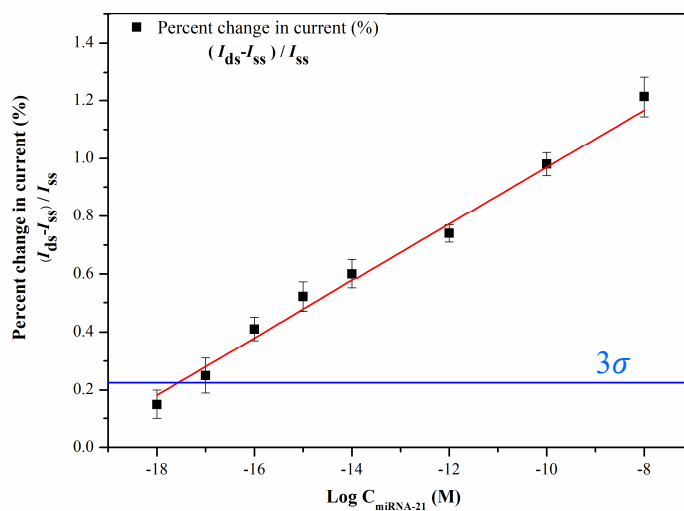


Figure III.14. The calibration curve of different concentrations of miRNA-21 in the buffer obtained at gold UME array by chronoamperometry.

III.2.3.4. Quantification of miRNA-21 in plasma based on RT-qPCR

miRNA-21 placed in plasma was quantified with RT-qPCR: poly(A)-tail extension and reverse transcription. The standard miRNA-21 was diluted into purified plasma solutions containing no miRNA-21, which are removed with a purification kit. Afterwards, this purified plasma was used to prepare diluted miRNA-21 solutions from 10^{-18} to 10^{-5} mol L⁻¹, a non-template control (NTC) and a blank. NTC is a sample without miRNA-21 and a control for the reverse transcription step, prepared in the initial step and undergoes the reverse transcription (poly(A)-tail extension method) and qPCR steps together with other miRNA-21 at different concentrations. Moreover, the blank is another control for qPCR step, which without cDNA and was prepared in the second step, ideally, no amplification curve will appear in any blank control. Then miRNA concentrations were measured by qPCR (Figure III.15).

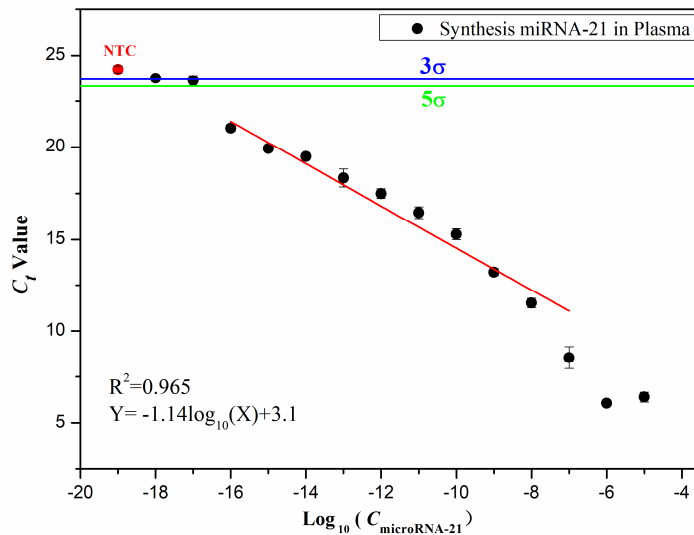


Figure III.15. The qPCR calibration curve of different concentration miRNA-21 sample in plasma of *TaqMan*[®] advanced microRNA assays.

The calculated PCR amplification efficiency is 99.66%. The dynamic range of PCR assay was between 10^{-16} mol L⁻¹ and 10^{-8} mol L⁻¹:

$$C_t = 1.14 \times \log(C_{miRNA-21}) + 3.1$$

LOD and LOQ that was estimated by taking the intersection between the linear part of the experimental data and 3-fold and 5-fold of the SD line of NTC. LOD and LOQ are respectively $8.7 \times 10^{-19} \text{ mol L}^{-1}$ and $1.85 \times 10^{-18} \text{ mol L}^{-1}$.

III.2.3.5. The comparison between electrochemistry and RT-qPCR

The Table III. shows the LOD of miRNA-21 by RT-qPCR and chronoamperometry using gold UME array, which are $8.7 \times 10^{-19} \text{ mol L}^{-1}$ and $5.7 \times 10^{-18} \text{ mol L}^{-1}$ and they are almost same. However, for the chronoamperometry method, it can directly detect miRNA-21 in serum and do not require additional step of reverse transcription compare with RT-qPCR. In addition, the chronoamperometry takes only about 30 min, while RT-qPCR requires at least 3h.

Table III.3. The low detection limit of miRNA-21 by chronoamperometry and RT-qPCR.

Method	LOD
Chronoamperometry	$5.7 \times 10^{-18} \text{ mol L}^{-1}$
RT-qPCR	$8.7 \times 10^{-19} \text{ mol L}^{-1}$

Conclusions

In this work, developed a gold UME array for the label-free quantification of miRNA-21 by chronoamperometry and comparing with the RT-qPCR. The LOD are $5.7 \times 10^{-18} \text{ mol L}^{-1}$ and $8.7 \times 10^{-19} \text{ mol L}^{-1}$ respectively, which shows that the electrochemical miRNA-21 biosensor we designed is feasible and the detection performance is as good as the gold standard detection method of miRNA, RT-qPCR. Otherwise, due to its simple procedure and short time-consuming, it has great potential in clinical diagnosis. For the UME array that we designed (w : 25 μm , gap: 200 μm), each band of UME array can be addressed independently, thus enabling

several measures quickly, and the strategy of averaging the measurements that measured on each band was chosen to reduce the variability of the measurements. This UME array design provides more reliability and sensitivity to the electrochemical DNA biosensor system.

References

1. Lee SY, Chang HN. High cell density cultivation of *Escherichia coli* W using sucrose as a carbon source. *Biotechnology letters* 1993,**15**:971-974.
2. Fabian MR, Sonenberg N, Filipowicz W. Regulation of mRNA translation and stability by microRNAs. *Annual review of biochemistry* 2010,**79**:351-379.
3. Vaucheret H, Béclin C, Fagard M. Post-transcriptional gene silencing in plants. *Journal of cell science* 2001,**114**:3083-3091.
4. Gillespie P, Ladame S, O'Hare D. Molecular methods in electrochemical microRNA detection. *Analyst* 2019,**144**:114-129.
5. Nordberg M, Duffus J, Templeton DM. Glossary of terms used in toxicokinetics (IUPAC Recommendations 2003). *Pure and Applied Chemistry* 2004,**76**:1033-1082.
6. Kosaka N, Iguchi H, Ochiya T. Circulating microRNA in body fluid: a new potential biomarker for cancer diagnosis and prognosis. *Cancer science* 2010,**101**:2087-2092.
7. Ortiz-Quintero B. Cell-free microRNAs in blood and other body fluids, as cancer biomarkers. *Cell proliferation* 2016,**49**:281-303.
8. Etheridge A, Lee I, Hood L, Galas D, Wang K. Extracellular microRNA: a new source of biomarkers. *Mutation Research/Fundamental and Molecular Mechanisms of Mutagenesis* 2011,**717**:85-90.
9. Kai K, Dittmar RL, Sen S. Secretory microRNAs as biomarkers of cancer. In: *Seminars in cell & developmental biology*: Elsevier; 2018. pp. 22-36.
10. de Planell-Saguer M, Rodicio MC. Analytical aspects of microRNA in diagnostics: a review. *Analytica chimica acta* 2011,**699**:134-152.
11. Hamidi-Asl E, Palchetti I, Hasheminejad E, Mascini M. A review on the electrochemical biosensors for determination of microRNAs. *Talanta* 2013,**115**:74-83.
12. Shabaninejad Z, Yousefi F, Movahedpour A, Ghasemi Y, Dokanehiifard S, Rezaei S, *et al.* Electrochemical-based biosensors for microRNA detection: Nanotechnology comes into view. *Analytical biochemistry* 2019:113349.
13. Tian T, Wang J, Zhou X. A review: microRNA detection methods. *Organic & biomolecular chemistry* 2015,**13**:2226-2238.
14. Burgos J, Ramírez C, Tenorio R, Sastre I, Bullido M. Influence of reagents formulation on real-time PCR parameters. *Molecular and cellular probes* 2002,**16**:257-260.
15. Ferre F. Quantitative or semi-quantitative PCR: reality versus myth. *Genome Research* 1992,**2**:1-9.
16. Klein D. Quantification using real-time PCR technology: applications and limitations. *Trends in molecular medicine* 2002,**8**:257-260.
17. Wen Y, Pei H, Shen Y, Xi J, Lin M, Lu N, *et al.* DNA nanostructure-based interfacial engineering for PCR-free ultrasensitive electrochemical analysis of microRNA. *Scientific reports* 2012,**2**:867.
18. Green JE, Choi JW, Boukai A, Bunimovich Y, Johnston-Halperin E, DeIonno E, *et al.* A 160-kilobit molecular electronic memory patterned at 10¹¹ bits per square centimetre. *Nature* 2007,**445**:414-417.
19. Basu N, Ho TH, Guillon FX, Zhang Y, Bigey P, Navakanta B, *et al.* Coupling Electrochemical Adsorption and Long-range Electron Transfer: Label-free DNA Mismatch Detection with Ultramicroelectrode (UME). *Electroanalysis* 2019,**31**:2232-2237.
20. Nassi A, Guillon F-X, Amar A, Hainque B, Amriche S, Maugé D, *et al.* Electrochemical DNA-biosensors based on long-range electron transfer: optimization of the amperometric detection in the femtomolar

- range using two-electrode setup and ultramicroelectrode. *Electrochimica Acta* 2016,**209**:269-277.
21. Faure M, Pallandre A, Chebil S, Le Potier I, Taverna M, Tribollet B, *et al.* Improved electrochemical detection of a transthyretin synthetic peptide in the nanomolar range with a two-electrode system integrated in a glass/PDMS microchip. *Lab on a Chip* 2014,**14**:2800-2805.
 22. Gamby J, Delapierre F-D, Pallandre A, Tribollet B, Deslouis C, Haghiri-Gosnet A-M. Dielectric properties of a single nanochannel investigated by high-frequency impedance spectroscopy. *Electrochemistry Communications* 2016,**66**:5-9.
 23. Aoki K, Tokuda K. Linear sweep voltammetry at microband electrodes. *Journal of electroanalytical chemistry and interfacial electrochemistry* 1987,**237**:163-170.
 24. Bard AJ, Faulkner LR. Fundamentals and applications. *Electrochemical Methods* 2001,**2**:580-632.
 25. Daniele S, Bragato C. From macroelectrodes to microelectrodes: Theory and electrode properties. In: *Environmental analysis by electrochemical sensors and biosensors*: Springer; 2014. pp. 373-401.
 26. Porat Ze, Crooker JC, Zhang Y, Le Mest Y, Murray RW. iR UNC Advantages and Real Geometrical Dimensions of Microband Electrodes. *Analytical Chemistry* 1997,**69**:5073-5081.
 27. Amatore C, Pebay C, Sella C, Thouin L. Mass transport at microband electrodes: transient, quasi-steady-state, and convective regimes. *ChemPhysChem* 2012,**13**:1562-1568.
 28. Pebay Cc, Sella C, Thouin L, Amatore C. Mass transport at infinite regular arrays of microband electrodes submitted to natural convection: theory and experiments. *Analytical chemistry* 2013,**85**:12062-12069.
 29. Mohr PJ, Taylor BN, Newell DB. CODATA recommended values of the fundamental physical constants: 2006. *Journal of Physical and Chemical Reference Data* 2008,**80**:633-1284.
 30. Faulkner L, Bard A. *Electrochemical Methods Fundamentals and Applications*, 2nd. 2001.

Supplementary information

Electrode set-up

A two-electrode system (Figure III. 16) is used to measure all stages of electrode surface change which the gold UME array (10 bands) was used as working electrode and an Au wire with a diameter of 1 mm used as counter electrode which is also considered as a pseudo-reference electrode.

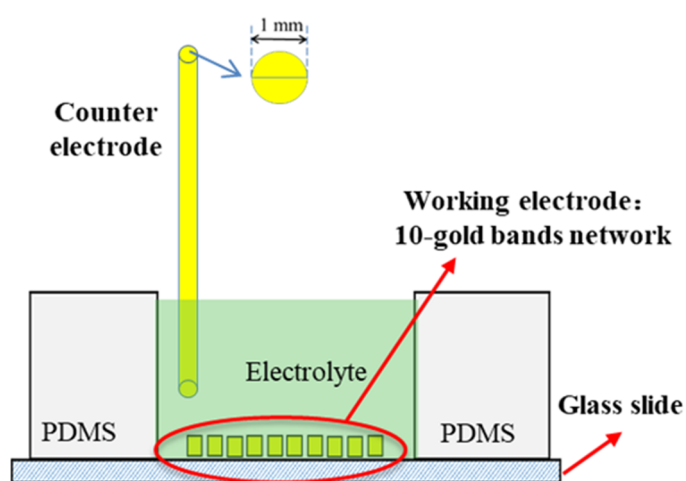


Figure III. 16. The vertical section of two-electrode setup of 10-gold bands UME array device.

Electrochemical response of gold UME array

The electrochemical behavior of gold UME array was studied by the methods of cyclic voltammetry (CV) and chronoamperometry (CA) which carried out using 5 mM $K_3[Fe(III)(CN)_6]$ and 5 mM $K_4[Fe(II)(CN)_6]$ in 0.5 M NaCl aqueous solution obtained using the two-electrode setup. Figure III.17 shows a cyclic voltammetric response of the gold UME array (10 gold microbands) in 0.5 M NaCl solution that absence (blue) and presence (red) of 5 mM $K_3[Fe(III)(CN)_6]$ and 5 mM $K_4[Fe(II)(CN)_6]$ at a scan rate of 50 mV/s. It is noted that it gets a typical cyclic voltammetry graph (red) in presence of redox couple system, and the current is very low when the electrolyte is only 0.5M NaCl (blue), it illustrated the perfect

electrochemical performance of gold UME array. The voltammetric profile of UME is related to the diffusion layer thickness, when the scan rate is low, the diffusion layer thickness is small and the diffusion is mainly convergent/radial diffusion, the voltammetric profile is a steady-state type. In addition, the peak shaped voltammograms was obtained since the scan rate increase, the diffusion layer thickness expanded and linear/planar diffusion predominated.

For band UME and the diffusion geometry is mix of radial and linear diffusion, the voltammetric theoretical peak current of microband as follows [1-4]:

$$I_p = n F C_o^* L D_o \left[0.439 p + 0.713 p^{0.108} + \frac{0.614 p}{1+10.9 p^2} \right] \quad (8)$$

$$p = (n F w^2 v / R T D_o)^{1/2} \quad (9)$$

Where n is electron number of the redox reaction, F is faraday constant (96485 C.mol⁻¹), D_o is the diffusion coefficient of [Fe (III)(CN)₆]³⁻ / [Fe (II)(CN)₆]⁴⁻ redox couple (6.4×10⁻⁶ cm².s⁻¹), C_o^* (mol.L⁻¹) is the bulk concentration of redox species, L (cm) and w (μm) are the length and width of electrode. Under the experiment condition with $L = 0.5$ cm and $w = 25$ μm, the theoretical peak current of one band was calculated at a scan rate of 50 mV/s to be 2.13 μA based on the equation (8 and 9). The experiment value of 10-band is 20.6 μA (Figure III.17 red), and the average current value per UME band is 2.06 μA which is near the theoretical current, this is due to the diffusion layers under the gold UME array structure and experimental conditions, the diffusion layers do not overlap.

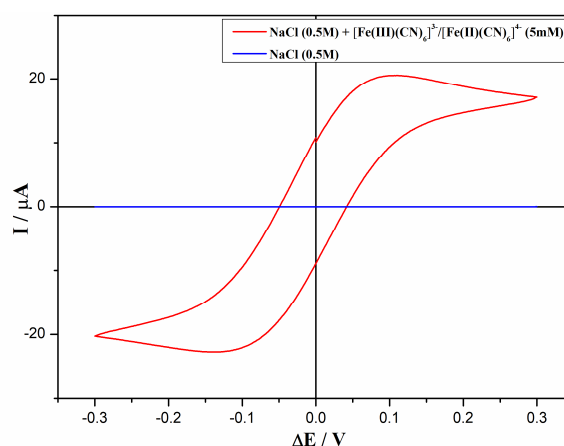


Figure III.17. Cyclic voltammograms of gold UME array (10 bands) in 5 mM $[\text{Fe}(\text{III})(\text{CN})_6]^{3-}$ and 5mM $[\text{Fe}(\text{II})(\text{CN})_6]^{4-}$ (red) with 0.5 M NaCl, and in NaCl 0.5 M (blue). The potential was swept from -0.3 V to +0.3 V at a scan rate of 50 mV/s.

To further analysis the relationship of single band UME in the array and the total band UME array, the CV and CA method were used. For cyclical voltammetry, the peak current was chosen for comparison, and for the CA which was applied 30 seconds at a constant potential of +0.05V and then selected the steady current at 30 s for comparison, which were shown in the Figure III.18 After the experiments of electrochemical characterization, the Figure III.18 shows the data of each single band UME current vs average current of each band in the band UME array which measured by CV (Figure III.18a) and CA (Figure III.18b). Both of them, the average current of each band is close to the single UME average current, which verified the response of each band UME is independent of the others and the diffusion layer thickness over the band UME does not overlap, in other words, electrodes are not coupled. Therefore, the design of the UME array is well choice where the $w_{\text{band}} = 25\mu\text{m}$ and $w_{\text{gap}} = 200\mu\text{m}$.

Due to each band of UME array can be addressed independently, thus enabling several measures quickly. Furthermore, the standard deviation of electrode responses of each band in the same UME array and different UME array (6 UME arrays were compared) are 0.096 and 0.19 respectively. Thus, this UME array design allows to decrease standard deviation of the measurement and provide more reliability and sensitivity to the electrochemical DNA biosensor system.

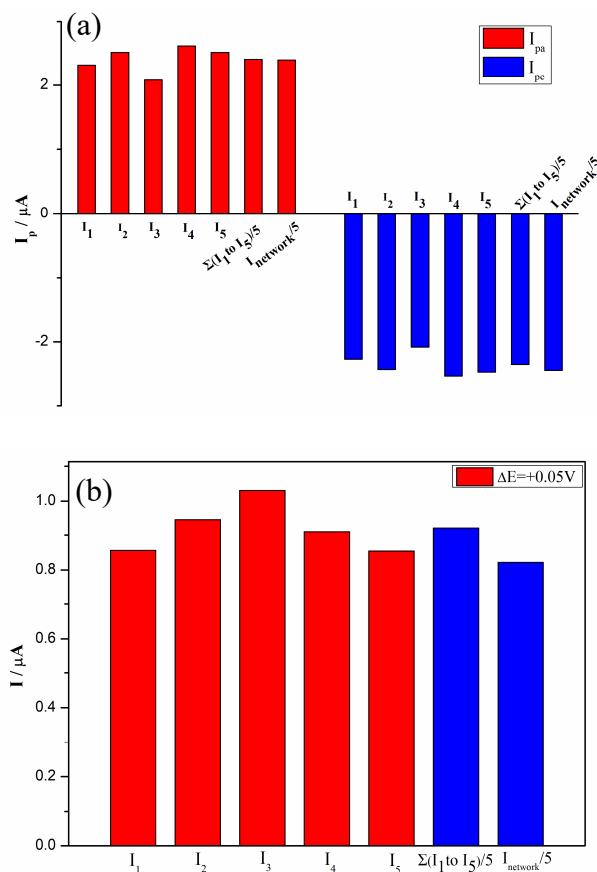


Figure III.18. The current of each single band UME vs average current of each band in the UME array which measured in 0.5M NaCl presence of 5 mM $[Fe(III)(CN)_6]^{3-}$ and 5 mM $[Fe(II)(CN)_6]^{4-}$ by cyclical voltammetry (a) and chronoamperometry (b).

References

1. Aoki K, Tokuda K. Linear sweep voltammetry at microband electrodes. *Journal of electroanalytical chemistry and interfacial electrochemistry* 1987,**237**:163-170.
2. Bard AJ, Faulkner LR. Fundamentals and applications. *Electrochemical Methods* 2001,**2**:580-632.
3. Daniele S, Bragato C. From macroelectrodes to microelectrodes: Theory and electrode properties. In: *Environmental analysis by electrochemical sensors and biosensors*: Springer; 2014. pp. 373-401.
4. Porat Ze, Crooker JC, Zhang Y, Le Mest Y, Murray RW. iR UNC Advantages and Real Geometrical Dimensions of Microband Electrodes. *Analytical Chemistry* 1997,**69**:5073-5081.

Conclusion of the Chapter III

DNA electrochemical biosensor provides a fast, simple, reliable and inexpensive DNA hybridization test method. It can directly transduce the DNA hybridization event into the electrochemical signal to detect, that can detect femtomolar to attomole DNA molecules. With these unique advantages, it has become a research hotspot in the field of DNA analysis. Electrochemical impedance spectroscopy, Cyclic voltammetry and Chronoamperometry are the commonly used electrochemical detection methods. Here, we constructed two electrochemical DNA platform that measured with EIS and CA, respectively. Then compare the performance with RT-qPCR and SPR described in chapter II.

First, we developed a label-free and non-amplified impedimetric genosensing of miRNA-21 using a bioanalytical platform rationally built by taking advantage of the carboxylic groups of GO to support CHIT. Impedance can analyze the electrode interface structure information by detecting the change in the resistance of the redox couple migration to the electrode surface (which is caused by the change in the state of the electrode surface). Which allowed the sensitive (femtomolar), selective, simple and fast quantification of miRNA-21 without any additional amplification step and successful application in different biological fluids.

Faraday AC impedance technology is an effective tool for studying electrode processes. It is widely used in the field of electrochemical research. It can obtain more kinetic information and electrode interface structure information than other electrochemical methods, such as electron transfer resistance, double electricity Layer capacitance, etc.

Moreover, we developed a gold UME array for the label-free quantification of miRNA-21 by chronoamperometry. And the use of catalyzed long-range electron transfer pathway that due to the faradic signal is not limited to the redox species adsorbed on the biosensor surface, thereby greatly improving the sensitivity of the biosensor. It allows attomole quantification of miRNA-21. In addition, by comparing with the impedimetric biosensor of this work, the UME array provides more reliability and sensitivity to the electrochemical DNA biosensor system. And the miniaturization and integration provided prospects for commercialization.

General Conclusions

In summary, this doctorate presents the technological development of analytical tools allowing a direct detection of miRNAs: electrochemical biosensor (EIS and CA) and optical techniques (RT-qPCR and SPR) for miRNA-21, which is a biomarker involved in liver cancers. As part of this thesis, the analytical performance of the biosensor was compared with PCR for the detection of miRNAs in human plasma samples.

Reverse transcription real-time fluorescence quantitative PCR (RT-qPCR) is a technology developed on the basis of traditional PCR technology for miRNA analysis and quantification. The doctorate evaluated and compared two methods of RT-qPCR for miRNA, which are stem-loop primer reverse transcription and poly(A)-tail extension method. As the results, the poly(A)-tail extension method is more sensitive and specific. Then it was used to detect miRNA-21 in plasma, and with a dynamic range between 10^{-8} M and 10^{-16} M, and with a LOD and LOQ of 0.87aM and 1.85aM, respectively. Which successfully detected the miRNA-21 in HCT116 cell line that contains a variety of miRNA types and shows an excellent selectivity.

Although RT-qPCR is the gold standard for miRNA analysis and has high sensitivity, it also has disadvantages, such as cumbersome amplification steps easy to cause errors, time-consuming, and expensive reagents. Currently, it is a challenge to detect miRNA without amplification, thus, the high sensitivity SPR and Electrochemical biosensor were developed and evaluated.

SPR biosensor is another method for quantifying miRNA-21 in this thesis, it relies on monitoring a shift in resonance angle due to a change in the refractive index of the dielectric material on the surface of SPR sensing resulting from the surface binding reaction. It can monitor the reaction process of biomolecules in real-time without labels. In order to improve the sensitivity of SPR miRNA biosensor, we reported a SPR biosensor based on a supramolecular architecture built at a thiolated gold platform containing GO, which can be successfully applied to the quantification of microRNA-21 in enriched urine samples. The incorporation of GO in the multistructure facilitates the covalent attachment of the NH_2 -DNA

probe and makes possible the enhancement of the SPR analytical signal, eliminating, in this way, the need for additional amplification scheme. There is a linear dependence between 1.0 fM and 10 nM, with a detection limit of 3×10^{-16} M. And has a high selectivity for non-complementary and one-base mismatch sequence.

DNA electrochemical biosensor can directly transduce the DNA hybridization event into the electrochemical signal to detect, it provides a fast, simple, reliable and inexpensive DNA hybridization test method. It is one of the more promising gene detection methods at present. Here we developed two kinds of electrochemical biosensor and measured miRNA-21 by EIS and CA respectively.

For the quantification of miRNA-21 with EIS, we reported a label-free and non-amplified impedimetric genosensing for miRNA-21 by using a bioanalytical platform that was built by taking advantage of the carboxylic groups of GO to support CHIT, which the conductive properties of RGO to improve the electroactivity of the platform, and the high density of the amine groups of chitosan to work as bridge between MPS and the aminated capture probe. Which the low detection limit is 3×10^{-13} M and a linear range of 10^{-12} M to 10^{-8} M, it was successfully discriminate non-complementary, even 1-base mismatch sequences and applied to different biological fluids (saliva, urine and serum).

For the quantitative analysis of miRNA-21 using CA, in order to improve the sensitivity, reliability and detection throughput of the sensor. We developed a gold band UMEs array (w : 25 μ m, gap: 200 μ m) for the label-free quantification of miRNA-21 by chronoamperometry, which has the simple immobilization procedure just by Au-S band and needn't any modification process. The design of the band UMEs array expanded the surface area, while improving the detection sensitivity by the strategy of averaging the measurements that measured on each band. In addition, each band of UMEs array can be addressed independently and the assembly of the PDMS well has greatly increased its detection throughput. Which the LOD is 5.7×10^{-18} and with a linear range from 10^{-18} M to 10^{-8} M.

Table C.1. Summary of the performance of four quantification techniques for miRNA-21.

Detection Techniques		Linear range	LOD (M)	Real sample
Optics	RT-qPCR	10^{-16} M to 10^{-8} M,	8.7×10^{-19}	Plasma
	SPR	10^{-15} M to 10^{-6} M	3×10^{-16}	Urine
Electrochemistry	EIS	10^{-12} M to 10^{-8} M	3×10^{-13}	saliva, urine and serum
	CA	10^{-18} M to 10^{-12} M	5.7×10^{-18}	-

The Table C.1 summarizes the performance of the four miRNA-21 quantification techniques. All of them got the wide dynamic range for miRNA-21 quantification, in which SPR and electrochemical biosensors allow detect miRNA-21 with high sensitivity without amplification and labels. SPR method achieved dynamic detection of up to 10 orders of magnitude and RT-qPCR can realize dynamic detection of 9 orders of magnitude. In addition, the CA and RT-qPCR techniques obtained excellent LOD, which can detect miRNA-21 as low as attomolar level, have high selectivity for non-complementary and one-base mismatch sequences, and successfully applied to the detection of miRNA-21 in the real body fluid samples. Otherwise, among the four detection methods proposed in this thesis, the chronoamperometry technique using gold band UMEs array is the best method to quantify miRNA-21, due to the miniaturization, integration and simple detection procedures.

Appendices

Contents

Appendices.....	235
LIST OF FIGURES	237
A.1. Introduction.....	239
A.2. Fabrication and Characterization of the Gold band UMEs array.....	239
A.2.1. Substrate Preparation	239
A.2.2. Photolithography Process.....	240
A.2.3. The metallization.....	243
A.2.4. Lift-off process.....	244
A.2.5. Fabrication of PolyDiMethylSiloxane wells (PDMS)	244
A.3. The gold band UMEs array surface cleaning.....	246
A.3.1. Gold UME array electrochemical response in sulfuric acid	246
A.3.2. Gold band UMEs array cleaning methods for bioanalytical purposes.....	249
A.3.2.1. Chemical and Electrochemical treatment method	249
A.3.2.2. Plasma treatment method	251
A.4. Gold electrode response in chloride solution.....	253
A.5. Electrochemical measurement methods.....	255
A.5.1. Mass Transport.....	256
A.5.1.1 Diffusion equations and current responses	257
A.5.2. The electrochemical measurement of planar electrode.....	258
A.5.2.1. Potential step methods (Amperometry)	258
A.5.2.2. Cyclic Voltammetry (CV).....	259
A.5.2.3. Electrochemical Impedance Spectroscopy (EIS).....	261
A.5.3. Ultramicroelectrodes (UME)	264
A.5.3.1. Potential step methods (Amperometry)	265
A.5.3.2. Cyclic voltammetry.....	266
A.5.4. Experiment set-up system	267
A.5.4.1. Three-electrode set-up.....	267
A.5.4.2. Two-electrode set-up.....	267
A.6. The concentration of nucleotides calculation	269

LIST OF FIGURES

Figure A.1. The photograph of plasma cleaner.	240
Figure A.2. Fabrication process of gold band UMEs array by lift-off method. (1) Coated a layer Ti primer on the glass slide. (2) Coated the photoresist AZ5214-E on Ti layer surface. (3) Covered the mask. (4) Exposed UV light. (5) The flood exposure of UV light without mask. (6) Developed with AZ 726 MIF developer. (7) Sputtered a thin layer of Ti. (8) Sputtered Au. (9) Removed the photoresist AZ-5214-E with ultrasonic cleaner in acetone. (10) Ti and Au electrode was left.....	240
Figure A.3. The picture of band microelectrodes array mask.	242
Figure A.4. The microscope picture of band UMEs array after different time development: a) 5s, b) 10s.	242
Figure A.5. K675X Turbo Large Chromium Coater 8.	243
Figure A.6. Photograph of lithographed gold band UMEs array.	244
Figure A.7. The chemical structure of PDMS.....	245
Figure A.8. Photo of the block PDMS with measurement wells.	246
Figure A.9. A typical cyclic voltammogram in different scanning potential ranges for gold electrode (1 mm diameter gold wire) in 1M H ₂ SO ₄ solution at 50 mV/s scan rate.	247
Figure A.10. Cyclic voltammetry, Electrochemical response of milli-electrode (1 mm diameter gold wire) in H ₂ SO ₄ (1M) when present of rinsing (blue) and absent of rinsing (red) after 30s oxidation by chronoamperometry (oxidation potential is 1.7 V).	248
Figure A.11. Cyclic voltammogram of gold band UMEs array in 0.5M NaCl solution contains 5 mM [Fe(III)(CN) ₆] ³⁻ / [Fe(II)(CN) ₆] ⁴⁺ , which undergoes different time of H ₂ SO ₄ . (1M) chemical treatment (a) and H ₂ SO ₄ . (0.05 M) electrochemical treatment (b).....	250
Figure A.12. The increased value of cyclic voltammetry on the electrode surface after treatment under different power of Ar plasma treatments (red). The DNA probe immobilization efficiency under the 1 W Ar plasma treatment during different time (black).....	252
Figure A.13. Chronoamperometry response of bare gold film (red), after self-assembly of DNA probe (blue), which was measured with a voltage of 0.05 V in 0.5M NaCl solution containing 5mM [Fe(III) (CN) ₆] ³⁻ and 5mM [Fe(II) (CN) ₆] ⁴⁺ , and the DNA immobilization efficiency after with or without the CV treatment in the chloride ion solution (black).	253
Figure A.14. Pathway of a general electrode reaction [23].....	256
Figure A.15. Diffusion mass transport of planar electrode [24].....	258
Figure A.16. AC excitation signal and sinusoidal current response in a Linear System.....	261
Figure A.17. Complex plane impedance plots at electrodes for the shown selected electrical equivalent circuits: (a) purely capacitive interfacial response, (b) faradaic electron-transfer reaction controlled by kinetics, (c) electron-transfer reaction with mass transfer control at low frequencies. R _Ω cell resistance, R _{ct} electron-transfer resistance, C _{dl} double-layer capacitance, Z _w Warburg impedance [24].	264
Figure A.18. Microelectrode configurations: (a) disk, (b) cylinder, (c) hemisphere, (d) band, (e) ring, (f) sphere cap, (g) cone, (h) nanopore, and (i) recessed microelectrode.	265
Figure A.19. Diffusional geometry at a band electrode. Normally the length of the electrode is very much	

larger than the width, and the three-dimensional diffusion at the ends does not appreciably violate the assumption that diffusion occurs only along the x and z axes.265

Figure A.20. A three-electrode-setup connected to a potentiostat with the electrodes in a cell.267

Figure A.21. Two-electrode electrochemical setup configuration. gold disc UME ranging from 25 μm -50 μm diameter (working electrode); gold disc in 2 mm diameter (counter electrode).268

Figure A.22. Cyclic voltammograms of two-electrode set-up and three-electrode set-up in a 5×10^{-3} M $\text{K}_3[\text{Fe}(\text{III})(\text{CN})_6]$, 5×10^{-3} M $\text{K}_4[\text{Fe}(\text{II})(\text{CN})_6]$, 0.5 M NaCl solution. (working electrode: gold disc UME in 50 μm diameter).....269

Figure A. 23.Ultraviolet absorption spectrogram of different concentration complementary DNA target.2700

A.1. Introduction

With the trend of analytical chemistry technology towards small volume and multi-channel detection, the interest of microelectrode array sensors continues to grow. Moreover, microelectrode array has some advantages such as small iR drop and capacitive charging currents, and easy to obtain a steady-state diffusion, which make it capture much interest in the field of electrochemical analysis. There are many kinds of microelectrodes array manufacturing technologies: photolithography, screen-printing technique, electrodeposition etc. Among them, photolithography is currently the most extensive metal microelectrode array manufacturing technology [1]. In addition, gold is one of the most extensive metal electrode materials in the manufacture of microarrays and was selected in this study for use in the manufacture of electrochemical biosensor due to its inertness, superior electrical conductivity, great stability and the strong affinity for thiol compounds.

For the band ultramicroelectrodes (UMEs) array, the size of the electrode affects its electrochemical response. Thus, the band UMEs array with a width of 25 μm , a length of 5 cm, and a gap of 200 μm was selected in this study and the electrochemical properties were studied. In addition, different gold surface cleaning methods were used and compared to obtain a cleaner gold surface and improve the affinity between gold and thiol.

A.2. Fabrication and Characterization of the Gold band UMEs array

Lift-off is a process for patterning structures with target material (e.g. metal) on the substrate surface (e.g. wafer, glass slide) [2]. It does not require etching step, so it will not destroy the substrate [3]. In general, the lift-off method contains the following steps: photolithography, metallization, resist stripping and metal lift-off. In the following subsections, the gold band UMEs array manufacturing process were described in detail.

A.2.1. Substrate Preparation

Glass slide are used as the substrate of gold band UMEs array, due to the fineness of the

microfabrication process, the cleanliness affects the quality of the photolithography step, dirty substrates cannot provide the necessary feature size and dimensional accuracy. The cleaning procedure was carried out with piranha method, first rinsed the surface of the slide with acetone and isopropanol, then immersed in the piranha solution for 15 minutes, then rinsed with deionized water and treated with oxygen plasma (50w, 100sccm) for 5 minutes, the cleaned glass slides were ready for next photolithography step. The plasma cleaning instrument shown in Figure A.1.



Figure A.1. The photograph of plasma cleaner.

A.2.2. Photolithography Process

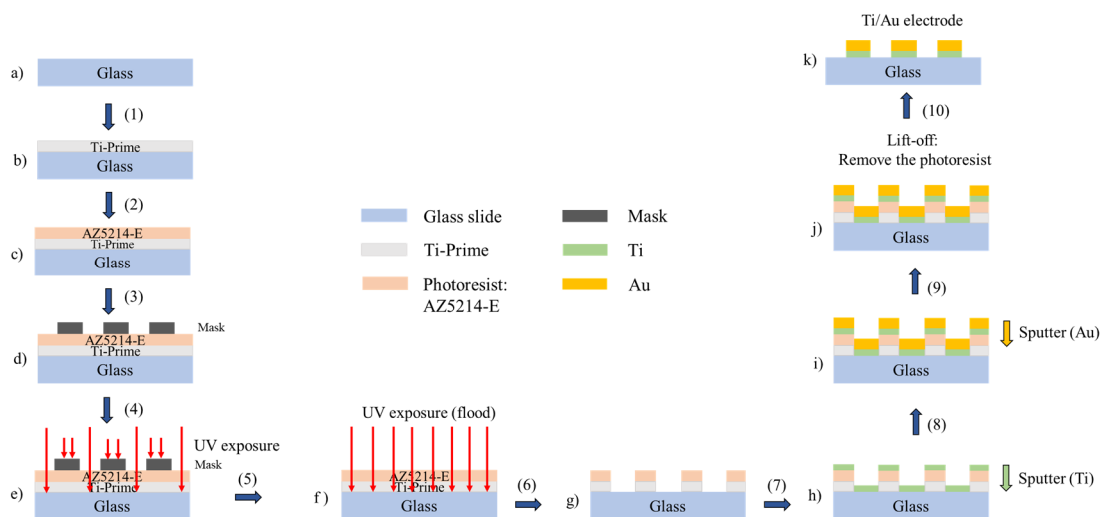


Figure A.2. Fabrication process of gold band UMEs array by lift-off method. (1) Coated a layer Ti primer on the glass slide. (2) Coated the photoresist AZ5214-E on Ti layer surface. (3) Covered the mask. (4) Exposed UV light. (5) The flood exposure of UV light without mask. (6) Developed with AZ 726 MIF developer. (7) Sputtered a thin layer of Ti. (8) Sputtered Au. (9) Removed the photoresist AZ-5214-E with ultrasonic cleaner in acetone. (10) Ti and Au electrode was left.

Figure A.2 shows total fabrication process of gold band UMEs array by lift-off method. The photolithography procedure illustrated in the Figure A.2 (1) – (6), photolithography refers to microfabrication process that can selectively remove parts of thin film (or substrate) based on the exposure step and development procedure for the UV sensitive photoresist. In our photolithography process, the image reversal resists AZ-5214E was used to pattern [4, 5]. Image reversal resists can be used both positively and negatively, in our study, a negative way was used and over the glass slide substrates, and its extended resolution feature can be applied to fabricate the small elementary dimensions pattern [6, 7]. Moreover, in the image reversal mode, the undercut resist sidewall reduces and allow to obtain a clean resist structures and edge in the lift-off procedure. The photolithography procedures are as follows:

(1). Process started from coating a layer of Ti-primer on the substrate to improve the adhesion for the following photoresist deposition. Which was spin-coated for 5 seconds at 1500 rpm followed for 30 seconds at 4000 rpm in a spin-coater. Then putted on a hot plate baking 2 minutes at 110 °C.

(2). Next, spin coated a layer of photoresist AZ-5214E for 5 seconds at 1500 rpm followed for 30 seconds at 4000 rpm, then subjected hot plate baking 2 min at 110 °C.

(3). Putted the mask on the photoresist coated surface and attached it tightly, then putted them on the UV-KUB2 aligner instrument. The photomask was designed through the use of CleWin software and showed in Figure A.3.

(4). Photoresist was exposed to UV light to make the photoresist selectively-soluble, which by a UV-LED masking system (UV-KUB 2) and operated for 10 seconds at 23.4 mW/cm².

Following, reversal bake was done at 125 °C for 2 minutes to complete the resin crosslinking chemical reaction and the exposed resist areas are converted to insoluble in the developer, while the unexposed resist without any change.

(5). The flood UV exposure of photoresist with done for 36 seconds without mask, which

made previously unexposed areas soluble in developer.

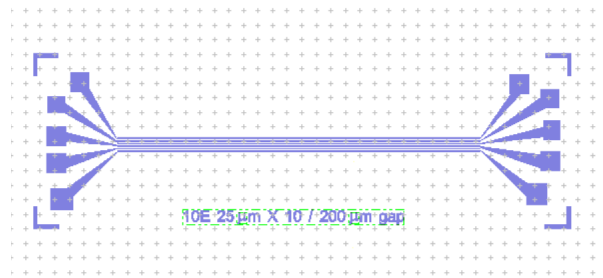


Figure A.3. The picture of band microelectrodes array mask.

(6). The last step is development, which the slide in the previous step immersed in AZ 726 MIF developer for 10 seconds, the first exposed area was retained, while the unexposed area was stripped and the pattern was formed on the glass substrate. Then rinsed with deionized water and dried with compressed air. Then observed the array microstructure under a microscope to determine whether its development is complete. Figure A.4 shows the microscope picture of band UMEs array after different development time, when the development time is 5s (Figure A.4a), it can be seen that part of the photoresist is still not dissolved on the pattern. And when the development time increase to 10s (Figure A.4b), the photoresist on the pattern dissolved completely and got a perfect pattern to the following metallization process.

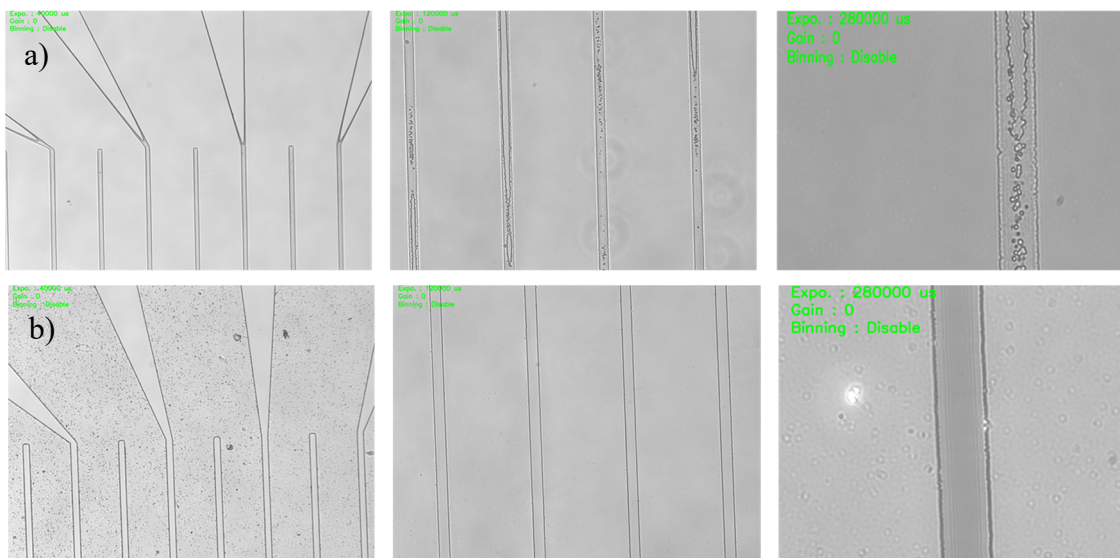


Figure A.4. The microscope picture of band UMEs array after different time development: a) 5s, b) 10s.

A.2.3. The metallization

There are three most common methods for vacuum depositing thin film: Thermal evaporation, electron beam evaporation, and sputtering. Among of them, sputter deposition used in this study, which the substrate that obtained in the step (6) and metal target (Ti and Au) that were deposited were putted in the vacuum chamber of K675X Turbo Large Chromium Coater 8 instrument (Figure A.5). Argon is the gas that forms the plasma due to it is inert, inactive, and will not cause unnecessary chemical reactions during our process. Which be ionized to form the plasma then it physically bombarde individual atoms of the target material with enough speed. These sputtered atoms then fly in all directions and condense on the substrate, including the substrate we want to coat. This process continues until the substrate is coated with the required thickness of material. The metallization steps are as follows (show in Figure A.2 (7) and (8)):

(7). A thin lay Ti (5 nm) was deposited on the patterned substrate that got from step (6), it can improve the adhesion of gold.

(8). Continue depositing gold layer (20nm) on the Ti thin lay, the thickness of the depositing metal is controlled by the design program.



Figure A.5. K675X Turbo Large Chromium Coater 8.

A.2.4. Lift-off process

Finally, the lift-off process was performed to remove the photoresist that on the glass substrate. Substrate was immersed in the acetone that can dissolve photoresist but remain inert to metal and glass, the Ti and Au layers on the photoresist were removed as the photoresist dissolved and the metal in other areas were left on the glass substrate surface to obtain the designed electrode pattern, the Figure A.6 is a photograph of a lithographic gold band UMEs array fabricate using the photolithography and lift-off procedures described above. The gold band UMEs array contains 10 bands which with a width of $25\ \mu\text{m}$, a length of 5 cm, and with a gap of $200\ \mu\text{m}$.



Figure A.6. Photograph of lithographed gold band UMEs array.

A.2.5. Fabrication of PolyDiMethylSiloxane wells (PDMS)

The microelectrode network is delimited by a block of PolyDiMethylSiloxane (PDMS) glued to the glass substrate and die-cut to the chosen dimension (5mm). PDMS block with 6 wells of 5 mm in diameter were selected, this model makes it possible to carry out 6 experiments on the same device (in 6 independent wells), realizing 10 measurements for each experiment.

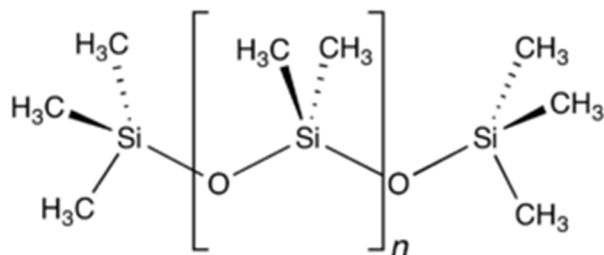


Figure A.7. The chemical structure of PDMS.

PolyDiMethylSiloxane (PDMS) are linear polymers, its chemical formula is $(C_2H_6OSi)_n$ and chemical structure fragmented formula is $CH_3[Si(CH_3)_2O]_n Si(CH_3)_3$, n is the number of monomers repetitions (Figure A.7).

The non-cross-linked PDMS are liquid (low n) or semi-solid in case of large chain length (high n). However, they can be cross-linked after mixing with a cross-linking agent and being heated to form a solid with elastomeric nature. It is widely used for microfluidic due to its excellent properties, for example, PDMS is easy to mold and inexpensive, it is transparent and easy to observe the contents in micro-channels. In addition, PDMS has good biocompatibility and it is almost inert that extremely resistant to oxidation, this makes it a hotspot in the application of biological analysis.

The PDMS used during this thesis is a kit Elecolit RTV615. First sufficiently mixed the supplied monomer and the cross-linking agent (the ratio of monomer and cross-linking agent is 9:1), then the mixture gel was poured into a Petri dish and pumped out all the bubbles. Next, putted it in an oven at 70 °C for about 60 minutes to cure it. The block PDMS obtained has a thickness of about 8 mm and can be cut to the size of a microscope slide (76 mm × 26 mm) to fit on the electrode arrays. Then 6 wells of 5 mm in diameter were cut on the PDMS by using a punch with 5 mm in diameter (Figure A.8). Then aligned the wells of the PDMS block with the band UMEs array and glued it by simple manual pressure.

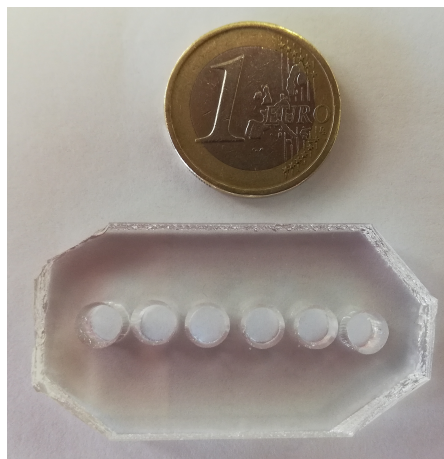


Figure A.8. Photo of the block PDMS with measurement wells.

A.3. The gold band UMEs array surface cleaning

A.3.1. Gold UME array electrochemical response in sulfuric acid

Gold, as one of the transition metals with unoccupied d-sublevels, possesses various oxidation states from +1 to +5, where compounds with the oxidation states +1 and +3 are most dominant in chemistry and the majority of biological research [8]. These studies prompted the investigation reported here into the oxidation of gold. Gold oxidation has been the subject of many studies over the years because noble metal oxidation provides a basis for the study of oxidation of industrially important non-noble metals and because of the importance of processes such as oxygen and chlorine evolution and of a renewed interest in the electrocatalytic properties of gold. The surface chemistry of gold has also seen a resurgence in interest through the discovery of the usefulness of gold nanoparticles in catalysis. Much work on anodic oxidation of gold in either acid or base has shown that the anodic oxidation falls into two stages with an initial and compact oxide (α oxide: AuO, Au(OH)₂, Au₂O₃) forming if the potential is cycled or held at moderate potentials and a second, hydrous or β oxide (Au₂O₃) developing when a more vigorous oxidation regime is applied, either through holding at high potentials (at which oxygen evolution also occurs) or by rapid potential cycling to similarly high potentials [9, 10].

Three-electrode setup was used to measure the CV behavior of gold in sulfuric acid, there are two gold wire (diameter 1mm, France), one worked as the working electrode, another one was counter electrode, and homemade AgCl-Ag wire (diameter 1mm, France) worked as reference electrode. Cyclic voltammetry carried out in 1M H₂SO₄ at the 50 mV/s scan rate with different scanning potential ranges, the initial potential is 0V and the end potential increased from 0.9V to 1.5V.

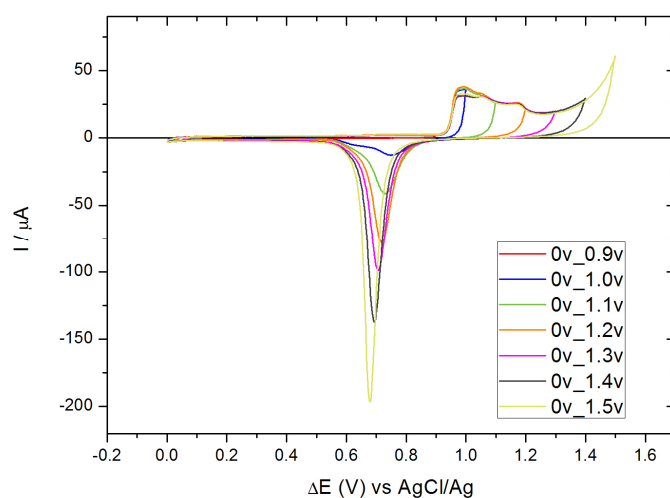


Figure A.9. A typical cyclic voltammogram in different scanning potential ranges for gold electrode (1 mm diameter gold wire) in 1M H₂SO₄ solution at 50 mV/s scan rate.

From the Figure A.9 there is no oxidation and reduction peak when the sweep is from 0 V to 0.9 V (red), until the potential range increased to 1.0 V or extended to 1.5, this indicates the monolayer oxide formation in acid extends from about 1.0 V to 1.5 V, meanwhile where there is also extensive oxygen evolution (oxygen evolution will take place at around 1.4 V). Then with further reverse negative scanning a reduction peak appeared and noticed its peak potential is around 0.7 V, where the oxides were reduced that oxides were formed in forward scan stage. And it has been noted that with the extension of forward scan rang, and the reduction peak of negative scan increased. It is due to that the time of oxide growth increases the amount of oxides of Au increased and the peak for oxide reduction grows and with a slight negative shift.

The electrochemical oxidation and reduction of gold in sulfuric acid

The gold electrochemical oxidation in sulfuric acid, the 1.7 V was selected as the oxidation potential of gold in 1M H₂SO₄ which during 30s by chronoamperometry. Then recorded the reduction current by the cyclic voltammetry from + 0.9 V to 0 V (*vs.* Ag/AgCl) at a rate of 50 mV/s in 1 M sulfuric acid, and the effect on the electrode was compared when the rinse step was present and absent and the corresponding cyclic voltammogram for oxide reduction is shown in Figure A.10a.

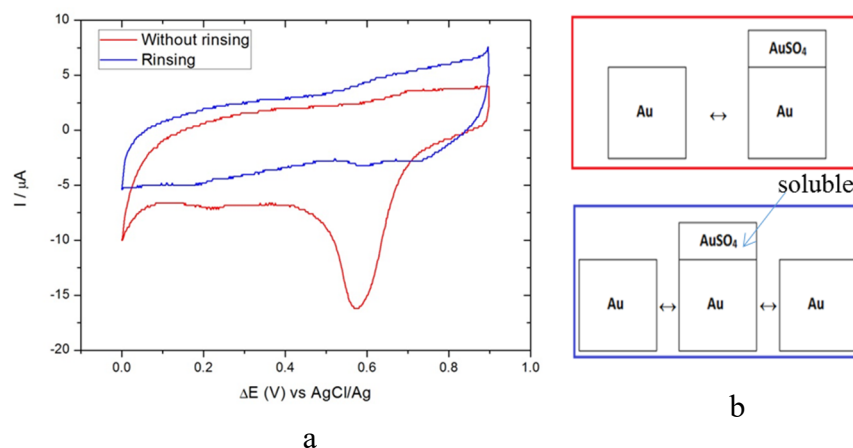


Figure A.10. Cyclic voltammetry, Electrochemical response of milli-electrode (1 mm diameter gold wire) in H₂SO₄ (1M) when present of rinsing (blue) and absent of rinsing (red) after 30s oxidation by chronoamperometry (oxidation potential is 1.7 V).

Gold can react with sulfuric acid under chemical or electrochemical conditions, after gold chemical or electrochemical reaction in sulfuric acid, it was oxidized and produced a thin layer of AuSO₄ (2). From the reduction current profile that was recorded after absent of rinsing and present of rinsing (Figure A.10), in the case where the electrode was without rinsing, a reduction reaction occurred on the surface of the electrode (Figure A.10a, red), and in the other case, the opposite was true (Figure A.10a, blue). This possible illustrates that the AuSO₄ monolayer which produced in anodic reaction is unstable (Figure A.10b), it is soluble in aqueous solution in rinsing step (3) [11].

Cathodic:



Anodic:



A.3.2. Gold band UMEs array cleaning methods for bioanalytical purposes

Gold is widely used in biological electrochemical application due to the excellent electrical conductivity and biological compatibility. As well, gold is the most noble of metal, but the gold microelectrode network is easy be contaminated during the lithography microfabrication procedure, the polluted surface can affect the interaction efficiency between gold surface and thiols and decrease the biological compatibility of gold [12], so in order to get the excellent modification efficiency the gold surface must be cleaned before it is modified by chemical or biological molecule.

Here described three methods procedures for cleaning gold electrode array surface for obtaining a reliably clean gold electrode surface, which are sulfuric acid chemical and electrochemical oxidation method [13-15] and argon plasma method [16, 17]. Then the peak-current of ferricyanide and ferrocyanide redox couple obtained from cyclical voltammetry and the steady-state current obtained from chronoamperometry after DNA probe immobilization were used to evaluate the efficiency of cleaning method.

A.3.2.1. Chemical and Electrochemical treatment method

Gold band UMEs array was cleaned by sulfuric acid chemical treatment method and sulfuric acid electrochemical oxidation method. For chemical treatment, sulfuric acid (1M) was kept stationary in the PDMS well for different time. For electrochemical oxidation method, chronoamperometry was used as oxidation method and performed at +1.2 V in sulfuric acid

(0.05M) during different time. Cyclic voltammetry was performed at before and after treatment step, then the peak current was chosen to evaluate the cleaning ability of them. Two-electrode setup was used to electrochemical treatment and cyclic voltammetry measurement.

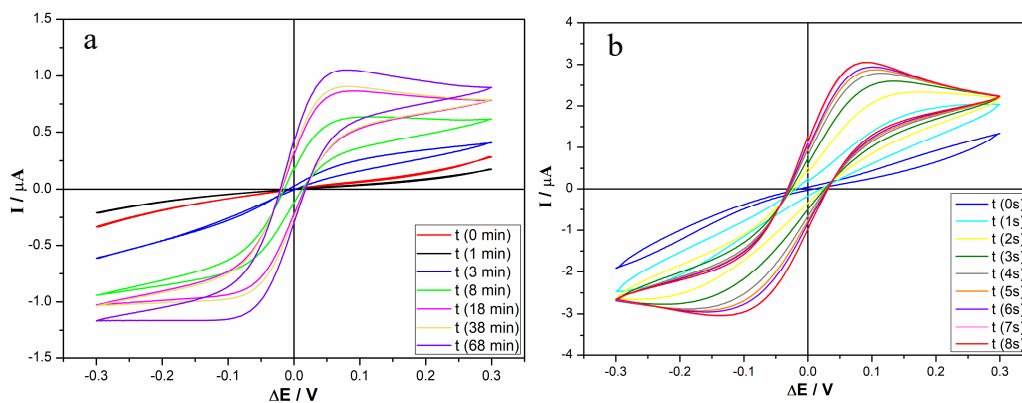


Figure A.11. Cyclic voltammogram of gold band UMEs array in 0.5M NaCl solution contains 5 mM $[\text{Fe}(\text{III})(\text{CN})_6]^{3-} / [\text{Fe}(\text{II})(\text{CN})_6]^{4-}$, which undergoes different time of H_2SO_4 . (1M) chemical treatment (a) and H_2SO_4 . (0.05 M) electrochemical treatment (b).

In this work the gold UME array was fabricated by the photolithography and lift-off procedures, during the microfabrication procedure, the gold band UMEs array was easy be contaminated by organic compounds and oxides, that deposited can have a significant impact in inhibit current of micron-sized electrode. See the Figure A.11, before chemical and electrochemical treatment the current of gold band UMEs array was low and it did not get a typical cyclic voltammogram of $\text{Fe}^{3+}/\text{Fe}^{2+}$ redox couple. It is due to the transfer of electrons of $\text{Fe}^{3+}/\text{Fe}^{2+}$ redox couple was blocked by the contamination of gold electrode surface. With the increased of treatment time, the current increased, and the cyclic voltammograms of $\text{Fe}^{3+}/\text{Fe}^{2+}$ redox couple was closer to the typical cyclic voltammograms. It illustrated that the sulfuric acid chemical and electrochemical treatment methods successfully cleaned the gold band UMEs array surface. From the Figure A.11a, it took about 68 minutes for chemical treatment method to reach the maximum current on the electrode surface, but for the electrochemical treatment method, which only required 8s to reach a maximum current of the gold band UME (Figure A.11b).

A.3.2.2. Plasma treatment method

Argon plasma treatment on the gold film electrode surface

Since gold oxides will be formed on the surface of gold cleaned by oxygen plasma, argon plasma was selected for gold treatment method, argon is a kind of inert gas that doesn't oxidize with gold even if under the state of plasma, so after argon plasma treatment, the gold film surface dose not form the new thin layer of gold compounds. The gold film that with the same properties (*thickness, metal and fabrication ways*) as the gold UME array was used as the sample to evaluate the plasma treatment method. Three electrodes setup which the gold film as working electrode, gold wire (1mm in diameter) and Ag/AgCl were control electrode and reference electrode respectively. Cyclic voltammetry was used to evaluate the effect of different power of argon plasma, before and after treatment, which measured in 0.5 M NaCl solution which contain 5 mM $[\text{Fe (III)(CN)}_6]^{3-}$ and $[\text{Fe (II)(CN)}_6]^{4-}$ redox couple, which the increased peak current value was used to evaluate the ability of treatment (Figure A.12 red column). In addition, chronoamperometry measured the electrochemical properties of gold film after 1W Ar plasma (gas flow is 50sccm) treatment under different time and then after DNA probe immobilized, which measured in the 0.5 M NaCl solution contains 5 mM $[\text{Fe (III)(CN)}_6]^{3-}$ and $[\text{Fe (II)(CN)}_6]^{4-}$ redox couple and 5 μ M MB, then calculated the DNA probe immobilization efficiency:

$$1 - \frac{I_{\text{ss}}}{I_{\text{Au}}}$$

to select the best treatment time (Figure A.12 black column).

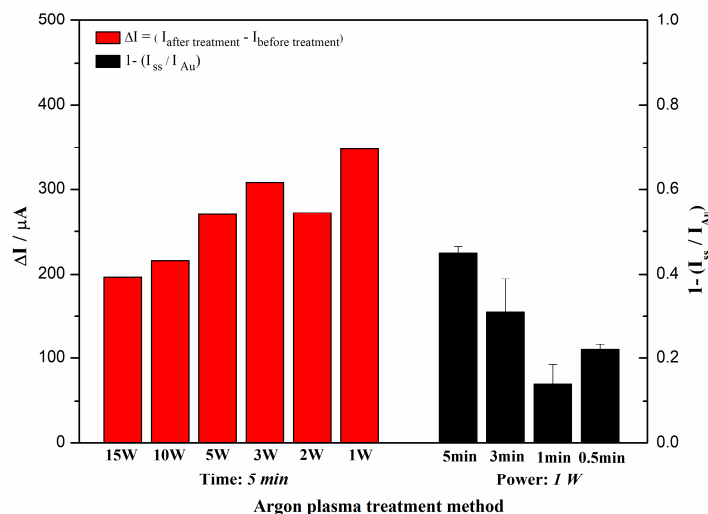


Figure A.12. The increased value of cyclic voltammetry on the electrode surface after treatment under different power of Ar plasma treatments (red). The DNA probe immobilization efficiency under the 1 W Ar plasma treatment during different time (black).

The red column in the Figure A.12 shows the increased CV peak current after treatment was compared with that before treatment by different Ar power. Since the increased value is the positive, this illustrates argon plasma treatment can effectively clean the gold film surface due to remove organic and oxide contaminants lead to expose gold atom and increase the conductivity of gold film [18]. Meanwhile, it can be seen that when the power is 1W, the current value increases the most, which is also because the high-power Ar plasma treatment is relatively easy to damage the gold film surface. Subsequently, selected the 1W Ar plasma then compared the effects of different treatment time (Figure A.12 black column), when the treatment time is 5 minutes, the DNA probe immobilization efficiency is the highest. Besides, there is a phenomenon that the current of some gold surfaces after Ar plasma treatment is higher than the theoretical current, it is maybe due to aggressive argon plasma potentially roughens the gold film surfaces through a mechanical treatment, it increase the surface area of gold film [17-19], same time which easy to lead to gold film surface erosion.

A.4. Gold electrode response in chloride solution

Chloride-induced gold dissolution has been well known in electrochemistry, therefore, in order to observe whether the chloride ion in the electrolyte affects the gold electrode surface during the electrochemical process when using the electrolyte (5mM [Fe(III)(CN)₆]³⁻ / [Fe(II)(CN)₆]⁴⁻, 0.5M NaCl) in this article, the self-assembled single stranded DNA immobilization efficiency was evaluated. The effect of chloride ion on the gold UME array surface was observed by the presence or absence of CV measurement reaction prior to DNA immobilization, which the gold film was chosen to as working electrode and were treated by 1W Ar plasma for 5 minutes before DNA probe immobilization.

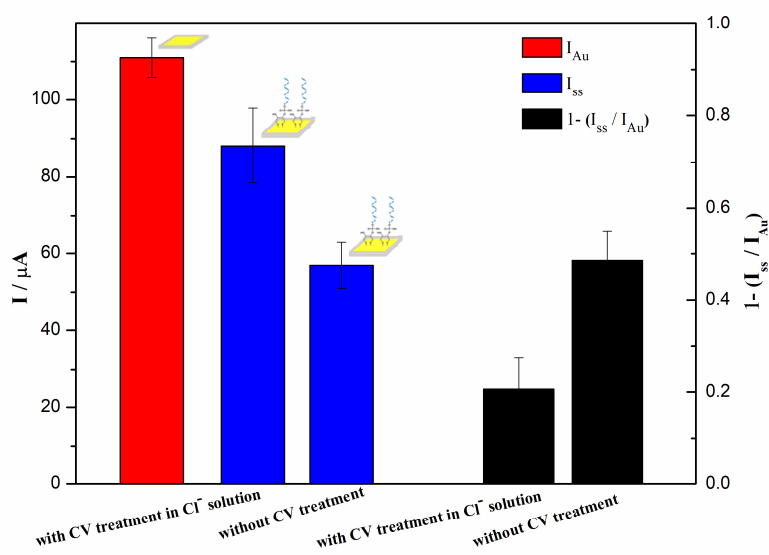


Figure A.13. Chronoamperometry response of bare gold film (red), after self-assembly of DNA probe (blue), which was measured with a voltage of 0.05 V in 0.5M NaCl solution containing 5mM [Fe(III)(CN)₆]³⁻ and 5mM [Fe(II)(CN)₆]⁴⁻, and the DNA immobilization efficiency after with or without the CV treatment in the chloride ion solution (black).

Figure A.13 shows the steady-state current of bare gold film electrode (I_{Au} , Figure A.13, red column) and after self-assembly of DNA probe (I_{ss} , Figure A.13, blue column) which includes

the situation that with and without cyclic voltammetry before DNA probe immobilization step. The current decreased after self-assembly of DNA probe on the gold film surface, it attributed to the DNA probe successfully immobilized on the surface of the gold film then cause the limited diffusion of the redox probe to electrode surface which by the negative the electrostatic repulsion and steric hindrance of negative charged phosphate backbone of probe DNA and negative redox probe. In addition, the DNA probe immobilization efficiency that was measured when absence of CV treatment in chloride ion electrolyte was higher than when presence of CV treatment (Figure A.13 black column), this result possible due to chloride ions corroded the gold surface the presence of chloride in the electrolyte can induced surface gold atom dissolution and redeposition results in corrosion of the electrode and the changes of gold surface characteristics (4), and this process was accelerated under electrochemical conditions. Asta Makaraviciute work has shown that the chlorine can also cause the desorption of the thiol-labeled probes [15].



Conclusions

In this work reported a various of cleaning methods for Au microelectrode and to find the right protocol for high efficiency cleaning of Au microelectrodes and keep the geometric structure of gold surface for sensing applications. Plasma treatment can effectively clean the gold microelectrode surface, however aggressive argon plasma potentially damaged the gold film surfaces through a mechanical cleaning and make the gold layer fall off. For the two sulfuric acid chemical and electrochemical cleaning protocols were effective in cleaning the surface and not easy to cause surface damages. Sulfuric acid treatment cleaning method trough oxidizing gold to produce AuSO_4 , which is unstable, it is soluble and easily dissolved in aqueous solution, then the gold atoms of gold electrode surface were exposed. The chemical treatment spent long time to get the optimized gold surface compare with the electrochemical oxidation treatment method.

A.5. Electrochemical measurement methods

Electrochemical biosensor possible to convert the biological event that occur on the surface of electrode directly into an electrical signal (e.g., current, potential, conductance, impedance and capacitance) without intermediate conversion. Which rely on the fact that during a biological interaction process, electrochemical species such as electrons are consumed or generated, thereby producing an electrochemical signal, which can be measured by an electrochemical detector and then the target is analyzed. Thus, electrochemical biosensors offer a faster, cheaper, and simpler detection protocols for nucleic acid analysis and able to provide a quantitative or semiquantitative analytical information [20].

There are many electrochemical measurement methods, and different detection methods can be selected for analysis according to the characteristics of biological events and the structure of sensors. The more commonly electrochemical measurements are voltammetry, amperometry and impedance[21, 22].

Electrochemistry is the study of the relationship between chemical material changes and charge transfer. Which the material changes include changes in substance concentration, valence state, type, and location. The charge transfer can be expressed as capacity, current, potential, impedance, etc. A typical electrode reaction involves the transfer of charge between an electrode and a species in solution, which the most common situation in electrochemistry is to study the chemical and electrical processes of the electron transfer at the electrode/solution interface when the chemical substance in the electrolyte undergoes a redox reaction. The simplest example is electron transfer between the oxidized species, O and the reduced species, R, which the general electrode reaction (Nernstian redox reaction): (5)



The electrode reaction usually referred to as electrolysis, the reduction process takes place at the cathode while oxidations take place at the anode, typically involves a series of steps (Figure A.14):

- (1). Oxidise species (O_{bulk}) in the bulk solution moves to the electrode/solution interface where the reaction occurs, which is termed mass transport.
- (2). Oxidise species (O_{bulk}) undergoes reduction to form the reduced form R and electron transfer to the electrode can then occur via quantum mechanical tunnelling.
- (3). The product (R) moves away from the electrode to allow fresh reactant (O_{bulk}) to the surface.

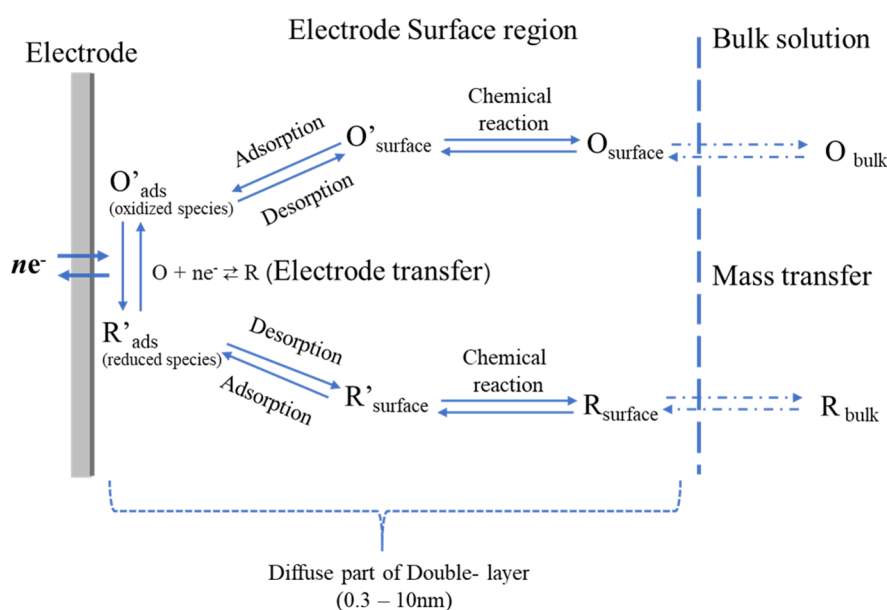


Figure A.14. Pathway of a general electrode reaction [23].

A.5.1. Mass Transport

In order to react electroactive species at an electrode it needs to be transported from bulk to electrode surface, which is termed mass transport. There are three forms of mass transport: diffusion, convection or migration

Diffusion: Movement of a species under the influence of a gradient of chemical potential (practically, a concentration gradient). from an area of high concentration to an area of low concentration.

Convection: material is moved by hydrodynamic transport that from external force such as natural thermal motion and/or stirring, or stirring.

Migration: The transport of a charged species under the influence of an electric field. charged particles move to equalize potential gradients in the electrolyte.

The mass transfer to an electrode is governed by the Nernst-Planck equation, which is written for one-dimensional mass transfer along the x-axis as:

$$J_i(x) = -D_i \frac{\partial C_i(x)}{\partial x} - \frac{z_i F}{RT} D_i C_i \frac{\partial \phi(x)}{\partial x} + C_i v(x) \quad [1]$$

The J_O ($\text{mol s}^{-1} \text{cm}^{-2}$) is the flux of species O at distance x from the surface, D_O is the diffusion coefficient (cm^2s^{-1}), The three terms on the right side represent the contributions of diffusion, migration and convection, respectively, to the flux. To simplify the mathematical models of the current flux in electrochemical measurements, one or two of the contributions are usually made negligible by controlling the experiment ways. Such the contribution of convection can be suppressed by preventing stirring the solution to kept still, and the effect of migration can be negligible by adding an inert supporting electrolyte (KCl, NaCl or KNO_3) to the solution at a concentration 10–100-fold excess with respect to the redox couple. By eliminating both migration and convection contributions, getting an expression that transport only by diffusion.

A.5.1.1 Diffusion equations and current responses

In generally electrochemical measurement, mass transfer is mainly by diffusion transfer, which can be described by Fick's first law and Fick's second law. Fick's law describes the flux of species and its concentration as functions of time and position. Fick's first law states that the flux is proportional to the concentration gradient (Eqs. 2) and the concentration gradient of species O at the electrode surface with time is described by Fick's second law (Eqs. 3).

$$J_o = -D_o \nabla C_o \quad [2]$$

$$\frac{\partial C_o}{\partial t} = D_o \nabla^2 C_o \quad [3]$$

The formula in equation 3 applies to all geometric shapes of the electrode, the ∇^2 is the

Laplacian operator, the different geometries has different boundary conditions that will give different forms of the operator and different equations. The concentration gradient at the electrode surface is obtained by solving Fick's second law, and Figure A.15 shows the diffusion mass transport for planar electrode. For planar electrode the diffusion equation expressed as:

$$\frac{\partial c}{\partial t} = D \left(\frac{\partial^2 c}{\partial x^2} \right) \quad [4]$$

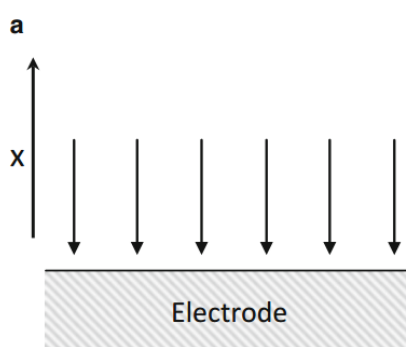


Figure A.15. Diffusion mass transport of planar electrode [24].

A.5.2. The electrochemical measurement of planar electrode

A.5.2.1. Potential step methods (Amperometry)

The measurement of the current after a step in the potential is applied is called chronoamperometry. The step is from a potential with an initial value where no electrode reaction occurs, to one where all the species that reach the electrode react, and which electrolysis proceeds at diffusion control rate.

For a planar electrode (with Fick's second law for this geometry):

$$\frac{\partial C_o(x,t)}{\partial t} = D_o \left(\frac{\partial^2 C_o(x,t)}{\partial x^2} \right) \quad [5]$$

Initial/boundary conditions:

$$C_o(x, 0) = C_o^* \quad [6]$$

$$\lim_{x \rightarrow \infty} C_o(x, t) = C_o^* \quad [7]$$

$$C_o(0, t) = 0 \text{ (for } t > 0) \quad [8]$$

Then based on the Fick's first law

$$-J_o(0, t) = \frac{i(t)}{nFA} = D_o \left[\frac{\partial C_o(x, t)}{\partial x} \right]_{x=0} \quad [9]$$

The current-time response is described by the *Cottrell equation* (Eqs. 10), that the current is inversely proportional to $t^{1/2}$.

$$i(t) = \frac{nFAD_o^{1/2}C_o^*}{\pi^{1/2}t^{1/2}} \quad [10]$$

The current i is measured as a function of the electrode area A , bulk concentration C_o^* of the species and the diffusion constant D_o . Its validity was verified in detail by the classic experiments of Kolthoff and Laitinen, who measured or controlled all parameters.

A.5.2.2. Cyclic Voltammetry (CV)

In cyclic voltammetry the current is measured constantly during the cycling of voltage, with the potential changes linearly with time, starting from an initial potential E_i (usually, where no electrode reaction occurs). Eventually, after reaching a potential E_λ , the sweep is reversed and the potential returns linearly to its initial value. The potential is swept linearly at ν , so that the potential at any time is given by $E(t) = E_i \pm \nu t$ where ν is the scan rate (or sweep rate, V/s). In case of the planar electrode, for the reversible reaction system which is assumed to be Nernstian in character. When combined with the solution of the diffusion equations of planar electrodes and the appropriate boundary conditions and the applications of numerical methods, provides the Eqs. 11.

$$i = nFAC_o^* (\pi D_o \sigma)^{1/2} \chi(\sigma t) \quad [11]$$

Which $\sigma = \left(\frac{nF}{RT}\right) v$; $\chi(\sigma t)$ are tabulated values.

This relation is the general response function for a step experiment in a reversible system, $\chi(\sigma t)$ is a pure number, i is proportional to C_o and $v^{1/2}$.

The maximum value of function $\pi^{1/2} \chi(\sigma t)$ is 0.4463 by calculating, so that, the peak current of CV in the forward scan, i_p , is

$$i_p = 0.4463 \left(\frac{F^3}{RT}\right)^{1/2} n^{3/2} A D_o^{1/2} C_o^* v^{1/2} \quad [12]$$

The backward (i_{pc}) to forward (i_{pa}) peak current ratio, i_{pc}/i_{pa} , is equal to 1 for a Nernstian wave with a stable product.

At 25 °C, with A in cm^2 , D_o is $\text{cm}^2 \text{s}^{-1}$, C_o^* in mol cm^{-3} and $v^{1/2}$ in V/s , i_p is

$$i_p = (2.69 \times 10^5) n^{3/2} A D_o^{1/2} C_o^* v^{1/2} \quad [13]$$

Theoretically, for planar diffusion, the diffusion conditions are only satisfied when the electrode surface is large. If it is a limited disk electrode, there will be an edge effect, and the diffusion of the overall electrode surface is not only linear diffusion but also radial diffusion that parallel to the electrode surface. However, if the radius of the disk electrode is sufficiently large relative to the thickness of the diffusion layer (like the commonly used millimeter-sized disk electrode), the edge effect can be ignored, and the *Cottrell equation* can accurately describe the current distribution on the electrode surface.

A.5.2.3. Electrochemical Impedance Spectroscopy (EIS)

Impedance technology is an effective tool for studying electrode processes. It is widely used in the field of electrochemical research. It can obtain more kinetic information and electrode interface structure information than other electrochemical methods, such as electron transfer resistance, double electric layer capacitance, etc. That data from impedance experiments contain more information than the data from voltammetric experiments. This means that it is a more sensitive technique for detecting changes in the electrode surface, but it also makes interpretation more difficult. Moreover, EIS has been widely used in numerous studies, such as immunosensing and genosensing, because of its high sensitivity, simplicity use, capacity for label-free detection and cost-efficient technique. The impedance can be simplified in some cases to a resistance (conductance) or capacitance.

Basically, EIS is based on applying a small sinusoidal potential perturbation with different frequencies to the electrochemical cell, and measure the ratio of the AC potential to the current signal (impedance, Z) as the sine wave frequency ω changes, or the phase angle φ of the impedance varies with ω the change

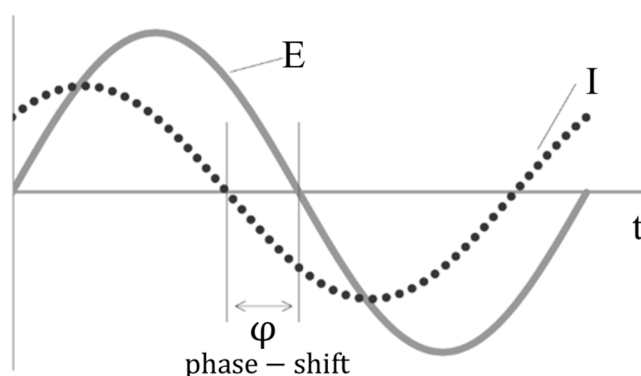


Figure A.16. AC excitation signal and sinusoidal current response in a Linear System.

In a linear (or pseudo-linear) system, the current response to a sinusoidal potential will be a sinusoid at the same frequency but shifted in phase (see Figure A.16).

The excitation signal as a function of time E_t ,

$$E_t = E_0 \cdot \sin(\omega t) \quad [14]$$

where E_t is the potential at time t , E_0 is the amplitude of the signal and ω is the radial frequency and f is the frequency expressed in Hertz (Hz).

$$\omega = 2\pi f \quad [15]$$

In a linear system, the response signal, I_t , is shifted in phase (φ):

$$I_t = I_0 \cdot \sin(\omega t + \varphi) \quad [16]$$

Thus, the impedance used ohm's law is:

$$Z_t = \frac{E_t}{I_t} = \frac{E_0 \cdot \sin(\omega t)}{I_0 \cdot \sin(\omega t + \varphi)} = Z_o \cdot \frac{\sin(\omega t)}{\sin(\omega t + \varphi)} \quad [17]$$

Furthermore, considering Euler's equation:

$$\exp(j\varphi) = \cos \varphi + j \sin \varphi \quad [18]$$

The impedance can be expressed as a complex number:

$$Z_\omega = Z_o \exp(j\varphi) = Z_o(\cos \varphi + j \sin \varphi) \quad [19]$$

The expression for Z_ω is composed of a real (Z') and an imaginary part (Z''),

$$Z_\omega = Z' - jZ'' \quad [20]$$

Therefore, the obtained EIS spectrum also takes these two parts as the x-axis and y-axis, which is also referred to as a “Nyquist plot”. In this plot, each point corresponds to a different frequency. An alternative representation is bode diagram that the impedance magnitude and phase angle as a function of the logarithm of frequency.

The analysis of AC impedance spectroscopy is generally carried out through an equivalent circuit. The basic components include: cell resistance R_{Ω} , electron-transfer resistance R_{ct} , double-layer capacitance C_{dl} , Warburg impedance Z_w .

1). When no electrode process occurs, the equivalent circuit is the cell resistance R_{Ω} in series with the double-layer capacitance C_{dl} . The impedance plot is a vertical straight line, as shown in Figure A.17a.

$$Z' = R_{\Omega} \quad Z'' = -1/(\omega C_{dl}) \quad [21]$$

2). The other case, at a different applied potential, an electrode process occurs, that is, charge transfer controlled over the whole frequency range, then this charge transfer can be represented by a charge-transfer resistance, R_{ct} . When without diffusive impedance, the equivalent circuit is the resistance R_{ct} is placed in parallel with the double-layer capacity, C_{dl} .

Analysis of the spectrum gives a semicircle of diameter R_{ct} , as shown in Figure A.17b.

$$Z' = R_{\Omega} + \frac{R_{ct}}{1+(\omega R_{ct}C_{dl})^2} \quad Z'' = -\frac{R_{ct}^2 C_{dl}}{1+(\omega R_{ct}C_{dl})^2} \quad [22]$$

The maximum of the semicircle corresponds to $\omega R_{ct}C_{dl} = 1$.

3). Faraday process can be further divided into two processes: charge transfer and mass transfer. The high-frequency region was dominated by charge-transfer, while the low-frequency region was controlled by mass-transfer (represented by a Warburg impedance, Z_w). The Warburg impedance appears on a Nyquist diagram as a diagonal line with a slope of 45°. The Nyquist

plot and equivalent circuit (Randles equivalent circuit) are shown in Figure A.17c.

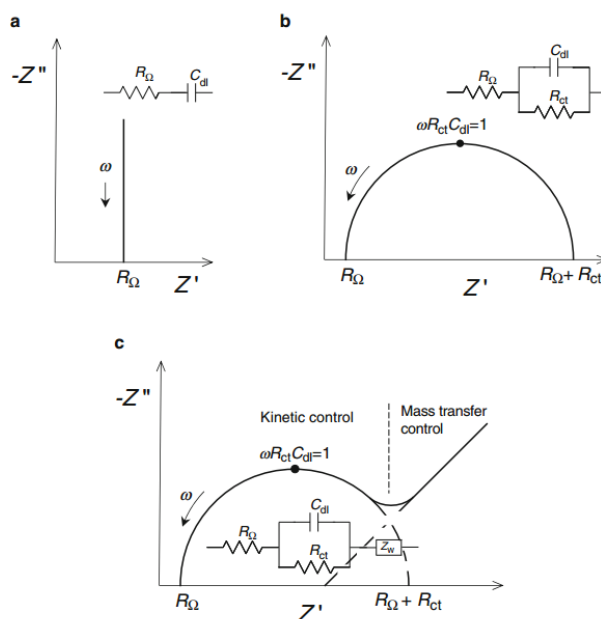


Figure A.17. Complex plane impedance plots at electrodes for the shown selected electrical equivalent circuits: (a) purely capacitive interfacial response, (b) faradaic electron-transfer reaction controlled by kinetics, (c) electron-transfer reaction with mass transfer control at low frequencies. R_{Ω} cell resistance, R_{ct} electron-transfer resistance, C_{dl} double-layer capacitance, Z_w Warburg impedance [24].

A.5.3. Ultramicroelectrodes (UME)

An ultramicroelectrode (UME) refers to only one dimension (such as the radius of a disk or the width of a band) of an electrode reaching a micron-nanoscale in a certain dimension, thus there are different shapes of UME (Figure A.18). The electrochemical signals obtained on the UME are different from conventional electrodes, for the UME, although which has a small area and a small polarization current, the current density on the electrode surface is very large, so the ohmic drop is very low. In this part the performance of band UME will be described. The band UME is quite different from other types UME, which the width (w) in the micron-nanoscale range. Nevertheless, the length (l) can be much larger and can be in the centimeter range. Thus, compared with the disk UME, the UME band can possess appreciable geometric area and can generate considerable current.

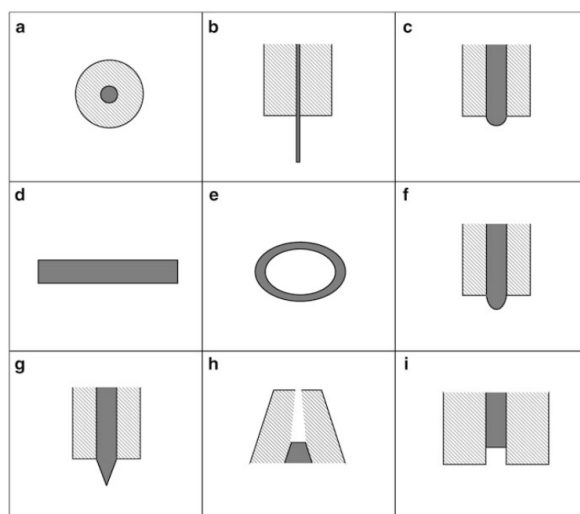


Figure A.18. Microelectrode configurations: (a) disk, (b) cylinder, (c) hemisphere, (d) band, (e) ring, (f) sphere cap, (g) cone, (h) nanopore, and (i) recessed microelectrode.

A.5.3.1. Potential step methods (Amperometry)

A band UME is a two-dimensional diffusion system in which the length of the electrode is very much larger than the width, which is much like the simpler hemicylindrical system. The coordinate system used to treat the diffusion problem at a band is shown in Figure A.19. Because of the $l \gg w$, the edge effects can be neglected, the diffusion essentially occurs only along the x - and z -axes, thus, the diffusion is considered as planar (the diffusion along the direction of L is neglected).

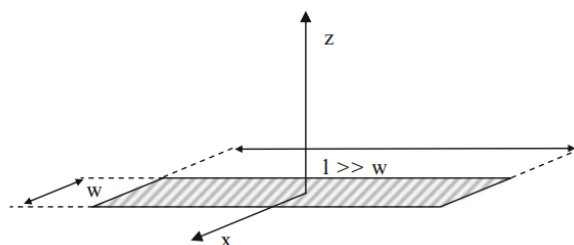


Figure A.19. Diffusional geometry at a band electrode. Normally the length of the electrode is very much larger than the width, and the three-dimensional diffusion at the ends does not appreciably violate the assumption that diffusion occurs only along the x and z axes.

At short times, the current converges to the Cottrell equation; at long times the current approaches a limiting form, The Cottrell equation describes the current at planar macroelectrodes (dimensions on the order of a mm) adequately for times as long as a few seconds. However, the diffusion current at a microelectrode will deviate significantly from Cottrell behavior even at very short times (ms or even μ s).

$$i = nFD_oC_o^*l \left\{ (\pi\theta)^{-1/2} + 0.97 - 1.10 \exp \left[\frac{-9.90}{|\ln(12.37\theta)|} \right] \right\} \quad [23]$$

$$\theta = D_o t / w^2$$

$$i = \frac{2\pi nFAD_oC_o^*}{w \ln(64D_o t / w^2)} \quad [24]$$

where n is the number of electrons transferred at the electrode, F is the Faraday constant. D_o ($\text{cm}^2 \text{ s}^{-1}$) is the diffusion coefficient of the electroactive species, C_o^* (mol cm^{-3}) its bulk concentration, l (cm) is the electrode length, w (cm) is its width, A in cm^2 and t (s) is time.

The current of band UME is related to the t , thus it does not provide a true steady-state current at long time, however, when the time t is long, the current attenuation can be slow, so called quasi-steady state.

A.5.3.2. Cyclic voltammetry

For microband geometries electrode, the theoretical expressions of voltammograms is derived contain the characteristic dimension parameters of the UME. Since the peak or maximum current characterizes quantitatively the voltammograms, relevant expressions are given in the equations 25 [24].

$$i_p = nFC_o^*D_o \left[0.439p + 0.713Pp^{0.108} + \frac{0.614p}{1+10.9p^2} \right] \quad [25]$$

$$p = (nFw^2v / RTD_o)^{1/2}$$

A.5.4. Experiment set-up system

A.5.4.1. Three-electrode set-up

The three-electrode system is designed to eliminate the large error of electrode potential due to polarization current. Figure A.20 shows a typical three-electrode set-up, which contains three electrodes: working electrode, counter electrode and reference electrode. Working electrode (WE) is also called or indicator electrode, that is where the electrode reaction occurs, in general, the material of the working electrode can be either solid or liquid, which cannot react with the components in the solvent or electrolyte. Counter electrode (CE) is also called auxiliary electrode, the auxiliary electrode and the working electrode form a circuit to make the current on the working electrode unblocked so as to ensure that the studied reaction occurs on the working electrode. Reference electrode (RE) has a known potential that approaches ideal non-polarizability and the potential is not affected by changes in the electrolyte composition. RE is used to provide precise control of potential at the WE, the potential is measured between the RE and the WE, and the current is transported between the WE and the CE by ionic transport.

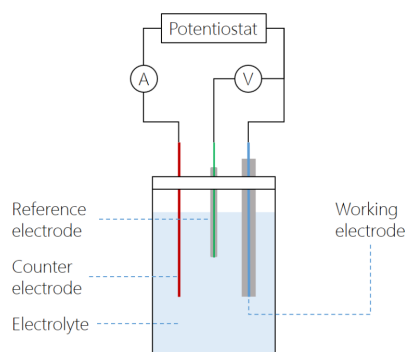


Figure A.20. A three-electrode-setup connected to a potentiostat with the electrodes in a cell.

A.5.4.2. Two-electrode set-up

Two electrode set-up system is the simplest electrode setup, which contains two electrodes working electrode (WE) and reference electrode (RE). The disadvantage is that RE carries current in this system and in order to prevent RE from polarizing, its size needs to be 100 times

that of WE, which is very difficult for large electrode systems, so CW was introduced to construct a three-electrode system. In addition, due to the size of UME, it is possible to construct a two-electrode system, and it can be miniaturized to adapted to the microliter samples and miniaturized high-density screening platform, such as biomolecule detection platform (eg. DNA).

In our microRNA electrochemical biosensor, the two-electrode set-up was chosen (Figure A.21). The laboratory has been developing this two-electrode circuit for biosensors for several years [25] and has successfully applied to microRNA biosensors, which consist of two electrodes of the same metal (Au), the working electrode is the gold UME (25 μ m) and the counter electrode is the gold millimeter electrode (2mm in diameter) which has very high area and the size is near 80-fold compare with UME, moreover, the surface area of working UME is small, the current will be small, so the iR drop is small and the polarization caused by the current is very small. Therefore, it can be considered as a pseudo-reference electrode allowing a feeble potential drift during measurements, which simplifies the experimental device. Both the two electrodes are made from same metal and are immersed in the same electrolyte containing the redox couple which thus makes it possible to eliminate any potential difference due to the materials of the electrodes and to obtain a signal centered on 0 V. As expected, a sigmoid shape voltammogram for a laminar flow was obtained and centered at zero potential (Figure A.22a).

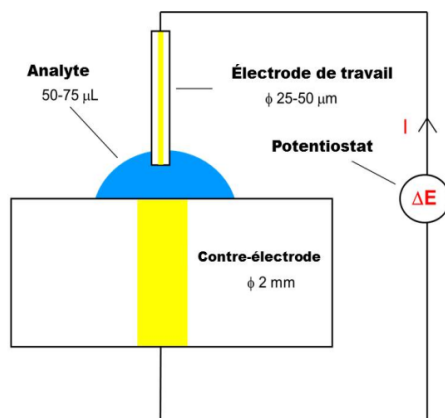


Figure A.21. Two-electrode electrochemical setup configuration. gold disc UME ranging from 25 μ m-50 μ m diameter (working electrode); gold disc in 2 mm diameter (counter electrode).

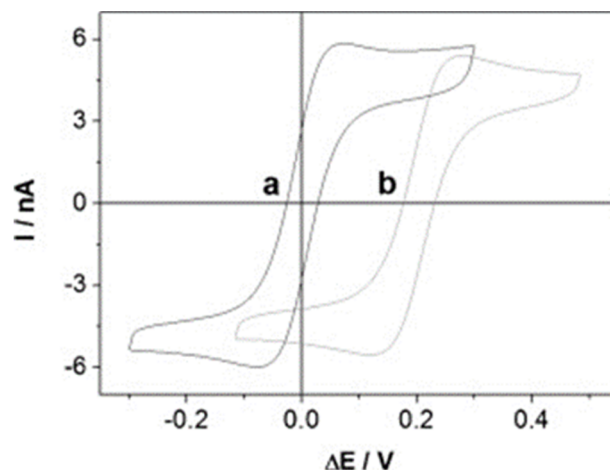


Figure A.22. Cyclic voltammograms of two-electrode set-up and three-electrode set-up in a 5×10^{-3} M $K_3[Fe(III)(CN)_6]$, 5×10^{-3} M $K_4[Fe(II)(CN)_6]$, 0.5 M NaCl solution. (working electrode: gold disc UME in 50 μ m diameter)

A.6. The concentration of nucleotides calculation

According to the Beer–Lambert law, the molar extinction coefficient (ϵ) of nucleotides is an important element in the calculation of nucleotide concentration. Currently there are a variety of molar extinction coefficient calculation methods based on the bibliography, however, the ϵ of DNA can also be obtained by ultraviolet absorption experiment. Here, we measured the ϵ experimental value of DNA target (T) then to compare the value obtained by different molar extinction coefficient calculation methods to evaluate the accuracy of the calculation method.

In the molar extinction coefficient (ϵ) experiment, 1cm long quartz cuvette and 0.5M NaCl were used as buffer solution to dilute a series of DNA targets for UV detection. 600 μ L of 0.5M NaCl solution is transferred into quartz cuvette then recorded the baseline UV absorbance from 225nm to 400nm as blank which operated by a UV-Vis Spectrophotometer. Following, the DNA was diluted by 2-fold gradient to 5 concentrations for UV measurement.

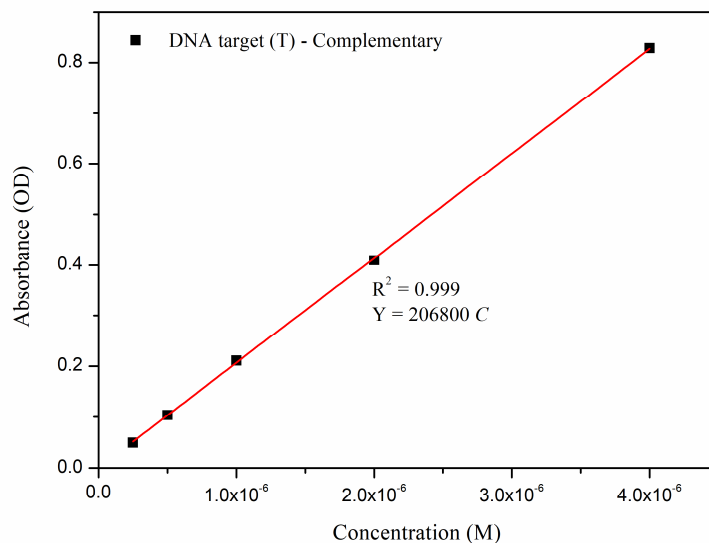


Figure A. 23. Ultraviolet absorption spectrogram of different concentration complementary DNA target.

After UV measurement of a series of DNA target concentrations, then the average value of the blank measurement was subtracted from the measurements made at each concentration and the results plotted which the concentration as the X-axis, and the UV absorption value at 260nm is the Y-axis. A linear regression fit was performed on the standard values (Figure A. 23). From the Figure A. 23, based on the Beer-Lambert law and the quartz cuvette length is 1cm, thus the slope of the curve indicated the extinction coefficient (ϵ) and it equal to $206800 \pm 1139.02 \text{ M}^{-1} \text{ cm}^{-1}$, and it approximates the values of the two most commonly used calculation methods, which one is based on the nearest-neighbors model ($217600 \text{ M}^{-1} \text{ cm}^{-1}$) and the other one is based on the base composition method ($217530 \text{ M}^{-1} \text{ cm}^{-1}$).

The base composition method is through to simply sums all the isolated nucleosides extinction coefficients and multiplies by a factor of 0.9 to account for base stacking [26-29]. And the nearest-neighbor model method takes into account interactions between adjacent bases. These nearest-neighbour parameters are measured empirically, and can give very accurate values for extinction coefficients of DNA [28, 30-32].

References

1. Huang XJ, O'Mahony AM, Compton RG. Microelectrode arrays for electrochemistry: approaches to fabrication. *Small* 2009,**5**:776-788.
2. Fredericks EC, Kotecha HN. Photoresist lift-off process for fabricating semiconductor devices. In: Google Patents; 1986.
3. Lee HS, Yoon J-B. A simple and effective lift-off with positive photoresist. *Journal of Micromechanics and Microengineering* 2005,**15**:2136.
4. Eliáš P, Gregušová D, Martaus J, Kostič I. Conformal AZ5214-E resist deposition on patterned (1 0 0) InP substrates. *Journal of Micromechanics and Microengineering* 2005,**16**:191.
5. Sheet PD. Az 5214 e image reversal photoresist. *AZ Electronic Materials*,**70**.
6. Galeano JA, Sandoz P, Zarzycki A, Robert L, Jaramillo JM. Microfabrication of position reference patterns onto glass microscope slides for high-accurate analysis of dynamic cellular events. *TecnoLógicas* 2017,**20**:117-128.
7. Jung J, Nakajima M, Kojima M, Fukuda T. Measurement of body volume of live *C. elegans* by microchip. In: *2011 International Symposium on Micro-NanoMechatronics and Human Science*: IEEE; 2011. pp. 204-209.
8. Đurović MD, Bugarčić ŽD, van Eldik R. Stability and reactivity of gold compounds—From fundamental aspects to applications. *Coordination Chemistry Reviews* 2017,**338**:186-206.
9. Burke L, Buckley D, Morrissey J. Novel view of the electrochemistry of gold. *Analyst* 1994,**119**:841-845.
10. Zhang W, Bas AD, Ghali E, Choi Y. Passive behavior of gold in sulfuric acid medium. *Trans. Nonferrous Met. Soc. China* 2015,**25**:2046.
11. Wickleder MS. AuSO₄: A True Gold (II) Sulfate with an Au²⁴⁺ Ion. *Zeitschrift für anorganische und allgemeine Chemie* 2001,**627**:2112-2114.
12. Sukeri A, Saravia LPH, Bertotti M. A facile electrochemical approach to fabricate a nanoporous gold film electrode and its electrocatalytic activity towards dissolved oxygen reduction. *Physical Chemistry Chemical Physics* 2015,**17**:28510-28514.
13. Bhalla V, Carrara S, Stagni C, Samori B. Chip cleaning and regeneration for electrochemical sensor arrays. *Thin Solid Films* 2010,**518**:3360-3366.
14. Carvalhal RF, Sanches Freire R, Kubota LT. Polycrystalline Gold Electrodes: A Comparative Study of Pretreatment Procedures Used for Cleaning and Thiol Self - Assembly Monolayer Formation. *Electroanalysis: An International Journal Devoted to Fundamental and Practical Aspects of Electroanalysis* 2005,**17**:1251-1259.
15. Makaraviciute A, Xu X, Nyholm L, Zhang Z. Systematic approach to the development of microfabricated biosensors: Relationship between gold surface pretreatment and thiolated molecule binding. *ACS Applied Materials & Interfaces* 2017,**9**:26610-26621.
16. Berman DS, Godazgar H, Godazgar M, Perry MJ. The local symmetries of M-theory and their formulation in generalised geometry. *Journal of High Energy Physics* 2012,**2012**:12.
17. Liu Y-C, Wang C-C. Effect of argon plasma treatment on surface-enhanced raman spectroscopy of polypyrrole deposited on electrochemically roughened gold substrates. *The Journal of Physical Chemistry B* 2005,**109**:5779-5782.
18. Berman D, Krim J. Impact of oxygen and argon plasma exposure on the roughness of gold film surfaces. *Thin Solid Films* 2012,**520**:6201-6206.
19. Wilson I, Kidd M. A study of cones developed by ion-bombardment of gold. *Journal of Materials Science* 1971,**6**:1362-1366.
20. Thévenot DR, Toth K, Durst RA, Wilson GS. Electrochemical biosensors: recommended definitions and classification. *Analytical Letters* 2001,**34**:635-659.
21. Chaubey A, Malhotra B. Mediated biosensors. *Biosensors and bioelectronics* 2002,**17**:441-456.
22. Rashid JIA, Yusof NA. The strategies of DNA immobilization and hybridization detection mechanism in the construction of electrochemical DNA sensor: A review. *Sensing and bio-sensing research* 2017,**16**:19-31.
23. Bard AJ, Faulkner LR, Leddy J, Zoski CG. *Electrochemical methods: fundamentals and applications*: wiley New York; 1980.
24. Moretto LM, Kalcher K. *Environmental analysis by electrochemical sensors and biosensors*: Springer; 2014.

25. Lazerges M, Tal V, Bigey P, Scherman D, Bedioui F. Electrochemical DNA-biosensors: Two-electrode setup well adapted for miniaturized devices. *Sensors and Actuators B: Chemical* 2013,**182**:510-513.
26. Brown T, Brown D, Eckstein EF. Oligonucleotides and analogues. *A Practical Approach* 1991:1-24.
27. Cavaluzzi MJ, Borer PN. Revised UV extinction coefficients for nucleoside-5'-monophosphates and unpaired DNA and RNA. *Nucleic acids research* 2004,**32**:e13-e13.
28. Kallansrud G, Ward B. A comparison of measured and calculated single-and double-stranded oligodeoxynucleotide extinction coefficients. *Analytical biochemistry* 1996,**236**:134-138.
29. Sambrook J, Fritsch EF, Maniatis T. *Molecular cloning: a laboratory manual*: Cold spring harbor laboratory press; 1989.
30. Borer P. Handbook of biochemistry and molecular biology. *Optical Properties of Nucleic Acids, Absorption and Circular Dichroism Spectra*, CRC Press, Cleveland 1975:589-595.
31. Richards E, Fasman G. Handbook of biochemistry and molecular biology: nucleic acids. by CD Fasman, CRC, Cleveland 1975,**1**:197.
32. Tataurov AV, You Y, Owczarzy R. Predicting ultraviolet spectrum of single stranded and double stranded deoxyribonucleic acids. *Biophysical chemistry* 2008,**133**:66-70.

RÉSUMÉ

Les micro-acides ribonucléiques (miARNs) sont des biomarqueurs émergents de nombreuses maladies, des cancers plus particulièrement. Ils présentent un intérêt majeur en santé humaine car leur quantification permet d'établir un diagnostic avec un nombre d'analyses nettement inférieur que celle fondée sur la quantification d'acides ribonucléiques messagers (ARNm). Leur détection s'effectue classiquement par une étape préliminaire d'amplification de leur concentration par réaction en chaîne par polymérase (RCP) suivi d'une mesure de fluorescence. Les limites de cette méthode sont son coût élevé, son temps d'analyse long et l'erreur induite par leur étape préliminaire d'amplification par RCP: des miARN de séquences différentes peuvent ne pas être amplifiés de la même manière dans des conditions opératoires identiques. La détection directe de miARN, c'est à dire sans amplification préalable par RCP, constitue de fait un challenge du diagnostic médical. Ce doctorat présente le développement technologique d'outils analytiques permettant une détection directe de miARN : des biocapteurs électrochimique et optique qui ciblent le miARN21, un biomarqueur impliqué dans des cancers hépatiques. Les performances analytiques des biocapteurs développés dans le cadre de ce doctorat sont comparées à celle de la RCP pour la détection de miARN dans des échantillons de sang d'origine humaine.

MOTS CLÉS

Biocapteur, Diagnostic medical, miARN, Electrochimie, RCP, RPS

ABSTRACT

Ribonucleic micro-acids (miRNAs) are emerging biomarkers for many diseases, particularly cancers. They are of major interest in human health because their quantification makes it possible to establish a diagnosis with a significantly lower number of analyzes than that based on the quantification of messenger-ribonucleic micro-acids (mRNAs). Their detection is carried out conventionally by a preliminary step of amplification of their concentration by polymerase chain reaction (PCR) followed by a fluorescence measurement. The limits of this method are its high cost, its long analysis time and the error induced by their preliminary amplification step by PCR: miRNAs of different sequences may not be amplified in the same way under identical operating conditions. The direct detection of miRNA, that is to say without prior amplification by PCR, constitutes a challenge in medical diagnosis. This doctorate presents the technological development of analytical tools allowing a direct detection of miRNAs: electrochemical and optical biosensors which target miRNA-21, a biomarker implicated in hepatic cancers. The analytical performance of the biosensors developed as part of this doctorate is compared to that of PCR for the detection of miRNAs in blood samples of human origin.

KEYWORDS

Biosensor, Medical diagnosis, miRNA, Electrochemistry, PCR, SPR

